Improved seismic analysis of unreinforced masonry buildings with flexible diaphragms

by

Yasuto Nakamura

A thesis submitted in partial fulfilment of the requirements for the degree of Doctor of Philosophy

School of Civil, Environmental and Mining Engineering
University of Adelaide

November 2016

Improved seismic analysis of unreinforced masonry buildings with flexible diaphragms

Yasuto Nakamura

B.E. (Civil Structural), M.Sc.

School of Civil, Environmental and Mining Engineering

University of Adelaide

November 2016

Abstract

The presence of flexible timber diaphragms in many existing unreinforced masonry buildings poses a significant challenge for the assessment of their seismic vulnerability. When diaphragms are flexible, different parts of a structure can interact with each other dynamically, in a way not typically encountered in modern structures with rigid diaphragms. As a result, the seismic analysis methods developed for buildings with rigid diaphragms, as well as our basic understanding of the dynamic behaviours of buildings under earthquake excitations, cannot be applied directly for buildings with flexible diaphragms. This thesis addresses two issues that require immediate attention in improving the seismic analysis of unreinforced masonry buildings with flexible diaphragms, namely (1) to enhance our understanding of the dynamic response characteristics of low-rise buildings with flexible diaphragms, and (2) to investigate the applicability of an array of existing analysis methods developed for rigid diaphragm structures.

The research work presented in this thesis begins with a basic analysis of the elastic behaviour of symmetric buildings with flexible diaphragms. Through an analytical study of their modal properties, it is shown that at least two dominant modes are present in the dynamic responses of buildings with flexible diaphragms. Using the results of modal analysis, an improvement to the linear static analysis method is proposed.

The inelastic behaviours of symmetric- and asymmetric-plan building systems with flexible diaphragms are then investigated through a systematic parametric analysis. It is shown that the effect of diaphragm flexibility varies depending on the level of stiffness- and strength-eccentricity of the system. A general diaphragm classification is developed to explain the influence of diaphragm flexibility on the global building response.

A simple numerical modelling technique to incorporate the dynamic behaviours of flexible diaphragms in a three-dimensional equivalent frame modelling approach is also investigated, and validated against shake table test data.

Finally, the applicability of nonlinear static procedures utilising single-mode, multi-mode and adaptive pushover analyses are investigated. Practical recommendations are provided for the use of various pushover analysis methods for unreinforced masonry buildings with flexible diaphragms.

Acknowledgments

I would like to express my gratitude to my principal supervisor, Professor Michael Griffith, for his continuous support, patience and enthusiasm throughout my PhD study. I am grateful for his guidance and for his critical reviews of my work. Without his support, it would not have been possible to complete this thesis.

I would also like to thank my co-supervisors, Associate Professor Hamid Sheikh and Professor Guido Magenes, for their thorough reviews of my work, encouragements and insightful comments.

Besides my supervisors, I would like to thank Professor Jason Ingham, who provided critical reviews of my manuscripts. I would also like to thank Dr. Hossein Derakhshan for his invaluable input on the current research needs for unreinforced masonry buildings and for his guidance through the course of my study.

Finally, I would like to thank my family and my wife, Vantho, for their enduring support and encouragement.

Table of Contents

List of Publications

Published Journal Papers and Papers Accepted for Publication

Nakamura, Y., Derakhshan, H., Ingham, J.M. and Griffith, M.C. (2014) "Seismic analysis of in-plane loaded walls in unreinforced masonry buildings with flexible diaphragms", Bulletin of New Zealand Society for Earthquake Engineering, 47(4), 275 – 289.

Nakamura, Y., Derakhshan, H., Magenes, G. and Griffith, M.C. (2016) "Influence of diaphragm flexibility on seismic response of unreinforced masonry buildings", Journal of Earthquake Engineering, published online 27 July 2016. DOI:10.1080/13632469.2016.1190799.

Nakamura, Y., Derakhshan, H., Sheikh, A.H., Ingham, J.M. and Griffith, M.C. (2016) "Equivalent frame modelling of an unreinforced masonry building with flexible diaphragms – a case study", Bulletin of New Zealand Society for Earthquake Engineering, 49(3), 234 – 244.

Manuscripts under Review

Nakamura, Y., Derakhshan, H., Griffith, M.C., Magenes, G. and Sheikh, A.H. (2016) "Applicability of nonlinear static procedures for low-rise unreinforced masonry buildings with flexible diaphragms", Submitted to Engineering Structures.

Peer-reviewed Conference Papers

Nakamura, Y., Magenes, G. and Griffith, M.C. (2014) "Comparison of pushover methods for simple building systems with flexible diaphragms", Proceedings of Australian Earthquake Engineering Society Conference, November 21 – 23, Lorne, Victoria, Australia.

Nakamura, Y., Derakhshan, H., Griffith, M.C. and Magenes, G. (2015) "Estimating the accuracy of single-mode pushover analysis for unreinforced masonry buildings with flexible diaphragms", Proceedings of the Ninth Pacific Conference for Earthquake Engineering, 6 – 8 November, Sydney, Australia.

Nakamura, Y., Derakhshan, H., Griffith, M.C. and Magenes, G. (2016) "Is Modal Pushover analysis accurate in estimating seismic demands for unreinforced masonry buildings with flexible diaphragms?", Proceedings of 16th International Brick and Block Masonry Conference, 26 – 30 June, Padova, Italy.

Statement of Original Authorship

I certify that this work contains no material which has been accepted for the award of any other degree or diploma in any university or other tertiary institution and, to the best of my knowledge and belief, contains no material previously published or written by another person, except where due reference has been made in the text. In addition, I certify that no part of this work will, in the future, be used in a submission for any other degree or diploma in any university or other tertiary institution without the prior approval of the University of Adelaide and where applicable, any partner institution responsible for the joint-award of this degree.

I give consent to this copy of my thesis when deposited in the University Library, being made available for loan and photocopying, subject to the provisions of the Copyright Act 1968.

The author acknowledges that copyright of published works contained within this thesis resides with the copyright holder(s) of those works.

I also give permission for the digital version of my thesis to be made available on the web, via the University's digital research repository, the Library catalogue and also through web search engines, unless permission has been granted by the University to restrict access for a period of time.

Signed: Date:

11/11/2016

(Yasuto Nakamura)

CHAPTER 1

INTRODUCTION

The poor performance of unreinforced masonry (URM) buildings during strong earthquake events is well recognised. Throughout history, and across different regions of the world, earthquake damages to URM buildings have led to countless number of fatalities, sometimes resulting in complete devastations of communities (Figure 1). Recognising the high vulnerability of URM buildings, New Zealand and California, two of the most seismically active regions with large representations of URM buildings, prohibited new URM building constructions in the 1930's after devastating earthquakes (i.e. 1931 Napier earthquake in New Zealand and 1933 Long Beach earthquake in California). Since then, the ban on URM buildings has spread throughout the seismically active areas of the western United States and Canada (Bruneau 1995). However, URM buildings still represent large proportions of total building stock in many parts of the world, and they continue to pose significant seismic risk, as evidenced by the successive earthquakes in the recent decades, including in Iran (2003), Pakistan (2005), Peru (2007), China (2008) and Nepal (2015). Even in those regions where the URM has become an archaic construction material, extensive damages to existing URM buildings still occur, as observed during the Christchurch earthquake sequence of 2011/2012 in New Zealand (Dizhur et al. 2011; Ingham and Griffith 2011; Griffith et al. 2013). Furthermore, the vulnerability of URM buildings is not confined to high-seismicity regions; the poor performances of URM buildings have been reported consistently in Australia (Griffith 1991; Edwards et al. 2010), where the seismicity is low to moderate.

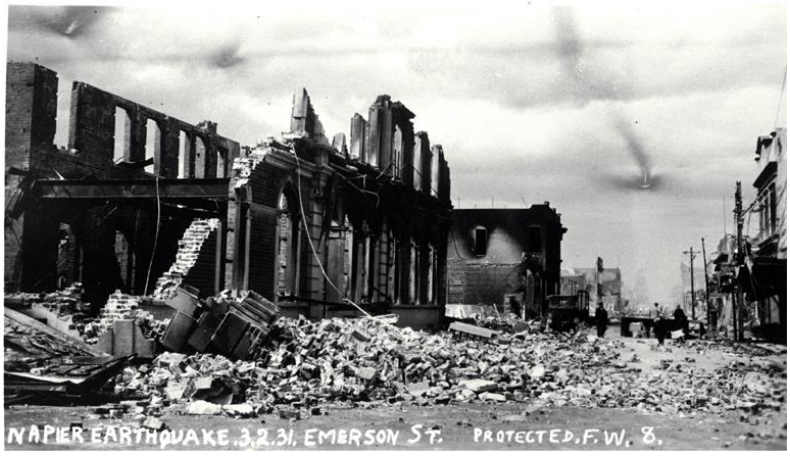

Figure 1. View of Emerson Street after the 1931 Napier earthquake. With permission from Christchurch City Libraries (CCL PhotoCD 4, IMG0041).

The high seismic vulnerability of URM buildings is not surprising, given that many existing buildings were built before the introduction of seismic codes and guidelines (Russel 2010), when the awareness of the importance of aseismic design was virtually non-existent. As a result, URM buildings contain several undesirable construction details in view of the modern seismic design principles, including:

- Brittle masonry material used for lateral load-resisting elements, which result in limited ductility and energy dissipation capacities;
- Lack of positive connections between floor/roof diaphragms and masonry walls, which can lead to the instability of out-of-plane loaded walls; and
- Use of timber floor and roof systems that have large in-plane flexibility, and the resulting lack of "box" type building behaviour.

Of the several weaknesses listed above, the present research focuses on the role of flexible diaphragms on the overall dynamic responses of URM buildings. The specific objectives addressed in this research are:

1. To develop a comprehensive understanding of the seismic behaviour of URM buildings with flexible diaphragms;
2. To investigate the accuracies of existing seismic analysis methods; and
3. To contribute towards the improvement of existing seismic analysis methods for URM buildings with flexible diaphragms.

The research needs as reflected in the above objectives are identified in the review of literature presented in Chapter 2. The literature review also contains a concise summary of the theoretical bases of nonlinear static analysis methods that are referenced in the subsequent chapters of this thesis.

The remaining chapters are a collection of manuscripts that are either in preparation, submitted, accepted or published in recognised journals. Each chapter takes the following format: an introduction explaining the background to the papers, the list of papers contained in the chapter, followed by the presentation of the papers.

In Chapter 3, the elastic behaviour of symmetric multistorey buildings with flexible diaphragms is firstly investigated using modal analysis to obtain a basic understanding of their dynamic response characteristics. It is shown analytically that at least two modes are typically required to capture the

majority of mass participation for buildings with flexible diaphragms. From the results of modal analysis, simplified expressions are developed to account for diaphragm flexibility in the context of the linear static analysis method. This chapter addresses research objectives 1 and 3.

In Chapter 4, a case study on the accuracy of the numerical model used throughout the present research is discussed. The investigated modelling approach is a minor extension of the equivalent frame analysis approach utilised in the TREMURI software, with the novelty of using multiple diaphragm elements to capture the dynamic behaviours of timber floors and roofs. The accuracy of the modelling approach is compared against existing shake table test results of a two-storey stone masonry building. This chapter addresses research objective 3.

In Chapter 5, the results of a comprehensive parametric study carried out using single-storey structural systems with inelastic in-plane loaded walls supporting flexible diaphragms are presented. The dynamic response characteristics, considering a wide range of diaphragm flexibility, are identified and characterised. This chapter addresses research objective 1.

In Chapter 6, the applicability of single-mode, multi-mode and adaptive nonlinear static procedures are evaluated for URM buildings with flexible diaphragms. The most suitable manner in which to apply each nonlinear static procedure for URM buildings with flexible diaphragms is identified. A measure of diaphragm flexibility developed in Chapter 4 is adapted for identifying the range of diaphragm stiffness values for which the single-mode nonlinear static method gives reasonable results. The accuracies of various analysis methods are discussed and recommendations are presented. This chapter addresses research objectives 2 and 3.

Chapter 7 summarises the results of the research, highlighting key findings, providing recommendations and identifying future research areas.

References

Bruneau, M. (1995) “Performance of masonry structures during the 1994 Northridge (Los Angeles) earthquake”, Canadian Journal of Civil Engineering, 22, 378 – 402.

Dizhur, D., Ingham, J., Moon, L., Griffith, M.C., Schultz, A., Senaldi, I., Magenes, G., Dickie, J., Lissel, S., Centeno, J., Ventura, C., Leite, J. and Lourenco, P. (2011) “Performance of masonry buildings and churches in the 22 February 2011 Christchurch Earthquake”, Bulletin of the New Zealand Society for Earthquake Engineering, 44(4), 279 – 296.

Edwards, M., Griffith, M. C., Whner, M., Lam, N., Corby, N., Jakab, M. and Habili, N. (2010) "The Kalgoorlie Earthquake of the 20th April 2010: Preliminary damage survey outcomes", Proceedings of Australian Earthquake Engineering Society 2010 Conference, Perth, Western Australia.

Griffith, M. C. (1991) "Performance of unreinforced masonry buildings during the Newcastle earthquake, Australia - Research Report No. R 86", School of Civil Engineering, University of Adelaide.

Griffith, M. C., Moon, L., Ingham, J. M. and Derakhshan, H. (2013) "Implications of the Canterbury earthquake sequence for Adelaide, South Australia", Proceedings of the 12th Canadian Masonry Symposium, Vancouver, British Columbia, June 2-5, 2013.

Ingham, J. and Griffith, M. C. (2011) "Performance of unreinforced masonry buildings during the 2010 Darfield earthquake", Australian Journal of Structural Engineering, Engineers Australia, 11(3), 207-224.

Russel, A. P. (2010) "Characterisation and seismic assessment of unreinforced masonry buildings", PhD thesis, Department of Civil and Environmental Engineering, University of Auckland.

CHAPTER 2

PREVIOUS RESEARCH ON BUILDINGS WITH FLEIXBLE DIAPHRAGMS

The seismic responses of buildings with flexible diaphragms are known to differ from those of rigid diaphragm structures. The role of diaphragm flexibility is reviewed in this chapter, focusing on unreinforced masonry (URM) buildings with timber diaphragms. This chapter also presents the review of seismic analysis methods commonly used in practice, namely the linear static and nonlinear static analysis procedures. In particular, the theoretical bases of single-mode and multi-mode nonlinear static procedures are outlined, providing background information for the subsequent chapters of this thesis. Problems associated with the application of the nonlinear static method for URM buildings with flexible diaphragms are discussed.

1. EXPERIMENTAL STUDIES ON BUILDING RESPONSE

The actual seismic behaviour of URM buildings with flexible diaphragms was reported by Tena-Colunga and Abrams (1992), who analysed the measured response of a two-storey unreinforced masonry building with timber floor and roof during the Loma Prieta earthquake of 1989. This heritage building, a former firehouse in Gilroy California (Figure 1), was constructed in 1890 and was instrumented with six accelerometers prior to the 1989 earthquake as part of the California Strong Motion Instrumentation Program. The construction system of the building comprised of the load bearing brick masonry walls with the first floor diaphragms consisting of timber joists anchored to the perimeter walls by 20 mm diameter steel rods, with diagonal sheathing boards and plywood overlay. The roof was also constructed of timber joists and boards, with layers of asphalt sheeting for waterproofing. Despite the large magnitude earthquake, the limited extent of cracking indicated that the structure responded more or less elastically during the earthquake.

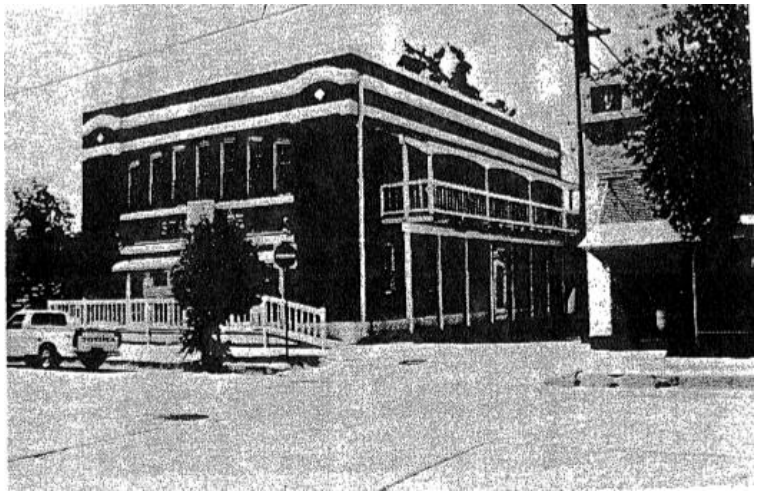

Figure 1. Gilroy Firehouse (Tena-Colunga & Abrams 1992)

The records from the accelerometers indicated large amplifications of acceleration and displacement at the centre of the roof diaphragm. In the east-west direction, the peak acceleration at the top of the internal wall was measured to be 0.41 g, while the peak acceleration at the mid-pan of the roof diaphragm reached 0.71 g. The normalised Fourier spectra indicated that the frequency content of the in-plane loaded wall was similar to the ground motion (Figure 2a), reflecting the stiff nature of masonry. In contrast, the normalised Fourier spectra of the roof diaphragm mid-span showed the dominant frequency occurring around the natural period of the diaphragm of approximately 0.5 s and filtering out of other frequency component (Figure 2b), leading the authors to concluded that, once excited, the diaphragms tended to respond independently from the in-plane loaded walls and the ground.

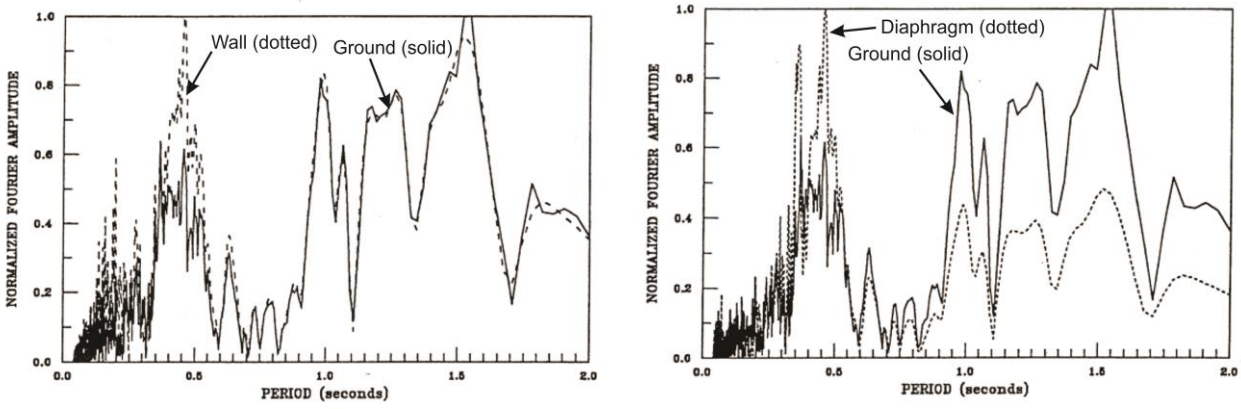

(a) Ground and wall (b) Ground and diaphragm

Figure 2. Normalised Fourier amplitudes of ground acceleration against the accelerations measured at the top of wall and diaphragm (Tena-Colunga & Abrams 1992)

The large amplifications of acceleration and displacement of the diaphragms were also observed in a subsequent experimental study by Costely and Abrams (1995). They tested two scaled brick masonry building models under the unidirectional input of Nahanni earthquake of 1985. To represent flexible diaphragms in a scaled model, steel beams with stiffnesses similar to timber diaphragms were used to construct the floor and the roof. Their experimental work confirmed the large amplifications and independent excitations of the diaphragms when the masonry walls remained elastic. However, when the walls cracked and started to rock, the diaphragm amplification reduced and in some cases became negligible. The post-cracking behaviour was dominated by the rocking of the in-plane loaded walls, as opposed to the excitation of the diaphragms.

Several experimental studies were also carried out in Europe during the 1990's and early 2000's, focusing on improving the seismic capacity of URM buildings with timber floors (Tomaževič et al. 1992; Tomaževič et al. 1996; Benedetti et al. 1998). These studies consistently found that when timber diaphragms were present without sufficient measures to maintain the integrity of the walls (such as anchor connections between the floor and walls, and tie rods between the walls), URM buildings tended to fail by the partial out-of-plane collapses of the walls. However, when the partial collapses were prevented, buildings with flexible diaphragms have been observed to perform satisfactorily.

By testing four different scaled models, Model A to Model D with different floor configurations under shake table excitations, Tomaževič et al. (1996) showed that the load-deformation capacity of flexible diaphragm structures could be comparable to that of an equivalent building with rigid diaphragms. In their experiment, Model A had timber diaphragms simply bearing onto the in-plane loaded walls without any positive connections. Model B had rigid reinforced concrete floors with tie beams around the perimeter of the walls. Models C and D had timber diaphragms identical to that of Model A, but the walls were tied around the perimeter by prestressed steel rods, or connected by internal struts (Figure 3). For Model A, failure occurred due to the partial collapse of the upper corner of the building. All other models with some form of strengthening activated global response mechanisms, with failures occurring in the in-plane loaded walls in the first storey. When such global response mechanism was achieved, the plots of base shear coefficients against the first storey drifts (Figure 4) showed good performances of timber floor systems, when compared to the reinforced concrete floor model.

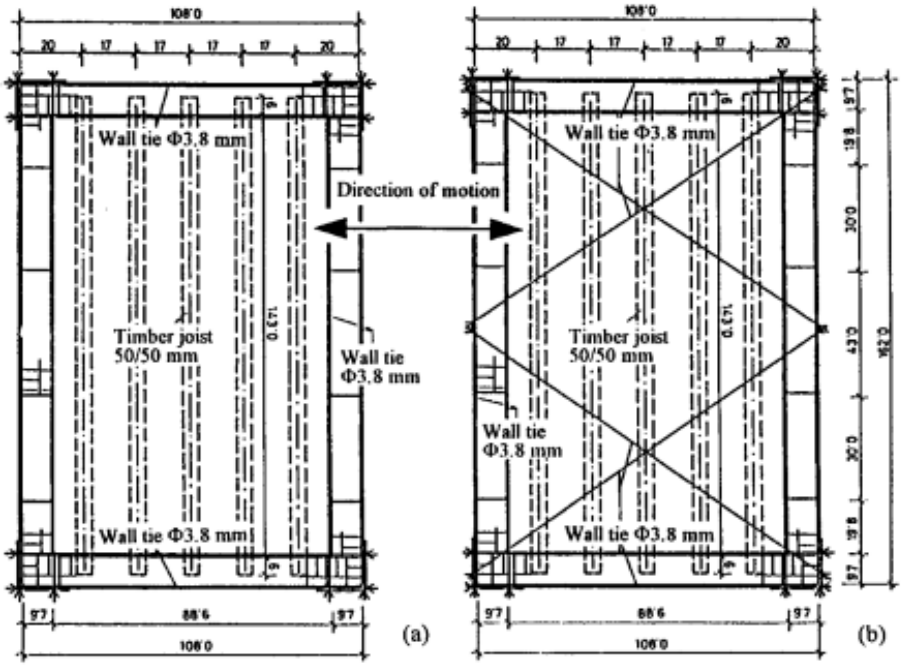

Figure 3. Plan view of models with wall ties, (a) Model C and (b) Model D. Model A is similar but without any wall ties (Tomaževič et al. 1996)

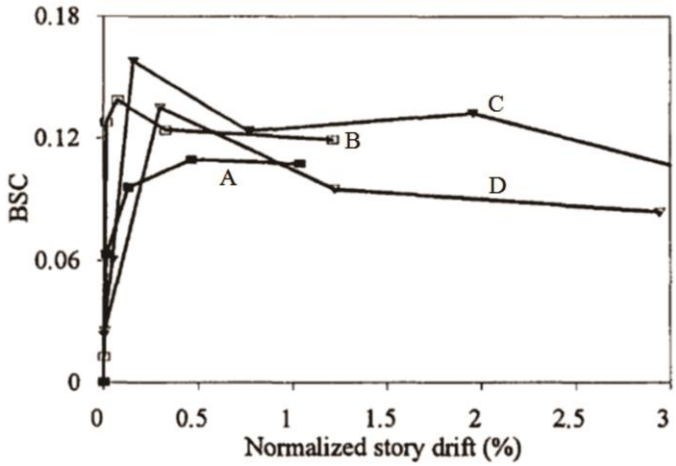

Figure 4. Plots of base shear normalised to the weight of the structure for timber diaphragms with no connections to the walls (A), reinforced concrete floor (B), and timber diaphragms with tied walls (C and D) (Tomaževič et al. 1996)

Paquette and Bruneau (2003) carried out pseudo-dynamic testing of a single-story brick masonry building with a timber diaphragm. The diaphragm was anchored to the perimeter walls by steel rods, and the loads were applied by hydraulic jacks to the mid-span of the diaphragm. The test results showed that the diaphragms remained essentially elastic even when extensive damage occurred to the in-plane loaded walls. As the observed damages consisted of stable rocking and sliding mechanisms, their study also

indicated that URM buildings with flexible diaphragms could undergo stable global responses under seismic excitations.

Cohen et al. (2003) conducted shake table testing of long and narrow single-storey scaled reinforced masonry buildings with timber and steel deck roofs. Similar to the findings by Costely and Abrams (1995), the test results showed high accelerations of the diaphragms in comparison to those of in-plane loaded walls (Figure 5). The results also showed that the responses of the stiff in-plane loaded walls contained noticeable participation of higher modes (shown by the arrows in Figure 5), while the response of the diaphragm appeared to be governed predominantly by a single mode.

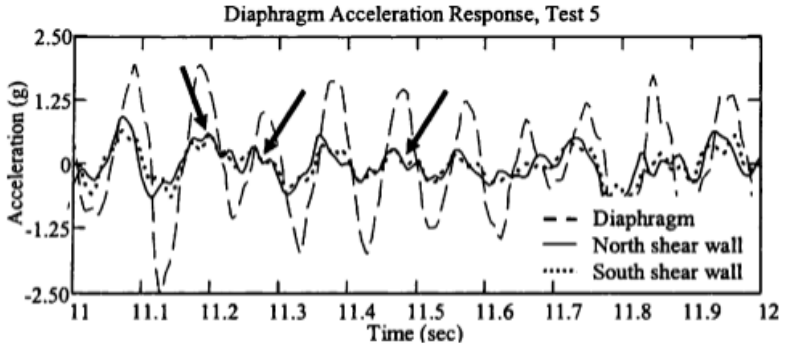

Figure 5. Acceleration response of diaphragm mid-span and the top of in-plane loaded walls (Cohen et al. 2003).

Yi et al. (2006) conducted a quasi-static testing of a full scale two-storey brick masonry building with timber diaphragms. Their experimental results indicated little coupling of the in-plane loaded walls because of diaphragm flexibility. However, the test results also showed that despite the weak diaphragm coupling, the global response of the building was achieved, as characterised by the variation in the vertical stresses in piers due to the overturning moments and the presence of flange effects where an additional rocking capacity could be attributed to the axial stresses developed in the out-of-plane walls acting as flanges (Figure 6).

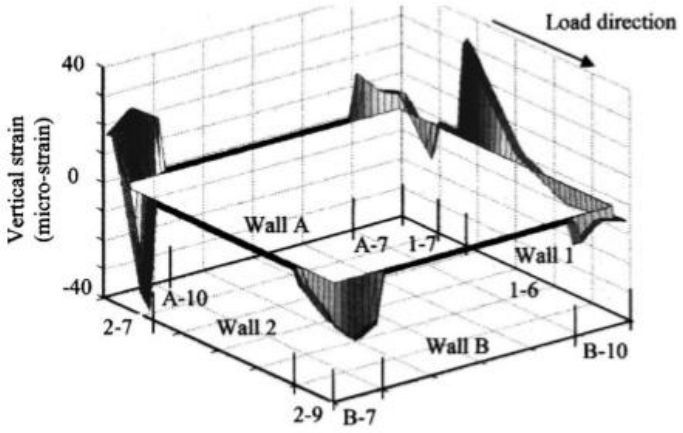

Figure 6. Vertical stress distribution at base of wall. The tensile and compressive stresses in the out-of-plane loaded walls A and B indicate flange effect (Yi et al. 2006). With permission from ASCE.

An extensive experimental investigation was recently conducted at the European Centre for Training and Research in Earthquake Engineering (EUCENTRE), aimed at understanding the dynamic behaviour of stone masonry buildings and to evaluate the effectiveness of retrofit strategies related to diaphragm stiffness (Magenes et al. 2014; Sinaldi et al. 2014). Three full scale two-storey buildings with different diaphragm materials (timber and concrete) and diaphragm to wall connection details were tested under shake table excitations. In general, the results were consistent with previous experimental observations, namely:

- out-of-plane wall failure occurred when flexible timber diaphragms were not positively anchored to the perimeter walls, and the in-plane capacities of the load bearing walls could not be exploited;

- even when diaphragms were not rigid, the seismic resistance of the building could be comparable to that of the rigid diaphragm condition, provided that the out-of-plane wall failure was prevented with sufficient connections between the walls and the diaphragm; and

- The flexible diaphragm provided limited coupling of in-plane loaded walls, and the walls tended to respond as independent components (Penna 2015).

A recent experimental study by Vintzileou et al. (2015) also confirmed the above response characteristics of URM buildings with flexible diaphragms.

2. ANALYTICAL STUDIES ON BUILDING RESPONSE

Analytical studies of the effects of diaphragm flexibility on the dynamic responses of buildings were carried out as early as in the 1960s by Shephard and Donald (1967). They proposed a lumped mass model with beam elements to capture the dynamic behaviour of flexible diaphragms. The application of this model to simple frame buildings (Figure 7) showed that the deformation of the diaphragm appeared only in higher modes. Based on this observation, the authors concluded that while flexible diaphragms may modify the higher mode shapes, they are likely to have little effect on the final loading of the lateral load-resisting elements.

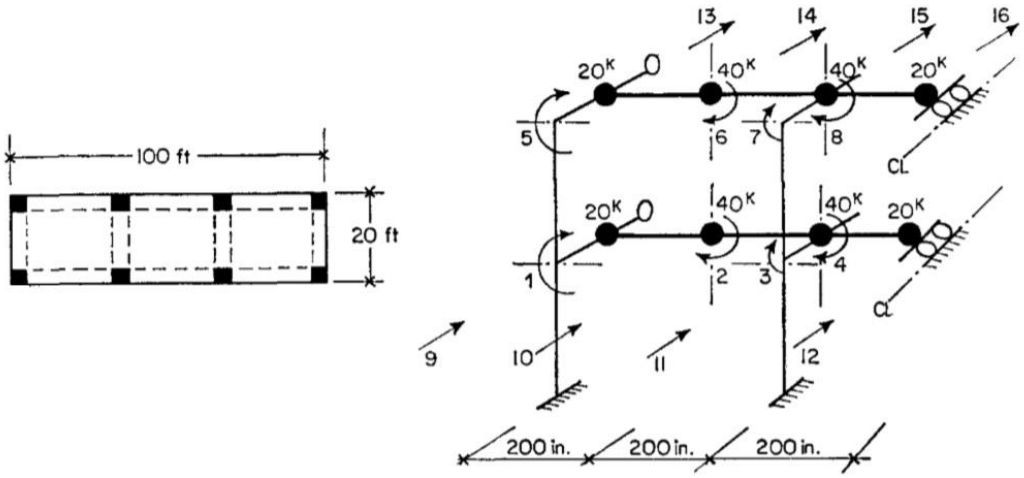

Figure 7. Early lumped mass and beam model (Shepherd & Donald 1967).

Jain and Jennings (1985) developed a mathematical model of symmetric long-span buildings with end shear walls by idealising the diaphragms as Timoshenko beams. Using the derived expressions, the modal properties of the Administrative Building of Arvin High School were investigated (Figure 8). In contrast to the conclusion of Shepherd and Donald (1967), the model showed that the largest contribution to the base shear resulted from the first two modes, which comprised mainly of the vibrations of the floor and the roof. It was postulated that for multistorey buildings with flexible diaphragms, lower modes may comprise of the independent vibrations of the floor diaphrams.

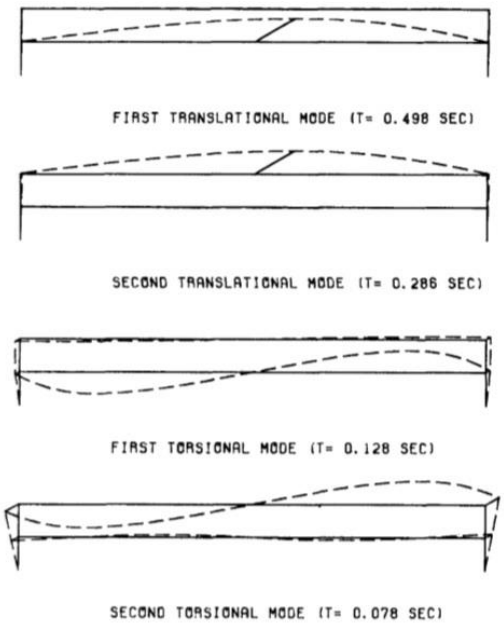

Figure 8. Modal properties of Administrative Building of Arvin High School (Jain & Jennings 1985).

Tena-Colunga and Abrams (1992) (see also Tena-Colunga 1992) developed discrete multi-degree of freedom (MDOF) linear models of the Gilroy firehouse (Figure 1), which had been instrumented before the Loma Prieta earthquake. The in-plane loaded walls and the timber diaphragms were represented by shear springs as shown in Figure 9. The out-of-plane loaded walls were not modelled, while the soil compliance was included. The calibration of the material parameters enabled the model to produce results compatible with the measured data. The sensitivity analyses on the calibrated model showed that:

- In agreement with Jain and Jannings (1985), the lower modes were governed by the independent vibrations of the diaphragms, while the higher modes contained the almost independent vibrations of the in-plane loaded walls (Figure 10). This result also supported the experimental observations of Costley and Abrams (1995) that in the elastic range, the diaphragms and the walls tended to respond independently.

- The distribution of the in-plane wall accelerations and displacements were uneven. The more flexible wall tended to experience larger accelerations and displacements compared to the stiffer wall.

- When compared to the same building model but with rigid diaphragms, in the presence of soil compliance the flexible diaphragms increased both the drifts and the accelerations of the walls. For a fixed-based model, the drifts increased but the accelerations reduced. Both the drifts and the

accelerations at the diaphragms' mid-spans, however, increased due to diaphragm flexibility regardless of the base fixity of the model.

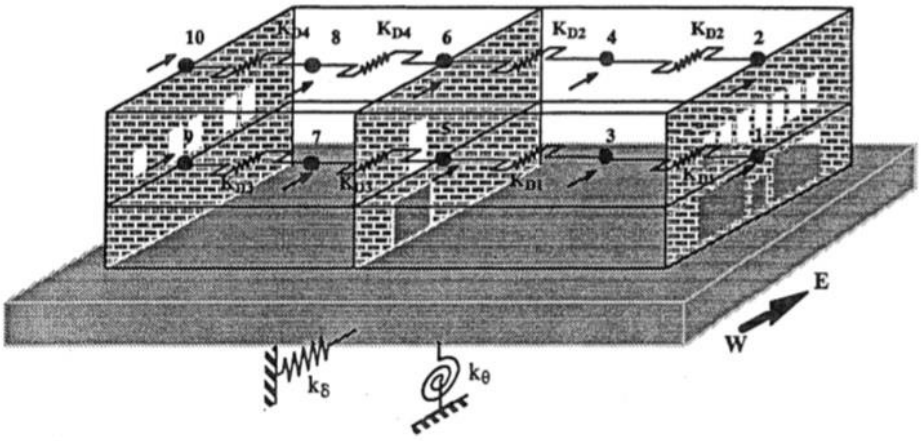

Figure 9. Lumped parameter model of Gilroy Firehouse in the east-west direction (Tena-Colunga & Abrams 1992).

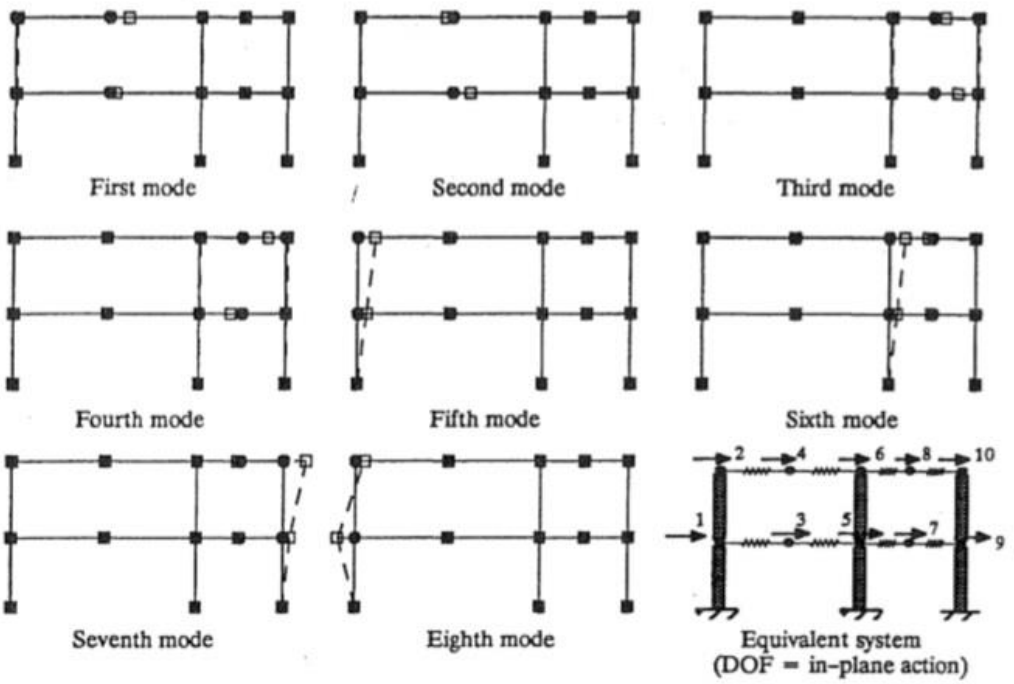

Figure 10. Mode shapes of Gilroy Firehouse in the east-west direction (Tena-Colunga & Abrams 1992)

The apparent contradictory finding of the earlier study by Shepherd and Donald (1967) that the flexible diaphragms did not significantly affect the dynamic response of the structure was explained by a study carried out by Saffarini and Qudaimat (1992), which focused on the relative stiffness of the diaphragm with respect to the stiffness of the lateral load-resisting elements. They conducted elastic static analyses

on 37 reinforced concrete (RC) buildings with varying storey heights, number of storeys, floor slab system, type of lateral load-resisting system and openings in slab. The results showed that even when the diaphragms were flexible, if the relative stiffness of the diaphragms in comparison to the stiffness of the lateral load-resisting elements was large, the response of the structure was similar to the rigid diaphragm case. In particular, the diaphragm flexibility was found to have more significant effects on shear wall structures when (1) storey height was reduced, (2) number of storey was reduced, and (3) plan aspect ratio of the building was increased. When the lateral load-resisting system was composed only of frames, as in the case of the study conducted by Shepherd and Donald (1967), the differences in the seismic base shear between flexible diaphragm system and the rigid diaphragm system were less than 1%.

Kim and White (2004a) developed a nonlinear MDOF discrete model with a diaphragm macroelement specifically developed for low-rise shear wall buildings with flexible diaphragms. In contrast to the similar model previously used by Tena-Colunga and Abrams (1992), the MDOF model of Kim and White (2004a) allowed the nonlinear hysteretic behaviours of the walls and the diaphragms, as well as the three-dimensional effects of the building response, to be captured. The in-plane and the out-of-plane walls were represented by shear springs with appropriate hysteretic properties. In order to model typical deformation modes of flexible diaphragms, a custom macroelement was developed as shown in Figure 11. The kinematics of the element was defined by six degrees of freedom, which could express the rigid body movements, shear and bending deformation modes. The authors applied the modelling approach to a single-storey half-scale reinforced masonry building previously tested by Cohen et al. (2004), with the element behaviours determined through model calibration against the test data.

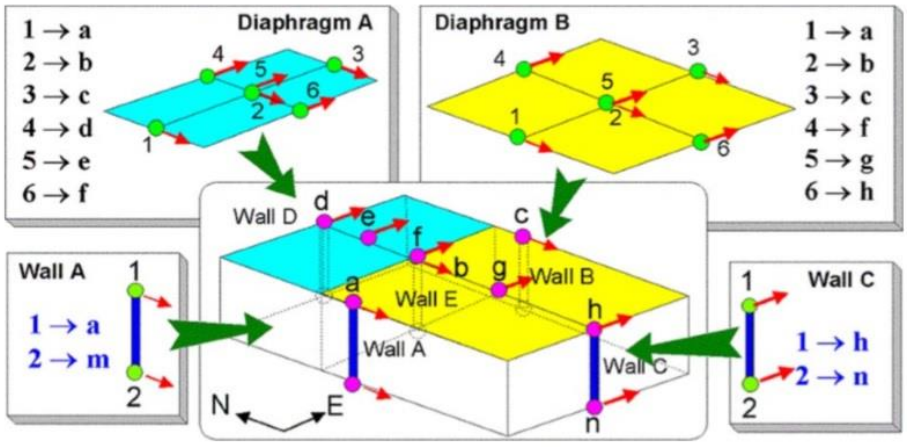

Figure 11. Discrete nonlinear model (Kim & White 2004a).

The calibration of the nonlinear MDOF model allowed the simulations of the peak responses that matched well with the experimental results, even at large damage levels. Using the calibrated element properties as

the reference values, sensitivity analyses were conducted by varying the stiffnesses and the strengths of the diaphragm, in-plane loaded walls and the out-of-plane loaded walls. In the sensitivity analysis, the stiffness and strength were considered to be inter-related; increasing the initial stiffness also increased the yield strength. The sensitivity analyses showed that

- Increasing the diaphragm stiffness reduced the drift demands on the out-of-plane loaded walls. However, the drift of the in-plane loaded walls increased initially, before reducing asymptotically to the rigid diaphragm condition (Figure 12);

- Increasing the in-plane wall stiffness reduced the drifts of both the in-plane and out-of-plane loaded walls; and

- Increasing the out-of-plane wall stiffness reduced the drifts of the out-of-plane loaded wall, but had limited effects on the response of the in-plane loaded wall.

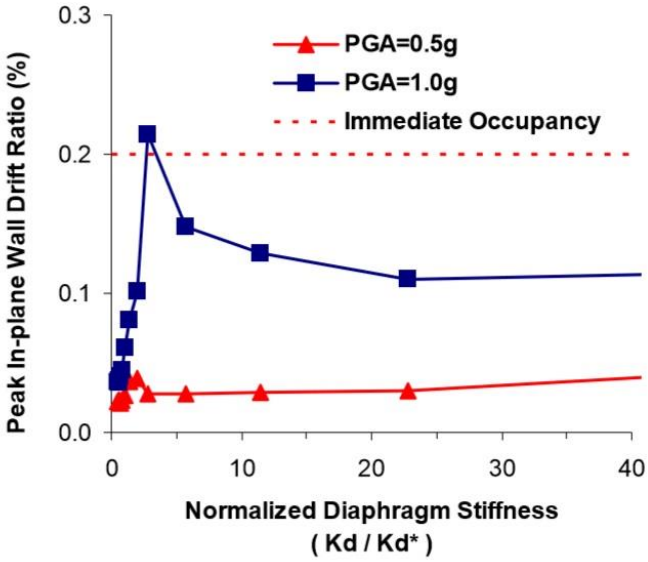

Figure 12. Peak drift ratio of in-plane loaded wall as a function of the normalised diaphragm stiffness (Kim & White 2003).

Sadashiva et al. (2012) conducted linear and nonlinear time-history analyses on one- to five-storey symmetric building systems with flexible diaphragms. Single- and two-bay structures were investigated. The diaphragm stiffness was expressed by the static flexibility ratio defined as

$$\gamma_s = \frac{\delta_{d\_flex}}{\delta_{w\_flex}} \quad (1)$$

where δ_{d_flex} was the mid-span deflection of the diaphragm subjected to a uniform static force, and δ_{w_flex} was the average displacement of the supporting walls below the diaphragm. The value of γ_s between 0 and 5 (increasing levels of diaphragm flexibility) were used in the study. Due to the large number of variables involved in the responses of buildings with flexible diaphragms, a number of constraints were imposed. These were:

- Equal amount of total mass at each floor level;
- Equal interstorey stiffness at all storeys;
- All diaphragms in a building to have the same static flexibility ratio; and
- For the two-span structures, the central wall to have twice the stiffness of the end walls.

The analyses showed that the fundamental period of the buildings increased with the diaphragm flexibility. The increase in the fundamental period was found to be most prominent for buildings with the reduction in the number storeys, which agreed with the previous findings by Saffarini and Qudaimat (1992). In general, the increase in the diaphragm flexibility resulted in the increased diaphragm displacements, but reduced forces and displacements of the in-plane loaded walls. The exception was the short period structures with the period T_{rig} (defined as the fundamental period of the rigid diaphragm system) of 0.1 s. For these structures, a tendency for increased displacements and forces of in-plane loaded walls were observed as the diaphragms were made flexible. The dependency of the effect of diaphragm flexibility on the natural period of the building suggested certain sensitivity to the input motion characteristics. The authors also proposed simple correction formulae for estimating the total mid-span displacement of the flexible diaphragms in a single-storey structure from the displacement of the corresponding rigid diaphragm system.

The effects of diaphragm flexibility on torsionally unbalanced buildings have also been investigated by several researchers.

Tena-Colunga and Abrams (1996) used three-dimensional elastic finite element models to show that the torsional behaviour reduced when diaphragm flexibility was increased.

De-La-Colina (1999) conducted nonlinear time-history analyses of simple torsionally unbalanced models (Figure 13) with stiffness eccentricity. The in-plane stiffness of the diaphragm was varied between values typical of timber floors to RC slabs. The lateral load-resisting elements were modelled with Clough-Otani

hysteresis. The yield forces of the elements were determined based on a rigid diaphragm configuration using a linear static design procedure typically used in seismic codes. The translational period of the rigid diaphragm system was varied between 0.2 s to 2 s, with the yield force reduction factor (R_y) between 1 and 6. In general, the peak displacements of the in-plane loaded walls (both the stiff and the flexible sides) reduced with the increase in diaphragm flexibility. However, large amplifications were observed when the period of the building (with a rigid diaphragm) was less than 0.4 s. The author explained that such difference in the effects of diaphragm flexibility was due to the shape of the input acceleration spectrum in relation to the elongation in the period of the system as the diaphragm flexibility increases.

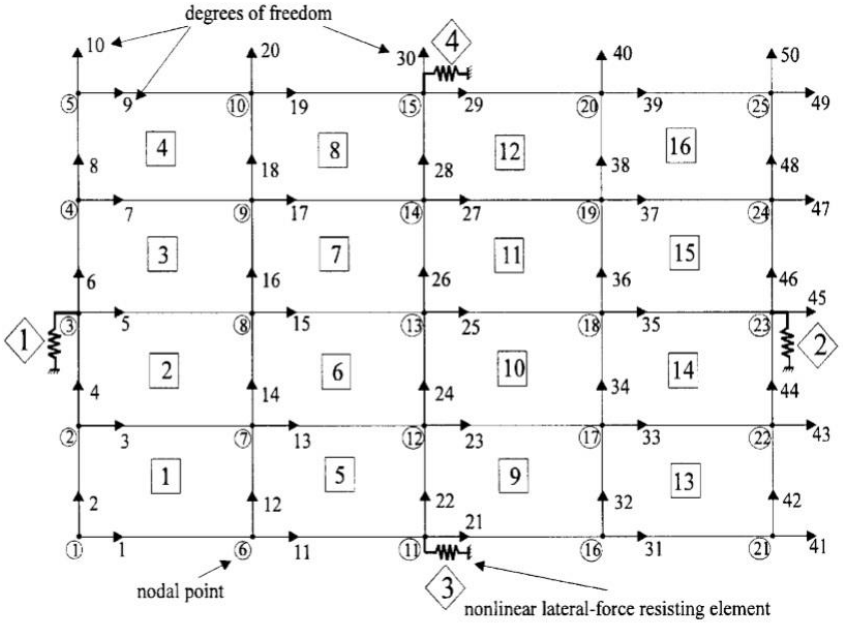

Figure 13. Stiffness eccentric model with flexible diaphragm (De-La-Colina 1999)

3. SEISMIC ANALYSIS METHODS

3.1 Overview of Analysis Methods

In general, seismic analysis methods can be classified into the linear elastic, linear dynamic, nonlinear static and nonlinear dynamic methods. Due to the low tensile strength of unreinforced masonry, the applicability of linear analysis methods are limited, even for low levels of loading. The need to consider the nonlinear behaviour of URM buildings has been long recognised, particularly after the Friuli earthquake of 1976 in Italy and Slovenia (Magenes & Penna 2009). However, in practice, engineers are still most familiar with the linear static analysis method and several specialised linear static analysis procedures have been developed for URM buildings with flexible diaphragms. These methods are

reviewed first. The remainder of this section is devoted to the review of the nonlinear static procedures, which are considered to be a viable alternative to the computationally intensive nonlinear time-history analysis.

3.2 Linear Static Method

A special procedure for the assessment and retrofit of existing URM buildings with flexible diaphragms was developed by ABK (1984) and described in detail by Bruneau (1994). This procedure is essentially empirical and contains the seismic capacity evaluation of the in-plane and out-of-plane loaded walls as well as the diaphragms. The method requires that the walls are adequately connected to the diaphragms so that partial out-of-plane wall failures are not expected to occur. To ensure the global behaviour, the span length and the strength of the diaphragms are firstly checked to be within an acceptable range to limit the amplification of the excitation applied onto the out-of-plane loaded wall. With the diaphragms so verified, the height-to-thickness (slenderness) ratio of the out-of-plane loaded walls are checked to ensure that stable dynamic rocking response can take place. The linear static method is then used to obtain the shear forces imposed on the in-plane loaded walls. In the linear static method, it is assumed that the in-plane walls are essentially rigid, so that the unamplified ground motion is transmitted to the diaphragms (Figure 14).

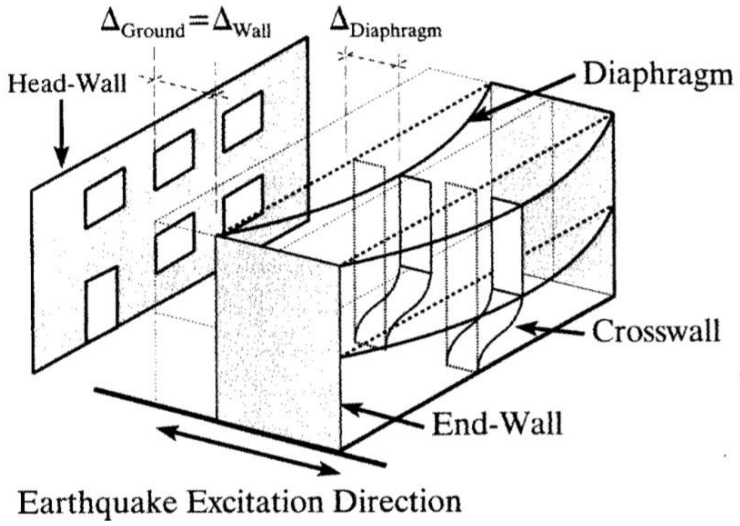

Figure 14. Rigid in-plane loaded wall assumption in ABK methodology (Bruneau 1994)

Based on this assumption, the maximum load applied on each in-plane loaded wall at any level is the tributary mass multiplied by the peak ground acceleration,

$$F_{wx} = \frac{a_g}{g}\left(W_{wx} + \frac{W_d}{2}\right) \tag{2}$$

where a_g is the peak ground acceleration, W_{wx} is the weight of the wall in the direction of loading and W_d is the weight attributed to the diaphragm. If the diaphragm yields, the force resisted by the in-plane loaded walls is limited to

$$F_{wx} = \frac{a_g}{g} W_{wx} + v_u D \tag{3}$$

where v_u and D are respectively the yield strength per unit length and the width of the diaphragm.

Kim and White (2004b) proposed an alternative method for calculating the in-plane loaded wall forces, recognising that the stiff walls and the flexible diaphragms tend to respond independently. In their method, a diaphragm subassembly consisting of a diaphragm span at any level and its supporting walls of the storey below (Figure 15) is considered to be subjected to the ground motion. The calculated diaphragm force is then distributed to the walls in proportion to their relative stiffnesses. The in-plane loaded walls are considered to be rigid, and their peak accelerations are set equal to the peak ground acceleration. The total storey force is then obtained as a direct sum of the forces from the diaphragm and the in-plane wall. Kim and White (2004b) reported good estimations of the peak base shear predictions of experimental data for single- and two-storey buildings.

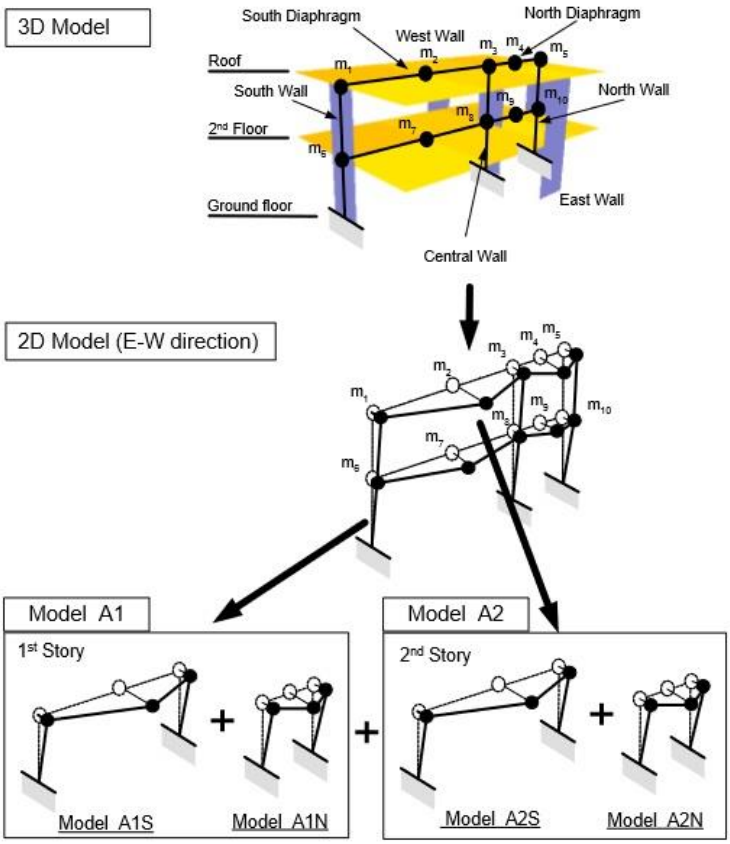

Figure 15. Diaphragm subassembly (Kim & White 2004b).

Knox (2012) proposed another approach, also based on the concept of the independent responses of the in-plane loaded walls and the diaphragms. In this method, the fundamental periods of the in-plane loaded wall and the diaphragms are calculated separately, and the individual components are considered to be subjected to the ground motion. The in-plane wall forces are then obtained by the square-root-of-sum-of-squares (SRSS) combination of the inertial forces from the diaphragm and the in-plane loaded walls at each level. In order to account for the possible response correlations resulting from the closely spaced diaphragm periods, the complete-quadratic-combination (CQC) rule is used to compute the total base shear. If the base shear obtained by summing the storey forces calculated using SRSS is smaller than the CQC value, the storey forces are scaled up accordingly. Knox (2012) also provided some discussions on the use of force reduction factors in the linear static analysis method.

3.3 Nonlinear Static Method

In the last decades, the development of performance-based seismic design and assessment has resulted in a series of nonlinear static procedures, starting with the Capacity Spectrum Method or CSM (Freeman et

al. 1975). Nonlinear static procedures are approximate methods for estimating the peak inelastic seismic responses through static analysis, and are designed to fill the gap between the simplistic linear analysis methods and the rigorous nonlinear time-history analysis. In the following sections, the N2 method developed by Fajfar and Gašperšič (1996) (considered to be representative of conventional nonlinear static procedure) contained in Eurocode 8 (CEN 2004) is firstly reviewed. Improved nonlinear static procedures including the multi-mode and adaptive methods are then described. The problems encountered in the application of nonlinear static procedures for unreinforced masonry buildings with flexible diaphragms are discussed.

3.4 N2 Method

The basic philosophy of the N2 method is that (1) the global behaviour of the building under seismic excitation can be characterised as an equivalent single-degree-of-freedom (SDOF) system, and (2) the properties of the equivalent SDOF system can be obtained from the static (and monotonic) pushover analysis of the nonlinear structural model. Once the equivalent SDOF system has been defined, the peak inelastic displacement demand can be obtained from the inelastic response spectrum appropriate for the site of interest.

The N2 method assumes that the displaced shape of the building can be approximated by an invariant shape $\boldsymbol{\phi}$, and the pushover analysis is carried out using lateral forces proportional to mass multiplied by the assumed displacement shape (Fajfar 2002)

$$\boldsymbol{p_s} = \boldsymbol{m}\boldsymbol{\phi}\lambda \tag{4}$$

where $\boldsymbol{p_s}$ is the vector of pushover forces, $\boldsymbol{m}$ is the mass matrix of the building model and λ is the increment in the applied forces.

Considering the equation of motion of a MDOF system (damping omitted for simplicity),

$$\boldsymbol{m}\ddot{\boldsymbol{u}} + \boldsymbol{f}_s = -\boldsymbol{m}\boldsymbol{\iota}\ddot{u}_g \tag{5}$$

where $\boldsymbol{u}$ is the nodal displacements of the building relative to the ground, $\boldsymbol{f}_s$ is the (nonlinear) restoring forces, $\boldsymbol{\iota}$ is the static transmission vector of the ground motion, and $\ddot{u}_g$ is the ground acceleration. Differentiation with respect to time is denoted by over-script dots. As stated previously, the N2 method approximates the displacement response by

$$\boldsymbol{u} = \boldsymbol{\phi}u_r \tag{6}$$

where u_r is the displacement time-history at a particular location (control node) of the building, and $\boldsymbol{\phi}$ is scaled to the displacement of the control node.

Substituting Eq. 6 in Eq. 5 and pre-multiplying both sides by $\boldsymbol{\phi}^{\mathrm{T}}$ gives

$$\boldsymbol{\phi}^{\mathrm{T}}\boldsymbol{m}\boldsymbol{\phi}\ddot{u}_r + \boldsymbol{\phi}^{\mathrm{T}}\boldsymbol{f}_s = -\boldsymbol{\phi}^{\mathrm{T}}\boldsymbol{m}\boldsymbol{\iota}\ddot{u}_g \tag{7}$$

The nonlinear restoring forces are considered to be approximated by the pushover analysis, such that

$$\boldsymbol{f}_s = \boldsymbol{p}_s = \boldsymbol{m}\boldsymbol{\phi}\lambda \tag{8}$$

Substituting Eq. 8 into Eq. 7 and performing simple mathematical operations gives the equation of motion of an equivalent SDOF system,

$$m^*\ddot{d}^* + \frac{V_b}{\Gamma} = -m^*\ddot{u}_g \tag{9}$$

Where with the equivalent mass is defined by

$$m^* = \boldsymbol{\phi}^{\mathrm{T}}\boldsymbol{m}\boldsymbol{\iota} \tag{10}$$

the equivalent displacement by

$$d^* = \frac{u_r}{\Gamma} \tag{11}$$

and the equivalent force by

$$f^* = \frac{V_b}{\Gamma} \tag{12}$$

where $\Gamma = \boldsymbol{\phi}^{\mathrm{T}}\boldsymbol{m}\boldsymbol{\iota}/\boldsymbol{\phi}^{\mathrm{T}}\boldsymbol{m}\boldsymbol{\phi}$.

As illustrated in Eq. 11 and Eq. 12, the relationship f^*- d^* (termed capacity curve) is computed from the pushover analysis by (1) subjecting the nonlinear structural model to the increasing lateral forces $\boldsymbol{p_s}$, (2) monitoring the base shear, V_b, and the displacement of the control node u_r (pushover curve), and (3) dividing both V_b and u_r by Γ. By bilinearising the capacity curve, the properties of the equivalent SDOF system can be obtained, i.e. the yield strength f_y^*, yield displacement d_y^*, initial stiffness $k^* = f_y^*/d_y^*$, the post yield stiffness and the initial period $T^* = 2\pi\sqrt{m^*/k^*}$.

Once the equivalent SDOF system is defined, the peak inelastic displacement (termed target displacement) is estimated through the inelastic spectrum derived by Vidic et al. (1994) in the N2 method. In general, however, the inelastic spectra used to estimate peak displacement should be appropriate for the site of interest and the structural system concerned, and numerous studies exist on this topic (e.g Mahin & Bertero 1981; Miranda 2000; Borzi et al. 2001; Ruiz-Garcia & Miranda 2003; Chopra & Chintanapakde 2004a; Chenouda & Ayoub 2008).

Once the target displacement of the SDOF system is obtained, the Eq. 11 is inverted to obtain the target displacement at the control node location. The result of the pushover analysis at that target displacement is considered to give a reasonable approximation to the actual dynamic response of the structure. The peak demands estimated from the pushover analysis (e.g. interstorey drifts, plastic hinge rotations) can then be compared against the required performance levels. Figure 16 provides a summary of the N2 method.

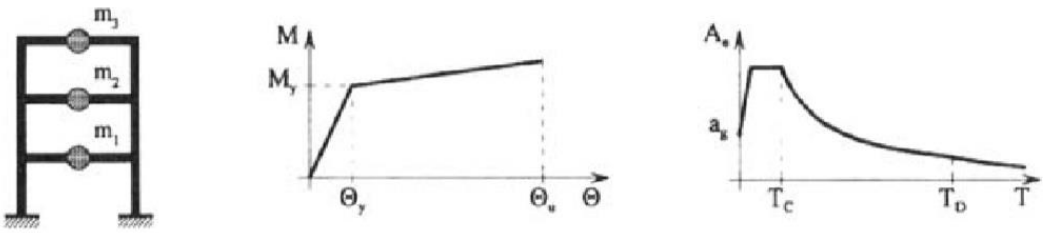

(a) Define structural model, input spectrum

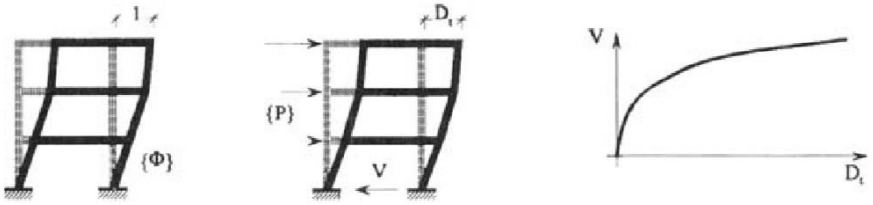

(b) Conduct pushover analysis

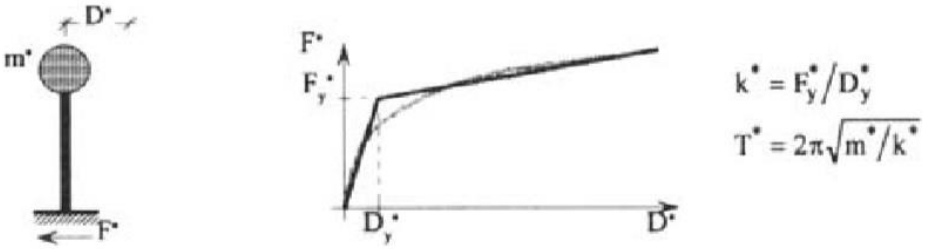

(c) Convert pushover curve to capacity curve and bilinearise

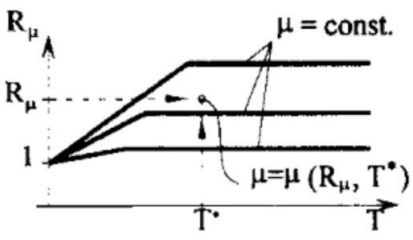

(d) Read off the peak displacemetn demand of the equivalent SDOF system

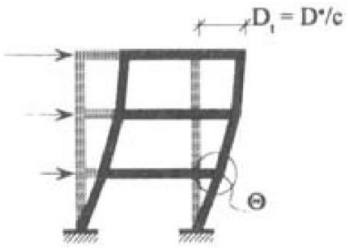

(e) Read off the pushover analysis result at the target displacement, evaluate the performance level

Figure 16. N2 method steps (Fajfar and Gašperšič 1996)

The conventional nonlinear static procedures such as the N2 method makes the critical assumptions that the building responds in a single displacement shape that remains constant throughout the excitation, and that such displacement shape can be determined a priori. These assumptions are clearly approximate, however, studies have shown adequate accuracies of the conventional nonlinear static procedures in predicting the peak inelastic responses of MDOF structures, provided that the response is governed by a single mode (Krawinker & Seneviratna 1998).

3.5 Multi-mode Nonlinear Static Methods

The single-mode nonlinear static procedures cannot account for (1) multi-mode behaviour where there is significant higher mode participation, and (2) changes in the inertial force distribution after the onset of inelastic response. Several multi-mode methods have been proposed to address the first shortcoming of the conventional method by conducting a series of separate pushover analyses with the lateral forces corresponding to a number of mode shapes (Paret et al. 1996; Sasaki et al. 1998; Chopra & Goel 2002). In this section, the Modal Pushover Analysis (MPA) formalised by Chopra and Goel (2002) is described.

The MPA has been developed as a direct extension of the response spectrum analysis method for linearly elastic structures. If the nonlinear MDOF structure is subjected to the nth effective earthquake force, and the resulting displacements are assumed be contained within the same mode with the mode shape $\boldsymbol{\phi}_n$, the nonlinear MDOF equation of motion may also be written as uncoupled equation of motion in each mode n,

$$\ddot{D}_n + 2\zeta_n\omega_n\dot{D}_n + \frac{F_{sn}}{L_n} = -\ddot{u}_g \tag{13}$$

where D_n is the modal displacement, ζ_n is the critical damping ratio and ω_n is the frequency in the nth mode, $F_{sn} = \boldsymbol{\phi}_n^T \boldsymbol{f}_s$ and $L_n = \boldsymbol{\phi}_n^T \boldsymbol{m\iota}$.

Eq. 13 is approximately valid if the modal coordinates are only weakly coupled during the inelastic response of the structure. Using a 9-storey steel building subjected to the El Centro record, Chopra and Goel (2002) showed that this uncoupled assumption can be appropriate for frame buildings (Figure 17).

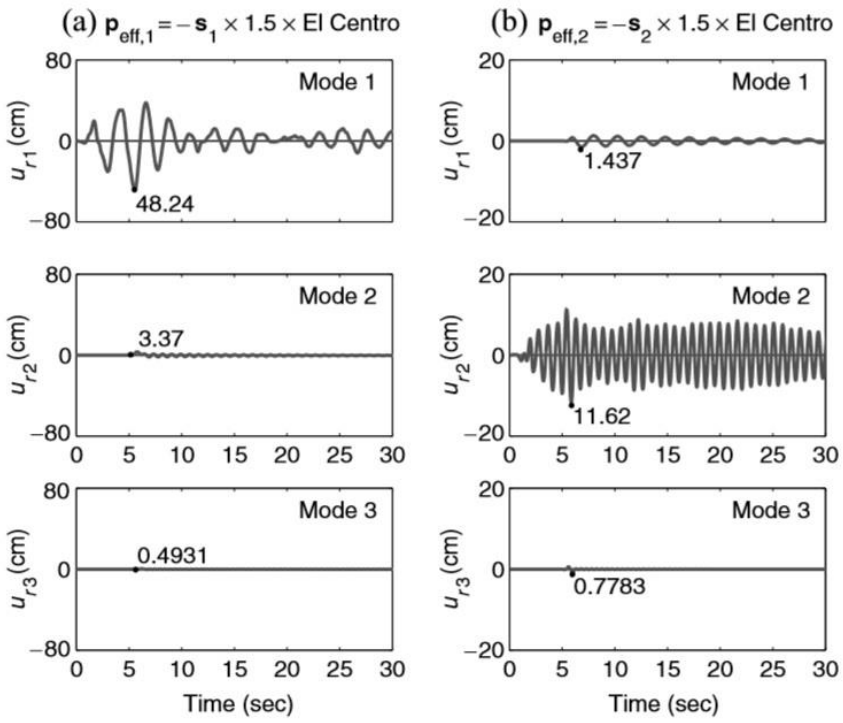

Figure 17. Participation of modal responses when the loading is imposed in (a) first mode, (b) second mode (Chopra & Goel 2002).

Based on the uncoupled equation of motion, the pushover analysis is conducted for each mode, using the force distribution $\boldsymbol{s}_n^* = \boldsymbol{m}\boldsymbol{\phi}_n$. The pushover curve is constructed, and the equivalent SDOF system is obtained by

$$\frac{F_{sn}}{L_n} = \frac{V_{bn}}{M_n^*} \tag{14}$$

$$D_n = \frac{u_{rn}}{\Gamma_n \phi_{rn}} \tag{15}$$

where V_{bn} is the base shear and u_{rn} is the displacement of the control node from the pushover analysis with the lateral load profile $\boldsymbol{s}_n^*$, ϕ_{rn} is the magnitude of mode shape at the control node and $M_n^* = \Gamma_n L_n$ is the effective modal mass in the nth mode.

Following an approach similar to the N2 method, the peak inelastic responses are obtained for each modal pushover analysis. The peak total responses are then combined using an appropriate mode combination rule (SRSS or CQC).

The accuracy of the MPA was tested in an extensive parametric analysis by Chintanapakdee & Chopra (2003) using 3 to 18 storey frame models. The analyses showed that MPA provided similar variations of storey drifts to the nonlinear time-history results when two or more modes were included. The comparison with the conventional method of FEMA 356 (ASCE 2000) also showed the superior predictions of MPA (Chopra & Chintanapakdee 2004b). The MPA has also been extended to assess the transverse response of bridges (Isakovič & Fischinger 2006; Paraskeva et al. 2006; Paraskeva & Kappos 2010). However, several issues have also been identified with the MPA. Firstly, it is difficult to quantify the error involved in the uncoupled modal assumption used in simplifying the nonlinear (inelastic) equation of motion. Secondly, as point out by Aydinoğlu (2003), the independent pushover analyses cannot account for the influence of all modes in the formulations of plastic hinges.

3.6 Adaptive Pushover Analysis

Several adaptive procedures have been proposed to address the inability of the single-mode nonlinear static methods in capturing the changes in the inertial force distribution after the onset of inelastic deformation. The development of the adaptive pushover methods have been broadly based on the idea that better predictions of the actual responses would be obtained if the pushover force is modified according to the current damage state of the structure.

Bracci et al. (1997) proposed the following procedure for modifying the pushover force distribution

$$\Delta F_i^{j+1} = V^j \left(\frac{F_i^j}{V^j} - \frac{F_i^{j-1}}{V^{j-1}} \right) + \Delta P^{j+1} \left(\frac{F_i^j}{V^j} \right) \tag{16}$$

where ΔF_i^{j+1} is the incremental pushover force of the ith floor, V^j is the base shear at the jth step, F_i^j is the resisting force of the ith storey at the jth step, and ΔP^{j+1} is the increment in the base shear force. The pushover analysis could commence with any reasonable initial force profile, F_i^0.

Antoniou and Pinho (2004a) proposed an adaptive procedure incorporating the higher modes and ground motion characteristics in an approximate manner. In their procedure, an eigenvalue analysis is conducted using the tangent stiffness matrix at each pushover step. The instantaneous inertial force is then obtained from

$$F_{ij} = \Gamma_j \phi_{ij} M_i S_{a,j} \tag{17}$$

where F_{ij} is the j[th] mode inertial force at the i[th] floor, Γ_j and ϕ_{ij} are the mode participation factor and mode shape respectively, M_i is the mass of the i[th] floor and $S_{a,j}$ is the (elastic) pseudo-acceleration of the j[th] mode.

The modal inertial forces of Eq. 17 is combined using the SRSS combination rule,

$$F_i = \sqrt{\sum_{j=1}^{N} F_{ij}^2} \tag{18}$$

The combined inertial force at the i[th] floor is then normaised as $\bar{F}_i = F_i / \sum F_i$, and the pushover force is applied either by the "total updating" (Eq. 19) or by the "incremental updating" (Eq. 20).

$$P_i = \lambda_i \, \bar{F}_i P_0 \tag{19}$$

$$P_i = P_{i-1} + \lambda_i \bar{F}_i P_0 \tag{20}$$

In these equations, λ_i is the increment magnitude and P_0 is a reference force profile, taken to be uniform. In their procedure, Antoniou & Pinho (2004a) did not derive a method to calculate the target displacement. Instead, the pushover curves and response parameters (drifts, shear forces etc.) obtained from the adaptive pushover analysis were compared against nonlinear time-history analysis results to validate the proposed algorithm. A similar adaptive procedure but applying displacements directly instead of pushover forces was also proposed (Antoniou & Pinho 2004b).

Several researchers have also investigated more complex analysis methods, such as the multi-mode adaptive procedures (Gupta & Kunnath 2000; Aydinoğlu 2003; Kalkan & Kunnath 2006). In these methods, multi-mode pushover analyses are conducted using mode properties based on the tangent or secant stiffness matrix at each analysis step. The modal response of the structure is then combined at each analysis step to update the stiffness matrix.

3.7 Problems with Pushover Analysis Method for Buildings with Flexible Diaphragms

Several issues have been identified when applying the nonlinear static analysis method to URM buildings with flexible diaphragms. Galasco et al. (2006) noted the following issues:

- There is no logical location for the control node to be used in the pushover analysis when diaphragm are flexible. Pushover curves obtained using different control node locations show significant differences in the deformation capacities of the structure (Figure 18); and

- The initial stiffness, strength and deformation capacities of the structure can be sensitive to the pushover force distribution (Figure 19).

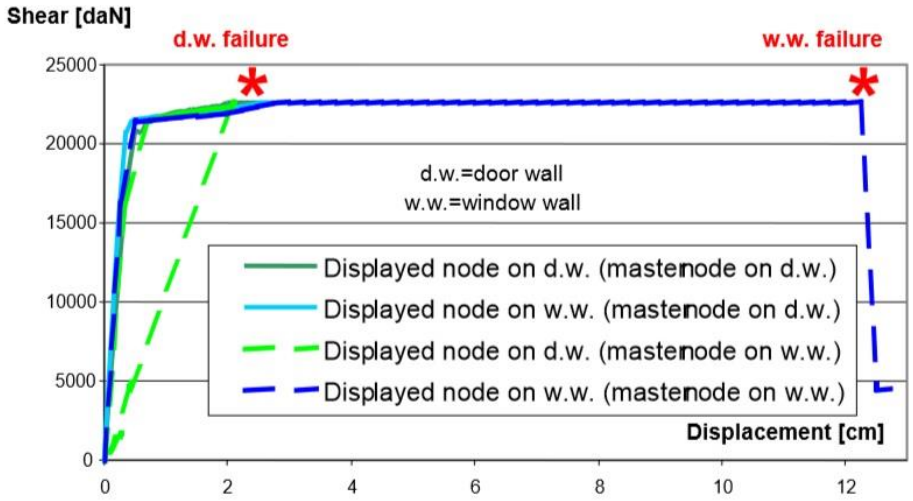

Figure 18. Control node sensitivity (Galasco et al. 2006)

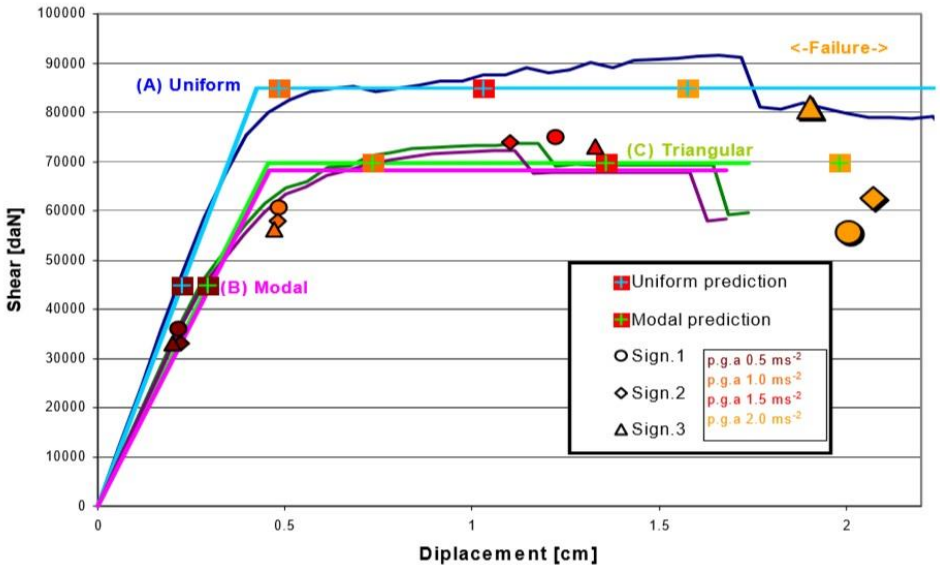

Figure 19. Pushover force profile sensitivity (Galasco et al. 2006)

In order to address the sensitivity of the pushover analysis to the assumed force distribution, Galasco et al. (2006) proposed an adaptive pushover algorithm. The proposed adaptive method applies the lateral force proportional to the displacement shape of the structure in the previous step,

$$\boldsymbol{p}_i = \lambda \boldsymbol{m} \boldsymbol{\psi}_{i-1} \tag{21}$$

where $\boldsymbol{p}_i$ is the pushover force at the ith step and $\boldsymbol{\psi}_{i-1}$ is the deformed shape of the structure in the previous step. The initial application of the pushover analysis showed that limitations had to be placed on the force distribution for reasonable results to be obtained.

Mendes & Lourenço (2009) investigated the applicability of single-mode and adaptive pushover analyses using a calibrated finite element model of a 5 storey URM building with timber floors. The comparisons of the pushover curves with the envelopes of the peak nonlinear time-history analysis results showed that none of the pushover analyses could accurately predict the time-history analysis results. They also reported differences in the failure mechanisms between the pushover and dynamic analysis results.

Due to the difficulties associated with the used of nonlinear static procedures for URM buildings with flexible diaphragms, Magenes and Penna (2009) presented an interim solution, in which each in-plane loaded wall may be analysed separately with its own tributary mass.

4. SUMMARY AND RESEARCH GAP

The measured data and experimental studies on URM buildings with flexible diaphragms have indicated the tendency for the diaphragms to respond independently of the in-plane loaded walls. In addition, the large amplifications of accelerations and displacements have also been consistently reported, especially in the elastic range of building behaviour. Experimental investigations have shown that the global behaviour could be attained only when the partial out-of-plane wall collapses could be prevented by means of sufficient connections between the diaphragms and the walls, as well as potentially tying the walls together. Once the global behaviour was triggered, however, the strength and deformation capacities of buildings with flexible diaphragm have been observed to be comparable to those of rigid diaphragm systems.

Early analytical studies on the behaviour of buildings with flexible diaphragms have focused on the elastic behaviour. In contrast, studies into the inelastic behavior have been limited. However, a number of studies have shown that the inelastic behaviour are significantly different to the elastic behaviour, and the present review has highlighted the need to characterise the inelastic behaviour of URM buildings with flexible diaphragm.

Several linear static analysis methods have been developed specifically for buildings with flexible diaphragms. However, it was found that none of the existing methods directly consider the dynamic interactions of the in-plane loaded walls and the diaphragms.

The theoretical bases of nonlinear static methods were summarised, and the assumptions inherent in various methods were detailed. It was found that the applicability of the nonlinear static methods to URM buildings with flexible diaphragms have not yet been fully investigated. Several problems have been identified when applying the nonlinear static procedures to URM buildings with flexible diaphragms, which are yet to be addressed.

REFERENCES

ABK (1984) "Methodology for mitigation of seismic hazards in existing unreinforced masonry buildings: the methodology", ABK Joint Venture, El Segndo, California.

Antoniou, S. and Pinho, R. (2004a) “Advantages and limitations of adaptive and non-adaptive force-based pushover procedures”, Journal of Earthquake Engineering, 8(4), 497 – 522.

Antoniou, S. and Pinho, R. (2004b) “Development and verification of a displacement-based adaptive pushover procedure”, Journal of Earthquake Engineering, 8(5), 643 – 661.

ASCE (2000) “Prestandard and commentary for the seismic rehabilitation of buildings”, FEMA 356, Federal Emergency Management Agency, Washington, D.C.

Aydinoğlu, M. N. (2003) “An incremental response spectrum analysis procedure based on inelastic spectral displacements for multi-mode seismic performance evaluation”, Bulletin of Earthquake Engineering, 1, 3 – 36.

Benedetti, D., Carydis, P. and Pezzoli, P. (1998) "Shaking table tests on 24 simple masonry buildings", Earthquake Engineering and Structural Dynamics, 27, 67 - 90.

Borzi, B., Calvi, G. M., Elnashai, A. S., Faccioli, E. and Bommer, J. J. (2001) "Inelastic spectra for displacement-based seismic design", Soil Dynamics and Earthquake Engineering, 21, 47 - 61.

Bracci, J. M., Kunnath, S. K. and Reinhorn, A. M. (1997) "Seismic performance and retrofit evaluation of reinforced concrete structures", Journal of Structural Engineering, 123(1), 3 - 10.

Bruneau, M. (1994) “Seismic evaluation of unreinforced masonry buildings - a state-of-the-art report”, Canadian Journal of Civil Engineering, 21(3), 512-539.

CEN (2004) “Eurocode 8: design of structures for earthquake resistance – part 1: general rules, seismic actions and rules for buildings”, European Committee for Standardization, Brussels, Belgium.

Chenouda, M. and Ayoub, A. (2008) "Inelastic displacement ratios of degrading systems, Journal of Structural Engineering, 134(6), 1030 - 1045.

Chintanapakdee, C. and Chopra, A. K. (2003) "Evaluation of modal pushover analysis using generic frames", Earthquake Engineering and Structural Dynamics, 32, 417 - 442.

Chopra, A. K. and Chintanapakdee, C. (2004a) "Inelastic deformation ratios for design and evaluation of structures: Single-degree-of-freedom bilinear systems", Journal of Structural Engineering 130(9), 1309 - 1319.

Chopra, A. K. and Chintanapakdee, C. (2004b) "Evaluation of Modal and FEMA pushover analyses: Vertically "regular" and irregular generic frames", Earthquake Spectra, 20(1), 255 - 271.

Chopra, A. K. and Goel, R. K. (2002) “A modal pushover analysis procedure for estimating seismic demands for buildings”, Earthquake Engineering and Structural Dynamics, 31, 561 – 582.

Cohen, G. L., Klinger, R. E., Hayes Jr., J. R. and Sweeney, S. C. (2003) "Seismic evaluation of low-rise reinforced masonry buildings with flexible diaphragms: I. Seismic and quasi-static testing", Earthquake Spectra, 20(3), 779 - 801.

Costley, A. C. and Abrams, D. P. (1995) “Dynamic response of unreinforced masonry buildings with flexible diaphragms”, Structural Research Series 605, Department of Civil Engineering, University of Illinois at Urbana-Champaign.

De-La-Colina, J. (1999) “In-plane floor flexibility effects on torsionally unbalanced systems”, Earthquake Engineering and Structural Dynamics, 28(12), 1705-1715.

Fajfar, P. and Gašperšič, P. (1996) “The N2 method for the seismic damage analysis of RC buildings”, Earthquake Engineering and Structural Dynamics, 25, 31 – 46.

Fajfar, P. (2002) "Structural analysis in earthquake engineering - a breakthrough of simplified non-linear methods", Proceedings of 12th European Conference for Earthquake Engineering, London, UK.

Freeman, S. A., Nicoletti, J. P. and Tyrell, J. V. (1975) "Evaluations of existing buildings for seismic risk - a case study of Puget Sound Naval Shipyard, Bremerton, Washington", Proceedings of U.S. National Conference on Earthquake Engineering, Berkeley.

Galasco, A., Lagomarsino, S. and Penna, A. (2006) "On the use of pushover analysis for existing masonry buildings", Proceedings of 1st European Conference on Earthquake Engineering and Seismology, Geneva.

Gupta, B. and Kunnath, S. K. (2000) "Adaptive spectra-based pushover procedure for seismic evaluation of structures", Earthquake Spectra, 16(2), 367 - 391.

Jain, S. K. and Jennings, P. C. (1985) "Analytical models for low-rise buildings with flexible floor diaphragms", Earthquake Engineering and Structural Dynamics, 13 (2), 225-241.

Isaković, T. and Fischinger, M. (2006) "Higher modes in simplified inelastic seismic analysis of single column bent viaducts", Earthquake Engineering and Structural Dynamics, 35, 95 - 114.

Kalkan, E. and Kunnath, S. K. (2006) "Adapive modal combination procedure for nonlinear static analysis of building structures", Journal of Structural Engineering, 132(11), 1721 - 1731.

Kim, S.-C., and White, D. W. (2003) "MDOF response of low-rise buildings", Final Report Project ST-5, Mid-America Earthquake Research Center, Georgia Institute of Technology.

Kim, S.-C. and White, D. W. (2004a) "Nonlinear analysis of a one-story low-rise masonry building with a flexible diaphragm subjected to seismic excitation", Engineering Structures, 26, 2053 - 2067.

Kim, S.-C., and White, D. W. (2004b) "Linear static analysis of low-rise buildings with flexible diaphragms using the structural separation method", Engineering Structures, 26, 83-93.

Knox, C. (2012) "Assessment of perforated unreinforced masonry walls responding in-plane", PhD thesis, Department of Civil and Environmental Engineering, University of Auckland.

Krawinkler, H. and Seneviratna G. D. P. K. (1998) "Pros and cons of pushover analysis of seismic performance evaluation", Engineering Structures, 20(4-6), 452 – 464.

Magenes, G. and Penna, A. (2009) "Existing masonry buildings: General code issues and methods of analysis and assessment", Proceedings of Eurocode 8 Perspectives from the Italian Standpoint Workshop, Naples, Italy.

Magenes, G., Penna, A., Senaldi, I., Rota, M. and Galasco, A. (2014) “Shaking table test of a strengthened full-scale stone masonry building with flexible diaphragms”, International Journal of Architectural Heritage: Conservation, analysis and restoration, 8(3), 349 - 375.

Mahin, S. A. and Bertero, V. V (1981) "An evaluation of inelastic seismic design spectra", ASCE Journal of Structural Division, 107(ST9), 1888 - 1795.

Mendes N. and Lourenço, P. B. (2009) "Seismic assessment of masonry "Gaioleiro" buildings in Lisbon, Portugal", Journal of Earthquake Engineering, 14(1), 80 - 101.

Miranda, E. (2000) "Inelastic displacement ratios for structures on firm sites", Journal of Structural Engineering, 126(10), 1150 - 1159.

Paret, M. J. N., Sasaki, K. K., Eilbeck, D. H. and Freeman, S. A. (1996) "Approximate inelastic procedures to identify failure mechanisms from higher mode effects", Proceedings of 11th World Conference on Earthquake Engineering.

Paraskeva, T. S., Kappos, A. J. and Sextos, A. G. (2006) "Extension of modal pushover analysis to seismic assessment of bridges", Earthquake Engineering and Structural Dynamics, 35, 1269 - 1293.

Paraskeva, T. S. and Kappos, A. J. (2010) "Further development of multimodal pushover analysis procedure for seismic assessment of bridges", Earthquake Engineering and Structural Dynamics, 39, 211 - 222.

Paquette, J. and Bruneau, M. (2003) "Pseudo-dynamic testing of unreinforced masonry building with flexible diaphragm", Journal of Structural Engineering, 129(6), 708 - 716.

Penna, A. (2015). “Seismic assessment of existing and strengthened stone-masonry buildings: critical issues and possible strategies”, Bulletin of Earthquake Engineering, 13 (4), 1051-1071.

Ruiz-Garcia, J. R. and Miranda, E. (2003) "Inelastic displacement ratios for evaluation of existing structures", Earthquake Engineering and Structural Dynamics, 32, 1237 - 1258.

Saffarini, H.S. and Qudaimat, M. M. (1992) “In-plane floor deformations in RC structures”, Journal of Structural Engineering, 118 (11), 3089-3102.

Sadashiva, V. K., MacRae, G. A., Deam, B. L., and Spooner, M. S. (2012) “Quantifying the seismic response of structures with flexible diaphragms”, Earthquake Engineering and Structural Dynamics, 41(10), 1365-1389.

Sasaki, K. K., Freeman, S. A. and Paret, T. F. (1998) "Multi-mode pushover procedure (MMP) - A method to identify the effects of higher modes in a pushover analysis", Proceedings of 6th U.S. National Conference on Earthquake Engineering, Seattle, Washington.

Senaldi, I., Magenes, G., Penna, A., and Galasco, A. (2014) “The effect of stiffened floor and roof diaphragms on the experimental seismic response of a full-scale unreinforced stone masonry buildings”, Journal of Earthquake Engineering, 18(3), 407 – 443.

Shephard, R. and Donald, R. A. H. (1967) "The influence of in-plane floor flexibility on the normal mode properties of buildings", Journal of Sound and Vibrations, 5(1), 29 - 36.

Tena-Colunga, A. (1992) "Seismic evaluation of unreinforced masonry structures with flexible diaphragms", Earthquake Spectra, 8(2), 305 - 318.

Tena-Colunga, A. and Abrams, D. P. (1992) “Response of an unreinforced masonry building during the Loma Prieta earthquake”, Structural Research Series 576, Department of Civil Engineering, University of Illinois at Urbana-Champaign.

Tena-Colunga, A. and Abrams, D. P. (1996) "Seismic behavior of structures with flexible diaphragms", Journal of Structural Engineering, 122(4), 439 - 445.

Tomaževič, M. and Lutman, M. (1996) "Seismic upgrading of old brick-masonry urban houses: tying of walls with steel ties", Earthquake Spectra, 12(3), 599 - 622.

Tomaževič, M., Velechovsky, T. and Weiss, P. (1992) "The effect of interventions in the floor structural system on the seismic resistance of historic stone-masonry buildings: An experimental study", Proceeding of 10th World Conference on Earthquake Engineering, Madrid, Spain, July 19 - 24.

Vidic, T., Fajfar, P. and Fischinger, M. (1994) “Consistent inelastic design spectra: strength and displacement”, Earthquake Engineering and Structural Dynamics, 23, 507 – 521.

Vintzileou, E., Mouzakis, C., Adami, C.-E., and Karapitta, L. (2015) “Seismic behaviour of three-leaf stone masonry buildings before and after interventions: Shaking table tests on a two-storey masonry model”, Bulletin of Earthquake Engineering, 13(10), 3107 – 3133.

Yi, T., Moon, F. L., Leon, R. T. and Kahn, L. F. (2006) "Lateral load tests on a two-story unreinforced masonry building", Journal of Structural Engineering, 132(5), 643 - 652.

CHAPTER 3

ELASTIC ANALYSIS

Background

This chapter contains the paper "Seismic analysis of in-plane loaded walls in unreinforced masonry buildings with flexible diaphragms", which investigates the modal properties of buildings with flexible diaphragms. The analytical consideration of modal properties reveals that two important modes generally exist when diaphragms are flexible. Mathematical formulae for such mode shapes and frequencies are derived, and expressions are proposed to modify the peak base shear force in the context of the linear static analysis method to account for diaphragm flexibility. An example application of the proposed expressions is provided.

List of Manuscripts

Nakamura, Y., Derakhshan, H., Ingham, J. M. and Griffith, M. C. (2014) "Seismic analysis of in-plane loaded walls in unreinforced masonry buildings with flexible diaphragms", Bulletin of New Zealand Society for Earthquake Engineering, 47(4), 275 – 289.

Statement of Authorship

Title of Paper	Seismic analysis of in-plane loaded walls in unreinforced masonry buildings with flexible diaphragms
Publication Status	☑ Published ☐ Accepted for Publication ☐ Submitted for Publication ☐ Unpublished and Unsubmitted work written in manuscript style
Publication Details	Nakamura, Y., Derakhshan, H., Ingham, J. M. and Griffith, M. C. (2014) "Seismic analysis of in-plane loaded walls in unreinforced masonry buildings with flexible diaphragms", Bulletin of New Zealand Society for Earthquake Engineering, 47(4), 275 – 289.

Principal Author

Name of Principal Author (Candidate)	Yasuto Nakamura
Contribution to the Paper	Prepared manuscript, performed all derivations and analyses
Overall percentage (%)	85%
Certification:	This paper reports on original research I conducted during the period of my Higher Degree by Research candidature and is not subject to any obligations or contractual agreements with a third party that would constrain its inclusion in this thesis. I am the primary author of this paper.
Signature	Date: 26/8/16

Co-Author Contributions

By signing the Statement of Authorship, each author certifies that:

i. the candidate's stated contribution to the publication is accurate (as detailed above);

ii. permission is granted for the candidate in include the publication in the thesis; and

iii. the sum of all co-author contributions is equal to 100% less the candidate's stated contribution.

Name of Co-Author	Hossein Derakhshan
Contribution to the Paper	Contributed to research and manuscript
Signature	Date: 26 Aug 2016

Name of Co-Author	Jason M. Ingham
Contribution to the Paper	Contributed to manuscript
Signature	Date: 24 August 2016

Name of Co-Author	Michael C. Griffith
Contribution to the Paper	Supervised and contributed to research and manuscript
Signature	Date 30/08/2016

Seismic Analysis of In-plane Loaded Walls in Unreinforced Masonry Buildings with Flexible Diaphragms

ABSTRACT

It is well recognised that the dynamic response of unreinforced masonry buildings with flexible timber diaphragms typically contains multiple dominant modes associated with the excitations of the diaphragms and the in-plane walls. Existing linear analysis methods for this type of structure commonly account for the multi-mode behaviour by assuming the independent vibrations of the in-plane loaded walls (in-plane walls) and the diaphragms. Specifically, the in-plane walls are considered to be rigid and the unmodified ground motion is assumed to be transmitted up the walls to the diaphragm ends. While this assumption may be appropriate for many low-rise unreinforced masonry buildings, neglecting the dynamic interaction between the diaphragms and the in-plane walls can lead to unreliable predictions of seismic demands. An alternative analysis approach is proposed in this paper, based on the mode properties of a system in which (1) the mass ratios between the diaphragms and the in-plane wall are the same at all levels, and (2) the periods of the diaphragms are the same at all levels. It is proposed that under these conditions, two modes are typically sufficient to obtain the peak seismic demands of the in-plane walls in elastically responding low-rise regular buildings. The applicability of the two-mode analysis approach is assessed for more general diaphragm configurations by sensitivity analysis, and the limitations are identified. The two-mode approach is then used to derive a response modification factor, which may be used in conjunction with a linear static procedure in the seismic assessment of buildings with flexible diaphragms.

1. INTRODUCTION

In older unreinforced masonry (URM) buildings, the floor and roof diaphragms are often constructed of flexible timber systems. The flexibility of the diaphragms introduce two dynamic effects that are absent in rigid diaphragm structures. Firstly, the non-rigid diaphragms lead to an intermediate coupling of the adjacent in-plane loaded walls (in-plane walls), resulting in a limited redistribution of inertial forces amongst the lateral-load resisting elements. Secondly, the excitations of the diaphragms themselves provide feed-back effects on the in-plane walls, potentially modifying the behaviour of the walls. As these older structures are highly vulnerable to seismic action, there is a need for a practical procedure to evaluate the seismic demand imposed on the in-plane walls for the global assessment of URM buildings with flexible diaphragms.

The simplest seismic analysis procedure, and likely the first choice of analysis in practice for typical low-rise regular URM buildings, is the linear static method. In the context of the performance-based assessment guideline of ASCE 41-13 (ASCE 2014), the equivalent static base shear is determined using a corresponding linear system,

$$V = C_1 C_2 C_m S_a W \tag{1}$$

where V is the elastic base shear, C_1 is a modification factor relating maximum inelastic displacement to the elastic displacement, C_2 expresses the modification for the effect of stiffness and strength degradations, C_m accounts for higher mode mass participation (taken to be 1.0 for URM), S_a is the spectral acceleration at the fundamental period of the structure, and W is the seismic weight of the structure. The elastic base shear in Equation 1 is not the actual base shear that the building would experience, but rather an equivalent force that would induce the expected inelastic displacement on the elastic system (Abrams 2001). The demand so calculated is compared against the component capacities to ensure,

$$\kappa Q_{CE} \geq Q_{UD}/m \tag{2}$$

where κ is the knowledge factor, Q_{CE} is the expected component strength (i.e. rocking or shear strength), Q_{UD} is the elastic demand (i.e. moments or shear forces) calculated based on Equation 1. m is the modification factor that accounts for the ductility of the component for a particular performance level (Abrams, 2001).

Several studies have been conducted to incorporate the effect of diaphragm flexibility in the demand estimation (Equation 1) of the linear static procedure. ASCE 41-13 and NZSEE (NZSEE 2006) stipulate that the fundamental period of unreinforced masonry buildings of less than six storeys in height, with single-span flexible diaphragms may be calculated as

$$T = \sqrt{3.07\Delta_d} \tag{3}$$

where Δ_d in metres is the maximum diaphragm deformation due to a lateral load of 1.0 g. Equation 3 has been shown to be the fundamental period of a fix-ended flexural beam (Wilson et al. 2013). Therefore, the expression considers the in-plane walls to remain rigid and the diaphragm to vibrate independent of the in-plane walls. An alternative procedure was proposed by Kim and White (2004). In their method, a subassembly consisting of the two adjacent in-plane walls at a given storey and the supported diaphragm is initially separated from the rest of the structure. The peak elastic demand of the subassembly is then

determined, considering the subassembly to be subjected to ground acceleration. Hence in this procedure, parts of the structure are assumed to remain rigid for the estimation of demand on each subassembly. The peak forces of the subassemblies are then combined together by direct summation to estimate the peak seismic demand of the actual structure. Recently, Knox (2012) proposed a method in which the equivalent seismic force of the in-plane wall and the diaphragms are firstly determined separately. The possible correlations in the responses are subsequently considered through the use of a modal combination rule to obtain the total demand. A set of modification factors similar to Equation 1 was also suggested to account for the inelastic behaviour.

For symmetric (or almost symmetric) structures, the coupling effect of the diaphragms may be considered negligible and the diaphragms can be idealised as single-degree-of-freedom (SDOF) systems mounted on a primary structure (in-plane wall) at floor levels (Fleischman & Farrow 2001; Lee et al. 2007). In this idealisation, the diaphragms can be viewed as heavy secondary systems. It is well recognised that heavy secondary systems have the potential to modify the dynamic behaviour of the primary structure (Chen & Soong 1988), and the response of the primary structure can only be evaluated accurately by considering the dynamics of the combined system. However, the foregoing review of the existing analysis methods incorporating the effects of diaphragm flexibility revealed that the interactions between the in-plane walls and the diaphragms are not explicitly considered. Therefore, the existing methods are strictly applicable when the following two conditions are met:

- the period of the diaphragm is sufficiently larger than the period of the in-plane walls (so that the in-plane walls may be considered as providing essentially rigid support conditions at diaphragm ends); and

- the period of the in-plane walls is sufficiently smaller than the dominant period of the ground motion (so that the important frequency content of the ground motion is not filtered out by the in-plane walls).

For many low-rise unreinforced masonry buildings, these conditions are satisfied. However, there are cases in which they may not be appropriate, including:

- long and narrow buildings with loading perpendicular to the narrow end;

- flexible in-plane walls with large openings; and

- stiffened/retrofitted diaphragms.

This study proposes an alternative, and more rational, method to account for diaphragm flexibility by explicitly considering the interaction between the elastically responding in-plane walls and the diaphragms.

In the first part of the paper, the modal properties of structures with an idealised diaphragm configuration are derived to show that two modes of the combined system are closely related to a given mode of the uncoupled in-plane wall. These two modes are further shown to retain the same proportion of the mass participation as the associated mode of the uncoupled in-plane wall, leading to the concept of the two-mode analysis in capturing the effect of diaphragm flexibility. The applicability of the two-mode analysis for more general diaphragm configurations is evaluated by sensitivity analysis, and the limitation of the approach is identified. In the second part of the paper, the two-mode approach is used to derive an expression for the modification of the peak base shear to account for flexible diaphragms in the context of the linear static method. A numerical validation is provided to demonstrate that the proposed method gives more consistent results in comparison to dynamic analyses than existing procedures for a wide range of diaphragm stiffnesses.

2. STRUCTURAL IDEALISATION

It is considered that symmetric, or essentially symmetric, unreinforced masonry buildings with flexible diaphragms can be idealised as planar discrete multi-degree-of-freedom (MDOF) systems as shown in Figure 1. In the idealisation, the out-of-plane walls are assumed to be cracked and their stiffness contributions are neglected, while their masses are appropriately distributed to the diaphragm and in-plane wall degrees of freedom.

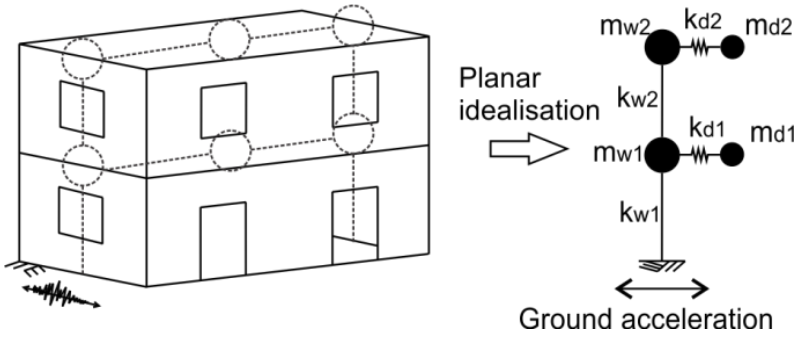

Figure 1. Idealisation of symmetric structures

Even though the in-plane walls are conceptually represented in a discrete manner, the difficulty associated with the derivation of storey stiffnesses of perforated walls (Tena-Colunga & Abrams 1992; Kim &

White 2003) is avoided in the analysis that follows, by characterising their elastic properties by the uncoupled wall's periods and mode shapes.

The SDOF idealisation of the diaphragm at each level requires the definitions of the equivalent mass and the period. The idealisation adopted in this study follows a similar approach to Sadashiva et al. (2012), in which the equivalent SDOF system is constructed such that it produces (1) the same period, and (2) the same total resisting force, of the diaphragm when it deforms in an assumed displacement shape. The first condition has been investigated by Wilson et al. (2013), who showed that the shear beam idealisation best approximates the deformed shape of single straight-sheathing diaphragms typically found in older URM buildings. By the generalised SDOF analysis (Chopra 2007), the period of the diaphragms deforming in shear has been shown to be

$$T_d = 0.7\sqrt{\frac{W_D L}{G_d B}} \tag{4}$$

where W_D is the total tributary weight of the diaphragm including any tributary weight of the out-of-plane walls, L and B are the dimensions of the diaphragms perpendicular and parallel to the direction of loading respectively, and G_d is the stiffness of the diaphragm. Using the consistent shear beam idealisation, the equivalent mass satisfying the second condition can also be derived by the generalised SDOF analysis as

$$m_d = \frac{126}{155}\frac{W_D}{g} \tag{5}$$

The equivalent SDOF idealisation of the diaphragm is hence defined by Equations 4 and 5 and the equivalent stiffness may also be obtained from these expressions. The mass and the stiffness of the combined structure ($\boldsymbol{m}$ and $\boldsymbol{k}$) can then be written in terms of the uncoupled component matrices, $\boldsymbol{m}_w$ and $\boldsymbol{k}_w$ for the in-plane wall and $\boldsymbol{m}_d$ and $\boldsymbol{k}_d$ for the diaphragms,

$$\boldsymbol{m} = \begin{bmatrix} \boldsymbol{m}_w & \boldsymbol{0} \\ \boldsymbol{0} & \boldsymbol{m}_d \end{bmatrix}, \qquad \boldsymbol{k} = \begin{bmatrix} \boldsymbol{k}_w + \boldsymbol{k}_d & -\boldsymbol{k}_d \\ -\boldsymbol{k}_d & \boldsymbol{k}_d \end{bmatrix} \tag{6}$$

As an example, for the two-storey model of Figure 1, the uncoupled matrices can be written as

$$\begin{aligned} \boldsymbol{m}_w &= \begin{bmatrix} m_{w1} & 0 \\ 0 & m_{w2} \end{bmatrix}, \qquad \boldsymbol{k}_w = \begin{bmatrix} k_{w1} + k_{w2} & -k_{w2} \\ -k_{w2} & k_{w2} \end{bmatrix} \\ \boldsymbol{m}_d &= \begin{bmatrix} m_{d1} & 0 \\ 0 & m_{d2} \end{bmatrix}, \qquad \boldsymbol{k}_d = \begin{bmatrix} k_{d1} & 0 \\ 0 & k_{d2} \end{bmatrix} \end{aligned} \tag{7}$$

3. MODAL ANALYSIS

3.1 Modal Properties of Idealised Diaphragm Configuration

The modal properties of the planar model in Figure 1 can be shown to be functions of the uncoupled in-plane wall's normal modes under a particular diaphragm condition.

Consider the undamped free vibration of the planar model

$$\begin{bmatrix} \boldsymbol{m}_w & \mathbf{0} \\ \mathbf{0} & \boldsymbol{m}_d \end{bmatrix} \begin{bmatrix} \ddot{\boldsymbol{u}}_w \\ \ddot{\boldsymbol{u}}_d \end{bmatrix} + \left(\begin{bmatrix} \boldsymbol{k}_w & \mathbf{0} \\ \mathbf{0} & \mathbf{0} \end{bmatrix} + \begin{bmatrix} \boldsymbol{k}_d & -\boldsymbol{k}_d \\ -\boldsymbol{k}_d & \boldsymbol{k}_d \end{bmatrix} \right) \begin{bmatrix} \boldsymbol{u}_w \\ \boldsymbol{u}_d \end{bmatrix} = \mathbf{0} \tag{8}$$

where $\mathbf{u}_w$ and $\mathbf{u}_d$ are the relative displacement vectors (with respect to the ground) of the in-plane wall and the diaphragms respectively, of size equal to the number of floors. Differentiation with respect to time is denoted by over-script dots. The dynamic properties of the combined structure can be related to the modal properties of the uncoupled components by the transformation (Suarez & Singh 1987),

$$\begin{bmatrix} \boldsymbol{u}_w \\ \boldsymbol{u}_d \end{bmatrix} = \begin{bmatrix} \boldsymbol{\Phi}'_w & \mathbf{0} \\ \mathbf{0} & \boldsymbol{\Phi}'_d \end{bmatrix} \begin{bmatrix} \boldsymbol{q}_w \\ \boldsymbol{q}_d \end{bmatrix} = \boldsymbol{\Lambda} \boldsymbol{q} \tag{9}$$

where the columns of the matrices $\boldsymbol{\Phi}_w'$ and $\boldsymbol{\Phi}_d'$ contain the eigenvectors of the uncoupled in-plane wall and the diaphragms respectively, normalised such that

$$\boldsymbol{\Phi}_w'^{\mathrm{T}} \boldsymbol{m}_w \boldsymbol{\Phi}'_w = \mathbf{I} \tag{10}$$

$$\boldsymbol{\Phi}_d'^{\mathrm{T}} \boldsymbol{m}_d \boldsymbol{\Phi}'_d = \mathbf{I} \tag{11}$$

where $\mathbf{I}$ is the identity matrix. Substituting Equation 9 in Equation 8 and pre-multiplying by $\boldsymbol{\Lambda}^{\mathrm{T}}$ gives

$$\boldsymbol{m}^* \ddot{\boldsymbol{q}} + \boldsymbol{k}^* \boldsymbol{q} = \mathbf{0} \tag{12}$$

where

$$\boldsymbol{m}^* = \begin{bmatrix} \boldsymbol{\Phi}_w'^{\mathrm{T}} & \mathbf{0} \\ \mathbf{0} & \boldsymbol{\Phi}_d'^{\mathrm{T}} \end{bmatrix} \begin{bmatrix} \boldsymbol{m}_w & \mathbf{0} \\ \mathbf{0} & \boldsymbol{m}_d \end{bmatrix} \begin{bmatrix} \boldsymbol{\Phi}'_w & \mathbf{0} \\ \mathbf{0} & \boldsymbol{\Phi}'_d \end{bmatrix} = \mathbf{I} \tag{13}$$

$$\boldsymbol{k}^* = \begin{bmatrix} \boldsymbol{\Omega}_w^2 & 0 \\ 0 & 0 \end{bmatrix} + \begin{bmatrix} \boldsymbol{\Phi}_w'^{\mathrm{T}} \boldsymbol{k}_d \boldsymbol{\Phi}'_w & -\boldsymbol{\Phi}_w'^{\mathrm{T}} \boldsymbol{k}_d \boldsymbol{\Phi}'_d \\ -\boldsymbol{\Phi}_d'^{\mathrm{T}} \boldsymbol{k}_d \boldsymbol{\Phi}'_w & \boldsymbol{\Omega}_d^2 \end{bmatrix} \tag{14}$$

The diagonal matrices $\boldsymbol{\Omega}_w$ and $\boldsymbol{\Omega}_d$ contain the modal frequencies of the uncoupled in-plane wall and diaphragms respectively. The eigenvalue problem of the transformed Equation 12 is

$$\left(\boldsymbol{k}^* - \omega_j^2 \mathbf{I}\right)\boldsymbol{\phi}_j^* = \mathbf{0} \tag{15}$$

where ω_j is the j^{th} frequency and $\boldsymbol{\phi}_j^*$ is the j^{th} mode shape (in the transformed coordinate) of the combined structure. Note that the size of $\boldsymbol{\phi}_j^*$ is twice the number of floor levels as it contains both the in-plane wall's and the diaphragms' degrees of freedom. Closed-form solutions are readily obtained, if the following conditions are imposed on the diaphragms configuration:

- the equivalent mass of the diaphragm at any floor level is a constant fraction R_m of the tributary mass of the in-plane wall at the same level; and
- the periods of the diaphragms are equal at all levels.

These conditions are expressed mathematically as

$$\boldsymbol{m}_d = R_m \boldsymbol{m}_w \tag{16}$$

$$\boldsymbol{\Omega}_d = \omega_d \mathbf{I} \tag{17}$$

By the dynamics of a SDOF system, it also follows that

$$\boldsymbol{k}_d = \omega_d^2 \boldsymbol{m}_d \tag{18}$$

By substituting Equations 16 to 18 in Equation 15 and writing out the equations corresponding to the in-plane wall and the diaphragms separately, $\boldsymbol{\phi}_j^* = [\boldsymbol{\phi}_{wj}^* \ \ \boldsymbol{\phi}_{dj}^*]^{\mathrm{T}}$, yields the following simultaneous equations

$$\left(\boldsymbol{\Omega}_w^2 - \omega_j^2 \mathbf{I}\right)\boldsymbol{\phi}_{wj}^* = -\omega_d^2\left(R_m \boldsymbol{\phi}_{wj}^* - \boldsymbol{\Phi}_w'^{\mathrm{T}} \boldsymbol{m}_d \boldsymbol{\Phi}_d' \boldsymbol{\phi}_{dj}^*\right) \tag{19}$$

$$-\omega_j^2 \boldsymbol{\phi}_{dj}^* = -\omega_d^2\left(-\boldsymbol{\Phi}_d'^{\mathrm{T}} \boldsymbol{m}_d \boldsymbol{\Phi}_w' \boldsymbol{\phi}_{wj}^* + \boldsymbol{\phi}_{dj}^*\right) \tag{20}$$

Equation 20 can be re-arranged to give the expression for the diaphragms' mode shape in terms of the mode shape of the in-plane wall

$$\boldsymbol{\phi}_{dj}^* = \frac{\omega_d^2}{\omega_d^2 - \omega_j^2}\left(\boldsymbol{\Phi}_d'^{\mathrm{T}} \boldsymbol{m}_d \boldsymbol{\Phi}_w'\right)\boldsymbol{\phi}_{wj}^* \tag{21}$$

Substituting Equation 21 in Equation 19 and applying the mass orthonormal condition (Equations 10 and 11) gives a diagonalised equation with the unknowns ω_j and $\boldsymbol{\phi}_{wj}^*$

$$\left[\omega_j^4\mathbf{I} - \omega_j^2\left(\boldsymbol{\Omega}_w^2 + \omega_d^2(1+R_m)\mathbf{I}\right) + \omega_d^2\boldsymbol{\Omega}_w^2\right]\boldsymbol{\phi}_{wj}^* = \mathbf{0} \tag{22}$$

For a nontrivial solution,

$$det\left[\omega_j^4\mathbf{I} - \omega_j^2\left(\boldsymbol{\Omega}_w^2 + \omega_d^2(1+R_m)\mathbf{I}\right) + \omega_d^2\boldsymbol{\Omega}_w^2\right] = 0 \tag{23}$$

Because the matrices in Equation 23 are triangular (more specifically, diagonal), the determinant is the product of the diagonal entries (Lay 2003). For the determinant to equal zero, each term of the product must equal zero, hence

$$\omega_j^4 - \omega_j^2\left[\omega_{wn}^2 + \omega_d^2(1+R_m)\right] + \omega_d^2\omega_{wn}^2 = 0 \tag{24}$$

where ω_{wn} denotes the n^{th} diagonal entry of $\boldsymbol{\Omega}_w$. As Equation 24 is a quadratic in ω_j^2, two solutions exist for ω_j^2 for each n^{th} mode of the uncoupled in-plane wall. Denoting these by $\omega_{n,L}{}^2$ and $\omega_{n,U}{}^2$ (*L* for *lower* and *U* for *upper* eigenvalues),

$$\omega_{n,L}^2 = \frac{\omega_{wn}^2 + \omega_d^2(1+R_m) - \sqrt{[\omega_{wn}^2 + \omega_d^2(1+R_m)]^2 - 4\omega_d^2\omega_{wn}^2}}{2} \tag{25}$$

$$\omega_{n,U}^2 = \frac{\omega_{wn}^2 + \omega_d^2(1+R_m) + \sqrt{[\omega_{wn}^2 + \omega_d^2(1+R_m)]^2 - 4\omega_d^2\omega_{wn}^2}}{2} \tag{26}$$

Equations 25 and 26 show that two modes of the combined system can be attributed to each mode of the uncoupled in-plane wall. The normal mode of the uncoupled in-plane wall is herein referred to as the "original mode". The two modes of the combined structure attributed to the n^{th} original mode are referred to collectively as the n^{th} "mode pair".

In Figure 2, the frequencies of the mode pair are plotted as normalised to the frequency of the original mode. When the diaphragm is overly flexible, the higher mode approaches the frequency of the uncoupled in-plane wall while the lower mode's frequency tends to zero. In addition, the frequencies of the mode pair become independent of the mass ratio. These observations suggest that the interactions between the diaphragms and the in-plane wall become negligible as the diaphragm becomes completely flexible. Conversely, when the diaphragm is very stiff, the higher mode increases exponentially, while the

lower mode approaches a frequency somewhat smaller than that of the uncoupled in-plane wall. This reduction in the lower mode's frequency depends on the mass ratio; in fact, the frequency approaches that of the rigid diaphragm condition, with the reduction in the frequency proportional to $1/\sqrt{(1+R_m)}$.

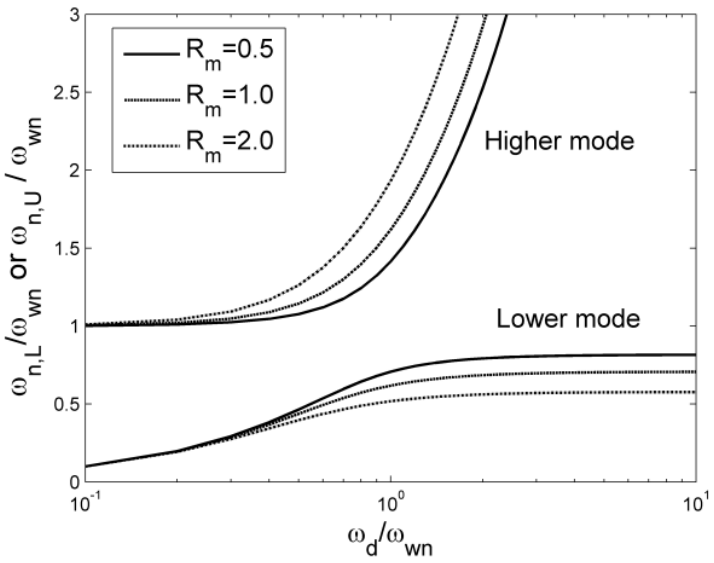

Figure 2. Frequencies of mode pair

The correspondence between the original mode and the mode pair can be further illustrated by their mode shapes. By substituting Equation 25 or 26 in the transformed Equation 22, it can be seen the standard basis vectors provide the required solution for $\boldsymbol{\phi}_{wn,L}^{*}$ and $\boldsymbol{\phi}_{wn,U}^{*}$

$$\boldsymbol{\phi}_{w1,\langle.\rangle}^{*} = [1 \quad 0 \cdots]^{\mathrm{T}}, \boldsymbol{\phi}_{w2,\langle.\rangle}^{*} = [0 \quad 1 \quad 0 \cdots]^{\mathrm{T}} \; etc. \tag{27}$$

To simplify the notation, ‹.› is used to replace the subscripts *L* or *U* in the above and the following expressions. Where ‹.› appears multiple times in an equation, they refer to the consistent component (*L* or *U*) of the mode pair. Applying the transformation back to the physical coordinate (Equation 9) yields

$$\boldsymbol{\phi}_{wn,\langle.\rangle} = \boldsymbol{\Phi}_{w}' \boldsymbol{\phi}_{wn,\langle.\rangle}^{*} = \boldsymbol{\phi}_{wn}' \tag{28}$$

where $\boldsymbol{\phi}_{wn}'$ is the n^{th} column vector of $\boldsymbol{\Phi}_{w}'$ and $\boldsymbol{\phi}_{wn,\langle.\rangle}$ is the eigenvector corresponding to the in-plane wall's degree of freedom of the n^{th} mode pair. The expression shows that the in-plane wall's mode shape (of the n^{th} mode pair) is proportional to the original, uncoupled in-plane wall's mode shape. The mode shape of the diaphragms in the n^{th} mode pair can be calculated from Equations 21, 28 and 9 as

$$\boldsymbol{\phi}_{dn,\langle.\rangle} = \frac{\omega_d^2}{\omega_d^2 - \omega_{n,\langle.\rangle}^2} \boldsymbol{\phi}'_{w\mathrm{n}} \tag{29}$$

In this expression, the displacement vector $\boldsymbol{\phi}_{dn,\langle.\rangle}$ is expressed as relative to the ground. Equation 29 also indicates that the mode shapes of the diaphragms are proportional to that of the original mode. Figure 3 shows the plot of the normalised mode shapes of the combined structure. The in-plane wall and the diaphragms are in-phase in the lower mode pair, and are out-of-phase in the higher mode pair.

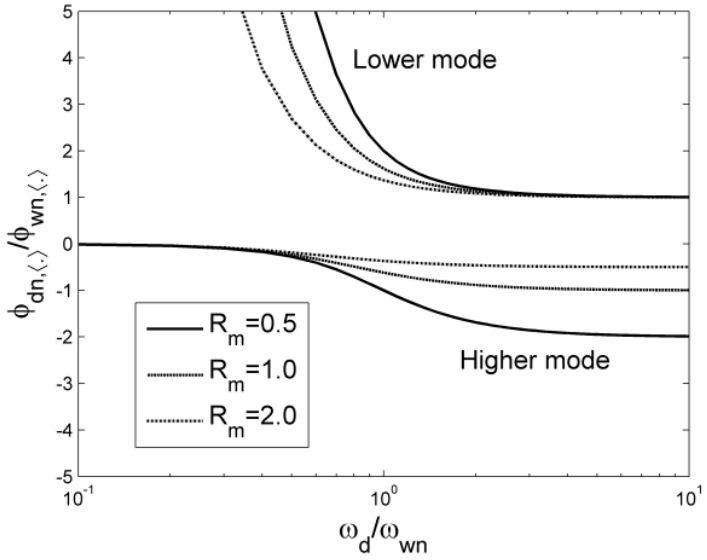

Figure 3. Mode shapes of mode pair

The properties of the mode pair derived in this section are specific to the diaphragm conditions of Equations 16 and 17. Under these conditions, a correspondence between the mode properties of the combined system and those of the uncoupled in-plane wall has been identified. Specifically, two modes (mode pair) of the combined system arise from each mode of the uncoupled in-plane wall (original mode). The mode shapes of the mode pair are proportional to that of the original mode. The in-plane wall and diaphragms are in-phase in the lower mode pair, and are out-of-phase in the higher mode pair. The significance of the mode pair is described in the next section.

3.2 Significance of Mode Pair for Seismic Analysis

In the seismic analysis of linearly elastic structures, it is usually sufficient to include only the first few modes to calculate the peak response quantities. A common parameter used to determine the number of modes to include, as typically specified in seismic codes, is the proportion of the effective modal mass to

the total seismic mass of the structure. The effective modal mass M_n may be obtained as the sum of the effective earthquake force distribution $\boldsymbol{s}_n$ (Chopra 2007),

$$M_n = \mathbf{1}^{\mathrm{T}}\boldsymbol{s}_n \tag{30}$$

where

$$\boldsymbol{s}_n = \Gamma_n \boldsymbol{m}\boldsymbol{\phi}_n = \frac{\boldsymbol{\phi}_n^{\mathrm{T}}\boldsymbol{m}\mathbf{1}}{\boldsymbol{\phi}_n^{\mathrm{T}}\boldsymbol{m}\boldsymbol{\phi}_n}\boldsymbol{m}\boldsymbol{\phi}_n \tag{31}$$

For the diaphragm configuration specified in Equations 16 and 17, Equation 31 for the mode pair can be evaluated as

$$\boldsymbol{s}_{n,\langle.\rangle} = \begin{bmatrix} f_{wn,\langle.\rangle}\boldsymbol{s}_{wn} \\ f_{dn,\langle.\rangle}\boldsymbol{s}_{wn} \end{bmatrix} \tag{32}$$

where $\boldsymbol{s}_{wn}$ is the effective earthquake force distribution of the original mode defined analogously to Equation 31. The coefficients $f_{wn,\langle.\rangle}$ and $f_{dn,\langle.\rangle}$ may be thought of as scaling factors applied to the in-plane wall and the diaphragms respectively,

$$f_{wn,\langle.\rangle} = \frac{1 + R_m\left(\dfrac{\omega_d^2}{\omega_d^2 - \omega_{n,\langle.\rangle}^2}\right)}{1 + R_m\left(\dfrac{\omega_d^2}{\omega_d^2 - \omega_{n,\langle.\rangle}^2}\right)^2}, \qquad f_{dn,\langle.\rangle} = R_m\left(\frac{\omega_d^2}{\omega_d^2 - \omega_{n,\langle.\rangle}^2}\right) f_{wn,\langle.\rangle} \tag{33}$$

The plots of $f_{wn,\langle.\rangle}$ and $f_{dn,\langle.\rangle}$ are shown in Figure 4 for the mode pair. The sum of $f_{wn,\langle.\rangle}$ of the mode pair, also indicated in Figure 4, is always 1, while the sum of $f_{dn,\langle.\rangle}$ is R_m. The total effective mass included in the analysis, if both modes of the mode pair are used (denoted by $M_{n,LU}$), can hence be given by

$$M_{n,LU} = \sum \mathbf{1}^{\mathrm{T}}\boldsymbol{s}_{n,\langle.\rangle} = \mathbf{1}^{\mathrm{T}}\boldsymbol{s}_{wn}\sum\left(f_{wn,\langle.\rangle} + f_{dn,\langle.\rangle}\right) = (1 + R_m)M_{wn} \tag{34}$$

where the summation is taken over the n^{th} mode pair and $M_{wn} = \mathbf{1}^{\mathrm{T}}\boldsymbol{s}_{wn}$ is the effective modal mass of the original mode. The ratio of the modal mass included in the analysis to the total seismic mass of the structure is

$$\frac{M_{n,LU}}{\mathbf{1}^{\mathrm{T}}(\boldsymbol{m}_w + \boldsymbol{m}_d)\mathbf{1}} = \frac{(1 + R_m)M_{wn}}{\mathbf{1}^{\mathrm{T}}\boldsymbol{m}_w(1 + R_m)\mathbf{1}} = \frac{M_{wn}}{\mathbf{1}^{\mathrm{T}}\boldsymbol{m}_w\mathbf{1}} \tag{35}$$

The significance of Equation 35 becomes clear by recognising that the right hand side of the equation expresses the proportion of the n^{th} modal mass of the uncoupled in-plane wall to its total seismic mass. Equation 35 therefore states that the mode pair retains the same proportion of the modal mass of the combined structure as that of the original mode. This property is particularly attractive for low-rise URM buildings, for which the uncoupled in-plane wall's behaviour is likely to be dominated by its fundamental mode. This leads to the concept of the two-mode analysis, whereby the response of the structure is approximated by the mode pair (defined by Equations 25, 26, 28 and 29) corresponding to the fundamental mode of the uncoupled in-plane wall. The applicability of this two-mode analysis concept is evaluated for more general diaphragm configurations in the next section.

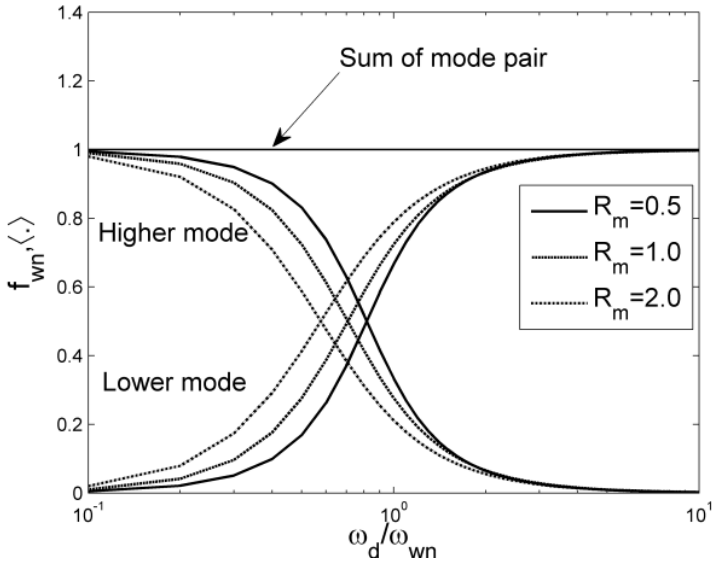

(a) In-plane walls

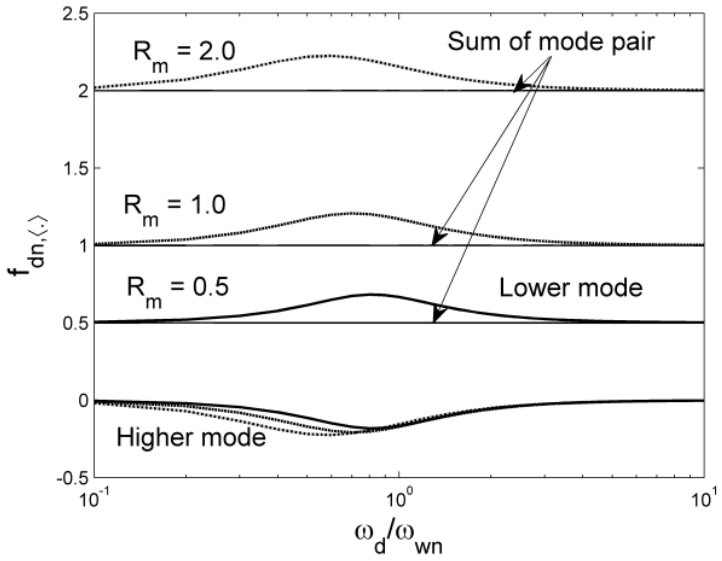

(b) Diaphragms

Figure 4. Scaling factors applied to the equivalent static force of uncoupled in-plane wall

4. SENSITIVITY ANALYSIS

4.1 Parameters Investigated

The validity of the assumptions and the errors inherent in the two-mode analysis approach is evaluated through a sensitivity analysis, by varying the number of storeys, characteristics of the input excitation, the reference mass ratio and the period of the diaphragms, as well as the variations introduced in the diaphragm configuration.

Two, three and four storey models are considered, with the reference fundamental periods of the uncoupled in-plane wall (T_w) corresponding to 0.178 s, 0.241 s and 0.3 s respectively. These period values are calculated based on the empirical period formula of AS 1170.4 (Standards Australia 2007),

$$T_{rig} = 0.0625h^{0.75} \quad (36)$$

where h is the height of the building, calculated assuming all storey heights to be 3.2 m. As T_{rig} applies to rigid diaphragm structures, T_w is obtained by eliminating the mass attributed to the diaphragms. For simplicity, it is considered that an equal amount of mass is attributed to the diaphragms (representing the mass of the out-of-plane loaded walls) and the in-plane wall, such that

$$T_w = \frac{T_{rig}}{\sqrt{2}} \tag{37}$$

The tributary mass of the in-plane wall is set to 10 tons at all levels except at the roof, where it is halved to approximate the reduction in the tributary height. The stiffnesses of the in-plane walls are adjusted so that the fundamental mode shape of the uncoupled in-plane wall is linear in all cases.

The *reference* diaphragm condition consistent with Equations 16 and 17 is determined by the *reference mass ratio* R_m and the *reference diaphragm period* T_d. The variations in these parameters are independently controlled by ε_m and ε_T respectively. Four different variation profiles are considered, as shown in Figure 5. The figure shows the profiles for the positive ε_m variation as applied to a three storey model. Similar variations are investigated for the diaphragm periods, by the parameter ε_T. For the linear and the alternating profiles, the reference values equal the average configurations of the diaphragms. For the top variation and the bottom variation profiles, all but one level have the reference values. The parameters ε_m and ε_T are varied independently from -0.5 to 0.5. The reference mass ratio R_m is varied from 0.5 to 2, and the diaphragm period T_d from 0.1 s to 2 s. These values are considered to encompass the likely range of parameters for typical existing URM buildings with timber diaphragms.

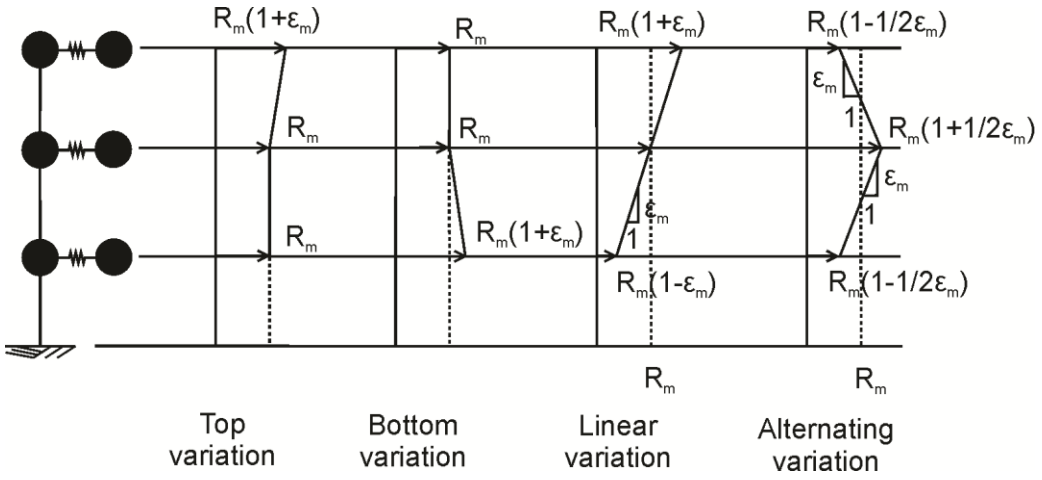

Figure 5. Variation in the reference mass ratio (for variation in reference period, replace R_m by T_d and ε_m by ε_T)

4.2 Acceleration Records

The sensitivity of the two-mode analysis to the input spectral shape is assessed by considering two sets of acceleration records. The first set consists of six natural accelerograms selected from the CUREE testing protocol (Krawinkler et al. 2000) as scaled by Christopoulos et al. (2002). As listed in Table 1, these records were measured in California on stiff soil (NEHRP site class C and D). The second set consists of artificial accelerograms compatible with AS 1170.4 on rock sites (Lam et al. 2005), which exhibit the dominance of high frequency content typical of intraplate regions. The mean pseudo-acceleration spectra of the two sets of records are shown normalised to their peak ground accelerations in Figure 6.

Table 1. List of natural accelerograms

Event	**Station**	**Year**	**M_w**	**Closest distance (km)**	**NEHRP site class**	**Scaling factor**
Superstition Hills	Plaster City	1987	6.7	21	D	2.2
Northridge	Canoga Park - Topanga Can	1994	6.7	15.8	D	1.2
Northridge	N. Hollywood - Colwater Can	1994	6.7	14.6	C	1.7
Loma Prieta	Gilroy Array # 4	1989	6.9	16.1	D	1.3
Cape Mendocino	Rio Dell Overpass - FF	1992	7.1	18.5	C	1.2
Landers	Yermo Fire Station	1992	7.2	24.9	D	2.2

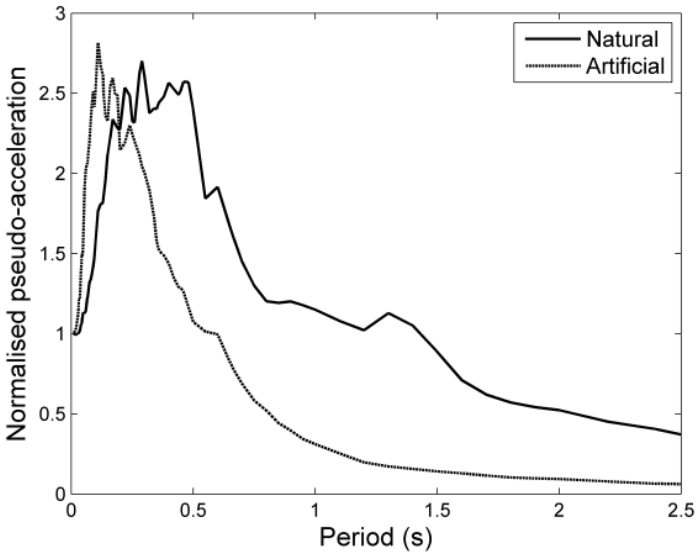

Figure 6. Comparison of the mean spectra of two sets of records

4.3 Analysis Procedure

For each parameter combination, two analyses are conducted. The first analysis is performed with the actual configuration of the diaphragms, including the variations in the mass ratio and the period. The time-history responses are calculated by Newmark's constant average acceleration method (γ = 0.5 and β = 0.25), with a constant damping ratio of 5% applied to all modes. The second analysis is carried out by using the reference values of diaphragms, R_m and T_d, and the mode pair corresponding to the fundamental mode of the uncoupled in-plane wall. For each mode, modal time-history displacements are solved and are superimposed to obtain the combined response of the mode pair. A constant damping ratio of 5% is also used in the second set of analyses to eliminate the influence of damping in the comparison of results.

4.4 Response Parameters

The two-mode analysis is evaluated based on the mean peak base shear and the interstorey drift of the in-plane wall. These are considered to represent the global and the local parameters most applicable in assessing the response of a building. Furthermore, the results are reported by the ratios of the mean peak responses (denoted generically as r) from the two-mode analysis (r_{est}) to the complete analysis (r_{act})

$$r = \frac{r_{est}}{r_{act}} \tag{38}$$

4.5 Error in Base Shear Estimation

The accuracy of the base shear estimation is found to depend on the flexibility of the diaphragms. In Figure 7, the range of the base shear ratios (Equation 38) for the four-storey model with ε_T of −0.3 is shown as a function of the period ratio, $R_T = T_d / T_w$. The plot shows the typical sensitivity characteristics observed, and includes all variation profiles. As shown in the figure, the two-mode analysis produces accurate results when the diaphragms become very flexible. The negligible influence of the very flexible diaphragms implies the in-plane wall to respond independent of the diaphragms. The largest error is generally observed when R_T is between 1 and 4, suggesting that the diaphragms have the most potential to modify the response of the in-plane wall when they are neither very stiff nor overly flexible.

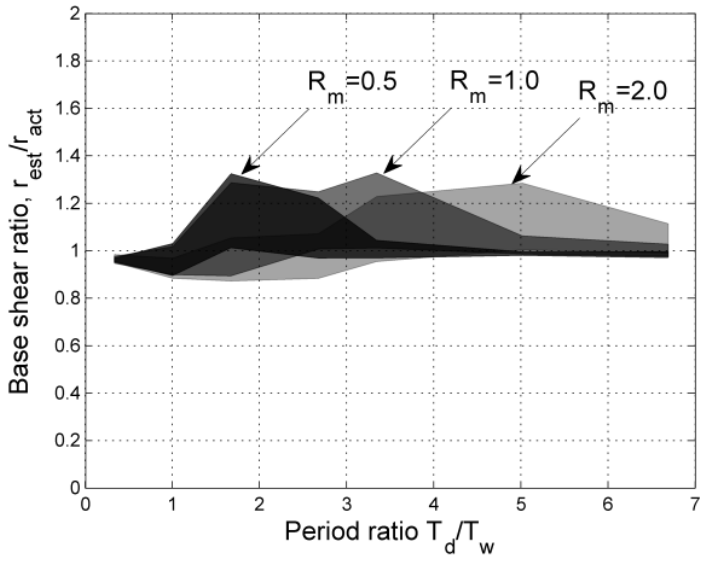

(a) Natural accelerograms

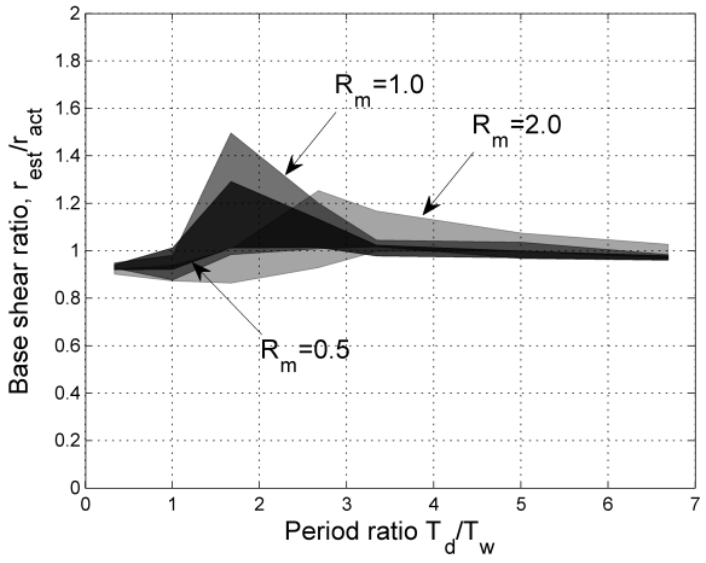

(b) Artificial accelerograms

Figure 7. Ratio of mean peak base shear of the two-mode analysis to the actual results for four-storey model with ε_T of −0.3

The reference mass ratio shows no consistent influence on the maximum error in the estimation of the base shear. However, larger R_m typically results in larger errors in the flexible diaphragm range, approximately for $R_T > 4$.

No significant differences in the maximum error are observed for the two sets of input accelerograms. However, the natural accelerograms tend to result in larger errors in the range $R_T > 4$.

The envelopes of the maximum and the minimum base shear ratios are shown in Figure 8 for the top variation and in Figure 9 for the linear ε_T variation profiles for the natural accelerogram records. While not shown, similar results are obtained for the artificial accelerograms. The errors resulting from the variations in ε_m are also found to be similar to those of ε_T. Furthermore, results for the bottom variation and the alternating variation profiles are similar to those obtained for the top variation profile. As Figure 8 and Figure 9 show, the linear variation results in the largest error of the two-mode analysis. While the errors in the other variation profiles are insensitive to the number of storeys, the error for the linear variation grows with the number of storeys.

For the top, bottom and alternating variation profiles, the error in the base shear estimation using the two-mode analysis can be limited to ±20% if ε_m and ε_T are within ±30% of the reference values. For the linear variation, up to +40% error can be observed for the four-storey structures by keeping ε_m and ε_T to within

±30% of the reference values. In general, there is a tendency for the two-mode analysis to overestimate the actual base shear. This may be attributed to the assumption of the equal diaphragm period inherent in the two-mode analysis, as this assumption results in the perfect correlation of the inertial forces transferred from the diaphragms to the in-plane wall.

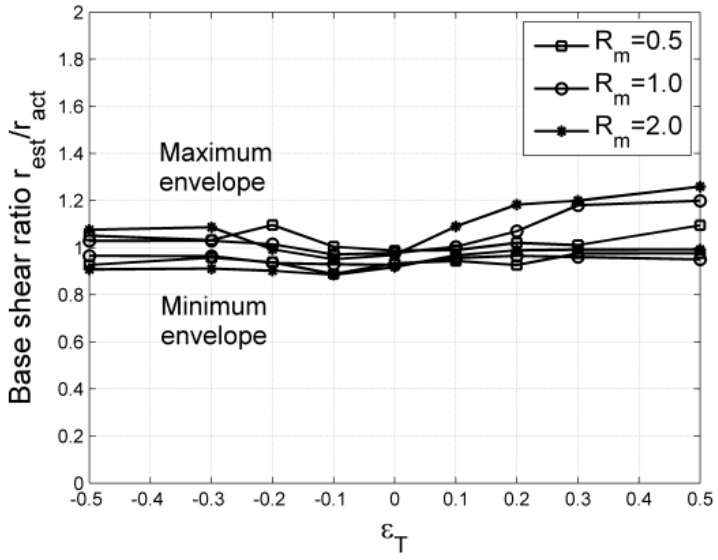

(a) Two-storey model

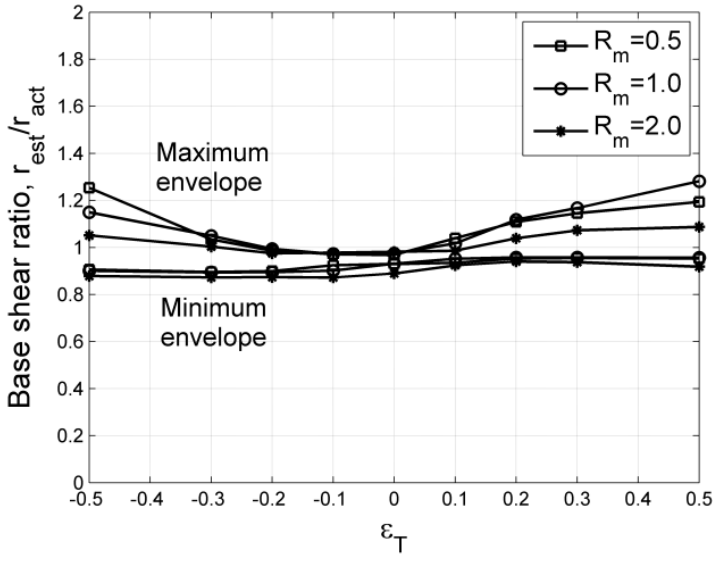

(b) Four-storey model

Figure 8. Envelope of mean peak base shear ratio of top variation in ε_T for natural accelerograms

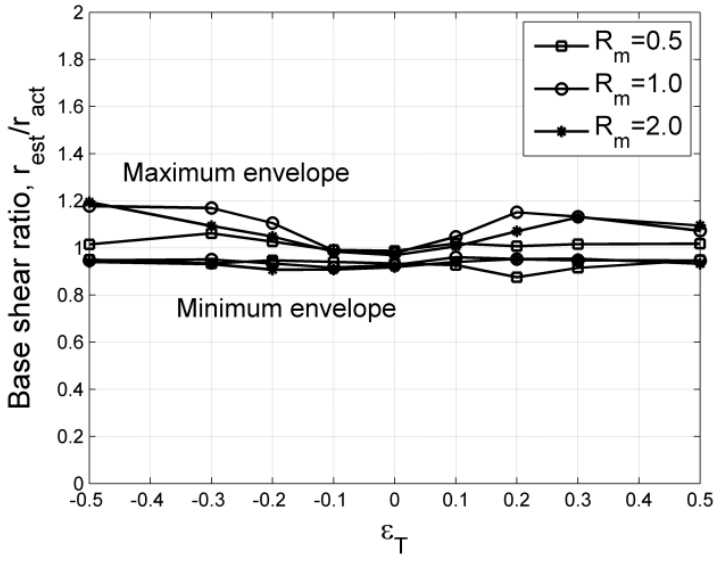

(a) Two-storey model

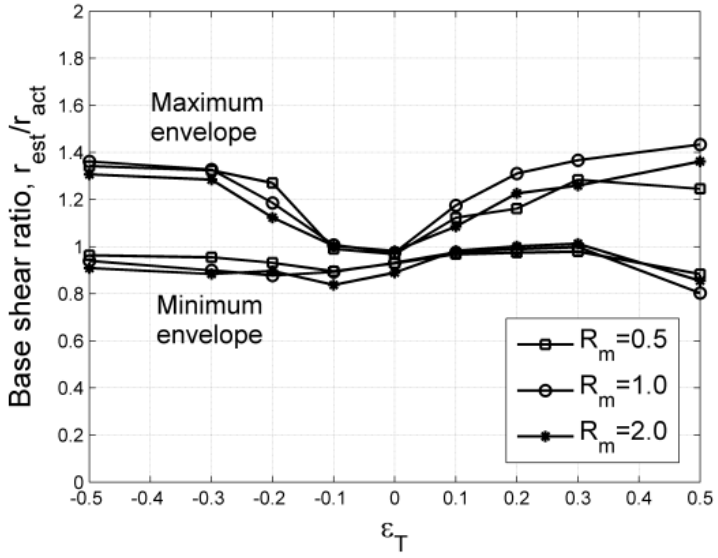

(b) Four-storey model

Figure 9. Envelope of mean peak base shear ratio of linear variation in ε_T for natural accelerograms

4.6 Error in Interstorey Drift Estimation

The two-mode analysis generally results in larger errors in the interstorey drift estimation in comparison to the base shear.

For the top and the linear variation profiles, the variation in ε_m results in larger errors than the variation in ε_T, while for the bottom and the alternating variation profiles, ε_m and ε_T lead to similar levels of errors. This finding is shown in the ratios of the interstorey drifts of the bottom and linear variation profiles for the four-storey model, corresponding to ε_T (Figure 10) and ε_m (Figure 11). While not shown, the maximum error envelope of the top variation profile is similar to that of the linear variation profile, while the alternating variation profile tends to be between the bottom and the top variation profiles.

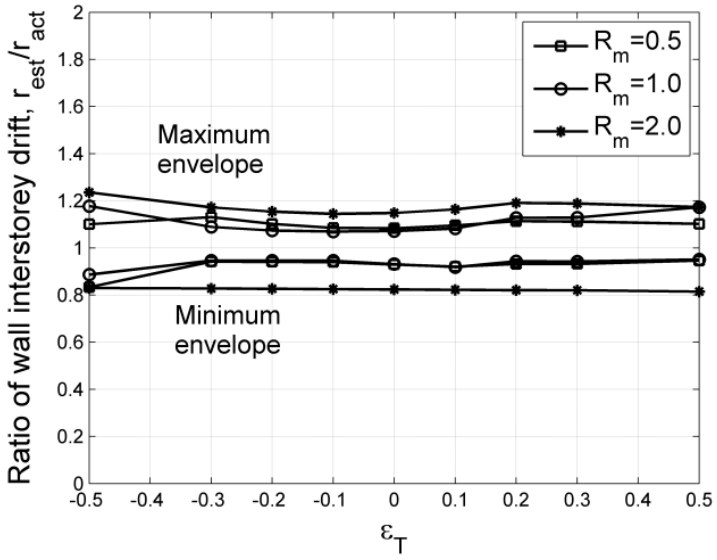

(a) Bottom variation profile

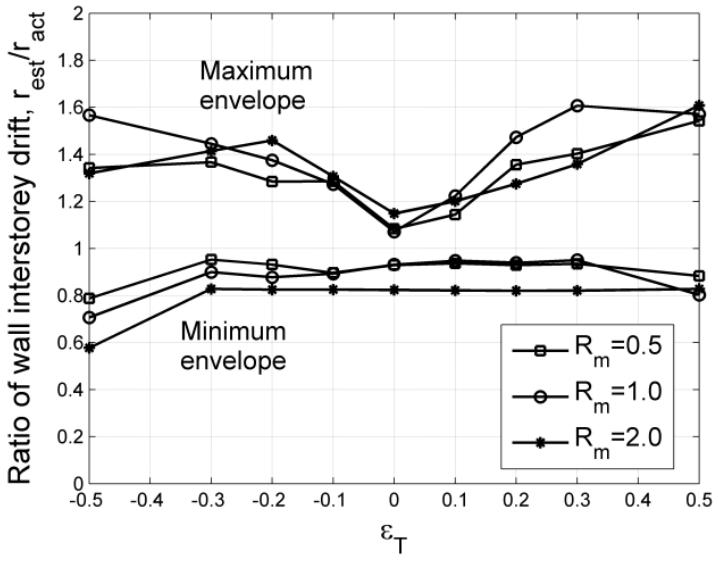

(b) Linear variation profile

Figure 10. Envelope of ratios of mean peak interstorey drift for four-storey model with variation in ε_T for natural accelerograms

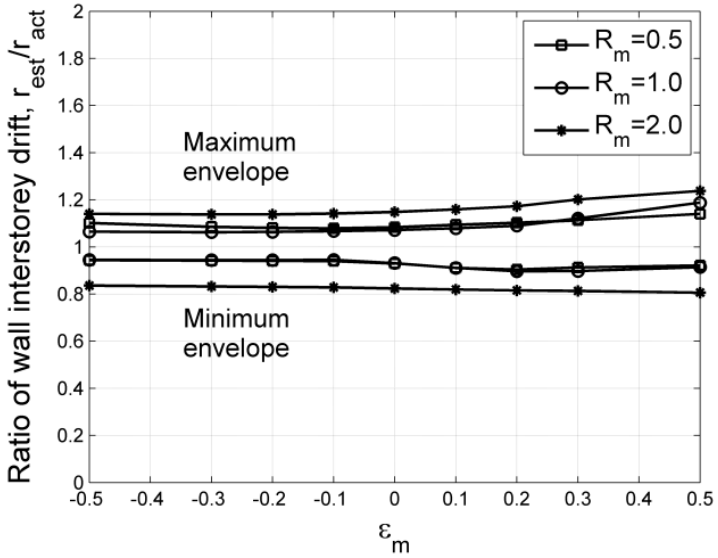

(a) Bottom variation profile

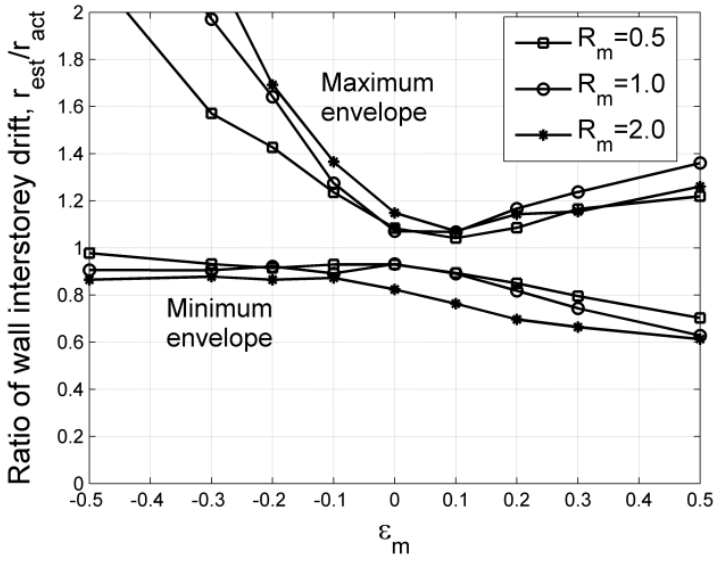

(b) Linear variation profile

Figure 11. Envelope of ratios of mean peak interstorey drift for four-storey model with variation in ε_m for natural accelerograms

From Figure 11, the two-mode analysis can be seen to produce conservative results when the mass ratio of the top level is less than the reference value ($\varepsilon_m < 0$), while noticeable underestimations may result when the top level has larger mass ratio ($\varepsilon_m > 0$). These observations have been consistently found for the top and the linear variation profiles, for both sets of accelerograms.

The estimation of the interstorey drift can also be somewhat sensitive to the spectral shape of the excitation. The artificial accelerograms appear to induce larger participation of higher modes that are not considered in the mode pair analysis. This is seen in Figure 12, in which a constant level of error persists even for very flexible diaphragms.

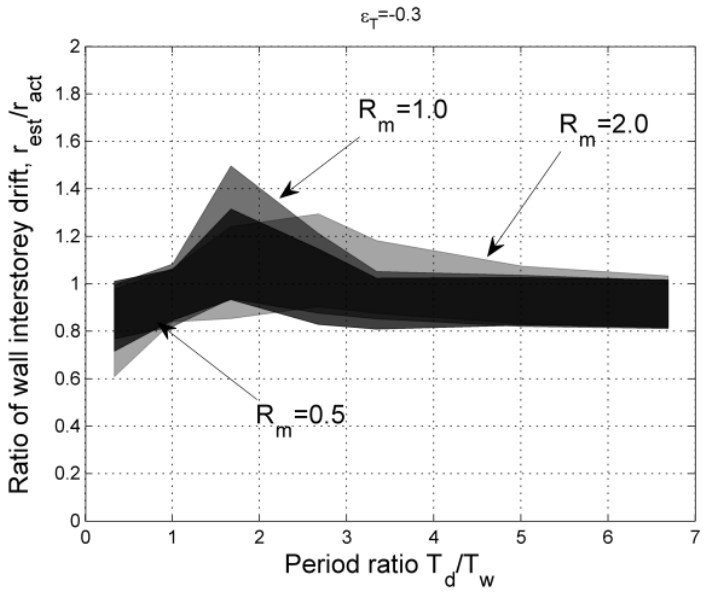

Figure 12. Ratio of mean interstorey drifts of the two-mode analysis to the actual results for four-storey mode with ε_T of −0.3

For buildings of up to three storeys, the error can be limited to between approximately −20% and +40% if ε_T is within ±30% of the reference value. For the four-storey models, an error of up to +60% may be obtained under the same condition. The variation in ε_m leads to even larger errors. For buildings of up to three storeys, errors between −20% and +60% are obtained for the bottom and the alternating variation profiles, if ε_m is within ±30% of the reference value. For the top and the linear variation profiles, the upper-bound errors increase to +90%. When the four-storey models are considered, significant overestimations (>100%) and underestimations (−60%) may be obtained.

The two-mode analysis appears to be appropriate in estimating the mean peak base shear of a structure with flexible diaphragms within the range of parameters investigated. However, the estimations of the local parameters, such as interstorey drifts, can become rather poor. It is envisaged that improved predictions of local demands can be achieved by modifying the mode shape assumed in the two-mode analysis.

4.7 Recommended Use of Two-Mode Analysis

From the sensitivity analysis, the following criteria are suggested for application of the two-mode analysis:

- the number of storey to be limited to three;

- the variation profile should be selected so that ε_m and ε_T are minimised, and within approximately ±0.3;

- the bottom variation profile is the most favourable for both ε_m and ε_T, followed by the alternating, top and linear profiles; and

- for conservative estimates, the mass ratio of the topmost level to be smaller than the reference value R_m, if the top or the linear variation profile is used.

These condition are aimed at limiting the error in the mean peak base shear estimations to ±20%, while eliminating the excessive errors observed for the interstorey drift predictions.

5. APPLICATION TO LINEAR STATIC PROCEDURE

An improvement to the linear static procedure is proposed by utilising the finding that the two-mode analysis can generally provide reasonable predictions of the mean peak base shear. Expressions for the mode pair to be used in the method are firstly summarised. A coefficient that captures the effect of diaphragm flexibility on the base shear (base shear modification factor) is then derived analytically.

5.1 Formulae for Mode Pair

The mode pair corresponding to the fundamental mode is used in the linear static method. For the uncoupled in-plane wall with the fundamental period T_w, the periods of the mode pair (from Equations 25 and 26) can be written as

$$T_1 = T_w \left(\frac{2R_T^2}{R_T^2 + (1 + R_m) - \sqrt{[R_T^2 + (1 + R_m)]^2 - 4R_T^2}} \right)^{0.5} \tag{39}$$

$$T_2 = T_w \left(\frac{2R_T^2}{R_T^2 + (1 + R_m) + \sqrt{[R_T^2 + (1 + R_m)]^2 - 4R_T^2}} \right)^{0.5} \tag{40}$$

where $R_T = T_d / T_w$ is the reference period ratio and R_m is the reference mass ratio. The scaling factors (Equation 33) of the effective earthquake force distribution are also given in an alternative dimensionless form as

$$f_{wi} = \frac{1 + R_m \beta_i}{1 + R_m \beta_i^2}, \qquad f_{di} = R_m \beta_i f_{wi}, \qquad i = 1,2 \tag{41}$$

where

$$\beta_i = \frac{T_i^2}{T_i^2 - (R_T T_w)^2}, \qquad i = 1,2 \tag{42}$$

5.2 Base Shear Modification Factor

The base shear modification factor, that expresses the effect of the flexible diaphragms on the peak base shear of the uncoupled in-plane wall, is herein derived analytically. Firstly considering the uncoupled in-plane wall, any peak response in the fundamental mode (denoted by r_w') can be written as (Chopra 2007)

$$r_w' = r_w'^{st} S_a(T_w) \tag{43}$$

where $r_w'^{st}$ is the static response of the wall subjected to $\boldsymbol{s}_w$, as defined in Equation 31 for the uncoupled in-plane wall, and S_a is the ordinate of the pseudo-acceleration spectrum at the fundamental period of the uncoupled in-plane wall.

For linearly elastic structures, a proportionality exists between the applied force and the response,

$$r_w'^{st} \propto \boldsymbol{s}_w \tag{44}$$

Using the expression of Equation 32, similar proportionality can also be written for the in-plane wall in the combined structure

$$r_{wi}^{st} \propto (f_{wi} + f_{di})\boldsymbol{s}_w, \qquad i = 1,2 \tag{45}$$

where f_{wi} and f_{di} can be obtained from Equation 41. Because the proportionality in Equations 44 and 45 is governed by the stiffness of the in-plane wall, which is identical in the uncoupled and the combined systems, the two expressions imply

$$r_{wi}^{st} = (f_{wi} + f_{di}) r_w'^{st}, \qquad i = 1,2 \tag{46}$$

The peak dynamic in-plane wall's response in the combined structure r_w can then be approximated by the square-root-of-sum-of-squares (SRSS) combination of the mode pair, because the modes are widely spaced (see Figure 2),

$$r_w = r_w'^{st} \sqrt{\sum_{i=1}^{2} [(f_{wi} + f_{di}) S_a(T_i)]^2} \quad (47)$$

where T_i is obtained from Equations 39 and 40. By specialising the response parameter to the base shear, the base shear modification factor is defined by

$$C_B = \frac{V_b}{V_b'} = \frac{\sqrt{\sum_{i=1}^{2} [(f_{wi} + f_{di}) S_a(T_i)]^2}}{S_a(T_w)} \quad (48)$$

where V_b is the approximated base shear of the combined structure and V_b' is the base shear of the uncoupled in-plane wall. Hence by knowing the base shear of the uncoupled in-plane wall, the base shear of the combined structure accounting for the diaphragm vibration is given by

$$V_b = C_B V_b' \quad (49)$$

5.3 Calculation of T_w

In evaluating Equations 39 and 40, the fundamental period of the in-plane wall is required. Several options are available to calculate T_w:

- The in-plane wall may be modelled using frame elements with rigid offsets at nodal regions. Eigenvalue analysis can then be conducted. This approach option requires the use of software.

- The stiffness of the solid walls may be calculated using the mechanics for homogeneous materials, considering both the shear and the flexural deformations. For walls with openings, the wall stiffness may be obtained from the individual stiffnesses of piers by assuming appropriate boundary conditions. The typical common assumptions on the boundary condition are (1) strong pier - weak spandrel (i.e. cantilever piers), or (2) weak pier - strong spandrel (i.e. each pier in double bending). Once the wall stiffness is calculated, the Rayleigh's method (ASCE 2014) may be used to obtain the fundamental period.

Alternatively, the estimation of T_w may be avoided completely if a simplified analysis method is used, as described in the following section.

5.4 Simplified Method

The calculation of T_w admittedly involves a large approximation, especially if a wall stiffness is estimated from the individual pier stiffnesses. The sensitivity of the modified base shear (Equation 49) to variations in T_w is therefore investigated. Figure 14 shows a contour plot of V_B (as normalised to the weight of the structure), against the uncoupled in-plane wall period and the diaphragm period. The plot is generated from the expressions in Equations 39 to 49, using the design spectrum of NZS 1170.5 (New Zealand Standard 2004a) on site subsoil class B (Figure 13), with the peak ground acceleration of 0.22 g. The mass ratio is set to 1. The transition periods of the design spectra are denoted as T_B and T_C as shown in Figure 13. These periods are also indicated in Figure 14. It can be observed that for a given value of T_d, the base shear is rather insensitive to variations in T_w. Furthermore, a reasonable conservative estimate can be made by setting $T_w = T_B$ for the typical period range of interest for URM buildings with flexible diaphragms (small T_w and moderate to large T_d). Consistent observations were made for other soil types and mass ratios. Hence a simplification is suggested for a practical application, by setting $T_w = T_B$.

In order to facilitate the use of the simplified method, the values of base shear modification factor (C_B) corresponding to $T_w = T_B$ are provided in Appendix B for the design spectra of NZS 1170.5. It is notable that C_B reduces with the increasing diaphragm flexibility. This suggests that the multi-mode behaviour associated with diaphragm flexibility leads to a general reduction in the base shear.

Note that the charts are developed using design spectra corresponding to the modal and time-history analyses (as opposed to the equivalent static analysis). This is because the spectra corresponding to the modal and time-history analyses reflect the hazard spectra, while those of the equivalent static analysis contain a cut-off period associated with the uncertainty involved in the estimation of short fundamental periods (New Zealand Standard, 2004b). However, accounting for such uncertainty does not seem appropriate in the proposed method.

Once T_d and R_m are calculated, these charts can be read off to obtain the value of the modification factor corresponding to the site subsoil class of interest. This avoids the need to calculate T_w. The base shear of the uncoupled in-plane wall can be obtained using the peak ordinate of the design spectra. It should be noted, however, that this simplified method is to be used only in conjunction with smooth design spectra, and not with individual earthquake records.

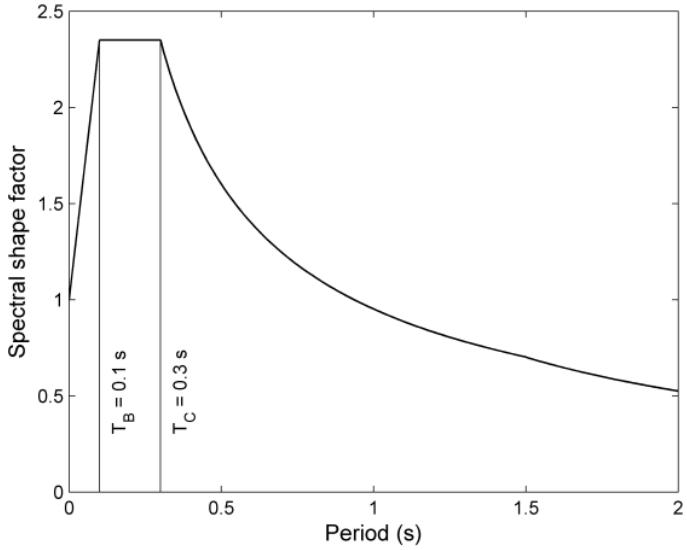

Figure 13. Design spectral shape factor of NZS 1170.5 for site subsoil class B

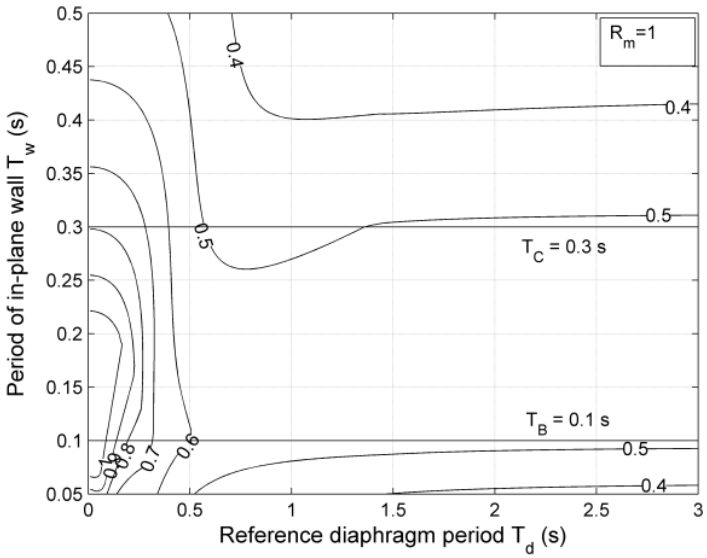

Figure 14. Contour plot of V_B (Equation 49)

5.5 Analysis Step

The proposed linear static method consists of the following steps, applicable to essentially symmetric structures of up to three storeys in height:

1. Calculate the tributary masses of the in-plane wall and the diaphragms.

2. Multiply the tributary masses of the diaphragms by 126/155 (Equation 5) to obtain the *effective* masses of the diaphragms. Calculate the mass ratio by dividing the effective diaphragm mass by the tributary mass of the in-plane wall at each level. Calculate the reference diaphragm mass ratio, R_m by selecting an appropriate variation profile of Figure 5, ensuring that ε_m is within ±0.3.

3. Calculate the periods of the diaphragms (Equation 4, also refer Wilson et al. (2013) and Giongo et al. (2014)) and the reference diaphragm period T_d by selecting an appropriate variation profile of Figure 5 (by replacing R_m and ε_m of Figure 5 by T_d and ε_T respectively), ensuring that ε_T is within ±0.3. Note that the variation in T_d does not need to assume the same profile as that of R_m.

4. Calculate the fundamental period (T_w) and the mode shape (ϕ) of the uncoupled in-plane wall. Alternatively, the simplified method can be used, by assuming $T_w = T_B$.

5. Calculate C_B from Equation 48, using the associated expressions in Equations 39 to 42. If the simplified method is used, C_B may be read off from one of the charts provided in Appendix B.

6. Calculate the peak base shear of the uncoupled in-plane wall (V_B'), by multiplying the seismic mass of the in-plane wall by $S_a(T_w)$, where S_a is the ordinate of the pseudo-acceleration spectrum. If the simplified method is used, the peak ordinate of the spectrum should be used.

7. In order to account for the inelastic deformation, the base shear may be further modified, for example, by C_1, C_2 and C_m of Equation 1. However, further studies are needed to confirm the validity of these coefficients for structures with flexible diaphragms.

8. The equivalent lateral forces on the in-plane walls are obtained by distributing the modified base shear in proportion to $m_j \phi_j / \sum m_i \phi_i$ for the j^{th} level. If the simplified method is used, ϕ may be approximated by the floor heights from the ground (linear variation), as typically specified in codes (New Zealand Standard 2004a; Standards Australia 2007; ASCE 2014). This approximation is consistent with the assumption of the first-mode dominance of the in-plane wall used in the two-mode analysis.

9. The resulting member forces (which can be evaluated using an equivalent frame model, or determined on the basis of the relative stiffnesses of the piers and spandrels) are compared to their capacities, for example using Equation 2.

5.6 Analysis Effort

The effort needed to carry out the proposed method is comparable to existing methods. This section provides the comparison of the analysis procedures of two existing methods, ASCE 41-13 and a method by Knox (2012), and the approach proposed in this study. The overview of the existing methods is provided in Appendix A. The following can be noted:

- All methods require the calculations of tributary masses and the diaphragm period of each span at each floor level. Hence the analysis steps 1 and 3 of the preceding section are identical for all methods.

- Analysis step 2 is unique to the proposed method. However, this step requires minimal effort.

- The calculation of the uncoupled in-plane wall period (step 4) is required in the rigorous version of the proposed method and in the method by Knox. However, as described previously, the simplified approach can be used to eliminate the need to compute the fundamental period of the wall.

- The calculation of C_B in step 5 is unique to the proposed method. However, this step requires minimal effort, especially if the simplified approach is used.

- ASCE 41-13 and Knox's methods require the computation of the equivalent static force for each diaphragm, while the proposed method requires the equivalent static force of the in-plane wall only.

- Knox's method requires the calculation of base shear by complete quadratic combination (CQC) of the diaphragm forces and the in-plane wall force to avoid the potential underestimation of storey forces obtained by SRSS. This may require certain additional effort in calculating the correlation coefficients.

The steps 7 onwards are identical in all methods. The foregoing discussion confirms that the effort needed to conduct the proposed method is comparable to the existing methods.

5.7 Numerical Validation

A two-storey symmetric building shown in Figure 15 is analysed using the proposed method. In addition, ASCE 41-13 and the method by Knox are also evaluated for comparison. In this validation, the rigorous

version of the method is used with the “actual” uncoupled in-plane wall period obtained from the modal analysis of the wall modelled by frame elements and rigid offsets. In addition, only the elastic response is evaluated, because the modification for the inelastic response is in principle identical for all methods.

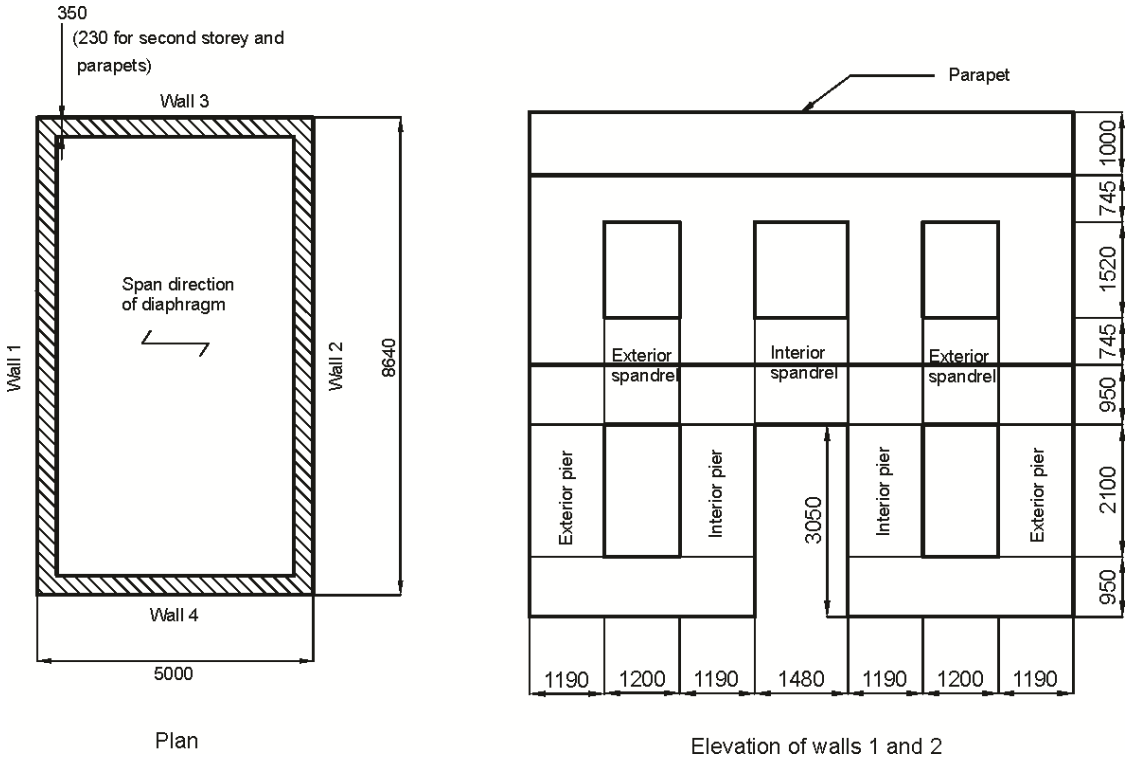

Figure 15. Example structure

In the analysis, the loading is considered in the direction parallel to walls 1 and 2, and perpendicular to the floor and roof joists. The out-of-plane walls (walls 3 and 4) are solid with no openings. The thicknesses of the walls are 350 mm in the first storey and 230 mm in the higher levels. The density of masonry is 1800 kg/m^3 and the Young's modulus is 2750 MPa. The shear modulus is assumed to be 40% of the Young's modulus.

Using an equivalent frame model, the fundamental period of the in-plane wall is calculated to be 0.097 s. The mode shape is 0.478 at the first floor and 1.0 at the roof level, indicating an almost linear profile. The effective mass of the fundamental mode is 85% of the total mass of the in-plane wall.

Three different diaphragm constructions are considered. The diaphragm stiffnesses of the first two cases are calculated using the procedure outlined in Giongo et al. (2014). The third case represents more heavily loaded stiff timber diaphragms.

In the first case (case 1), the first level diaphragm is considered to be in a "fair" condition and sheathed with single straight floor board, while the roof has single diagonal sheathing and is in a "poor" condition (see Giongo et al. (2014)). Using the procedure of Giongo et al. (2014), and neglecting for simplicity the effects of floor opening and additional stiffness of the out-of-plane wall, the diaphragm stiffness G_d is calculated to be 215 kN/m at the first floor and 340 kN/m at the roof. Assuming 18 mm thick sheathing and 55 mm by 240 mm deep joists spaced at 405 mm centres, with the timber density of 610 kg/m^3, the self-weight of the floor is calculated to be 0.3 kPa. The self-weight of the roof is considered to be 0.6 kPa, accounting for an additional 0.3 kPa for the roofing. The floor is also subjected to an additional 0.9 kPa (3 kPa imposed load multiplied by the seismic load factor of 0.3) imposed load.

In the second case (case 2), the floor diaphragm is considered to have been strengthened with blocked 9 mm plywood overlay (unchorded), increasing G_d to 1460 kN/m. The roof is also strengthened with an additional layer of diagonal sheathing, resulting in G_d of 2385 kN/m. In addition, the self-weight of the floor and the roof increase to 0.36 kPa and 0.72 kPa respectively, due to the additional strengthening material.

The third case (case 3) represents a more heavily stiffened case in which the floor and the roof diaphragms have the same stiffness G_d of 3150 kN/m. This value represents the upper-bound expected stiffness of timber diaphragms in ASCE 41-13. The dead load of the floor and the roof are considered to be 1.5 kPa, taken as an average value reported for a two-storey building by Bruneau (1994), which contains large mass contributions from the ceiling and wood partitions. In addition, a 1.5 kPa imposed load is considered for the floor (5 kPa live load with the seismic load factor of 0.3).

The calculated diaphragm mass ratio and periods are shown in Table 2 for the three cases. In this example, the linear profile has been chosen for both parameters, resulting in the reference parameters R_m and T_d being the average values of the mass ratios and the diaphragm periods. The values of ε_m and ε_T can then be calculated from Figure 5. For example, using the first floor mass ratio of 0.425 and the reference R_m of 0.457 for case 1 (see Table 2), the value of ε_m is obtained by substituting the above values in the expression given in Figure 5 for the linear profile; i.e. $0.457(1 - \varepsilon_m) = 0.425$, resulting in ε_m of 0.07.

Table 2. Diaphragm configuration (case 1: as-built; case 2: plywood overlay; case 3: heavily stiffened)

Level	Mass ratio (effective diaphragm mass / in-plane wall mass)			Diaphragm period (from Equation 4)		
	Case 1	Case 2	Case 3	Case 1	Case 2	Case 3
1	0.425	0.432	0.639	0.45 s	0.17 s	0.14 s
2	0.490	0.515	0.678	0.29 s	0.11 s	0.11 s
Average	0.457	0.474	0.658	0.37 s	0.14 s	0.13 s

The calculated values of ε_m are 0.071, 0.089 and 0.029 respectively for the first, second and the third cases. Similarly, the values of ε_T are -0.22, -0.21 and -0.12 respectively for the three cases. It is noted that all ε_m and ε_T values are within the suggested limit of ± 0.3.

The structures are analysed with the proposed method using the mean spectrum of the natural records listed in Table 1. In order to assess the accuracy of the method, linear dynamic analyses are conducted in SAP2000 (CSI 2012) using the six accelerograms. The in-plane walls are modelled as equivalent frames with rigid offsets, while the diaphragms are modelled by beam elements with artificially large bending stiffness to simulate the shear deformation compatible with Equation 4. In addition, the existing linear static method by Knox, as well as the method contained in ASCE 41-13 for URM buildings with flexible diaphragms, are also evaluated. In the ASCE 41-13 method, the updated diaphragm period expression of Equation 4 by Wilson et al. (2013) is used. In all analyses, a constant modal damping ratio of 5% is used. The results from the three linear static methods are compared against the time-history results.

Table 3 shows the predicted mean peak moments of the in-plane wall elements, indicated in Figure 15 for the first storey, as normalised to the dynamic analysis results for case 1. Similar results are shown in Table 4 and Table 5 for case 2 and 3 respectively. The comparison shows that the proposed and the Knox's methods produce comparably good predictions of the dynamic results for the flexible diaphragms in case 1. The method of ASCE 41-13, however, results in large overestimations. When the diaphragm stiffness is increased in case 2, the proposed method reports the same level of accuracy as in case 1, while Knox's method results in some underestimations. The overestimation of ASCE 41-13 reduces, although the method is still overly conservative. For the most stiff and heavy diaphragms of case 3, the proposed method provides reasonably consistent results with the dynamic analysis, while Knox's method results in further underestimations. The method in ASCE 41-13, on the other hand, provides a comparable level of accuracy to that as the proposed method.

It appears that the ASCE 41-13 is more suited to the analysis of structures when the diaphragms are relatively stiff, as this method assumes the total tributary mass to respond in a single period. Conversely, the method of Knox appears more suitable when the diaphragms are relatively flexible, as it treats the in-plane wall and the diaphragms to vibrate independently. In comparison to these existing procedures, the proposed method is capable of providing consistent predictions of seismic demand for a wide range of diaphragm stiffnesses.

Table 3. Peak moments from linear static methods normalised to mean peak dynamic results for case 1

Element	Location	Proposed method		Method by Knox		ASCE 41-13	
		Storey 1	Storey 2	Storey 1	Storey 2	Storey 1	Storey 2
Pier	Exterior	1.13	1.29	1.25	1.08	2.41	1.99
	Interior	1.07	1.24	1.16	1.08	2.25	2.00
Spandrel	Exterior	1.27	1.26	1.33	1.11	2.54	2.04
	Interior	1.16	1.24	1.19	1.10	2.89	2.04

Table 4. Peak moments from linear static methods normalised to mean peak dynamic results for case 1

Element	Location	Proposed method		Method by Knox		ASCE 41-13	
		Storey 1	Storey 2	Storey 1	Storey 2	Storey 1	Storey 2
Pier	Exterior	1.08	1.29	0.91	0.77	1.54	1.14
	Interior	1.03	1.23	0.85	0.78	1.45	1.14
Spandrel	Exterior	1.24	1.25	0.98	0.79	1.63	1.16
	Interior	1.14	1.22	0.87	0.79	1.43	1.17

Table 5. Peak moments from linear static methods normalised to mean peak dynamic results for case 3

Element	Location	Proposed method		Method by Knox		ASCE 41-13	
		Storey 1	Storey 2	Storey 1	Storey 2	Storey 1	Storey 2
Pier	Exterior	0.95	1.22	0.69	0.63	1.11	0.92
	Interior	0.90	1.15	0.64	0.62	1.03	0.91
Spandrel	Exterior	1.07	1.19	0.73	0.64	1.16	0.94
	Interior	0.98	1.12	0.65	0.62	1.01	0.91

5.8 Discussions on Inelastic Behaviour

The basic premise of the linear static procedure, when used in the performance-based assessment, is that the peak inelastic displacement can be estimated from the displacement of the corresponding elastic system. For example, the modification factor C_1 in Equation 1 accounts for the presumed difference

between the peak inelastic displacement and the elastic displacements. In FEMA 356 (FEMA 2000) (and adopted by Knox), C_1 is given as 1.0 if the period of the structure is larger than the characteristic earthquake period (T_C) and as 1.5 if the building period is less than 0.1 s. Linear interpolation is allowed between these period values. In ASCE 41-13, a more elaborate expression is provided

$$C_1 = 1 + \frac{\mu_{strength}{}^{-1}}{aT^2} \tag{50}$$

where a is a factor that depends on the site subsoil classification, T is the fundamental period of the structure, and $\mu_{strength}$ is the strength ratio defined by

$$\mu_{strength} = \frac{S_a}{V_y/W} \tag{51}$$

where V_y is the base shear capacity.

These expressions were derived from analytical and experimental investigations of earthquake response of yielding systems (ASCE 2014), considering the diaphragm to be rigid. It is beyond the scope of this paper to assess the adequacy of these expressions for structures with flexible diaphragms, which is an ongoing area of research activity at the University of Adelaide and the University of Auckland.

6. CONCLUSIONS

A method for the seismic analysis of in-plane loaded walls in a symmetric, low-rise building with flexible diaphragms has been presented. The method approximates the peak response of the in-plane walls using two modes of the structure assuming (1) equal ratio of diaphragm mass to the in-plane wall mass at all levels, and (2) equal diaphragm period at all levels. Under these conditions, the modal analysis has shown that two modes are typically sufficient to capture the majority of mass participation for regular low-rise buildings. Sensitivity analysis has been conducted to show that the two-mode analysis gives reasonable predictions of the base shear, even when the diaphragm configurations deviate from the assumed conditions. However, the predictions of interstorey drifts were less accurate, as the variations in the mass ratio and the period of the diaphragms resulted in modified mode shapes from those assumed in the two-mode analysis. Further studies are envisaged to address this issue.

An improvement to the linear static method has been proposed by utilising the two-mode analysis. Simple expressions are provided to capture the effect of flexible diaphragms. A simplified version of the method is also proposed to facilitate a rapid use of the procedure in practice. The proposed method provides an

improvement to the existing procedures, as it explicitly considers the dynamic interaction between the in-plane wall and the diaphragms. The method has been shown to produce results consistent with dynamic analysis for a wide range of diaphragm stiffness values in the elastic range of building behaviour. Further studies are needed to assess the general suitability of the linear static procedure for URM buildings, and how the inelastic displacement should be obtained from the corresponding elastic system response when flexible diaphragms are present.

ACKNOWLEDGMENTS

The financial support for this work was provided by the Australian Federal Government through an Australian Research Council grant (DP120100848) and an Australian Postgraduate Award.

REFERENCES

Abrams, D. P. (2001) "Performance-based engineering concepts for unreinforced masonry building structures", Progress in Structural Engineering and Materials, 3(1), 48-56.

ASCE (2014) "Seismic evaluation and retrofit of existing buildings", ASCE/SEI 41-13, American Society of Civil Engineers, Reston, Virginia.

Bruneau, M. (1994) "Seismic evaluation of unreinforced masonry buildings - a state-of-the-art report", Canadian Journal of Civil Engineering, 21(3), 512-539.

Chen, Y., and Soong, T. T. (1988) "State-of-the-art review seismic response of secondary systems", Engineering Structures, 10, 218-228.

Chopra, A. K. (2007) "Dynamics of structures – theory and applications to earthquake engineering", 3rd Edition. Pearson Prentice Hall, New Jersey.

Christopoulos, C., Filiatrault, A., and Folz, B. (2002) "Seismic response of self-centring hysteretic sdof systems", Earthquake Engineering and Structural Dynamics, 31, 1131-1150.

CSI (2012) SAP2000 v15, Computers and Structures Inc. Berkeley, CA.

FEMA (2000) "Prestandard and commentary for the seismic rehabilitation of buildings", FEMA 356, Federal Emergency Management Agency, Washington, D.C.

Fleischmann, R. B., and Farrow, K. T. (2001) “Dynamic behaviour of perimeter lateral-system structures with flexible diaphragms”, Earthquake Engineering and Structural Dynamics, 30, 745-763.

Giongo, I., Wilson, A., Dizhur, D, Derakhshan, H., Tomasi, R., Griffith, M., Quenneville, P., and Ingham, J. (2014) “Detailed seismic assessment and improvement procedure for vintage flexible timber diaphragms”, Bulletin of the New Zealand Society for Earthquake Engineering, 47(2), 97-118.

Kim, S.-C., and White, D. W. (2003) “MDOF response of low-rise buildings”, Final Report Project ST-5, Mid-America Earthquake Research Center, Georgia Institute of Technology.

Kim, S.-C., and White, D. W. (2004) “Linear static analysis of low-rise buildings with flexible diaphragms using the structural separation method”, Engineering Structures, 26, 83-93.

Knox, C. (2012) “Assessment of perforated unreinforced masonry walls responding in-plane”, PhD thesis, Department of Civil and Environmental Engineering, University of Auckland.

Krawinkler, H., Parisi, F., Ibarra, L., Ayoub, A., and Medina, A. R. (2000) “Development of a testing protocol for wood frame structures”, CUREE Report Np. W-03, Richmond, CA.

Lam, N., Wilson, J., and Venkatesa, S. (2005) “Accelerograms for dynamic analysis under the new Australian Standard for Earthquake Actions”, Electronic Journal of Structural Engineering, 5, 10-35.

Lay, D. C. (2003) “Linear algebra and its applications 3rd Edition”, Pearson Education, New Jersey.

Lee, H. J., Aschheim, M. A., and Kuchma, D. (2007) “Interstory drift estimates for low-rise flexible diaphragm structures”, Engineering Structures, 29, 1375-1397.

New Zealand Standard (2004a) “Structural design actions Part 5: Earthquake actions - New Zealand”, NZS 1170.5:2004, Standards New Zealand, Wellington, New Zealand.

New Zealand Standard (2004b) “Structural design actions Part 5: Earthquake actions - New Zealand - Commentary”, NZS 1170.5 Supp1:2004, Standards New Zealand, Wellington, New Zealand.

NZSEE (2006) “Assessment and improvement of the structural performance of buildings in earthquakes”, New Zealand Society for Earthquake Engineering, Wellington, New Zealand.

Sadashiva, V. K., MacRae, G. A., Deam, B. L., and Spooner, M. S. (2012) "Quantifying the seismic response of structures with flexible diaphragms", Earthquake Engineering and Structural Dynamics, 41(10), 1365-1389.

Standards Australia (2007) "Structural design actions. Part 4: Earthquake actions in Australia", AS 1170.4-2007, Standards Australia, Sydney, Australia.

Suarez, L. E., and Singh, M. P. (1987) "Seismic response of SDF equipment-structure system", Journal of Engineering Mechanics, 113(1), 16-30.

Tena-Colunga, A., and Abrams, D. P. (1992) "Response of an unreinforced masonry building during the Loma Prieta earthquake", Civil Engineering Studies – Structural Research Series No. 576, Department of Civil Engineering, University of Illinois at Urbana-Champaign.

Wilson, A., Quenneville, P., and Ingham, J. (2013) "Natural period and seismic idealization of flexible timber diaphragms", Earthquake Spectra, 29(3), 1003-1019.

Appendix A - Overview of Existing Methods

ASCE 41-13

ASCE 41-13 contains a linear static procedure for unreinforced masonry buildings with single-span flexible diaphragms with six stories or less in height. In this procedure, the fundamental period is calculated as given in Equation 3. The peak static force for each diaphragm is then obtained as in Equation 1. The static force calculated for each diaphragm is then distributed to the in-plane walls in accordance with their tributary masses, and the design actions in each component is evaluated.

Knox

The method by Knox considers the uncoupled fundamental periods of the in-plane wall (T_w) and diaphragms (T_i) separately. T_w may be evaluated by modelling the wall using frame elements, and T_i is evaluated from Equation 4. Using the calculated period, the diaphragm force is evaluated as

$$V_{di} = C_1 C_3 S_a(T_i) W_D \tag{A3}$$

where W_D is the tributary weight of the diaphragm. The in-plane wall base shear is calculated by

$$V_w = C_1 C_3 S_a(T_w) W_w \tag{A4}$$

where W_w is the total weight of the in-plane wall. The coefficients C_1 and C_3 have been adopted from FEMA 356, and account for the inelastic behaviour and P-delta effects respectively. The in-plane wall's base shear from Equation A4 is distributed up the height of the wall in proportion to the tributary wall mass at the i^{th} level. The equivalent static force at the i^{th} level is then approximated by the SRSS combination of the diaphragm and in-plane wall forces,

$$V_{si} = \sqrt{\left(\frac{V_{di}}{2}\right)^2 + (V_{wi})^2} \tag{A5}$$

where V_{wi} is the distributed in-plane wall's base shear.

In order to account for closely spaced modes, the total base shear is also evaluated by combining V_{di} and V_w using the complete quadratic combination (CQC) rule. If the sum of equivalent static forces calculated from Equation A5 is smaller than the base shear obtained using CQC, they are scaled up accordingly.

Note that while the SRSS estimation may be carried out without calculating T_w, the CQC base shear check requires the periods of all components.

Appendix B - Plots of C_B for Simplified Approach

The plots of base shear modification factor C_B generated for the design spectra of NZS 1170.5 are provided in Figure B1 for different site subsoil classes. The plots correspond to $T_w = T_B$ and can be used to simplify the proposed method.

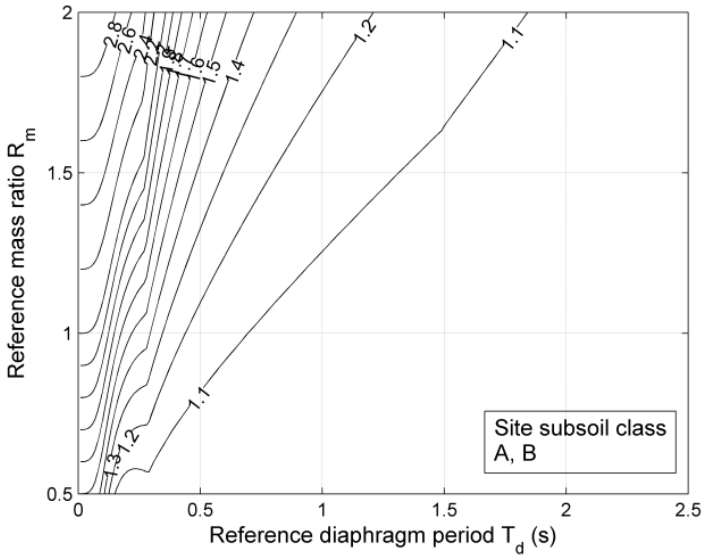

(a) C_B *for site subsoil class A or B*

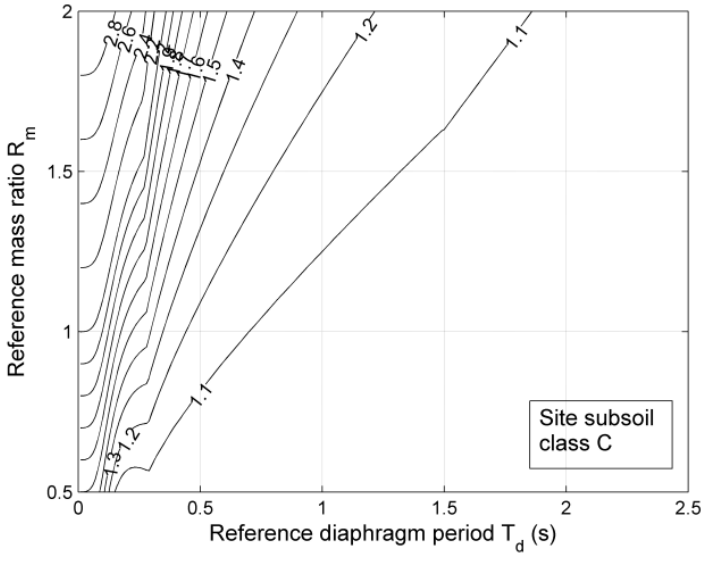

(b) C_B *for site subsoil class C*

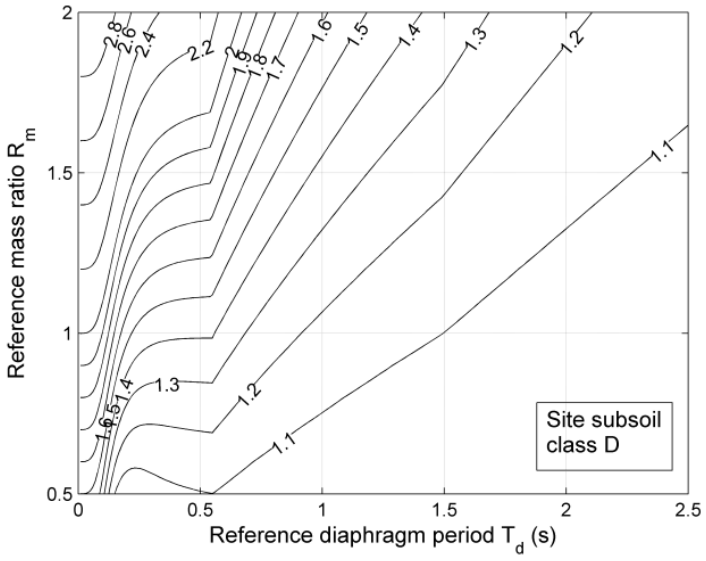

(c) C_B *for site subsoil class D*

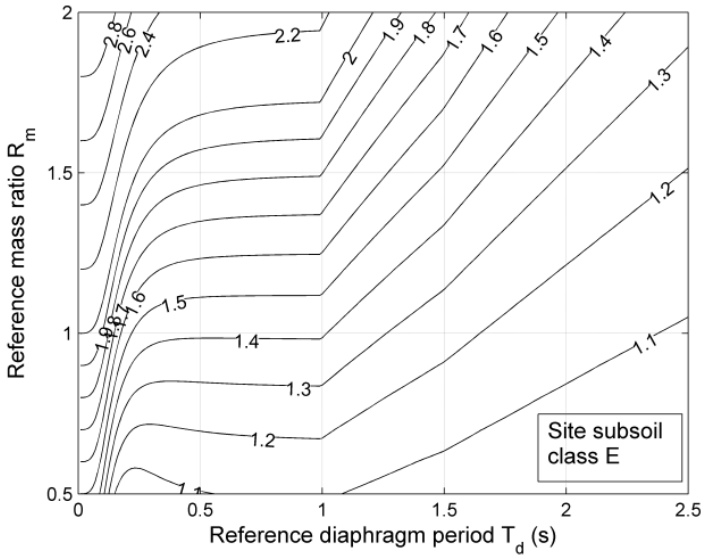

(e) C_B *for site subsoil class E*

Figure B1: Values of C_B for different site subsoil classes

CHAPTER 4

EQUIVALENT FRAME MODELLING

Background

This chapter presents a case study of a simplified numerical modelling of unreinforced masonry buildings that is used throughout the remaining sections of this thesis. The investigated modelling approach is a minor extension of the existing three-dimensional modelling used in the TREMURI software, in which several membrane elements are used to model the dynamic behaviour of the flexible diaphragms. The development of the model is described and the shortcomings/limitations are identified. A preliminary parametric study on the effect of diaphragm flexibility on the global building behaviour is presented.

List of Manuscripts

Nakamura, Y., Derakhshan, H., Sheikh, A. H., Ingham, J. and Griffith, M. C. (2016) "Equivalent frame modelling of an unreinforced masonry building with flexible diaphragms - a case study", Bulletin of New Zealand Society for Earthquake Engineering, 49(3), 234 – 244.

Statement of Authorship

Title of Paper	Equivalent frame modelling of an unreinforced masonry building with flexible diaphragms – a case study
Publication Status	☐ Published ☑ Accepted for Publication ☐ Submitted for Publication ☐ Unpublished and Unsubmitted work written in manuscript style
Publication Details	Nakamura, Y., Derakhshan, H., Sheikh, A. H., Ingham, J. and Griffith, M. C. (2016) "Equivalent frame modelling of an unreinforced masonry building with flexible diaphragms - a case study", Bulletin of New Zealand Society for Earthquake Engineering.

Principal Author

Name of Principal Author (Candidate)	Yasuto Nakamura
Contribution to the Paper	Prepared manuscript, developed model, performed all analyses
Overall percentage (%)	85%
Certification:	This paper reports on original research I conducted during the period of my Higher Degree by Research candidature and is not subject to any obligations or contractual agreements with a third party that would constrain its inclusion in this thesis. I am the primary author of this paper.
Signature	Date 26/8/16

Co-Author Contributions

By signing the Statement of Authorship, each author certifies that:

i. the candidate's stated contribution to the publication is accurate (as detailed above);

ii. permission is granted for the candidate in include the publication in the thesis; and

iii. the sum of all co-author contributions is equal to 100% less the candidate's stated contribution.

Name of Co-Author	Hossein Derakhshan
Contribution to the Paper	Contributed to research and manuscript
Signature	Date 26 Aug 2016

Name of Co-Author	Abdul H. Sheikh
Contribution to the Paper	Supervised and contributed to research and manuscript
Signature	Date 26/8/2016

Name of Co-Author	Jason M. Ingham
Contribution to the Paper	Contributed to manuscript
Signature	Date: 24 August 2016

Name of Co-Author	Michael C. Griffith
Contribution to the Paper	Supervised and contributed to research and manuscript
Signature	Date: 30/08/2016

Equivalent Frame Modelling of an Unreinforced Masonry Building with Flexible Diaphragms – A Case Study

ABSTRACT

A case study was conducted to investigate the applicability of the equivalent frame modelling for the nonlinear time-history analysis of unreinforced masonry buildings with flexible diaphragms. The dynamic responses calculated from the equivalent frame models were compared against shake table test results of a full-scale two-storey stone masonry building. The investigated modelling approach reflected the simplifications commonly assumed for the global analysis of buildings; namely, considering the diaphragms to behave elastically and neglecting the stiffness and strength contributions of the out-of-plane responding walls. The sensitivity of the analysis to different idealisations of the equivalent frame, as well as to the diaphragm stiffness values, were also investigated. Discussions are provided on the accuracies and limitations of the investigated modelling approach, which may serve as a useful guidance for practical application.

1. INTRODUCTION

Unreinforced masonry (URM) buildings make up a substantial proportion of existing building stock, and continue to pose large seismic risk in many parts of the world. In evaluating their seismic vulnerability, efficient numerical models are required, that are capable of simulating the inelastic building behaviour. The equivalent frame modelling procedure (Magenes & Della Fontana 1998) has been shown to be a promising practical approach capable of simulating the salient response mechanisms of URM buildings, without incurring the large computational penalty of finite element analysis.

The equivalent frame idealisation considers the in-plane response of a wall as comprising of deformable pier and spandrel elements connected to nodes, which may have rigid offsets (Figure 1(a)). The minimum deformable length of the piers (spandrels) is commonly assumed to be dictated by the smallest height (width) of adjacent openings. Alternatively, to account for the deformability of the node panels, the deformable length of piers may be extended making use of 30° lines emanating from the corners of the door or window openings as shown in Figure 1(a). The piers and spandrels are conceptually represented as elastic frame members with lumped nonlinearity capturing the shear or rocking failure modes (Figure 1(b)). The initial validation of the equivalent frame modelling procedure was focused on individual in-plane loaded walls in isolation (Magenes & Della Fontana 1998; Kappos et al. 2002; Salonikios et al. 2003).

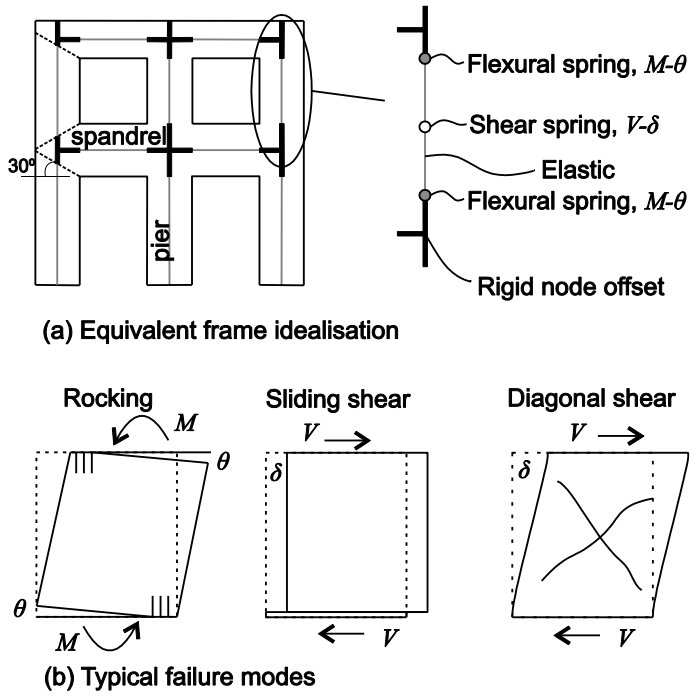

Figure 1. Equivalent frame idealisation and typical failure modes

Subsequent developments have explored the feasibility of modelling the global three-dimensional response of buildings by assembling two-dimensional equivalent frames coupled by diaphragms (Lagomarsino et al. 2013).

In such three-dimensional models, floor and roof diaphragms are often treated as stiffness contributing elements but do not have dynamic or vibration characteristics (Lagomarsino et al. 2013). However, it is well recognised that the in-plane motions of flexible timber diaphragms, which commonly exist in URM buildings, can dominate the response of these buildings. This recognition is reflected in some guidelines (ASCE 2014) where the natural frequency of a building is considered to be approximately equal to the frequency of the diaphragm itself. Measurements taken from an instrumented URM building with timber diaphragms during the Loma Prieta earthquake (Tena-Colunga & Abrams 1992) showed that the flexible diaphragms have the tendency of vibrating almost independently of the supporting walls, with amplified displacements and accelerations at their mid-spans. Similar behaviours were also observed in shake table tests by Costely and Abrams (1995). Evidence of significant diaphragm deformation was also found in at least one building during the 22 February 2011 Christchurch earthquake (Dizhur et al. 2011) where excessive in-plane diaphragm deformation was believed to have led to the out-of-plane collapse of a wall (Figure 2).

Figure 2. Out-of-plane wall failure caused by excessive diaphragm deformation (Dizhur et al. 2011)

Despite the importance of the dynamic characteristics of flexible diaphragms, the accuracy of an equivalent frame analysis incorporating such behaviour has not been investigated in detail so far. A notable exception is found in a recent study undertaken by Aleman et al. (2015) who developed a numerical model of a typology of URM buildings commonly found in New York City. In their model, the in-plane walls were represented by equivalent frames and the timber floor joists and sheathing were represented as elastic beam elements that were connected through nonlinear springs to capture nail-slip behaviour, together with calibrated rotational springs representing the one-way vertically spanning out-of-plane loaded walls.

Such detailed nonlinear modelling, however, poses several problems in practice. The modelling of a timber diaphragm requires an individual nail force-slip relationship, which is typically not available in seismic codes and guidelines. The actual nonlinear behaviour of diaphragms also depends on the specific locations of the nail connections and on the spacing of the nail couple, which may be difficult to capture. The inclusion of one-way vertical bending corresponding to the out-of-plane deformation of walls, as done in Aleman et al. (2015), increases computational demand but does not necessarily enhance the analysis accuracy; recent research (Derakhshan et al. 2015) has suggested that even for one-way (vertically) spanning wall modelling, an additional failure mode needs to be considered due to diaphragm flexibility. Such detailed modelling for the out-of-plane loaded wall is considered to be impractical.

The aim of this paper is to explore the applicability of the equivalent frame modelling approach for the prediction of global response of URM buildings with flexible diaphragms, considering the above limitations currently faced by practising engineers. To this end, a relatively simple modelling approach based on commonly accepted assumptions is investigated. Specifically, the diaphragms are represented by elastic membrane elements, while the out-of-plane wall stiffness and strength contributions are neglected. Dynamic test data of a full-scale stone masonry building with strengthened timber floor and roof (Magenes et al. 2014) is used to verify the potential, and to identify the limitations, of the modelling

approach. The sensitivity of the analysis for different choices of modelling are also explored through two different equivalent frame idealisations and diaphragm stiffness values. While the analyses are conducted using TREMURI (Lagomarsino et al. 2013) with certain modelling concepts specific to that program, results reported in this paper have general applicability.

2. CASE STUDY BUILDING

A two-storey stone masonry building with a timber floor and a timber roof diaphragm tested at the EUCENTRE (Magenes et al. 2014) is analysed in this study. This is a retrofitted building (Figure 3), whose diaphragms had been strengthened with a layer of diagonal timber boards nailed to the original single straight sheathing. In addition, the connections between the floor/roof diaphragms and the walls were also strengthened. At the floor level, 140 mm x 140 mm x 10 mm steel sections were attached to the interior faces of the walls, and bolted through the thickness of the wall using 14mm diameter threaded bars. At the roof level, a continuously reinforced masonry ring beam was constructed using solid brick exterior layers and a cement grouted core. Two 12mm or 16mm diameter longitudinal reinforcements were placed in the central core, with horizontal truss reinforcements connecting the two brick faces at each bed joint. These strengthening measures ensured the global building behaviour to take place, while still allowing some level of diaphragm flexibility.

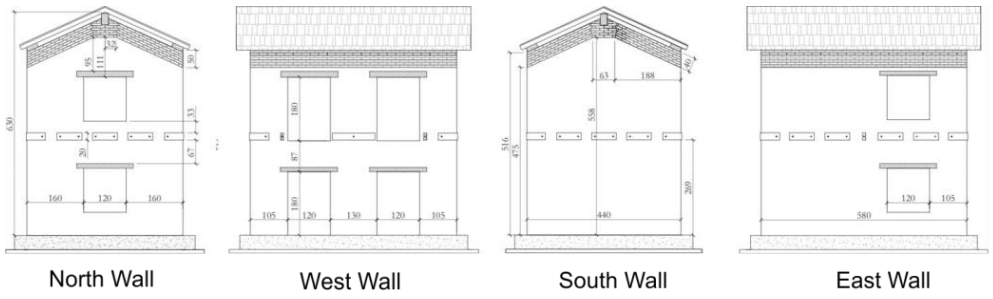

(a) Wall elevations

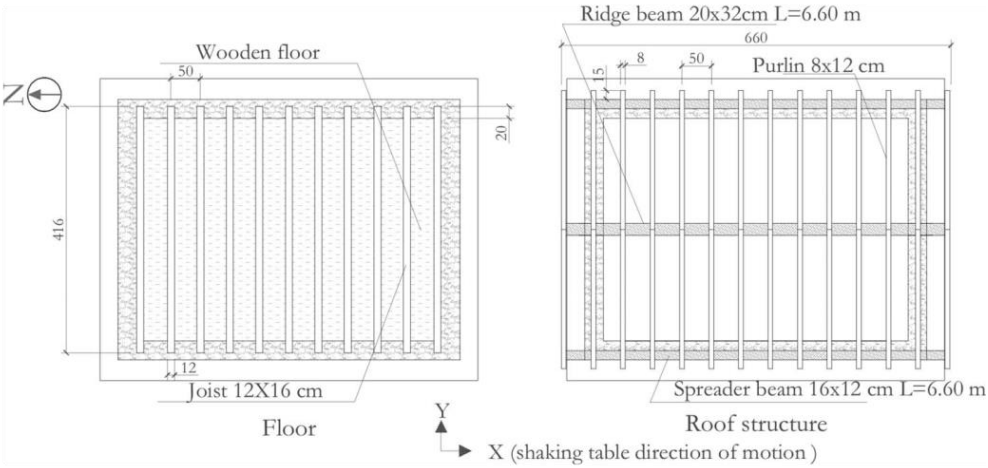

(b) Floor plan view

Figure 3. Construction details of tested building, dimensions in cm (Magenes et al. 2014)

The building was tested under shake table excitations using the motions of the 15 April 1979 Montenegro earthquake measured at the Ulcinj-Hotel Albatros station with some scaling (Figure 4). The nominal peak ground acceleration (PGA) was gradually increased from 0.05g to 0.7g, for which the actual acceleration (peak) of the table motion varied from 0.06g to 1.16g. In this paper, the excitation levels are referred to by the nominal PGA.

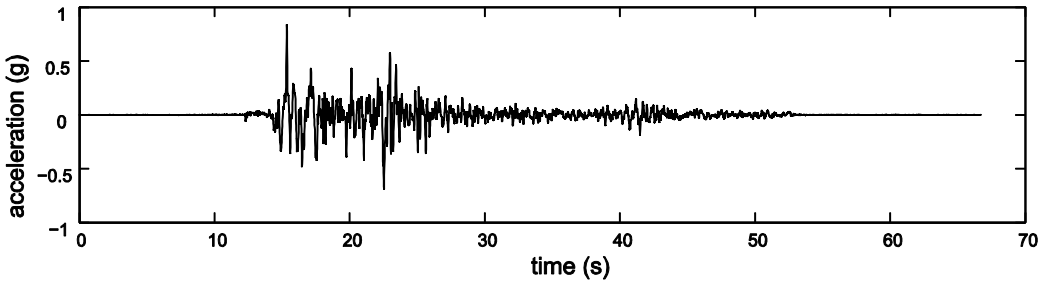

Figure 4. Table acceleration for the 0.6 g test

The building suffered some damage during its transportation to the testing facility. Thus, the initial stiffness of the building would have been smaller than if the building had remained undamaged at the start of testing. The response of the building was almost elastic up until the 0.5g excitation. Significant

cracking appeared during the 0.6g test sequence, followed by the near-collapse state with the 0.7g excitation. A detailed description of the response characteristics of the building can be found in Magenes et al. (2014).

3. MODELLING APPROACH

3.1 General Descriptions of Numerical Model

Figure 5 schematically shows a three-dimensional building model built up as an assemblage of two dimensional components. Each wall is idealised as equivalent plane (2D) frame members consisting of piers and spandrels. These members are connected to nodes (2D wall nodes) at their two ends, with each node having in-plane local degrees of freedom u_{loc}, u_z and ϕ_{rot} (e.g. $u_{loc} = u_x$ for a wall laying in the *x*-*z* plane). Three-dimension nodes (3D wall nodes) are used at the intersections of walls, for example at corners of a building, with the global degrees of freedom u_x, u_y, u_z, ϕ_x and ϕ_y. These degrees of freedom are obtained by projecting the local degrees of freedom of the intersecting 2D walls onto the global coordinates. As the contributions of out-of-plane stiffness and strength of a wall are usually small compared to its in-plane stiffness and strength, the out-of-plane degrees of freedoms are neglected. Furthermore, the compatibility of the two intersecting walls is strictly satisfied for the vertical translation, but not for the horizontal translational or the rotational components. This modelling concept allows the direct adoption of the 2D equivalent frame idealisation developed for the individual walls in isolation. In this way, flange effects at wall intersections associated to normal deformations are captured in an approximate way, allowing free warping of the flanged section, whereas no flange effect is captured for shear deformation.

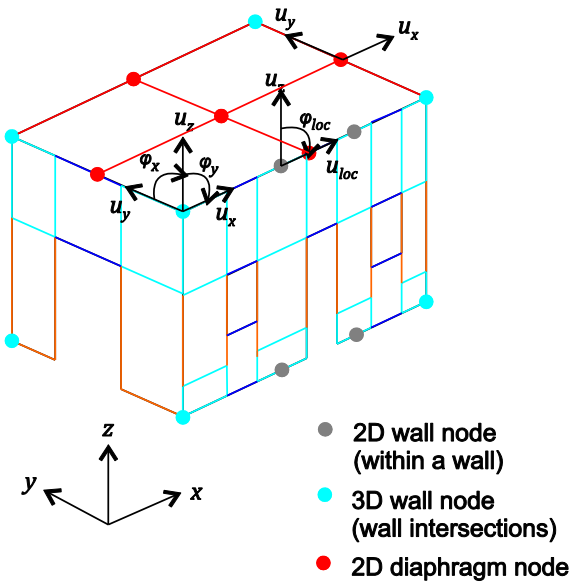

Figure 5. Modelling concept

The diaphragms are modelled with plane stress or membrane elastic elements where the element node (2D diaphragm node) consists of two in-plane (horizontal) translational degrees of freedom, which permit a linear variation of displacements within an element. These elements are defined by the Young's modulus, shear modulus, and the thickness of the diaphragms. In this study, four elements are used to model a single diaphragm, which is the simplest possible idealisation that can capture the vibration characteristics of the diaphragms.

The masses are assigned by considering simple tributary areas for inertial (horizontal) loading, as shown in Figure 6 and Figure 7 respectively for the floor and wall masses. It should be noted that distributing the mass in this manner does not provide the correct internal force distribution under gravity loading. Thus, additional static nodal forces (vertical forces and moments) are applied in order to obtain the correct gravity forces prior to the dynamic analysis.

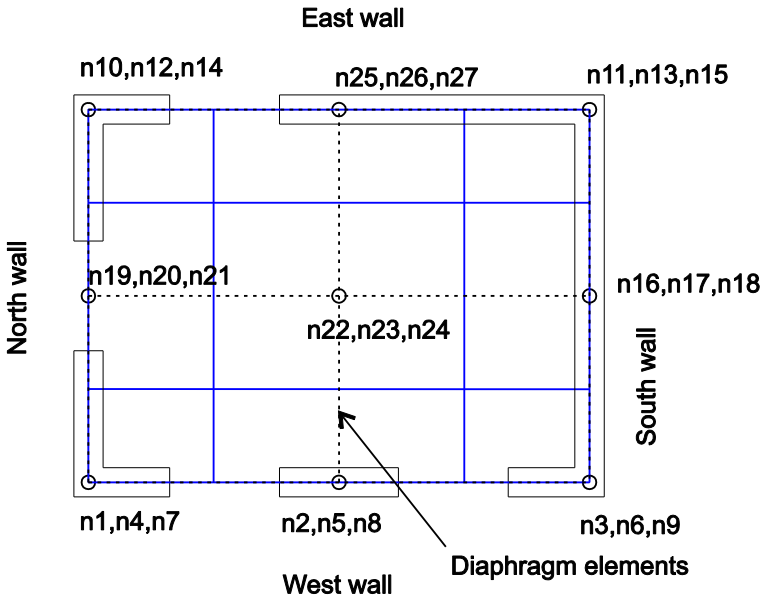

Figure 6. Tributary areas for the distribution of the floor mass

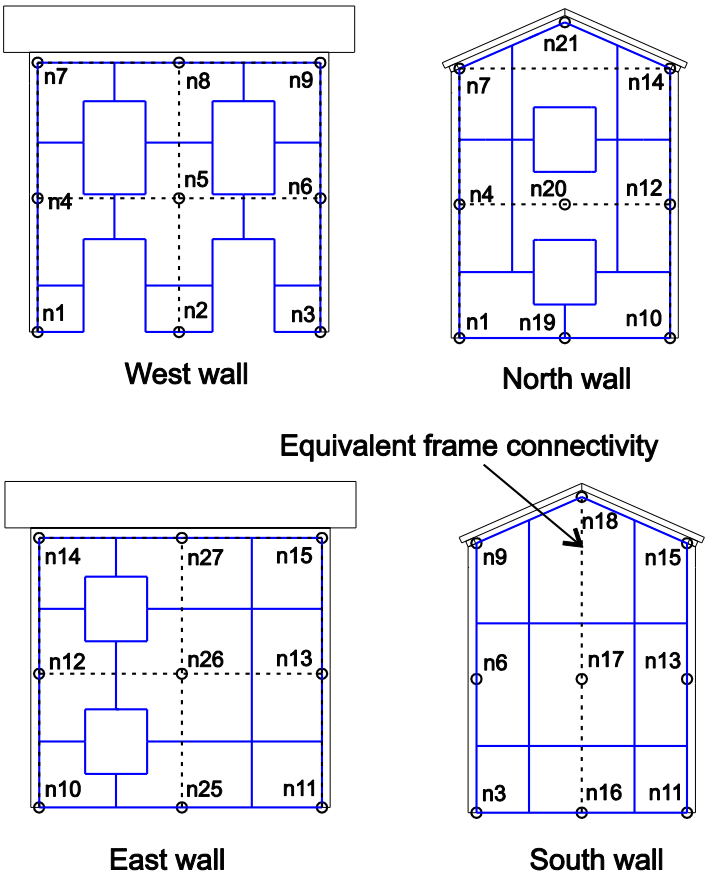

Figure 7. Tributary areas for the distribution of the wall mass

3.2 Limitations of Diaphragm Modelling

The model used for the diaphragms in this study has several limitations, which warrant clarification. Specifically: (1) the diaphragms are considered to be elastic even though the actual behaviour of a timber diaphragm can exhibit highly nonlinear material behaviour, (2) full compatibility between the walls and diaphragms is assumed, and (3) only four elements are used to model the diaphragm. These issues are discussed in this section.

Considering the first limitation, even though flexible timber diaphragms can exhibit large deformations, the amount of energy dissipation due to inelastic deformation is usually limited, and the strength degradation is typically not detected for the conceivable range of deformation (Giongo et al. 2014). For these reasons, the elastic representation of flexible diaphragms in URM buildings can be considered appropriate.

The second assumption related to the full compatibility condition between the walls and diaphragms may not always be appropriate for existing buildings, where floor joists may simply rest within a recess created in the walls without having any strong connection. However, buildings with such poor connections tend to undergo local collapses, before the in-plane wall capacities can be reached. The global building response governed by the in-plane wall resistances can occur only if the wall-diaphragm connections are improved and the local failures are prevented. Hence, assumption of full compatibility between the diaphragms and walls can also be considered as an appropriate simplification when the analysis concerns the global response of the building. Nevertheless, it is possible to include connection flexibility in the stiffness calculation of the diaphragm elements, as suggested by some researchers (Brignola et al. 2012).

The lumped mass modelling of a diaphragm using four membrane elements introduces some inaccuracy. In particular, the peak inertial force of the diaphragm may be reduced to 60% of the more realistic, distributed mass idealisation, due to the smaller effective mass (Appendix A). Despite this discrepancy, lumped mass idealisations have been used successfully in past studies (Tena-Colunga & Abrams 1992; Kim & White 2004). The reason for this success may be that the discrepancy becomes more significant when the diaphragm flexibility increases, but the natural periods of such flexible diaphragms typically fall in the velocity- or displacement-sensitive region of the response spectra associated with small spectral accelerations, or force demands, compared to those of the stiff masonry walls. Hence, the discrepancy of the lumped mass diaphragm idealisation may not significantly affect the overall computed building

responses. In this study, lumped mass idealisation of the diaphragm is considered to be an acceptable simplification, given the simplified nature of the overall model.

3.3 Macroelement Definition

The inelastic behaviours of the piers and spandrels are simulated using the macroelement definition of TREMURI (Penna et al. 2014). Each macroelement (pier or spandrel) consists of three segments (Figure 8) with eight in-plane degrees of freedom. The degrees of freedom consists of axial (w_i and w_j) and lateral (u_i and u_j) translations and a rotation (ϕ_i and ϕ_j) at element ends *i* and *j*, with two rigid-body displacements defined in the middle segment (w_e and ϕ_e). The top and the bottom interfaces capture the combined axial-rocking interaction and the shear behaviour is concentrated in the middle segment. The axial-rocking behaviour accounts for the limited compressive capacity, while the strength and stiffness degradations occur under shear deformation, as governed by an internal damage parameter. The material properties used in the present analyses (Table 1) were obtained from the results of complementary component tests as part of the experimental campaign (Magenes et al. 2010).

Table 1. Masonry material properties from component tests

Young's modulus (MPa)	Shear modulus (MPa)	Compressive strength f_m (MPa)	Cohesion f_{v0} (MPa)	Friction coefficient μ
2537	841	3.28	0.14	0.14

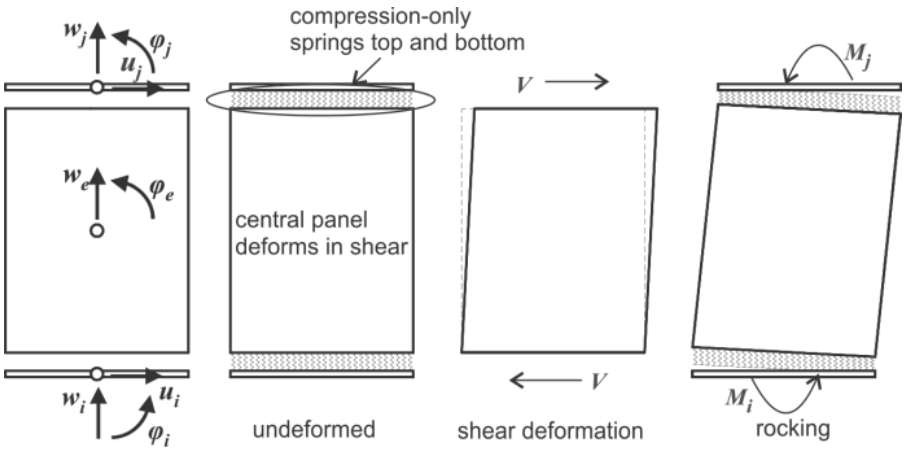

Figure 8. Kinematics of macroelement (Penna et al. 2014)

3.4 Analysis Cases

In order to explore the uncertainties associated with the choice of modelling, four different analysis cases were considered. These cases corresponded to two different idealisations of the equivalent frame definitions, and diaphragm stiffness values calculated using two different approaches.

The two equivalent frame idealisations of the walls oriented in the direction of loading are shown in Figure 9. The first idealisation corresponds to the "full" rigid offsets of the nodes where the rigid zones extend across the full width or the depth of pier and spandrel. The second pattern more accurately reflects the actual crack patterns of the tested building, capturing both the initial damage suffered during the transportation of the building as well as the crack pattern observed from the final stage of testing (reported in a subsequent section of this paper). The second idealisation was developed considering the following:

- the rigid nodes on the upper storey of the West wall were removed to reflect the cracking occurred during the transportation of the tested building, which separated the reinforced masonry beam from the wall;
- the effective heights of the exterior piers were increased to account for the diagonal crack lines observed in the final run of the test; and
- the thickness of the timber lintels were omitted from the spandrel depth.

Figure 10 shows the two equivalent frame idealisation (of Figure 9) superimposed on the final crack patterns observed from the shake table tests. The consideration of the diagonal crack patterns resulted in the increase in the effective (or deformable) heights of the exterior piers of approximately 1.1 to 1.3 times the "full" rigid offset case. In practice, the effective heights reflecting the likely crack patterns may be determined, for example, by making use of assumed 30º crack lines (Figure 1(a)) or by using empirical effective heights derived by Dolce (1989).

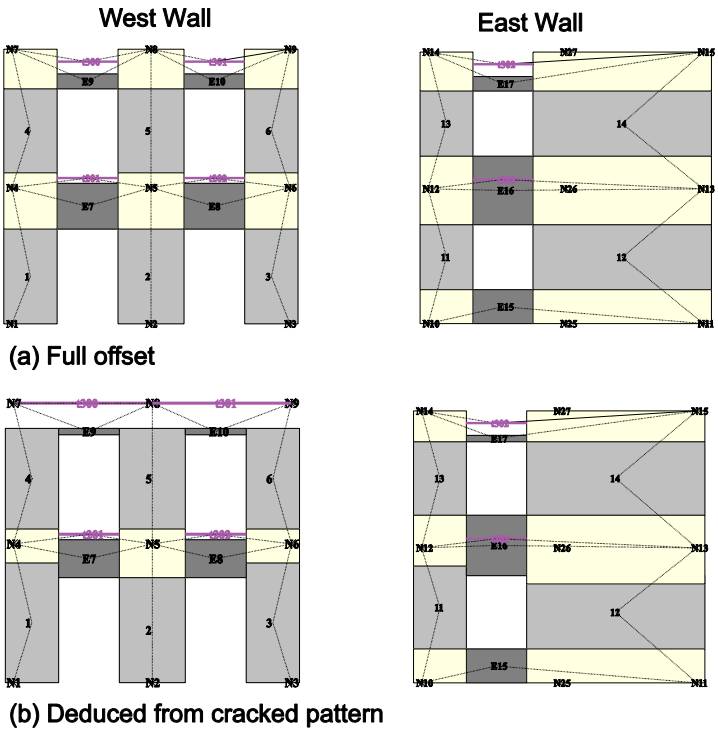

Figure 9. Equivalent frame idealisation of longitudinal walls

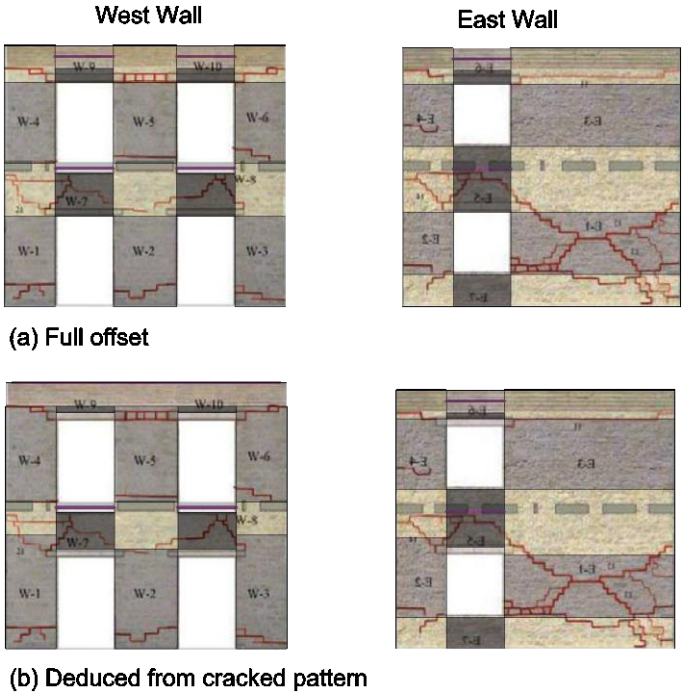

Figure 10. Equivalent frame idealisations superimposed on the final crack patterns

The two diaphragm stiffness values considered in the present analyses are summarised in Table 2, where the stiffness values (G_d) are defined as the material shear modulus multiplied by the thickness of

diaphragm. The first value (D1) corresponds to the expected diaphragm stiffness suggested by ASCE 41-13 (ASCE 2014). The second stiffness value (D2) was calculated more rigorously using the procedure proposed by Brignola et al. (2012), by considering the timber joists to act as flexural beams in parallel. In the latter approach, the interior joists were assumed to be pinned at wall connections, while the end joists were fixed, with the fixity provided by the perimeter steel beams. In addition, the steel beam and the uncracked portion of the masonry wall, as observed from the final test run, were also considered to provide additional stiffness for the floor diaphragm. For the roof diaphragm, the perimeter reinforced masonry beam was included in the stiffness calculation.

The four models analysed were:

- Case 1: full rigid offset with D1
- Case 2: full rigid offset with D2
- Case 3: cracked pattern with D1
- Case 4: cracked pattern with D2

Table 2. Diaphragm stiffness values corresponding to retrofitted floor and roof with large joist cross sections

Type	Diaphragm stiffness G_d (kN/m)	
	Floor	Roof
D1	3150	3150
D2	7036	5189

4. ANALYSIS RESULTS AND DISCUSSIONS

The accuracies of the numerical models were assessed by comparing the results predicted by these models with the experimental data in terms of the modal properties (frequencies and mode shapes), peak displacements and the distribution of damage.

The modal properties are presented in Figure 11 and Figure 12 for the experiment and numerical results respectively. The experimental mode properties reported by Magenes et al. (2014) were identified from the signal analysis of the ambient and random vibrations with peak table accelerations ranging between ± 0.03g. The mode shapes and frequencies of Figure 11 were obtained prior to the 0.05g test run, and hence represent the initial (elastic) mode properties of the experimentally tested building.

The same number of significant modes in the direction of excitation were identified from the experimental results and the numerical analysis. The fundamental mode of vibration in the direction of excitation is reasonably well captured by all analysis models. It can be seen that the increase in the displacement value up the height of the building is better captured when the diaphragm stiffnesses are calculated using the more refined procedure (Cases 2 and 4). In particular, the closest fundamental mode shape is achieved by Case 4, where the mid-span deformations of the diaphragms relative to the supporting walls are the smallest. In general, the numerical models exhibit larger deformations of the diaphragms relative to the walls, and underestimate the fundamental frequency in comparison to the experimental result.

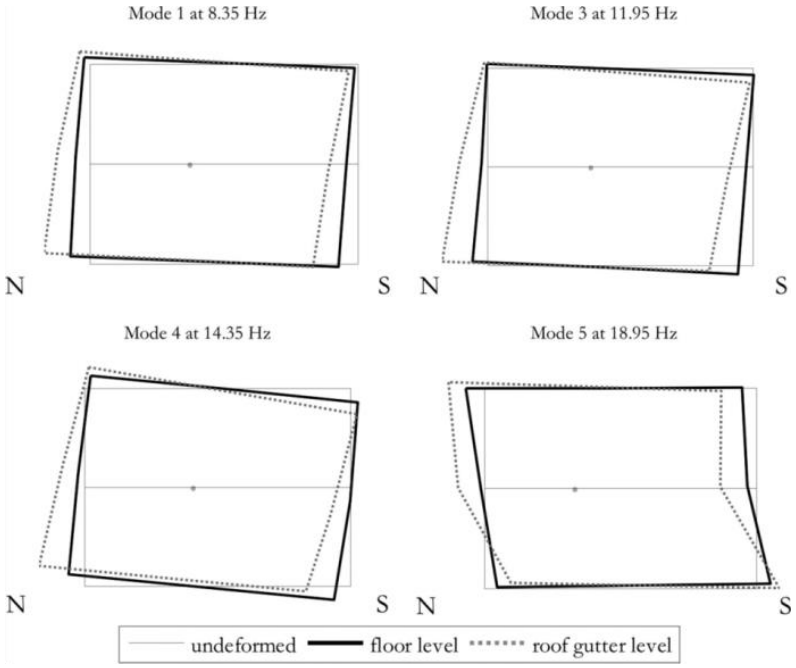

Figure 11. Mode shapes and frequencies identified from ambient and random vibrations (Magenes et al. 2014)

In contrast to the fundamental mode, the displacement shapes of the higher modes are not captured so well. The out-of-phase vibration of the floor and the roof diaphragms is more pronounced in the numerical analysis compared to that observed experimentally (2nd significant mode). The 3rd experimentally observed mode resembling the rotation of the diaphragms as a rigid-body could not be identified by the numerical models. The highest significant mode shape found in the experiment appears to be a mixture of the two highest modes predicted by the numerical models.

The larger diaphragm displacements and the reduced torsional rotation are due to the lack of coupling between the diaphragms at adjacent levels, as well as a lack of coupling between diaphragms and the in-

plane loaded walls. This coupling is provided by the out-of-plane deformations of walls, which were neglected in the analysis. The implication is that the out-of-plane walls may play an important role (particularly if the height-to-thickness ratio of the wall is not large, as in the tested building), at least within the elastic range of the building response.

The notion that the out-of-plane walls affect the elastic building response can also be inferred from the normalised Fourier amplitudes of displacements calculated at the diaphragm mid-spans (Figure 13). For the 0.4g excitation (when the building remains almost elastic), the numerical analyses show large responses occurring near 10 Hz, which corresponds to the natural frequency of the diaphragm. In contrast, the experimental data do not show significant peaks corresponding to those frequencies. This discrepancy may be due to the effect of out-of-plane motions of walls, which act to "restrain" the independent motions of the diaphragms.

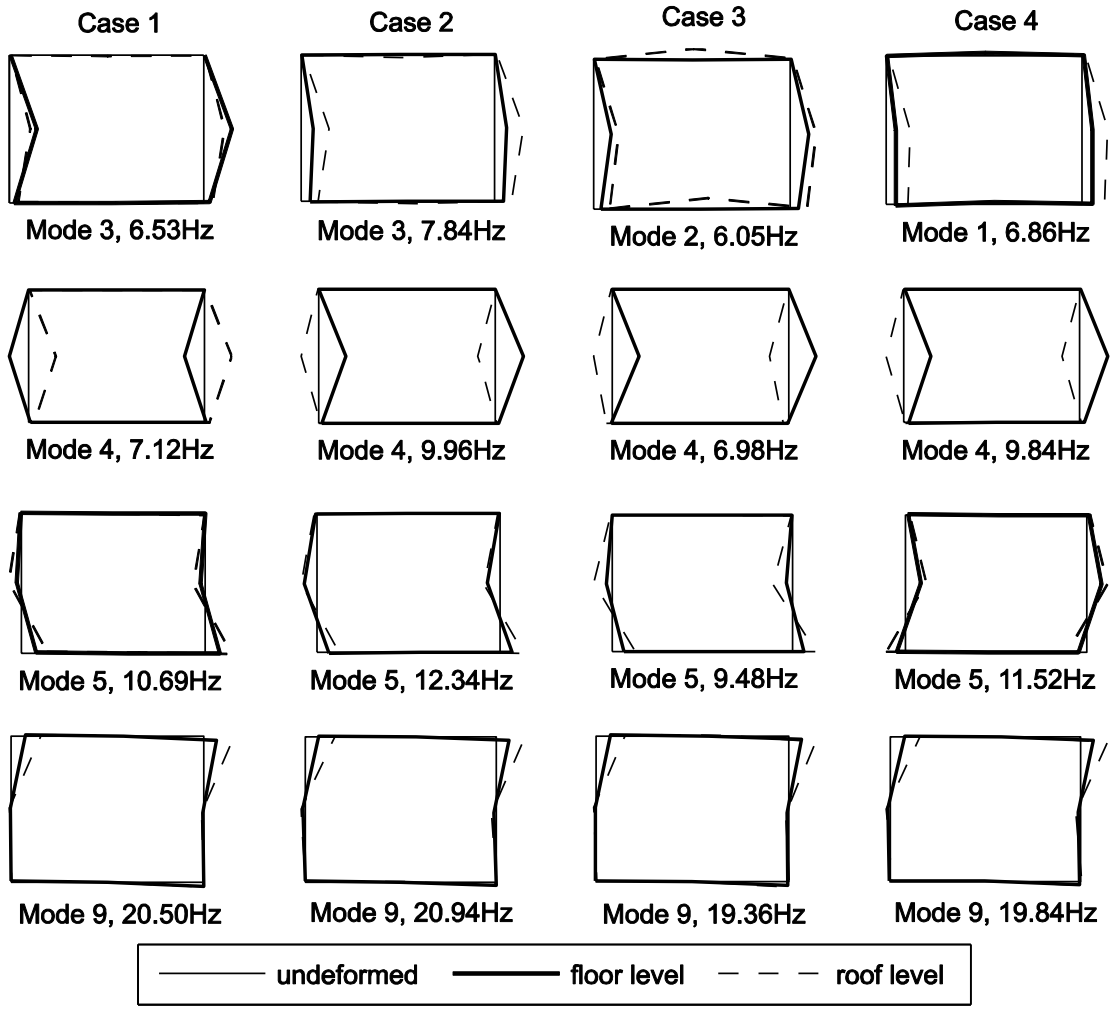

Figure 12. Significant mode shapes and frequencies from numerical analysis

The importance of the out-of-plane loaded walls to the global building response appears to become less significant as the building becomes inelastic, which is reflected in the form of increased consistency of the Fourier amplitude for the 0.6g excitation. However, Figure 13 shows that this increased consistency is due to the reduced diaphragm motion as the in-plane loaded walls become inelastic, and may not necessarily be due to the reduced effect of the out-of-plane responding walls. Nevertheless, neglecting the out-of-plane wall appears to be generally more appropriate in the inelastic range of the building response.

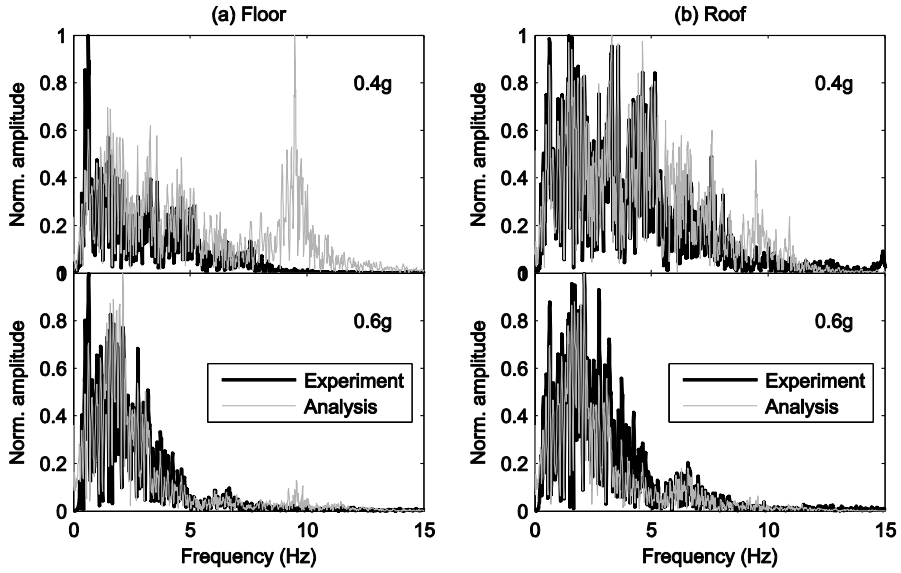

Figure 13. Normalised Fourier amplitudes of displacements at (a) floor mid-span, (b) roof mid-span for Case 4.

The peak displacement envelopes found experimentally, as well as numerically, are compared in Figure 14 for the West and East walls as well as at the diaphragm mid-spans. The results corresponding to 0.4g, 0.5g, 0.6g and 0.7g excitation intensities are shown for the four analysis cases. The general trends of the experimental results show that the peak displacements of the walls and the diaphragms approach towards each other as the excitation intensity increases. This trend is captured by all numerical models also. In general, the sensitivity of the analysis to the diaphragm stiffness is small, although the elastic response (0.4g and 0.5g intensities) is affected to some degree. The discretisation of the equivalent frame appears to have more importance. The upper storey displacements of the West wall are better captured by Cases 3 and 4 in the elastic range, implying that the equivalent frame idealisation based on the cracked pattern provides a better correlation with the experimental data. However, when significant inelastic response occurs during the 0.7g excitations, no significant differences of these responses predicted by the four

different models are found, and all models exhibit soft-storey behaviour with damage concentration in the ground storey.

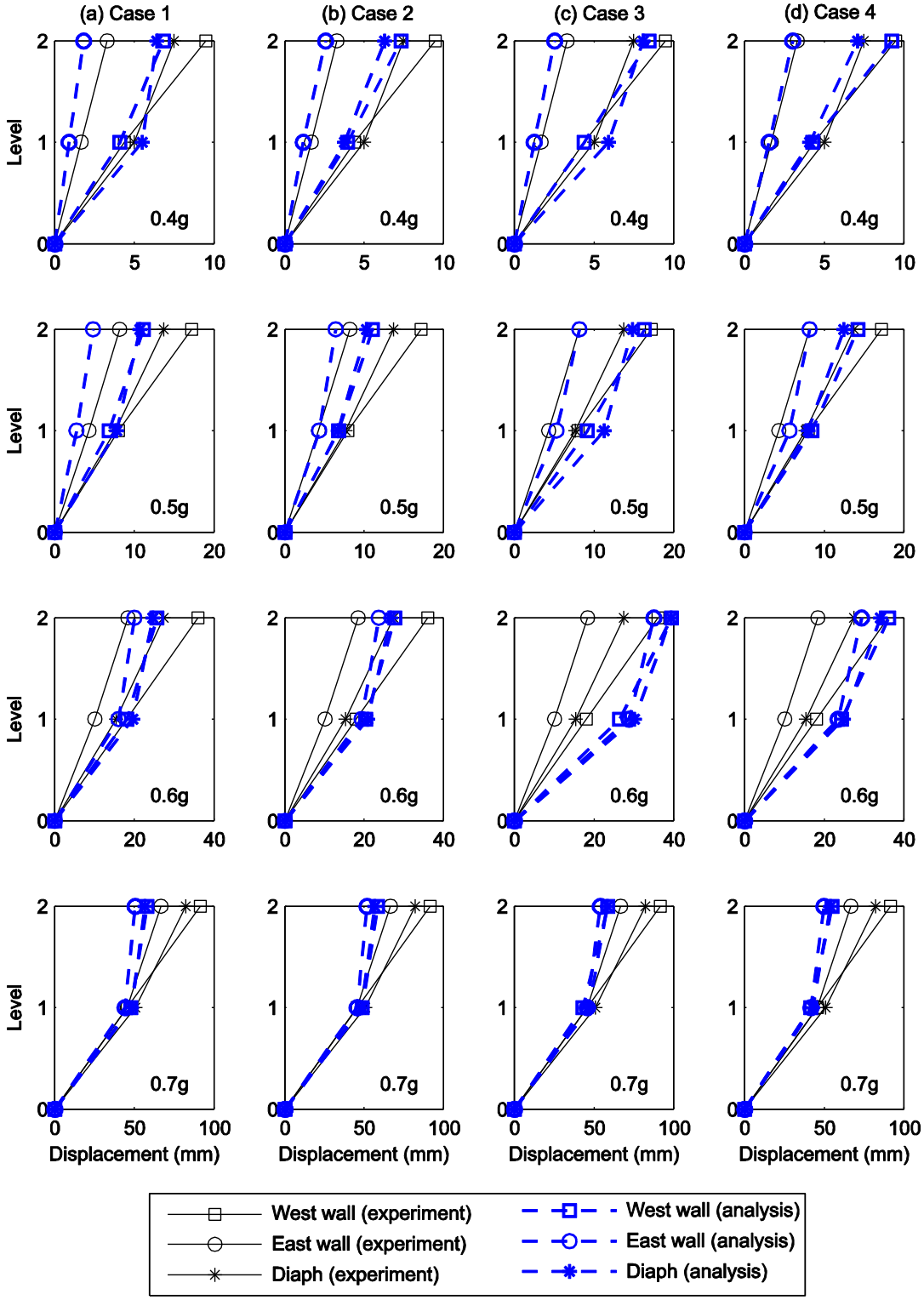

Figure 14. Comparisons of peak displacement envelopes

The distribution of damage is assessed using the ratios between the rotations due to rocking and drifts due to shear (δ_b and δ_s) and their corresponding ultimate capacities ($\delta_{b,ult}$ and $\delta_{s,ult}$) for a given macroelement. The rocking rotations and shear drifts are expressed as the flexural and the shear components of chord rotation (Penna et al. 2014) (Figure 8), which may be expressed as

$$\delta_b = \frac{\phi_i + \phi_j}{2} + \phi_e \tag{1}$$

$$\delta_s = \frac{u_j - u_i}{h} + \phi_e \tag{2}$$

where h is the deformable height of the pier or length of the spandrel. The definitions of the other variables are given in Figure 8.

The ultimate rocking and drift capacities obtained from the component tests (Magenes et al. 2010) were $\delta_{b,ult}$ = 0.6 % and $\delta_{s,ult}$= 0.3 %, which were used in the present study. These values corresponded to the deformations of the statically tested piers when the lateral resistance reduced to 80% of the peak value. The damage ratios are hence defined as $DL_b = \delta_b/\delta_{b,ult}$ and $DL_s = \delta_s/\delta_{s,ult}$ for rocking and shear respectively. Ratios greater than 1 indicate the notional failure of that component under the considered failure mechanism for the purpose of seismic assessment.

The damage ratios estimated for the 0.6g and 0.7g excitations are compared against the experimental crack patterns in Figures 15 and 16 respectively. The top and bottom values for each element of the figures indicate DL_b and DL_s, respectively. Results for the analysis Cases 2 and 4 are shown, and where the damage ratios exceed 1, indicative failure patterns are also shown (straight lines at the element ends indicate the rocking failure, and the diagonal lines across the element indicate the shear failure). For the 0.6g excitation intensity, the analysis based on Case 4 predicted rocking-dominant behaviour of the West wall, which is consistent with the experimental observation. In contrast, Case 2 predicted predominant shear damage. Hence, the damage mechanism is also better captured when the equivalent frame idealisation is based on the actual crack patterns. For the 0.7g excitation, however, both models show qualitatively identical damage distribution, which indicated that they generated almost identical displacements. At this near-collapse state, however, the predicted failure patterns are not in good agreement with the experimental results. In particular, for the West wall, the numerical analysis shows a failure governed by shear damage, while the experimental crack patterns actually indicate predominantly rocking failure.

Comparing the peak displacement shapes (Figure 14) and the damage distributions for the 0.7g excitation, the rocking responses of the upper storey piers of the West wall are found to be generally underestimated by the numerical analyses. A number of variations of the material properties were investigated with the aim of achieving larger upper storey (rocking) deformations for the final test run. However, in all simulations, initial flexural-rocking behaviour of the bottom storey piers was followed by significant shear damage. Once shear damage occurred, the models underwent soft-storey collapse, and the increased deformation of the upper-storey could not be attained. To some extent, this outcome may be considered as the limitation of the equivalent frame approach in capturing the dynamics of extensively damaged URM buildings.

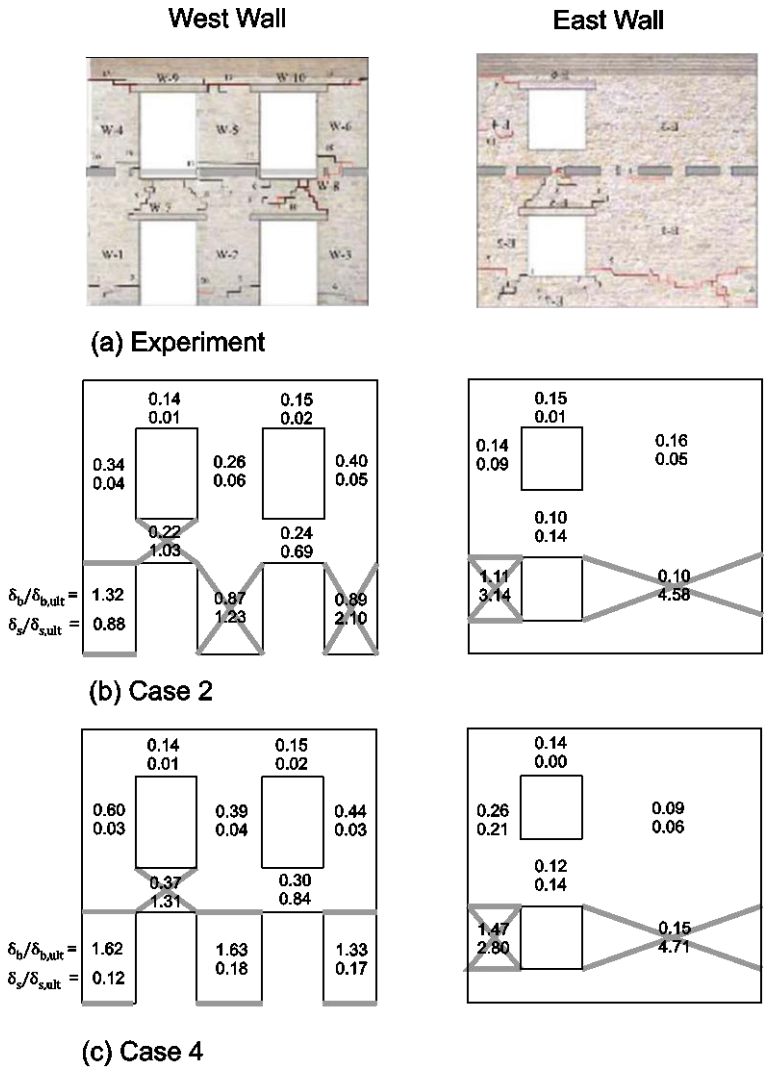

Figure 15. Comparison of (a) experimental crack patterns, (b) damage ratios predicted by Case 2, and (c) damage ratios predicted by Case4, for 0.6 g excitation.

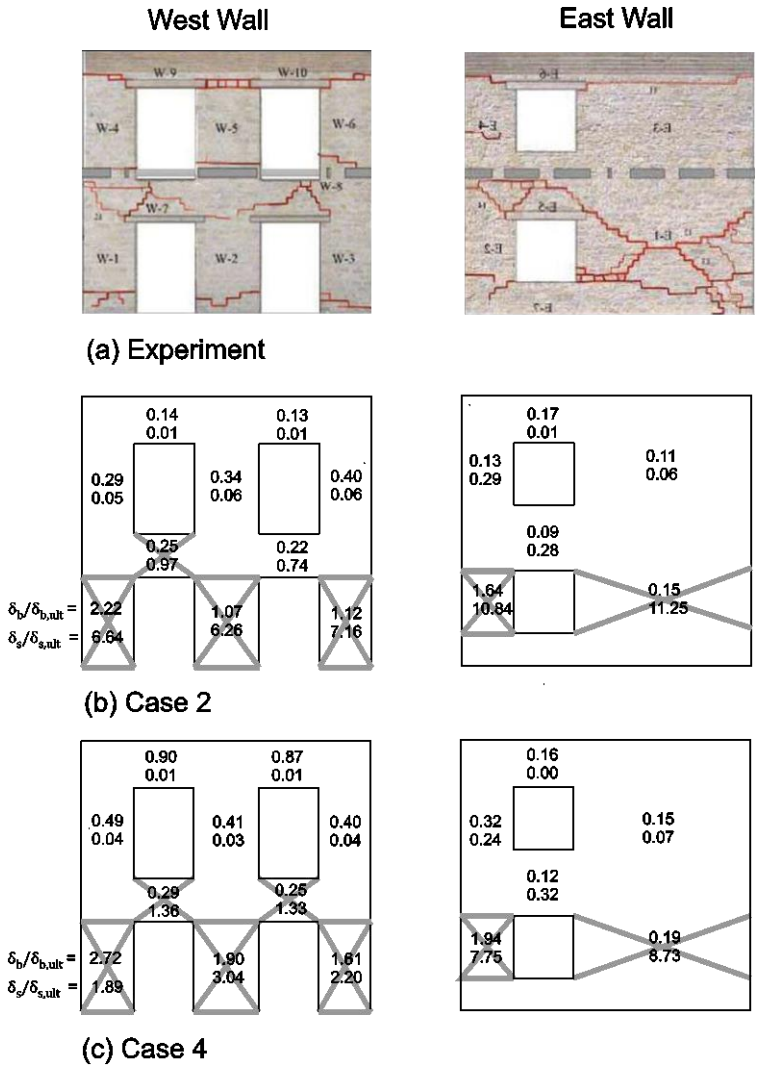

Figure 16. Comparison of (a) experimental crack patterns, (b) damage ratios predicted by Case 2, and (c) damage ratios predicted by Case4, for 0.7 g excitation.

5. INFLUENCE OF DIAPHRAGM FLEXIBILITY

The sensitivity of the building response due to relatively large diaphragm flexibility was investigated numerically. Using the analysis Case 4, the stiffnesses of the floor and the roof diaphragms were reduced from their original values (D2 in Table 2) to 0.005 times these original values. The stiffness values of 0.005 times the original values are likely to be unrealistically low for the test building, but were analysed to observe the general trends of the responses. Figure 17 shows the peak displacement variations of the West and the East walls at the roof level (u^r_{west} and u^r_{east} respectively) as well as the peak deformation of the roof diaphragm mid-span relative to the walls (Δ^r_d). Note that Δ^r_d is the diaphragm displacement relative to the average displacement of the in-plane loaded walls, and not to the ground. The peak deformations of the floor diaphragm showed similar trends to those of the roof diaphragm and are not

shown for clarity. The results correspond to the 0.6g excitation, and are plotted against the average diaphragm period (T_d) of the floor and the roof (the two diaphragms had almost identical period values). The diaphragm periods approximately corresponding to the diaphragm stiffness D1 (Table 2) and the lower-bound stiffness suggested by ASCE 41-13 (ASCE 2014) are also indicated, which represents single straight sheathing diaphragms. It can be observed that the diaphragm flexibility has significant effects on the seismic demands of the in-plane response of walls. In particular, for the West wall, which is more flexible, a displacement amplification of 220% is observed between the as-built diaphragm D2 and the lower-bound values.

Such amplification is due to two factors associated with flexible diaphragms; namely, (1) the variation of the diaphragms' inertial forces and (2) reduced coupling between the walls when the diaphragm are flexible. The effect of the first factor can be seen in Figure 18, where the spectral acceleration of the 0.6g table motion is plotted with respect to the diaphragm periods (normalised with respect to values corresponding to the original diaphragm). The comparison between the spectral accelerations and the peak wall displacements (Figure 17) indicates that the wall displacement amplifications occur when the spectral accelerations (or inertial forces) of the diaphragms are amplified. Once the spectral acceleration is reduced for T_d greater than approximately 0.7 s, the peak wall displacement is also reduced. The peak inertial force of the diaphragm hence directly affects the displacement demands of the walls. This observation also implies that the amplification is dependent on the ground motion characteristics. The second factor exacerbates the amplification of the weaker/flexible side (i.e. West wall) due to the limited coupling provided by flexible diaphragms in redistributing the internal forces.

It can be seen that the peak diaphragm deformation (Figure 17) closely reflects the spectral displacement (Figure 18), suggesting that the diaphragm deformation may be estimated directly from the elastic spectrum. The similarity occurs because the diaphragms are modelled as being elastic, and the in-plane loaded walls are generally much stiffer than the diaphragms. Hence, the diaphragms essentially behave as elastic single-degree-of-freedom systems with rigid supports. When the diaphragms are relatively stiff (and the walls can no longer be considered as rigid supports), some deviations can be seen between the peak diaphragm deformations and the elastic displacement spectrum.

Even though the diaphragm deformation may be approximated by the spectral displacement, it is questionable if the diaphragm deformation actually matches the displacement spectrum when the diaphragm is overly flexible, without causing instability of the out-of-plane responding walls. Further studies are needed to investigate the effect of the dynamic response of the out-of-plane walls (particularly

for the two-way spaning walls) on the building response when the diaphragm becomes excessively flexible.

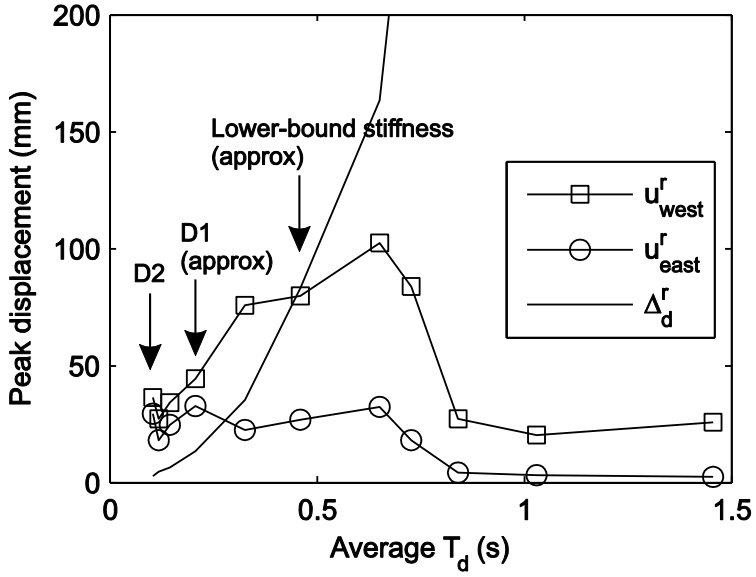

Figure 17. Influence of diaphragm stiffness on the wall displacement and roof deformation, subjected to the 0.6 g excitation intensity

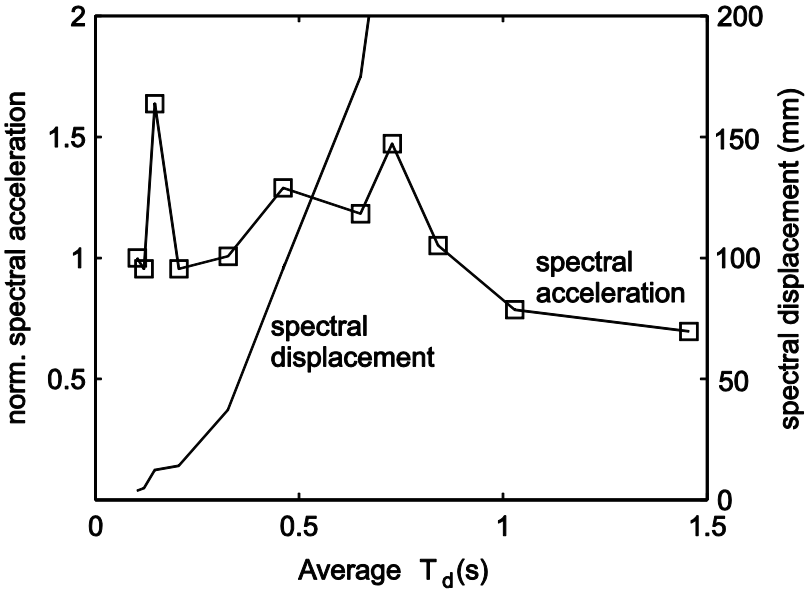

Figure 18. Plots of normalised spectral acceleration and displacement corresponding to the average diaphragm period for the 0.6 g excitation

6. CONCLUSIONS

In this paper, results of a case study are reported on the applicability of the equivalent frame modelling approach for the global analysis of URM buildings with flexible diaphragms, when the local out-of-plane failure mechanisms have been mitigated. Reflecting the current modelling practice, the diaphragms were considered to remain elastic and the out-of-plane wall stiffness and strength contributions were neglected.

The simple modelling approach was able to capture, with reasonable accuracy, the fundamental mode characteristics and the evolution of the peak displacements as the excitation intensity increased. On the other hand, the higher modes and the damage mechanisms were not as accurately simulated, particularly towards the near-collapse state.

Concerning the damage mechanisms, different failure mechanisms were obtained (prior to the ultimate state) depending on the assumed length of the rigid node offset. More consistent results (with respect to the experimental data) were achieved when the equivalent frame idealisation reflected the actual crack pattern.

For the case study building, the analyses did not indicate large sensitivity to the diaphragm stiffness values. When the diaphragms were made relatively flexible, however, the numerical models indicated the potential for significant sensitivity, including amplification, of the wall displacements due to the diaphragm stiffness values.

The analyses also revealed that perhaps the most significant limitation of the investigated modelling approach is the omission of the out-of-plane walls. The discrepancies in the mode properties were identified as primarily due to the lack of out-of-plane wall stiffness. The interaction between the out-of-plane responding wall and flexible diaphragm is also expected to play an important role as the diaphragm flexibility increases.

Considering these points, the following conclusions can be drawn for practical application:

- The analyses are sensitive to the frame geometry (deformable lengths of piers) and the best agreement with the actual response is expected when the geometry is guided by the crack pattern. Clearly, when the frame model is used for prediction of the response, the final crack pattern may not be obvious, in which case the engineer may need to consider the sensitivity of the results by varying the length of the piers. In such sensitivity analysis, an absolute minimum deformable

length of the frame should correspond to height of the adjacent openings. In addition, any pre-existing crack should be reflected in the idealisation;

- Neglecting out-of-plane loaded walls may render the results inaccurate if the diaphragm deformation is significant, and/or the building response is predominantly elastic;

- If diaphragm stiffness is known, then the likely level of diaphragm deformation (relative to the supporting walls) may be gauged from the elastic displacement spectrum as a preliminary consideration;

- If the diaphragm deformation is deemed to be excessively large, alternative analysis approaches that can account for two-way spanning out-of-plane wall behaviour, such as the finite element method, may be warranted; and

- If diaphragm stiffness is unknown, a sensitivity analysis on the stiffness value is recommended due to the relatively flexible diaphragms significantly affecting the wall displacement demand.

ACKNOWLEDGEMENTS

This work was supported by the Australian Research Council, through the grant DP120100848. The first author received financial support through the Australian Postgraduate Award. The authors would like to thank Prof. Magenes, Asst. Prof. Penna and Dr. Senaldi from the University of Pavia and EUCENTRE for their suggestions on the numerical modelling of the experimentally tested building. The authors would also like to thank Prof. Magenes for reviewing the original manuscript.

REFERENCES

Aleman J., Mosqueda G. and Whittaker, A. (2015) “Seismic analysis of multi-story unreinforced masonry buildings with flexible diaphragms”, MCEER Report-15-0001, University of Buffalo, State University of New York.

ASCE (2014) “Seismic evaluation and retrofit of existing buildings ASCE/SEI 41-13”, American Society of Civil Engineers, Reston, Virginia.

Brignola, A., Pampanin, S. and Podesta S. (2012) “Experimental evaluation of the in-plane stiffness of timber diaphragms”, Earthquake Spectra. 28(4), 1687 - 1709.

Chopra, A. (2007) “Dynamics of Structures - theory and application to earthquake engineering”, Prentice Hall, New Jersey.

Costley, A. C. and Abrams, D. P. (1995) “Dynamic response of unreinforced masonry buildings with flexible diaphragms”, Structural Research Series 605, Department of Civil Engineering, University of Illinois at Urbana-Champaign.

Derakhshan, H., Griffith, M. C. and Ingham, J. M. (2015) “Out-of-plane seismic response of vertically spanning unreinforced masonry walls connected to flexible diaphragms”, Earthquake Engineering and Structural Dynamics. In Press. DOI: 10.1002/eqe.2671.

Dizhur, D., Ingham, J. M., Moon, L., Griffith, M. C., Schultz, A., Senaldi, I., Magenes, G., Dickie, J., Lissel, S., Centeno, J., Ventura, C., Leite, J. and Lourenço, P. (2011) “Performance of masonry buildings and churches in the 22 February 2011 Christchurch earthquake”, Bulletin of New Zealand Society for Earthquake Engineering, 44(4), 279 - 296.

Dolce, M. (1989) “Schematizzazione e modellazione degli edifice in muratura sogetti ad azioni sismiche (Modelling of masonry buildings under seismic loads)”, L’industria delle Construzioni, 242, 44 – 57. (in Italian).

Giongo, I., Wilson A., Dizhur, D., Derakhshan, H., Tomasi, R., Griffith, M. C., Quenneville, P. and Ingham J. M. (2014) “Detailed seismic assessment and improvement procedure for vintage flexible timber diaphragms”, Bulletin of New Zealand Society for Earthquake Engineering, 47(2), 97 - 118.

Kappos, A. J., Penelis, G. G. and Drakopoulos, C. G. (2002) “Evaluation of simplified models for lateral load analysis of unreinforced masonry buildings”, Journal of Structural Engineering, 128(7), 890 – 897.

Kim, S.-C. and White, D. W. (2004) “Nonlinear analysis of a one-story low-rise masonry building with a flexible diaphragm subjected to seismic excitation”, Engineering Structures, 26, 2053 - 2067.

Lagomarsino, S., Penna, A., Galasco, A. and Cattari, S. (2013) “TREMURI program: An equivalent frame model for the nonlinear seismic analysis of masonry buildings”, Engineering Structures, 56, 1787 - 1799.

Magenes, G. and Della Fontana, A. (1998) “Simplified non-linear seismic analysis of masonry buildings”, Proceedings of the British Masonry Society, 8, 190 – 195.

Magenes, G., Penna, A., Galasco, A. and Da Paré, M. (2010) "In-plane cyclic shear tests of undressed double-leaf stone masonry panels", Proceedings of 8th International Masonry Conference (8IMC), Dresden, Germany, July 4 – 7, Paper No 216.

Magenes, G., Penna, A., Senaldi, I., Rota, M. and Galasco, A. (2014) "Shaking table test of a strengthened full-scale stone masonry building with flexible diaphragms", International Journal of Architectural Heritage: Conservation, analysis and restoration, 8(3), 349 - 375.

Penna, A., Lagomarsino, S. and Galasco, A. (2014) "A nonlinear macroelement model for the seismic analysis of masonry buildings", Earthquake Engineering and Structural Dynamics, 43(2), 159 - 179.

Salonikios, T., Karakostas, C., Lekidis, V. and Anthoine, A. (2003) "Comparative inelastic pushover analysis of masonry frames", Engineering Structures, 25, 1515 – 1523.

Standards Australia (2007) "AS 1170.4 - 2007: Structural design actions. Part 4: Earthquake actions in Australia", Standards Australia, Sydney.

Tena-Colunga, A. and Abrams, D. P. (1992) "Response of an unreinforced masonry building during the Loma Prieta earthquake", Structural Research Series 576, Department of Civil Engineering, University of Illinois at Urbana-Champaign.

Wilson, A., Quenneville, P. and Ingham, J. M. (2013) "Natural period and seismic idealization of flexible timber diaphragms", Earthquake Spectra, 29(3), 1003 - 1019.

Appendix A – Limitation of Lumped Mass Diaphragm Idealisation

The lumped mass idealisation of the diaphragm introduces some inaccuracies, in particular, concerning the forces generated by the diaphragm motion. Two idealised elastic diaphragm models are analysed to illustrate this point, considering the supporting in-plane walls to be rigid. The first model corresponds to a generalised SDOF system of a shear beam with uniformly distributed mass, assuming the displacement shape, ψ, to be the deformed shape of the beam subjected to a parabolic load. This model may be considered to be representative of actual timber diaphragms (Wilson et al. 2013). The generalised mass $\tilde{m}$, generalised stiffness $\tilde{k}$ and the period T of the system are

$$\tilde{m} = \frac{3968}{7875} m \ , \qquad \tilde{k} = \frac{4352}{875} \frac{GA}{\kappa L} \ , \ T = 2\pi \sqrt{\frac{\tilde{m}}{\tilde{k}}} \tag{A.1}$$

where m is the total mass of the diaphragm including the contributions from out-of-plane walls, G is the shear modulus, A is the diaphragm cross section area, L is the span length and κ is the cross section shape factor for shear.

The peak displacement at mid-span u_0 and the peak elastic restoring force V_0 of the shear beam are given by (Chopra 2007)

$$u_0 = \tilde{\Gamma} D, \qquad V_0 = \tilde{\Gamma} \tilde{L} A \tag{A.2}$$

where $\tilde{L} = \int_0^L \bar{m} \psi dx$, with $\bar{m}$ =mass per unit length, and $\tilde{\Gamma} = \tilde{L}/\tilde{m}$. D and A express the peak displacement and pseudo-acceleration correspondingly.

The equivalent mass and the stiffness corresponding to the lumped mass idealisation of the diaphragm used in this study are

$$\tilde{m} = \frac{1}{2} m \ , \qquad \tilde{k} = 4 \frac{GA}{\kappa L} \tag{A.3}$$

The peak mid-span displacement and the base shear force of the lumped mass system are

$$u_0 = D, \qquad V_0 = \tilde{m} A \tag{A.4}$$

Figures A.1 shows the comparisons of the period, peak mid-span displacement and the peak elastic restoring force obtained from the two idealisations, subjected to the design spectrum of AS 1170.4 (Standards Australia 2007) with a peak ground acceleration of 0.1g on site class C_e. The diaphragm stiffness G_d, defined as the shear modulus multiplied by the thickness, was set to 1750kN/m (approximately representing a diaphragm with double layered sheathing (ASCE 2014)), and results correspond to the span length of 10 m and several different aspect ratios (L/B). It can be seen that both the periods and the peak displacements of the two idealisations match well. However, the elastic force demand of the lumped mass model is consistently smaller than the generalised SDOF idealisation of the distributed mass model. This discrepancy is mainly attributed to the difference in the "effective" mass of the two models. For the generalised SDOF shear beam, the "effective" mass, which produces the peak base shear when multiplied by the spectral acceleration, is equal to $\tilde{\Gamma}\tilde{L} = 0.815m$ (from Eq. A.2). For the lumped mass idealisation, the corresponding value is $\tilde{m} = 0.5m$ (from Eq. A.4). Hence the peak elastic force imposed on the lumped mass idealisation is approximately 60% of the more representative, shear beam model with distributed mass.

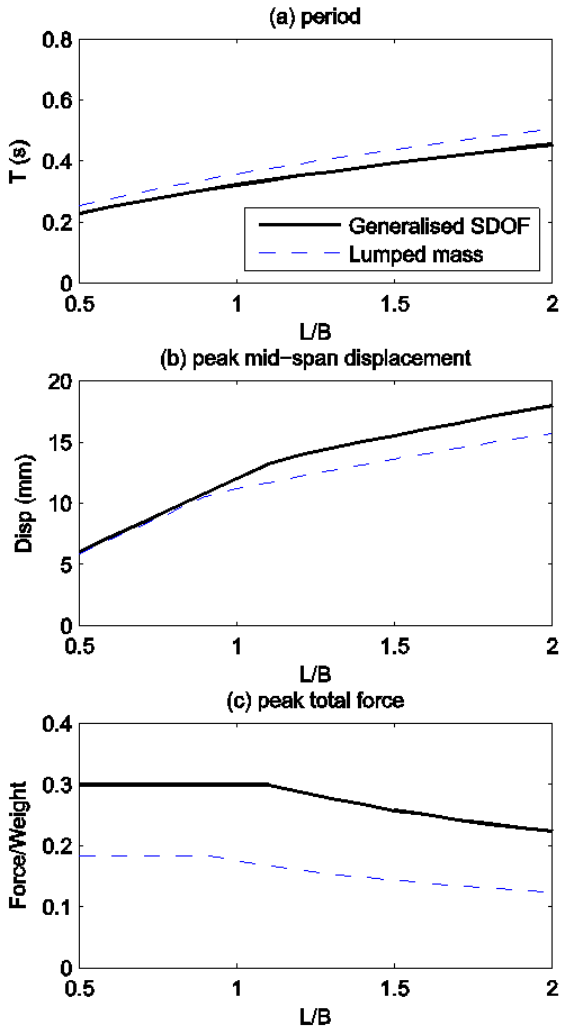

Figure A.1. Comparisons of (a) period, (b) peak mid-span displacement, and (c) peak base shear of the diaphragm idealisations. L is the span length and B is the width of the diaphragm.

Despite the theoretical discrepancy, the lumped mass idealisation has been used successfully in past studies (Tena-Colunga and Abrams 1992; Kim and White 2004). The reason may be that the discrepancy is most significant when the diaphragm is relatively flexible. For stiff diaphragms, the wall supports do not remain rigid, and the participation of the wall mass will likely reduce the discrepancy. Indeed, at the limiting condition of a rigid diaphragm, the two idealisations will yield identical results, as governed by the total mass of the diaphragm and the stiffness of the walls. Hence the lumped mass model is expected to be appropriate when the diaphragm is relatively stiff, while it can underestimate the force demand by up to 40% when the diaphragm becomes overly flexible. However, for such flexible diaphragms the force demands are also usually small, and hence, may have only limited effects on the building response. In this study, lumped mass idealisation is considered to be an acceptable simplification, given the simplified nature of the overall model.

CHAPTER 5

INFLUENCE OF DIAPHRAGM FLEXIBILITY

Background

This chapter presents the results of an extensive parametric study carried out using idealised plan-asymmetric systems to identify and characterise the effects of diaphragm flexibility. The paper "Influence of diaphragm flexibility on seismic response of unreinforced masonry buildings with flexible diaphragms" shows that there are multiple effects of diaphragm flexibility on the peak structural responses, which are dependent on the level of the stiffness- and, more significantly, the strength-eccentricity of the system. A qualitative diaphragm classification is developed, and is used to characterise the effects of diaphragm flexibility. A simple measure based on the ratio of diaphragm deformation to the average wall displacement is proposed to determine when the multi-mode behaviour becomes significant.

List of Manuscripts

Nakamura, Y., Derakhshan, H., Magenes, G. and Griffith, M. C. (2016) "Influence of diaphragm flexibility on seismic response of unreinforced masonry buildings with flexible diaphragms", Journal of Earthquake Engineering, published online 27 July 2016.

Statement of Authorship

Title of Paper	Influence of diaphragm flexibility on seismic response of unreinforced masonry buildings with flexible diaphragms
Publication Status	☐ Published ☑ Accepted for Publication ☐ Submitted for Publication ☐ Unpublished and Unsubmitted work written in manuscript style
Publication Details	Nakamura, Y., Derakhshan, H., Magenes, G. and Griffith, M. C. (2016) "Influence of diaphragm flexibility on seismic response of unreinforced masonry buildings with flexible diaphragms", Journal of Earthquake Engineering

Principal Author

Name of Principal Author (Candidate)	Yasuto Nakamura
Contribution to the Paper	Prepared manuscript, developed model, performed all analyses
Overall percentage (%)	85%
Certification:	This paper reports on original research I conducted during the period of my Higher Degree by Research candidature and is not subject to any obligations or contractual agreements with a third party that would constrain its inclusion in this thesis. I am the primary author of this paper.
Signature	Date 26/8/16

Co-Author Contributions

By signing the Statement of Authorship, each author certifies that:

i. the candidate's stated contribution to the publication is accurate (as detailed above);

ii. permission is granted for the candidate in include the publication in the thesis; and

iii. the sum of all co-author contributions is equal to 100% less the candidate's stated contribution.

Name of Co-Author	Hossein Derakhshan
Contribution to the Paper	Contributed to research and manuscript
Signature	Date 26 Aug 2016

Name of Co-Author	Guido Magenes
Contribution to the Paper	Supervised and contributed to research and manuscript
Signature	Date 25/8/16

Name of Co-Author	Michael C. Griffith
Contribution to the Paper	Supervised and contributed to research and manuscript
Signature	Date 30/8/2016

Influence of Diaphragm Flexibility on Seismic Response of Unreinforced Masonry Buildings with Flexible Diaphragms

ABSTRACT

The effects of diaphragm flexibility on the seismic response of low-rise unreinforced masonry buildings are examined using one-way stiffness- and strength-eccentric single-storey systems subjected to unidirectional ground excitation. A wide range of diaphragm stiffnesses are considered. Results show that diaphragm flexibility can induce different effects depending on the configuration of the system and the level of diaphragm flexibility. When diaphragm is relatively stiff, amplified displacement demands can be imposed on the flexible side of the structure. When diaphragm is relatively flexible, peak displacements of in-plane loaded walls generally reduce. A diaphragm classification is developed to capture these salient effects.

keywords: flexible diaphragm, unreinforced masonry, plan asymmetry, inelastic response.

1. INTRODUCTION

Seismic design and assessment of buildings are typically carried out assuming the floor and roof diaphragms to be rigid in their own planes, provided they have adequate in-plane stiffness properties. While the rigid diaphragm assumption is appropriate for many construction types, certain structural systems have deformable diaphragms that render the rigid diaphragm assumption questionable. One particular structural system with pronounced diaphragm flexibility is unreinforced masonry (URM) buildings with the floor and roof diaphragms constructed of timber boards and joists. Due to the limited coupling provided by the flexible diaphragms, the in-plane loaded shear walls (in-plane walls) tend to respond independently of each other (Penna 2015). Consequently, multiple dominant modes can be present even though URM buildings are typically low-rise (of generally up to 5 storeys), and their response characteristics can deviate from those typical of rigid diaphragm structures (Tena-Colunga & Abrams 1996).

Previous research into the effects of diaphragm flexibility on elastic building response has shown that increased diaphragm flexibility results in the elongation of the fundamental period of the structure and an increase in the multi-mode behaviour (Jain & Jennings 1985; Saffarini & Qudaimat 1992; Moon & Lee 1994; Tena-Colunga & Abrams 1996; Ju & Lin 1999). The structural configuration most affected by diaphragm flexibility is consistently reported as low-rise shear wall buildings, with a large number of

bays. Moon and Lee (1994) noted that diaphragm flexibility can also lead to modified mode shapes, as well as a phenomenon they referred to as "mode shifts", whereby two modes of a rigid diaphragm system appear in the flexible diaphragm system with their modal orders switched. Fleischman and Farrow (2001) have shown that the increase in diaphragm flexibility results in the separation of the masses attributed to the in-plane walls and the diaphragms into different modes; the lower modes typically comprising of the vibrations of the diaphragms, while the higher modes containing the deformations of the walls.

The inelastic response of buildings with flexible diaphragms has so far received less attention than the elastic response. De-La-Colina (1999) analysed single-storey, plan-asymmetric frame structures designed by a typical code procedure and found that for medium- to large-period systems, the increase in diaphragm flexibility reduced the in-plane displacement of walls. For short-period systems, some increases in the wall displacements were observed. These effects of diaphragm flexibility were found to reduce with the increase in the level of yielding and the initial period of the system. A similar period-dependent behaviour was also reported by Sadashiva et al. (2012) for symmetric systems. Kim and White (2004) conducted a parametric analysis of a nonlinear model initially calibrated to experimental tests conducted on a single-storey symmetric reinforced masonry building with a timber roof. Their parametric analysis indicated the occurrence of the largest in-plane wall displacement when the diaphragm was neither absolutely rigid nor completely flexible.

Experimental studies on URM buildings with flexible diaphragms showed that partial failures (such as out-of-plane wall collapse) were likely to occur when the diaphragms were excessively flexible, or if the diaphragm to wall connections were poor (Tomaževič et al. 1991; Magenes et al. 2014; Senaldi et al. 2014; Vintzileou et al. 2015). When partial failures were prevented by strengthening the diaphragms and diaphragm to wall connections, URM buildings with flexible diaphragm generally achieved comparable base shear resistances as those of similar buildings with rigid (reinforced concrete) diaphragms (Tomaževič et al. 1993). However, some test results have indicated that buildings with flexible diaphragms experienced larger wall displacement demands compared to those with rigid diaphragms under a similar level of excitation (Magenes et al. 2014; Senaldi et al. 2014).

While previous studies have identified various aspects of response characteristics of buildings with flexible diaphragms, several issues remain unanswered. These include (1) whether the diaphragm flexibility is beneficial or detrimental to the seismic demands imposed on the lateral load resisting walls, and (2) whether qualitatively consistent building responses are obtained regardless of the level of diaphragm flexibility. This paper reports on a parametric study conducted to address these issues concerning the influence of flexible diaphragms on the global seismic responses of URM buildings. An

idealised simple numerical model, intended to capture the main response characteristics of the building typology concerned, is used in order to carry out systematic nonlinear dynamic analyses encompassing a wide range of diaphragm stiffness values. While the focus of the present study is URM buildings, the results of the parametric study may also be applicable to other structural systems which have relatively stiff in-plane loaded walls supporting flexible diaphragms. The results show that (1) relatively flexible diaphragms can reduce the peak displacements of the in-plane walls, while relatively stiff diaphragm can lead to increased seismic demands, and (2) the non-rigid diaphragms can be broadly categorised into four ranges based on their salient effects on the building behaviour.

2. DESCRIPTION OF NUMERICAL MODEL

Analyses are conducted on idealised single-storey models, consisting of a rectangular diaphragm supported by four walls at its perimeter (Figure 1(a)). The perimeter walls are considered to resist loading in the in-plane loaded directions only, and the wall stiffnesses in the out-of-plane directions are neglected. The centre of mass (CM) coincides with the geometric centroid, while uniaxial stiffness eccentricity (e_{sx}, defined as the distance between the CM and the centre of stiffness, CR) and strength eccentricity (e_{px}, defined as the distance between the CM and the centre of strength, CP) are introduced by making wall 2 stiffer and stronger than wall 1. The system is subjected to unidirectional excitations applied in the y direction of the model.

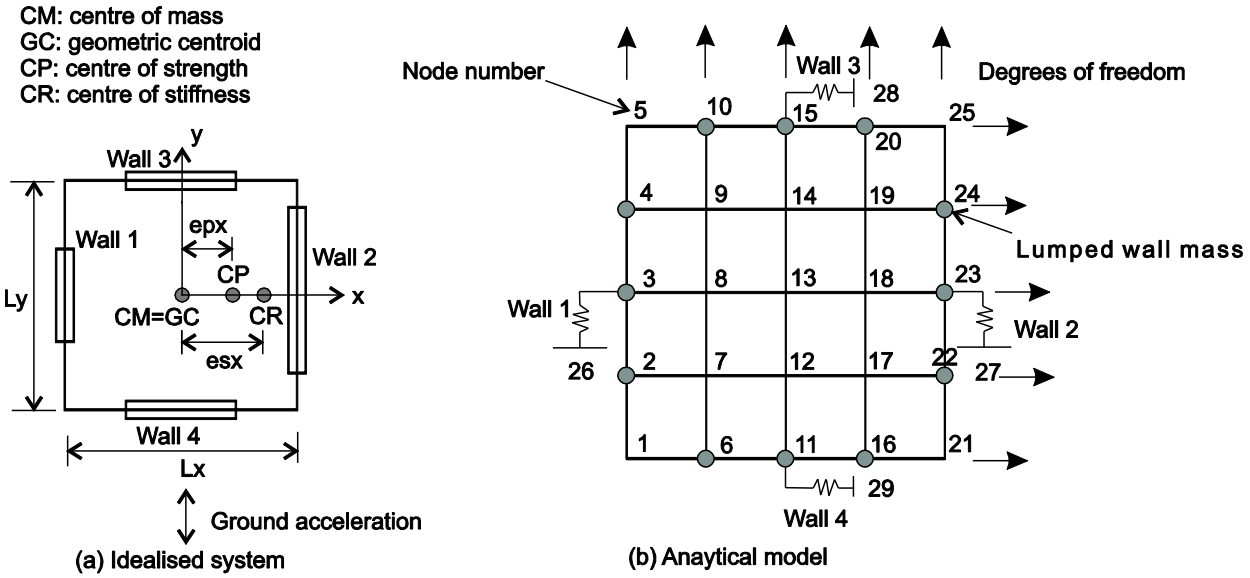

Figure 1. Plan view of (a) idealised system, and (b) analytical model.

Numerical modelling of URM buildings poses significant challenges due to their distributed mass, low tensile strength and the dependence of their lateral strengths on the vertical (axial) forces. In order to

capture such details, finite element analysis may at first appear to be the most suitable modelling approach. However, nonlinear (dynamic) finite element analysis capable of identifying all possible failure mechanisms requires significant computational resources, and the required constitutive properties, as well as generally accepted constitutive models, are currently lacking. It may also be thought that the dominant global response characteristics of buildings with flexible diaphragms could be captured by relatively simple models, even if they do not fully account for the specific response mechanisms of URM construction. This study uses such simplified models in order to discern the main trends of the dynamic behaviour, where the simplifications introduced include:

- no connections between the orthogonal walls;
- the diaphragm is considered to remain linearly elastic, and is perfectly and continuously attached to the perimeter walls;
- the out-of-plane wall failures are considered to have been prevented;
- the dependence of URM wall strength on the level of axial forces is neglected; and
- the span direction of the floor joists are not explicitly considered.

The analytical model representing the idealised system is shown in Figure 1(b). RUAUMOKO (Carr 2008) is used for the analysis. The force-deformation relationship of each wall is assumed to be captured by the "thin" Takeda hysteresis model (Figure 2(c)), which is typically used to simulate the response of reinforced concrete walls and columns (Priestley et al. 2007). The post-yield stiffness is set to zero for all walls. Implicit in this behavioural model is the assumption that the masonry walls can deform inelastically, in a ductile manner. Even though the conventional notion of ductility does not apply to masonry due to its lack of tensile resistance after cracking, typical failure modes of masonry piers (Figure 2(a) and Figure 2(b)) do exhibit inelastic behaviours that can be represented by the bilinear idealisations of their backbone curves, with appropriate levels of energy dissipation depending on the failure mode (Magenes & Calvi 1997). Therefore, the use of the Takeda hysteresis model was considered to be an appropriate simplification for the purpose of this study, in which the in-plane behaviour of each wall is assumed to be produced by a combination of flexural and shear failure modes of several piers.

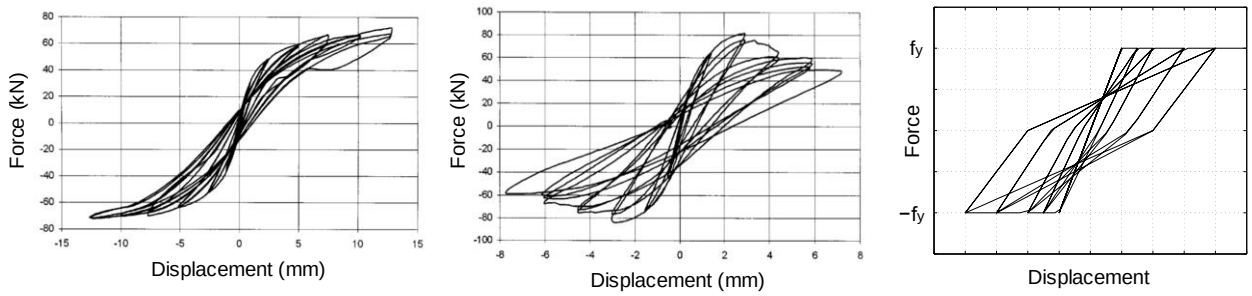

(a) Rocking (b) Diagonal shear (c) Takeda model

Figure 2. Typical force-displacement relationships of unreinforced masonry piers (Magenes & Calvi, 1997), for (a) rocking, (b) diagonal shear failure modes. The "thin" Takeda model used in the analysis is shown in (c).

The diaphragm is modelled by 16 quadrilateral membrane elements (Carr 2008). The degrees of freedom of the collinear nodes in the x and y directions are slaved to achieve the shear-dominant deformation mechanism consistently observed for timber diaphragms, typical of those found in existing URM buildings (Brignola et al. 2012; Wilson et al. 2013; Giongo et al. 2014; Whitney and Agrawal 2015). For example in Figure 1(b), the displacements in the y direction are slaved for nodes 1 to 5, nodes 6 to 10, nodes 11 to 15, nodes 16 to 20, and nodes 21 to 25. The mesh sensitivity and the validity of node slaving were checked by comparing the fundamental frequency of the numerical model against the theoretical value of a shear beam. The configuration used in this study resulted in small errors of about 1 %.

Note that the behaviour of a timber diaphragm is typically orthotropic (Giongo et al. 2014). However, an isotropic membrane was used in the present study to reduce the number of variables. This was considered to be an appropriate simplification because the diaphragm deformations orthogonal to the direction of loading were small. In the direction of loading, the investigated range of diaphragm stiffness encompassed the conceivable stiffness range of timber floor systems.

URM buildings with timber floors are essentially distributed mass systems, in which a large proportion of the seismic mass is attributed to the mass of the masonry. In fact, the floor masses typically account for only 10 - 20 % of the total building mass. In order to reflect this, the wall masses are directly lumped at the location of the wall elements (shown in Figure 1(b) by grey circles), while the floor masses are distributed across the diaphragm elements.

The configuration of the analytical model is defined by the following parameters, where the total mass of the structure is denoted by m, the stiffness and strength of the i^{th} wall oriented in the direction of loading are defined by k_{yi} and f_{yi} respectively, with the wall located at a distance x_i from the CM,

- The translational period of the symmetric system in the direction of loading under the rigid diaphragm condition, $T_y = 2\pi\sqrt{m/K_y}$, where $K_y = \sum k_{yi}$ is the lateral stiffness of the structure.

- The ratio of the uncoupled torsional to lateral frequencies of the rigid diaphragm system, $\Omega_\theta = \sqrt{K_{\theta s} m / I_O K_y}$, where I_O is the mass moment of inertia of the rigid diaphragm about the CM and $K_{\theta s}$ is the torsional stiffness of the structure about the CR.

- The stiffness eccentricity, $\varepsilon_{sx} = \frac{e_{sx}}{L_x} = \frac{1}{L_x}\frac{\sum k_{yi} x_i}{K_y}$, expressed as normalised to the dimension of the diaphragm perpendicular to the direction of excitation.

- The total strength of the system in the direction of excitation, $F_y = \sum f_{yi}$.

- The strength eccentricity, $\varepsilon_{px} = \frac{e_{px}}{L_x} = \frac{1}{L_x}\frac{\sum f_{yi} x_i}{F_y}$, expressed as normalised to the dimension of the diaphragm perpendicular to the direction of excitation.

- The total strength orthogonal to the direction of excitation, $F_x = \sum f_{xi}$.

- The fraction of the mass attributed to each wall oriented in the direction of loading (wall 1 and 2, denoted by m_1 and m_2) to the total mass of the system, $\rho_y = \frac{m_1}{m} = \frac{m_2}{m}$.

- The fraction of the mass attributed to each wall oriented in the direction orthogonal to loading (wall 3 and 4, denoted by m_3 and m_4) to the total mass of the system, $\rho_x = \frac{m_3}{m} = \frac{m_4}{m}$.

- The fraction of the mass attributed to the diaphragm to the total mass of the system, $\rho_d = \frac{m_d}{m}$.

- The fundamental period of the diaphragm, $T_d = 2\sqrt{\frac{m_{d,tot} L_x}{\kappa G t_d L_y}}$ where $m_{d,tot} = (\rho_d + 2\rho_x)m$ is the total mass attributed to the diaphragm including those of the out-of-plane loaded walls, G is the shear modulus, t_d is the diaphragm thickness and κ is the shape factor, which equals 1 for the model (because of the node slaving, uniform shear stress is enforced in the diaphragm). This is the theoretical fundamental period of a fix-ended shear beam, which is almost identical to the approximate expression proposed for timber diaphragms by Wilson et al. (2013), derived using a shear beam with a uniform mass distribution, responding in a displacement shape corresponding to a parabolic load. $G_d = G t_d$ is often referred to as the characteristic timber diaphragm stiffness (ASCE 2014).

- Damping ratio, assumed to be constant 5% critical damping for all modes.

Note that while the notions of stiffness and strength eccentricities (typically associated with the torsional behaviour of rigid diaphragm structures) are used as convenient definitions, analyses will show (Section 4) that the torsional behaviour becomes small as the diaphragm becomes flexible. Therefore the eccentricities are better understood as asymmetries in the distributions of stiffness and strength rather than as parameters governing the torsional behaviour of the system. For this reason, eccentric systems will be referred to as stiffness- or strength-asymmetric systems. For the systems considered in this study, the relative stiffness and strength of wall 1 and 2 can be obtained from the defined eccentricities by $\frac{k_{y1}}{k_{y2}} = \frac{0.5-\varepsilon_{sx}}{0.5+\varepsilon_{sx}}$ and $\frac{f_{y1}}{f_{y2}} = \frac{0.5-\varepsilon_{px}}{0.5+\varepsilon_{px}}$.

3. RANGE OF PARAMETERS AND GROUND MOTIONS

The variables considered in the parametric analysis were the lateral period of the system (T_y), frequency ratio (Ω_θ), yield force levels (F_y), strength of orthogonal walls (F_x), stiffness and strength eccentricities (ε_{sx} and ε_{px}), and the distribution of mass (ρ_x, ρ_y, and ρ_d). No particular design code requirements were followed in the selection of the parameters.

The values of T_y ranged from short (0.1 s) to moderate (0.6 s) periods, which ranged from the acceleration- to the velocity-sensitive regions of the ground motions, and were considered to encompass the likely range of URM buildings. As URM buildings almost always have shear walls located at the perimeter of the structure, they were assumed to be torsionally stiff ($\Omega_\theta \geq 1$). The values of Ω_θ corresponding to 1 and 1.4 were analysed. Four different values of the normalised stiffness eccentricity, ε_{sx}, were selected, ranging from 0 to 0.3. The total mass (m) and the dimension perpendicular to the direction of loading (L_x) were kept constant so that the stiffnesses of the walls oriented in the direction of loading were determined uniquely by setting T_y and ε_{sx}. The mass moment of inertia (I_O) was also kept constant so that the stiffness of the walls in the x direction was uniquely determined by setting values for T_y and Ω_θ.

The total strength in the y direction was determined based on the rigid diaphragm configuration through the expression $F_y = \frac{f_o}{R_y}$, where f_o was the mean peak elastic force attained from the set of ground motions used in the analysis, and R_y was the force reduction factor assigned to the system. In order to investigate the effect of yield levels, R_y was varied between 1 (elastic), 2.5 and 4. The strength eccentricity, ε_{px}, was

set to either 0 or equal to ε_{sx}. $\varepsilon_{px} = 0$ occurs when walls of equal strength are placed symmetrically about the CM, while $\varepsilon_{px} = \varepsilon_{sx}$ implies a linear relationship between stiffness and strength (Peruš and Fajfar, 2005). As stiffness and strength are usually correlated, these two cases were considered to reflect the likely range of the wall strength distributions. The total strength of the walls in the x direction was set by $F_x = F_y R_F$, where R_F was varied between 0.5 and 1.

Two sets of mass ratios representing different scenarios were investigated. The first set consisted of 22.5% of total mass equally distributed on the walls ($\rho_y = \rho_x = 0.225$), with 10% of total mass assigned to the diaphragm ($\rho_d = 0.1$). Such condition may represent buildings which are almost square in plan. The second set consisted of 45% more masses on the walls oriented in the x direction than those of the walls in the y direction ($\rho_y = 0.164$ and $\rho_x/\rho_y = 1.45$), and the diaphragm mass was set to 19.6% of the total mass. Hence the second condition represented a case in which a significantly larger mass was excited by the deformation of the diaphragm, for instance buildings which are rectangular in plan, loaded in the direction perpendicular to the long dimension. Finally, for each combination of variables, the diaphragm periods were varied from 0.01 s to 2.0 s in eleven increments.

The ranges of variables considered in the analysis are summarised in Table 1. The parameters kept constant in the analyses are listed in Table 2. The constant plan dimensions for L_x and L_y were used to keep the same diaphragm mesh size for all analyses.

Table 1. Range of variables

Variable	Values
T_y	0.1, 0.2, 0.35 and 0.6 s
Ω_θ	1 and 1.4
ε_{sx}	0, 0.1, 0.2 and 0.3
ε_{px}	0, 0.1, 0.2 and 0.3
R_y	1 (elastic), 2.5 and 4
R_F	0.5 and 1
ρ_y	0.225 and 0.164
$(\rho_d + 2\rho_x)/\rho_y$	2.444 and 4.085
T_d	0.01, 0.05, 0.075, 0.1, 0.3, 0.5, 0.75, 1, 1.25, 1.5 and 2 s

Table 2. Constant parameters

Variable	Values
m	25 tons
I_O	1633.125 tons-m^2
L_x	12 m
L_y	18 m
Hysteretic behaviour	Modified Takeda (Figure 2(c))
Damping	5% of critical damping for all modes

The ground motion records were obtained from the Pacific Earthquake Engineering Research Center (PEER) database (PEER 2014), and consisted of waveforms processed into the fault-normal and fault-parallel components. The selected records are listed in Table 3. The ground motions were measured on stiff soil with the top 30 m soil shear velocity (V_{s30}) between 360 m/s and 720 m/s, with distances from the rupture plane between 15 km and 62 km. The records were scaled so that the mean spectrum of the record set (shown in Figure 3) corresponded well with the design spectrum of AS 1170.4 (Standards Australia, 2007) on a site classified as "rock" (soil subclass type B_e, V_{s30} > 360 m/s) with the peak ground acceleration of 0.2 g.

Table 3. Records used in analysis

Event	Year	Station	M_w	Mechanism	Closest distance (km)	V_{s30} (m/s)	Scale factor
Northridge	1994	LA - UCLA Grounds	6.69	Reverse	22.5	398.4	0.6789
Northridge	1994	Santa Susana Ground	6.69	Reverse	16.7	715.1	0.8073
Northridge	1994	San Gabriel - E Grand Ave	6.69	Reverse	39.3	401.4	1.2641
Irpinia	1980	Rionero In Vulture	6.9	Normal	30.1	530	1.848
Loma Prieta	1989	San Jose - Santa Teresa Hills	6.93	Reverse-Oblique	14.7	671.8	0.7638
Loma Prieta	1989	Fremont - Mission San Jose	6.93	Reverse-Oblique	39.5	367.6	1.5848
Hector Mine	1999	Twentynine Palms	7.13	Strike-Slip	42.1	684.9	3
Hector Mine	1999	Heart Bar State Park	7.13	Strike-Slip	61.2	684.9	2.6688

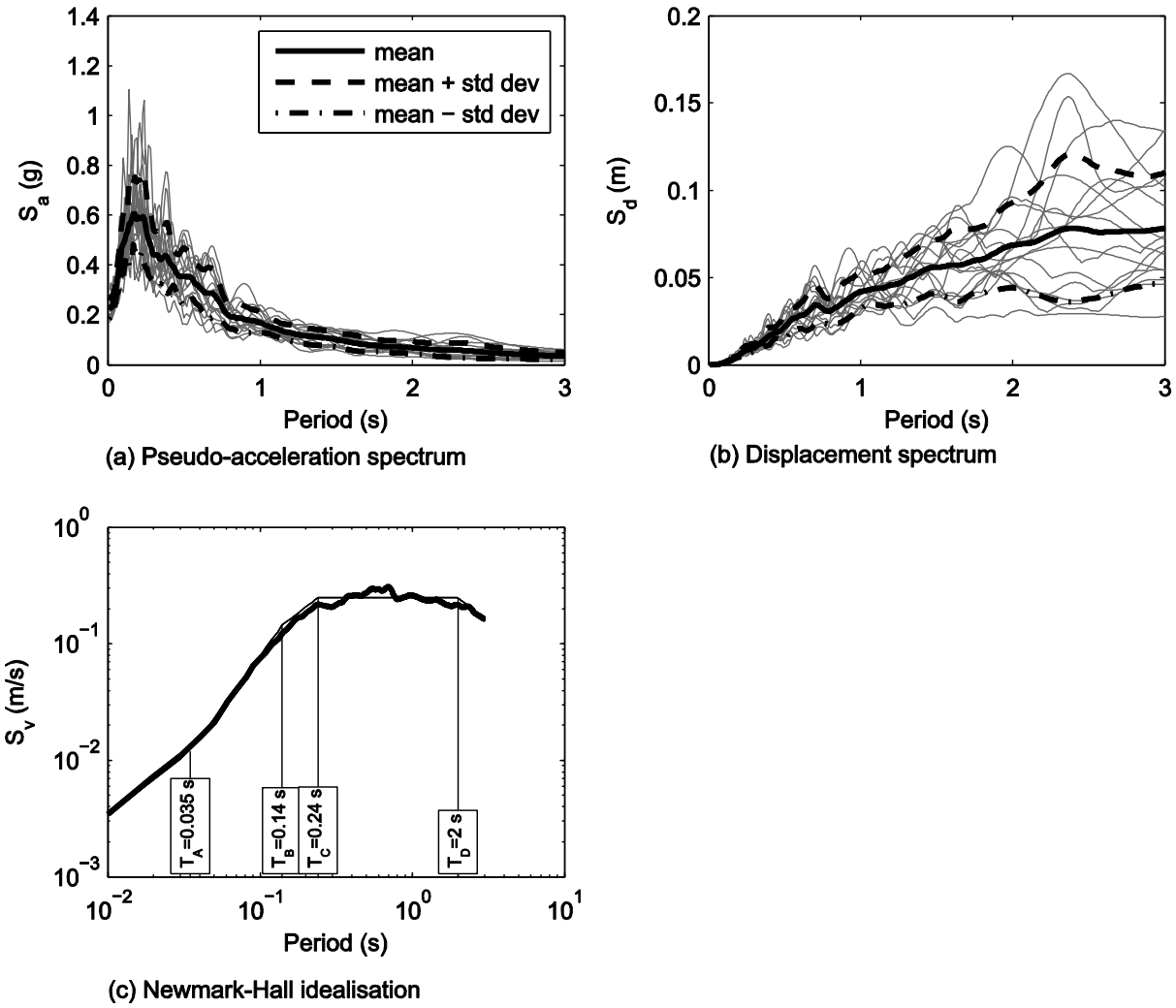

Figure 3. Mean spectrum of records and Newmark-Hall idealisation

4. EFFECT OF DIAPHRAGM FLEXIBILITY

4.1 Response of Symmetric Systems

The mean peak displacements of wall 1 and wall 2 (main lateral-load resisting elements oriented in the direction of loading) are shown in Figure 4 corresponding to the elastic and the inelastic systems with R_y of 2.5 and 4. As the structure is symmetric, the displacements of the two walls are identical, and the walls perpendicular to the direction of loading are not excited. For brevity, the distribution of mass is expressed by the ratio ρ_x/ρ_y, and the results correspond to $\rho_x/\rho_y = 1$ (i.e. representative of almost square plan structures). Four different values of T_y are presented and the displacement variations are plotted against the diaphragm period, T_d.

In general, the inelastic response of the symmetric systems is qualitatively similar to the elastic response, and characterised by the reductions in the wall displacements as the diaphragm flexibility increases. For the short-period system of T_y = 0.1 s, however, some amplification of the flexible side can occur as the yield level increases. For elastic systems, this reduction can be shown to arise from the reduced interactions of modal masses associated with the walls and the diaphragms (Fleishman and Farrow 2001). When the diaphragm becomes very flexible, the diaphragm mass responds independently of the walls, and each wall behaves as though it is an isolated element, resisting its own inertia only. This is reflected in the constant wall displacements beyond T_d of approximately 1 s in Figure 4. The similarity between the displacement variations of the elastic and the inelastic systems suggests that the walls also behave as independent elements for inelastic systems with the increase in diaphragm flexibility. The response reduction is most prominent for short-period systems (e.g. T_y = 0.1 s) with large levels of yielding.

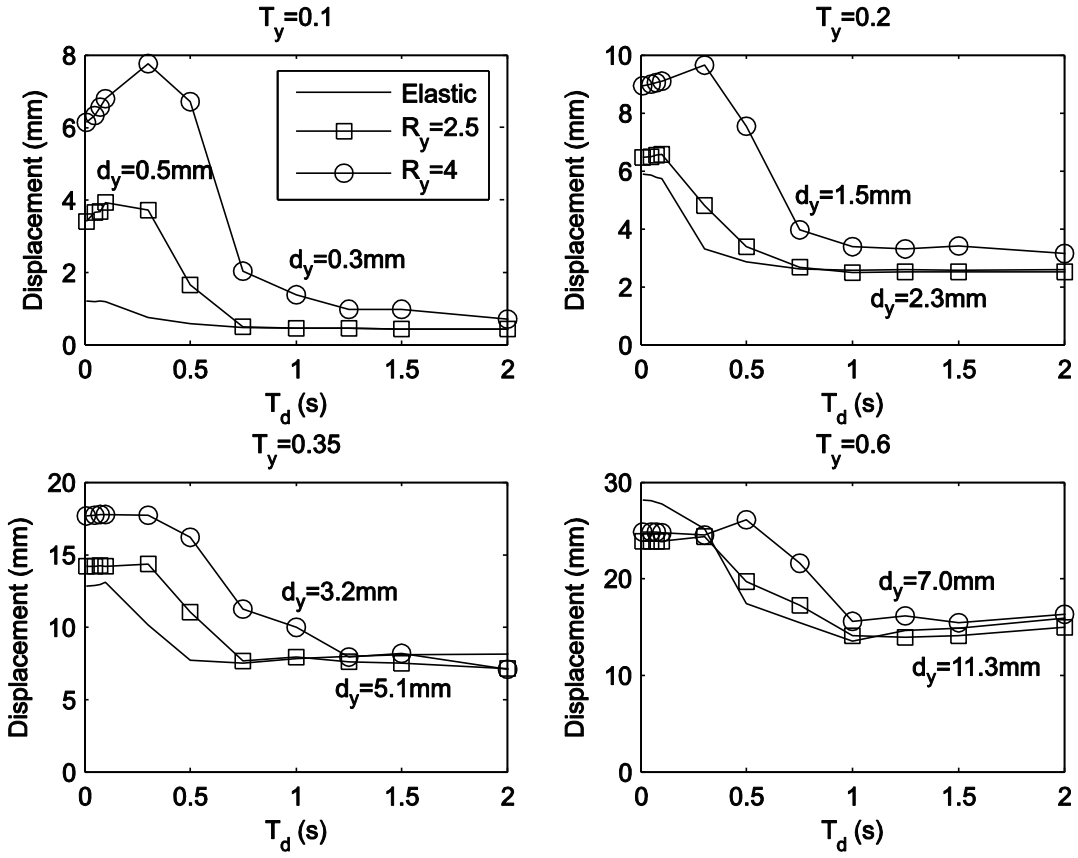

Figure 4. Mean peak displacement of walls in symmetric system, $\rho_x/\rho_y = 1$. Yield displacements (d_y) of the walls are indicated.

4.2 Response of Stiffness Asymmetric Systems

The mean peak wall displacements of stiffness-asymmetric, but strength-symmetric ($\varepsilon_{px} = 0$) systems are shown in Figure 5 for wall 1 (flexible side) and wall 2 (stiff side). The stiffness eccentricity ε_{sx} is varied from 0.1, to 0.3 and the results are shown with respect to T_d. Each figure presents results corresponding to three different values of lateral period (T_y = 0.1, 0.2 and 0.35 s), and three levels of yielding (elastic, R_y of 2.5 and 4). In all plots, the responses of the symmetric systems are also shown for comparison.

The overall displacement variations of the flexible and the stiff sides can be seen to resemble the symmetric response. In addition, the response variations are also qualitatively similar to the elastic behaviour. However, the displacement of the flexible side increases, and that of the stiff side reduces, in comparison to the symmetric system in almost all ranges of diaphragm stiffness. The amplification of the flexible side's displacement over the rigid diaphragm condition can be observed when the diaphragm is relatively stiff. This amplification becomes more pronounced with the increase in stiffness asymmetry.

The mean peak wall displacements of the inelastic systems of Figure 5 are shown normalised to the yield displacements of walls (i.e. as ductility) in Figure 6. In contrast to the displacement demand, the ductility demand of the stiff side increases, and the flexible side reduces, in comparison to the symmetric system. This effect is most significant when the diaphragm is stiff. As the diaphragm flexibility increases, the discrepancy in the ductility demand between the two sides disappears. This result implies that the diaphragm flexibility generally leads to a more uniform distribution of damage between the in-plane loaded walls, if the strength eccentricity of the building is small.

The mean peak displacements of walls 3 and 4 (orthogonal sides) are shown in Figure 7 for T_y of 0.35 s, for three levels of yielding and stiffness eccentricities. The displacements are largest when the diaphragm is rigid. As the diaphragm flexibility increases, rapid reductions in the wall displacements take place, suggesting that the orthogonal sides are excited predominantly by the torsional rotation of the diaphragm. The yielding of the main lateral-load resisting walls causes the reduction of the orthogonal displacements, which appears to be consistent with the reduction in torsional behaviour expected as the strength distribution is symmetric.

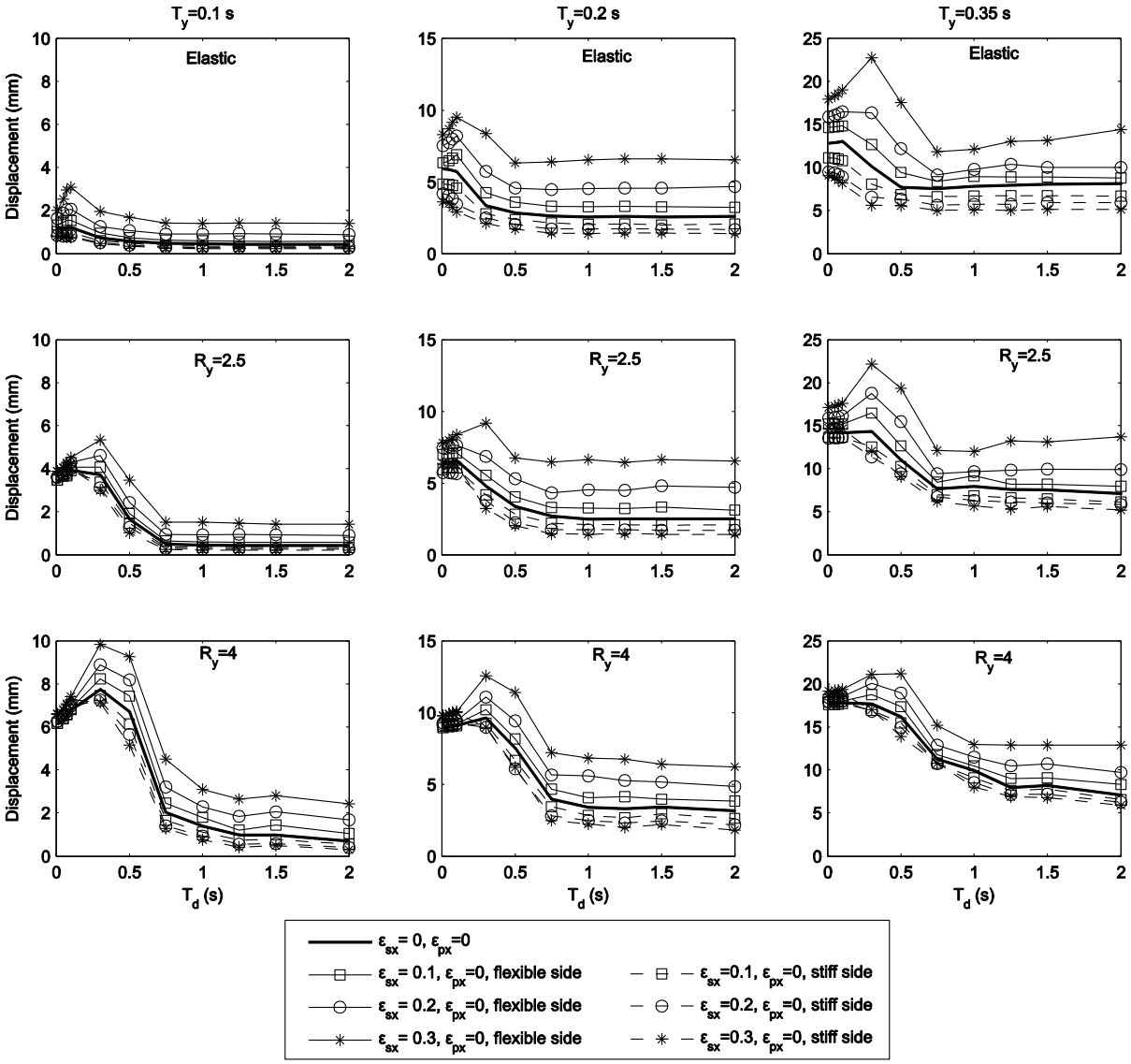

Figure 5. Mean peak displacement of flexible (wall 1) and stiff (wall 2) sides, stiffness-asymmetric systems with $\Omega_\theta = 1$, $R_F = 1$ and $\rho_x/\rho_y = 1$.

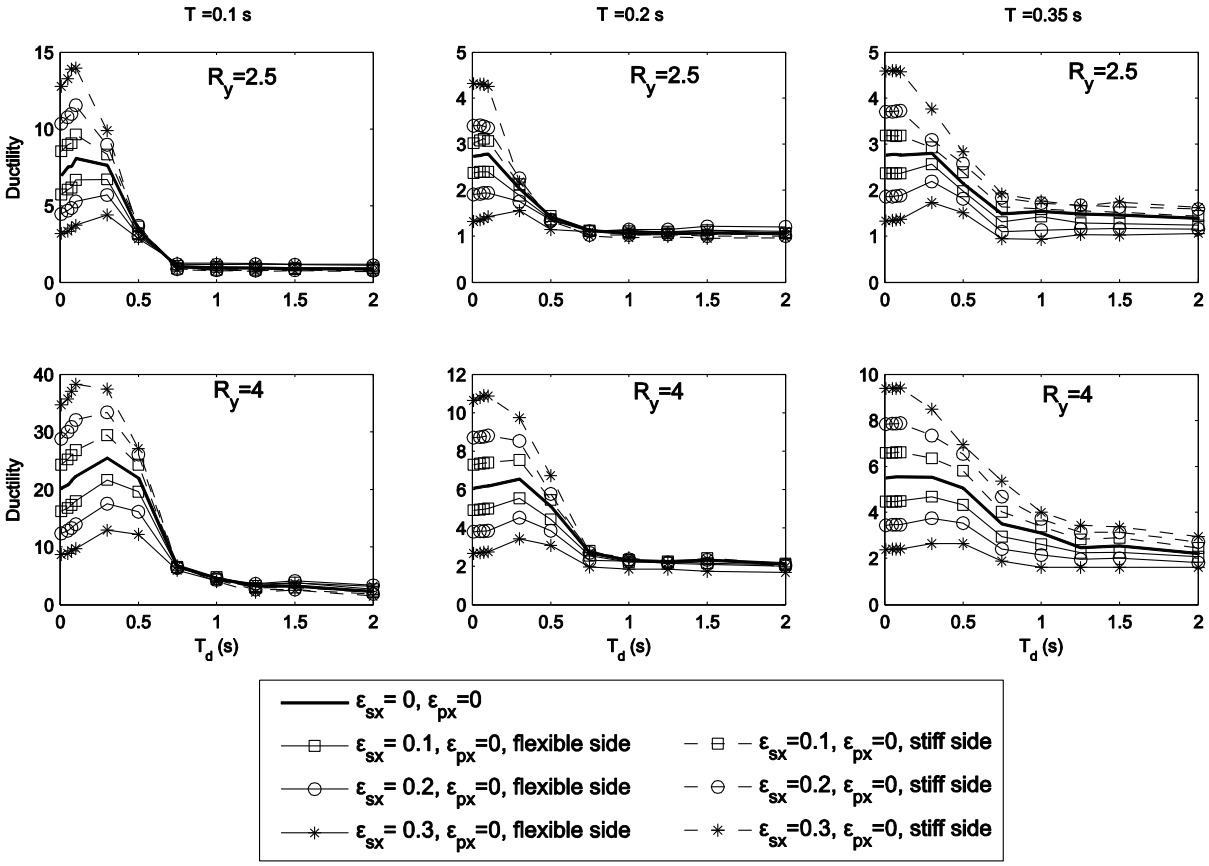

Figure 6. Mean peak ductility of flexible (wall 1) and stiff (wall 2) sides, stiffness-asymmetric systems with $\Omega_\theta = 1$, $R_F = 1$ and $\rho_x/\rho_y = 1$.

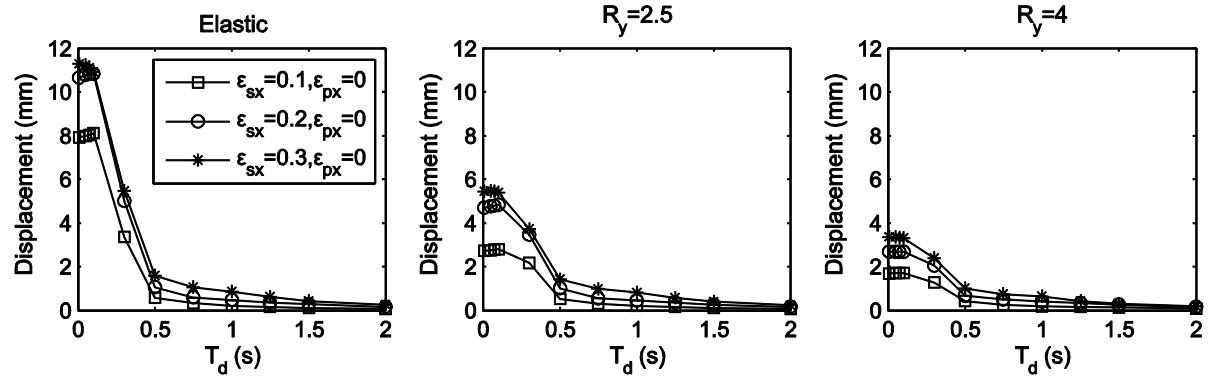

Figure 7. Mean peak in-plane displacement of orthogonal (wall 3 and wall 4) sides, stiffness-asymmetric systems with $T_y = 0.35$ s, $\Omega_\theta = 1$, $R_F = 1$ and $\rho_x/\rho_y = 1$.

The effects of variations in the stiffnesses and the strengths of the orthogonal sides, as expressed by Ω_θ and R_F, as well as the differences in the mass ratio ρ_x/ρ_y, are shown in Figure 8 for T_y of 0.35 s and R_y of 2.5. The parameters Ω_θ and R_F affect stiff diaphragm systems, but have negligible influences as the diaphragm flexibility increases. This is because the orthogonal sides are primarily engaged by the torsional behaviour of the diaphragm, hence changes in their properties affect systems that undergo

torsional response, i.e. for relatively stiff diaphragms only. On the other hand, the variation in the mass ratio affects relatively flexible diaphragm systems and has negligible influences for stiff diaphragm systems, because the rotational inertia (I_O) has been kept constant in the analysis. In general, the aforementioned effects remain small for the range of parameters investigated, and they may be considered as secondary parameters insofar as the effects of diaphragm flexibility are concerned. For the remainder of the paper, the system configurations will consist of $\Omega_\theta = 1$, $R_F = 1$ and $\rho_x/\rho_y = 1$.

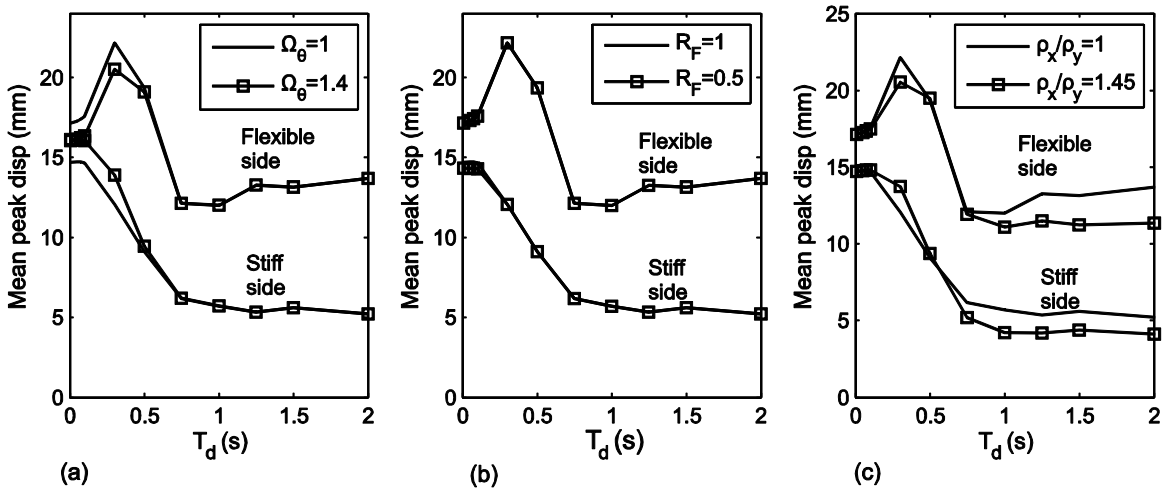

Figure 8. Mean peak displacements of stiffness-asymmetric systems with, $T_y = 0.35\ s$, $R_y = 2.5$ $\varepsilon_{sx} = 0.3$, and $R_F = 1$, (a) variation in Ω_θ, keeping constant R_F = 1 and $\rho_x/\rho_y = 1$, (b) variation in R_F, keeping constant $\Omega_\theta = 1$ and $\rho_x/\rho_y = 1$, and (c) variation in ρ_x/ρ_y, keeping constant $\Omega_\theta = 1$ and R_F = 1.

4.3 Response of Strength Asymmetric Systems

The effect of strength asymmetry on the mean peak displacements of the main lateral-load resisting elements are shown for the same structural configurations as for the stiffness-asymmetric systems with R_y of 2.5 and 4, with the exception that the strength eccentricity is now made equal to the stiffness eccentricity, $\varepsilon_{px} = \varepsilon_{sx}$ (Figure 9). The responses of the corresponding symmetric systems are again presented for comparison.

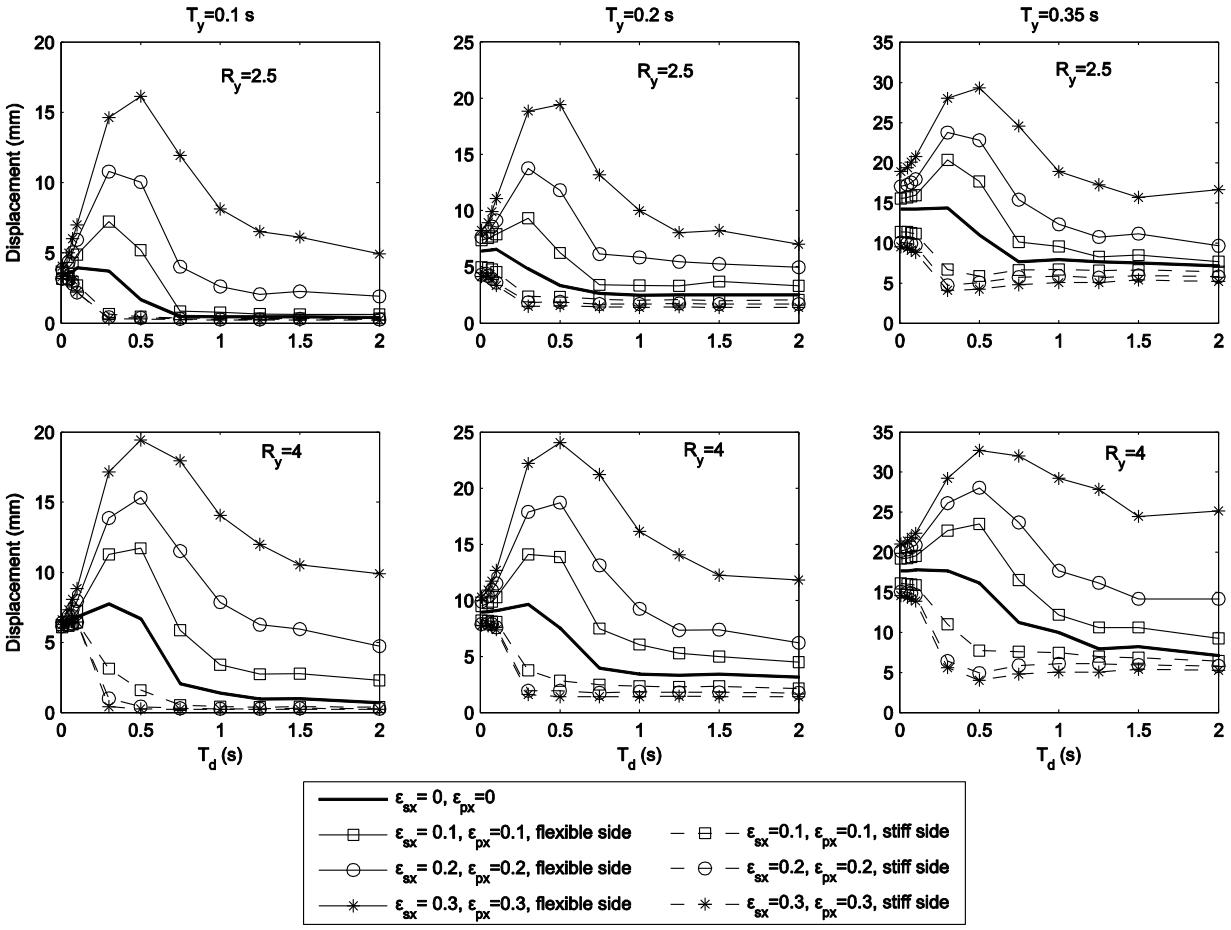

Figure 9. Mean peak displacement of flexible and stiff sides of strength asymmetric systems.

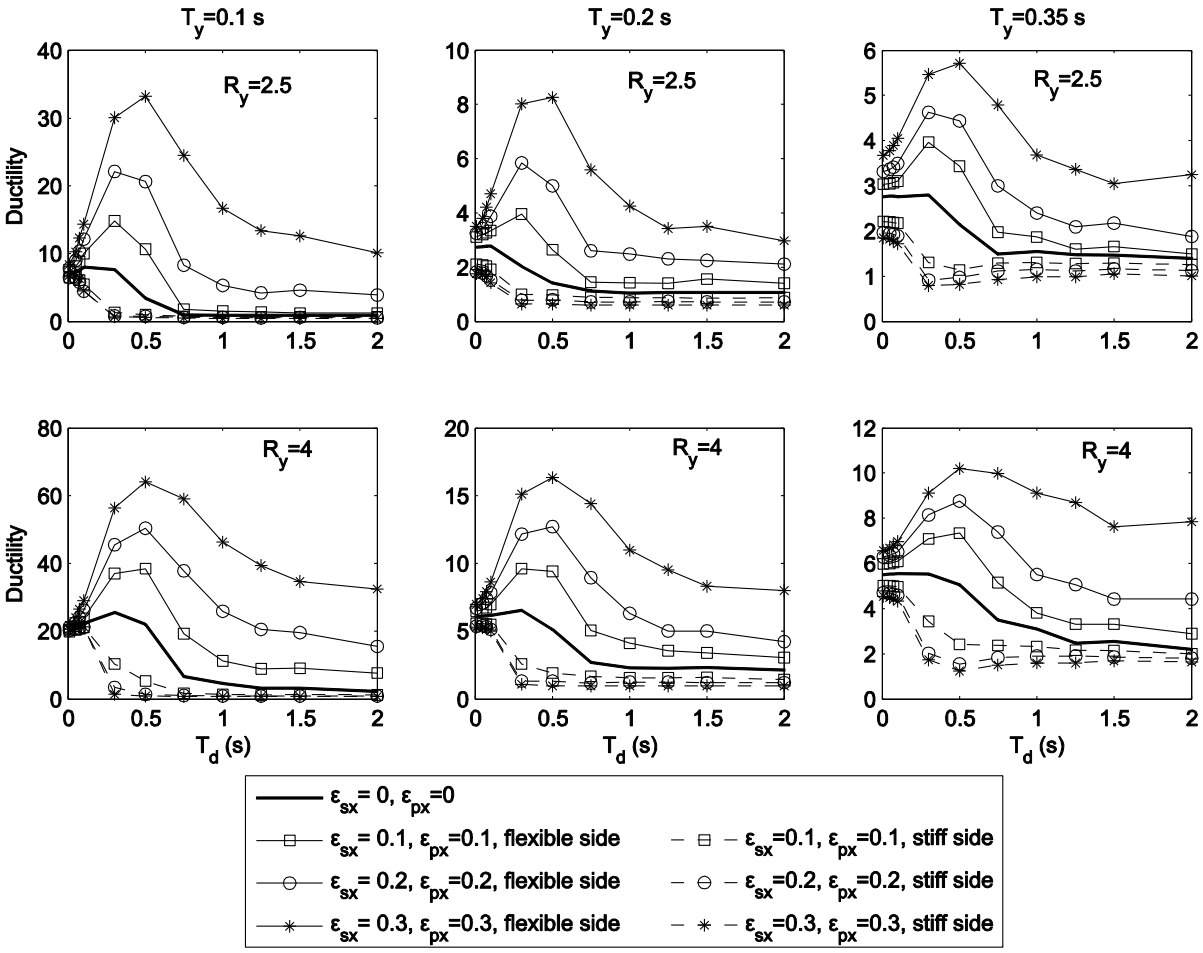

Figure 10. Mean peak ductility of flexible and stiff sides of strength asymmetric systems.

The response characteristics show significant deviations from the symmetric, and even the stiffness-asymmetric, systems. They also differ considerably from the elastic response (Figure 5). The inelastic response of strength-asymmetric systems are characterised by the large amplification of the flexible side's displacement, and the rapid reduction of the stiff side's displacement. While the amplified displacement of the flexible side also occurs for stiffness-asymmetric systems, it becomes much more pronounced.

The ductility demands of strength-asymmetric systems are shown in Figure 10. In contrast to the stiffness-asymmetric (but strength-symmetric) systems, the flexible side is subjected to a consistently larger ductility demand than the stiff side, and the increase in the level of strength eccentricity exacerbates this effect. Furthermore, the discrepancy in the ductility demand between the flexible and stiff walls remains even when the diaphragm flexibility is increased. This result suggests that for buildings with strength eccentricity, the flexible side is likely to experience more damage than the stiff side for all levels of diaphragm stiffness.

The maximum value of the peak displacement of the flexible side ($u_{1,max}$), which generally occurs at T_d between 0.3 s and 0.5 s (Figure 9), can be significantly larger than the displacement of the flexible side under the rigid diaphragm configuration at T_d = 0 s ($u_{1,rig}$). The maximum displacement amplification ratio, $u_{1,max}/u_{1,rig}$, has been found to be primarily a function of, and almost linearly related to, the strength eccentricity ε_{px} (or the level of strength asymmetry). The amplification was also more pronounced when the period T_y of the structure was less than the period at the beginning of constant velocity segment of the spectrum, T_C (Figure 3c). Other parameters, including T_d and R_y did not significantly affect the maximum amplification ratio of the flexible side. Eq. 1 was derived for the maximum displacement amplification of the flexible side as a linear function of ε_{px}, in which the influence of T_y was included by fitting an exponential function using least squares. The reasonable correlations of the empirical expression with the numerical results are shown in Figure 11.

$$\frac{u_{1,max}}{u_{1,rig}} = 1 + \left[3.363\left(\frac{T_y}{T_C}\right)^{-0.95}\right]\varepsilon_{px} \tag{1}$$

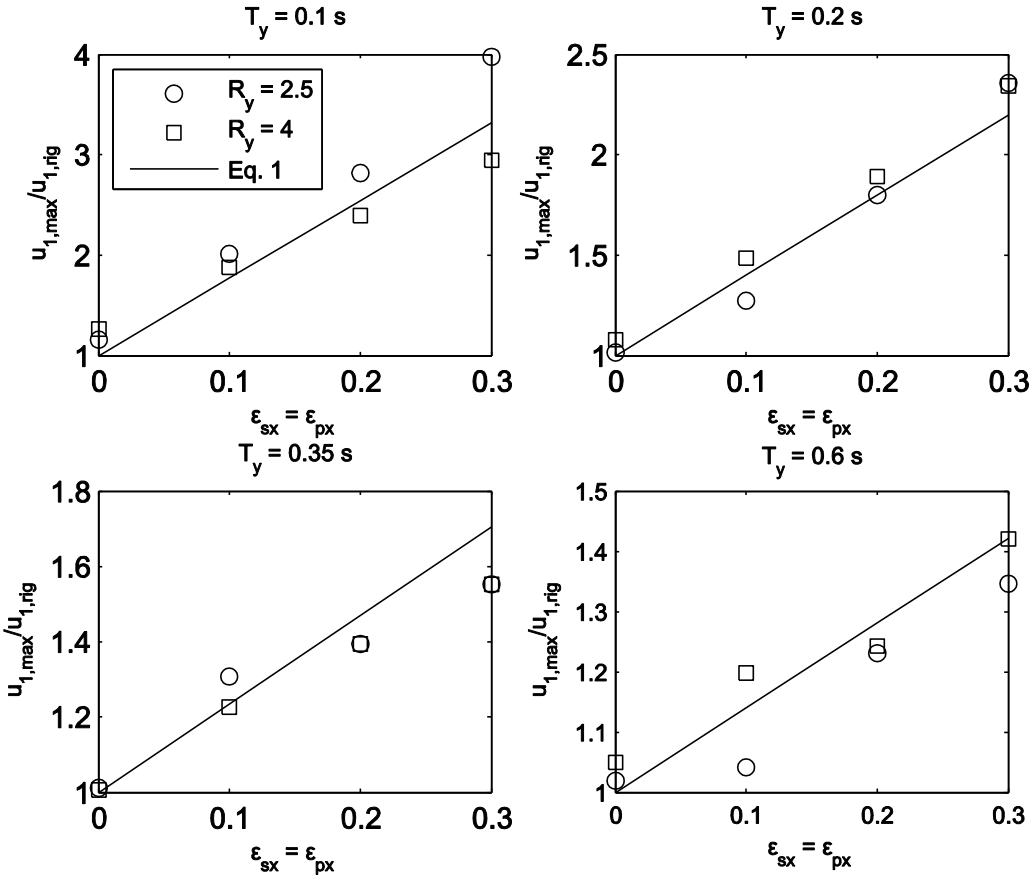

Figure 11. Comparison of Eq. 1 against displacement amplification of the flexible side obtained from time-history analysis.

The displacement variations of the strength-asymmetric systems also show similarities with those of symmetric systems when the diaphragm flexibility becomes large. In all cases analysed, the asymptotic reduction in the displacement of the flexible side, and the almost constant response of the stiff side indicate the walls to behave as if they are uncoupled elements. To confirm this premise, each wall was analysed as a single-degree-of-freedom (sdof) system with its own mass only, and the mean peak displacements from the sdof analysis (u_{sdof}) were compared with those of the actual model (u_{flex}) at the large diaphragm period of $T_d = 2.5$ s (Figure 12). The near-unity ratios between the two analyses indeed confirm that the walls respond as uncoupled elements when the diaphragm becomes overly flexible.

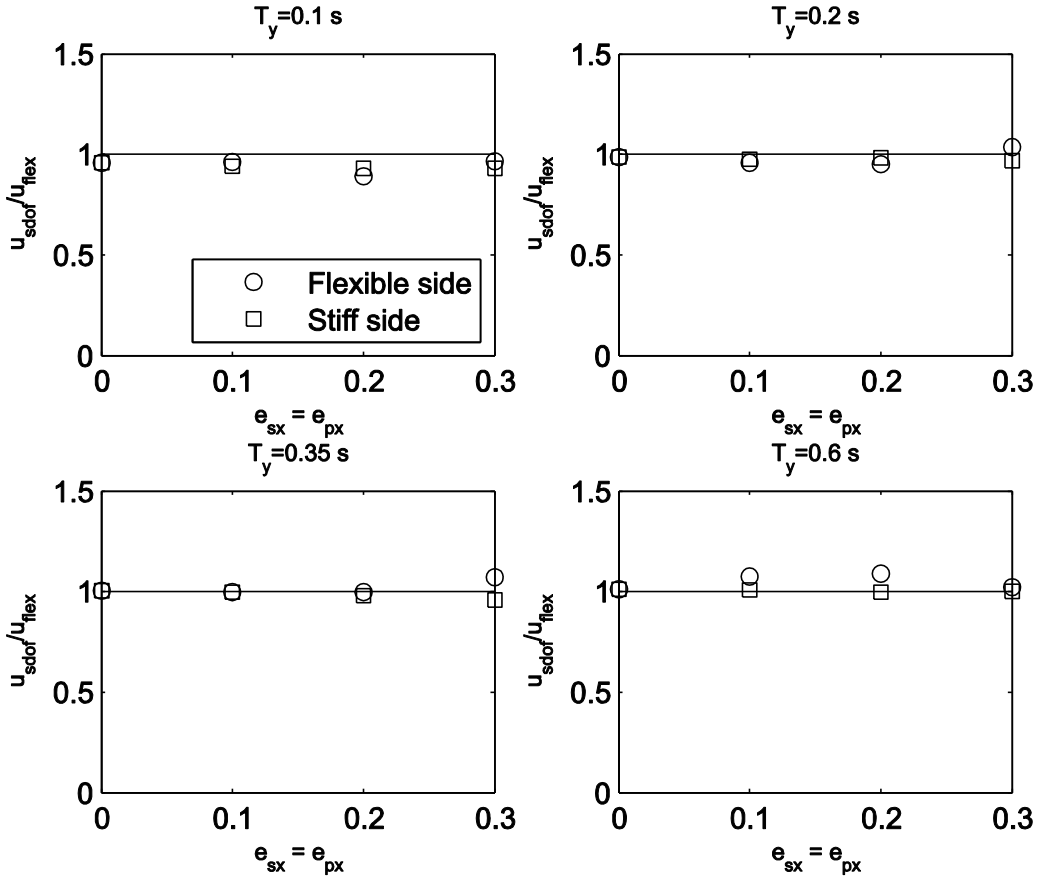

Figure 12. Ratios of mean peak displacements of uncoupled walls to the results obtained from the actual model with $T_d = 2.5$ s.

4.4 Summary of Parametric Study

The parametric analysis has shown that diaphragm flexibility can induce two different effects on the in-plane wall responses. The first effect is common to all systems (symmetric, stiffness- and strength-asymmetric) and characterised by the reduction of the wall responses and ultimately of the uncoupled

wall behaviour as the diaphragm flexibility becomes large. The second effect concerns the plan-asymmetric systems, in particular those with strength asymmetries. When the diaphragm is relatively stiff, significant amplification of the flexible side's response can occur. In comparison, diaphragm flexibility has been observed to be generally beneficial for the stiff side of the structure in reducing both displacement and ductility demands. For strength-asymmetric structures, the maximum conceivable amplification of the flexible side's displacement has been observed to be primarily a function of the initial period of the structure and the level of strength asymmetry, and can be estimated using Eq. 1.

5. CHARACTERISATION OF DIAPHRAGM FLEXIBILITY

5.1 Diaphragm Classification

The diaphragms can be classified into distinct ranges based on how an incremental flexibility of the diaphragm affects the wall responses. For the most general configuration of strength-asymmetric systems, four diaphragm stiffness ranges can be readily identified from the variations of the peak wall displacements. An example is shown in Figure 13 for $T_y = 0.35$ s, $R_y = 2.5$ and $\varepsilon_{sx} = \varepsilon_{px} = 0.3$. Using similar terminologies to those commonly used in seismic codes and guidelines (ASCE 2014), these ranges are referred to as "rigid", "stiff", "semi-flexible" or "flexible". The qualitative descriptions of these ranges are as follows:

- The "rigid" range defines the diaphragm stiffnesses for which an incremental diaphragm flexibility has little effects on the wall responses because the diaphragm remains almost rigid.

- In the "stiff" range, an incremental diaphragm flexibility increases the response of the flexible side, and reduces that of the stiff side.

- In the "semi-flexible" range, an increase in diaphragm flexibility induces a reduction in the flexible side's response.

- The "flexible" range defines the diaphragm stiffnesses for which the walls behave as though they are isolated elements, and an incremental diaphragm flexibility has no effect on the wall behaviour.

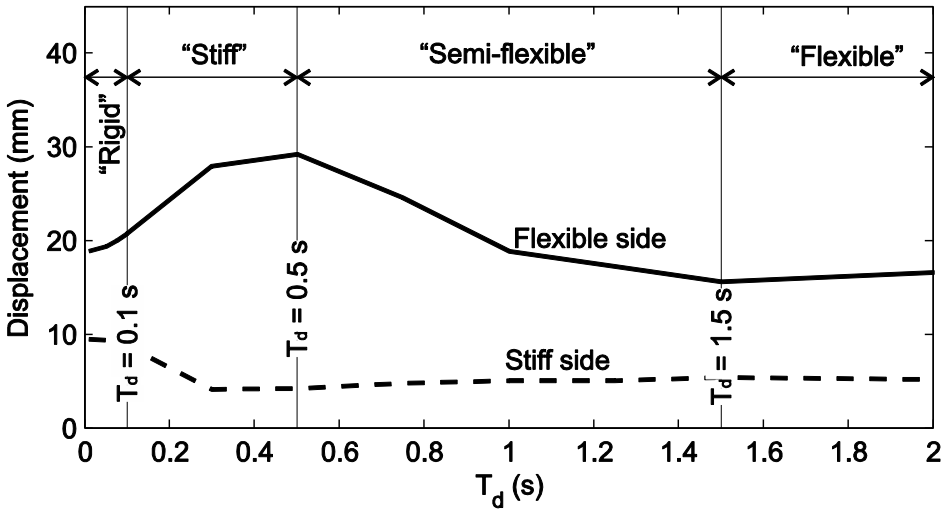

Figure 13. Diaphragm classification, illustrated for $T_y = 0.35$ s, $R_y = 2.5$ and $\varepsilon_{sx} = \varepsilon_{px} = 0.3$.

The classification also reflects the differences in the dominant diaphragm deformation characteristics. For the unidirectional loading considered in this study, the diaphragm deformation may be decomposed into four components - translation, torsional rotation, shear and bending - as shown in Figure 14. The first two components express the rigid-body motion, while the latter two capture the deformational modes of the diaphragm. Note that "shear" and "bending" refer to the overall deformation shapes as indicated in Figure 14, and have no relations to the deformation components of a Timoshenko beam. The relative importance of these components can be gauged by comparing the derived displacements Δ_w, Δ_θ, Δ_s and Δ_d respectively for translation, torsion, shear and bending (Figure 14). They can be computed from the actual displacements measured at 3 different locations of the model in the direction of loading (u_1 to u_3 in Figure 14(a)) and at two locations in the direction orthogonal to loading (v_1 and v_2 in Figure 14(a)),

$$\Delta_w = \frac{u_1 + u_3}{2} \tag{2}$$

$$\Delta_\theta = (v_1 - v_2)\frac{L_x}{L_y} \tag{3}$$

$$\Delta_s = (u_1 - u_3) - \Delta_\theta \tag{4}$$

$$\Delta_d = u_2 - \Delta_w \tag{5}$$

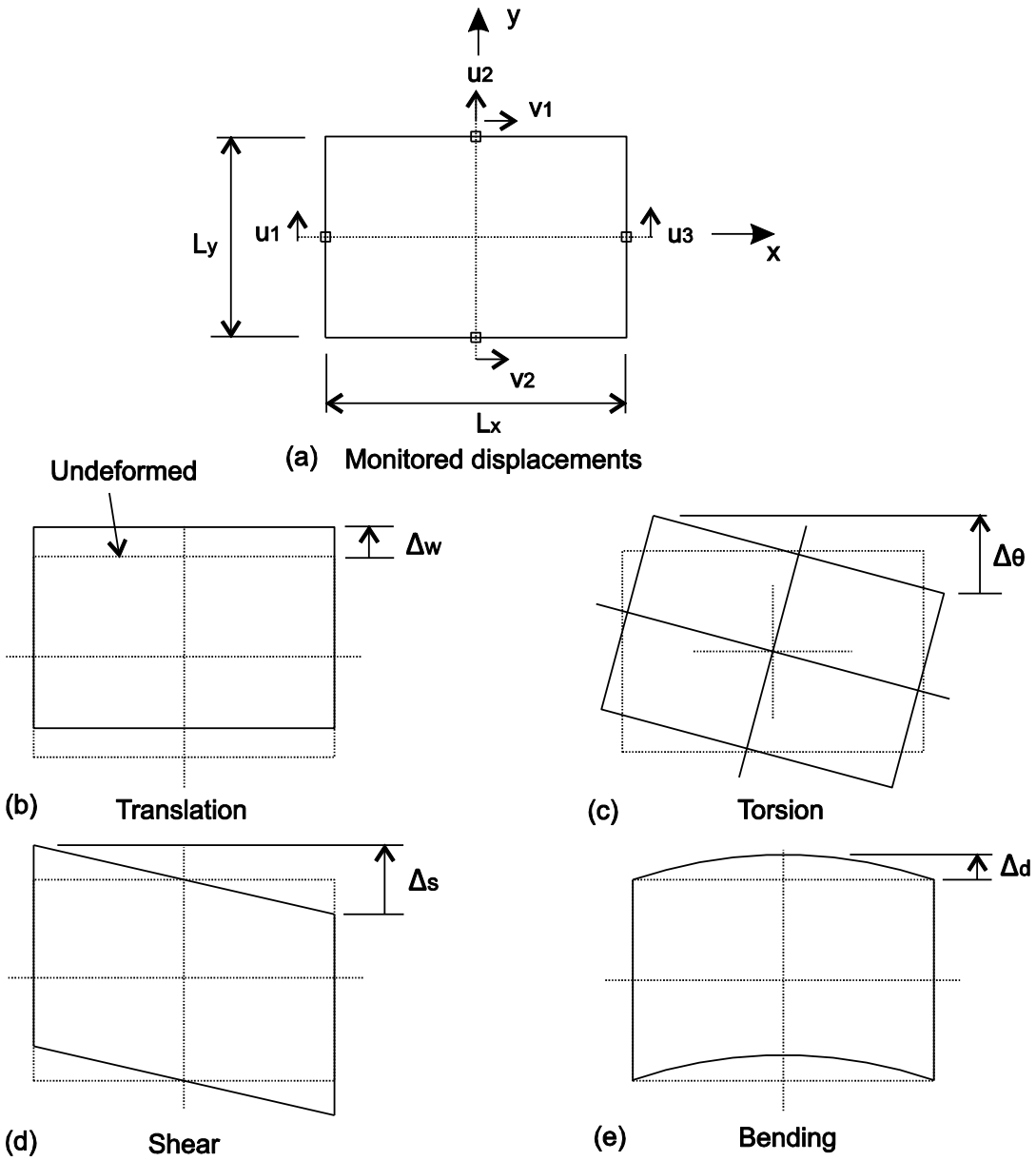

Figure 14. Deformation components of the diaphragm, (a) measurement locations of model, (b) translation, (c) torsion, (d) shear and (e) bending.

The mean of the peak values of Δ_w, Δ_θ, Δ_s and Δ_d are plotted in Figure 15 for the same system configuration as for Figure 13. It can be seen that:

- The "rigid" diaphragm range is characterised essentially by the rigid-body motion of the diaphragm. The shear (Δ_s) and the bending (Δ_d) components are negligible in this range;

- The "stiff" diaphragm range is characterised by the mix of the rigid-body, the shear and the bending deformations. The shear component is dominant, while the torsional motion becomes small;
- The "semi-flexible" diaphragm range is also characterised by the mix of the shear and the bending deformations, while the torsional behaviour is almost negligible. In contrast to the "stiff" range, bending becomes the dominant component;
- The "flexible" diaphragm range is dominated by the bending component.

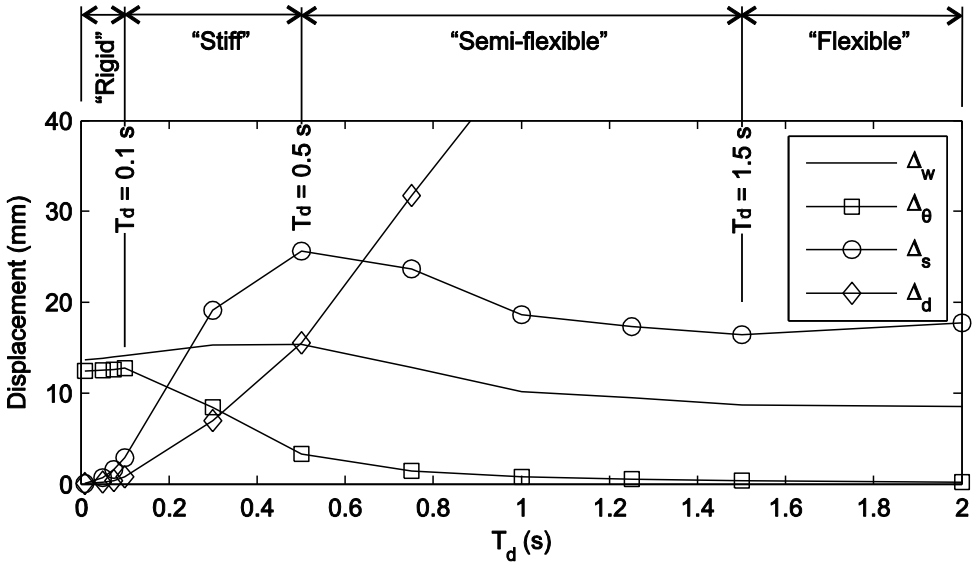

Figure 15. Mean peak deformation components of the diaphragm for $T_y = 0.35$ s, $R_y = 2.5$, ε_{sx} = 0.3, ε_{px} = 0.3.

In the "stiff" range, the shear deformation of the diaphragm occurs with the amplification of the flexible side (Figure 13) because the flexible side, being also the weaker side when ε_{sx}=ε_{px}, tends to yield first, while the stiff side may remain almost elastic. A large difference in the instantaneous wall stiffnesses hence exists, and as the diaphragm is not rigid, the displacement of the flexible side is not restrained by the stiff side. This results in the large yielding of the flexible side accompanied by the shear-dominant deformation of the diaphragm.

In the "semi-flexible" range, the same phenomenon as the "stiff" range essentially occurs. However, because the diaphragm becomes flexible enough to vibrate between the walls in a different mode, it leads

to the reduction of the inertia force to be resisted by the walls. This results in the reduction in the flexible side's displacement (Figure 13).

Similar associations between the diaphragm classification and the dominant diaphragm deformation can be established for the stiffness-asymmetric system. The main difference between the stiffness- and strength-asymmetric systems is that the shear mode does not become a dominant component for stiffness-asymmetric systems (Figure 16(b)). This is because the flexible and the stiff sides tend to yield at the same time when ε_{px} = 0, resulting in no significant differences in the instantaneous wall stiffnesses. For the symmetric system (Figure 16(a)), the shear mode does not exist, and the "stiff" diaphragm range disappears, so that the "rigid" range is followed by the "semi-flexible" range.

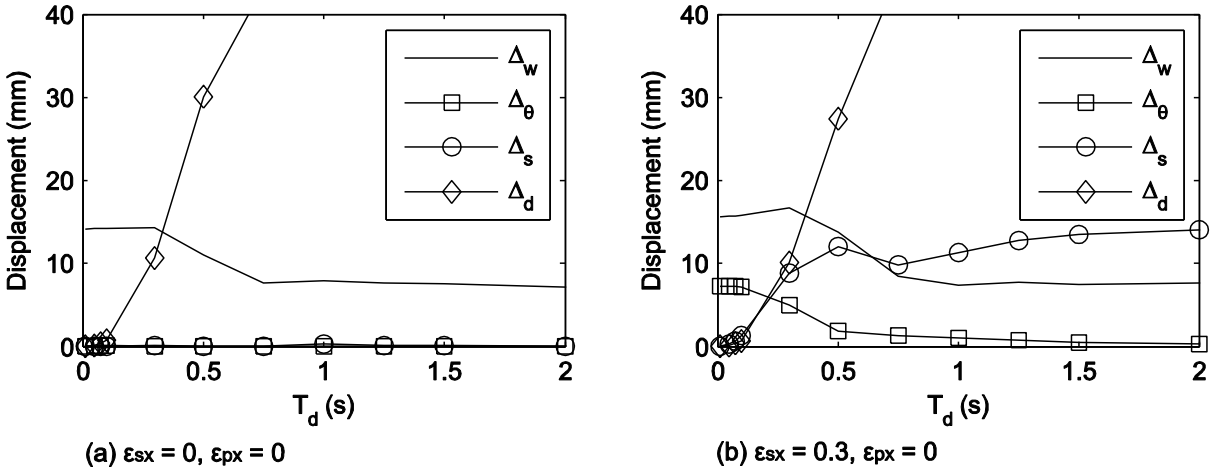

Figure 16. Mean peak deformation components of the diaphragm for $T_y = 0.35$ s, $R_y = 2.5$, (a) symmetric (ε_{sx} = 0, ε_{px} = 0), (b) stiffness-asymmetric (ε_{sx} = 0.3, ε_{px} = 0)

5.2 Characteristics of Dynamic Behaviour

The dominance of the bending component of the diaphragm deformation strongly affects the dynamic behaviour of the system, and the transition point between the "stiff" and the "semi-flexible" diaphragms marks a change in the response characteristics of the system from being governed essentially by a single mode to a multi-mode behaviour. This can be identified from the Fourier amplitudes of the displacements of the flexible and the stiff sides, as well as the diaphragm mid-span. Using the same structural configuration as for Figure 13, a Fourier analysis is conducted over the windowed duration of 5% to 95% of the Arias intensity for each ground motion. The calculated amplitudes are then averaged and normalised to the peak value (Figure 17). The plots show that a dominant mode exists in the "rigid" and the "stiff" diaphragm ranges ($T_d < 0.5$ s). Even though the higher mode associated with torsion also affects the stiff side, the fundamental mode can be considered to govern the response in these ranges. In

the "semi-flexible" range ($0.5 \leq T_d < 1.5$ s), however, the response of the stiff side becomes independent of the rest of the structure. In the "flexible" range ($T_d \geq 1.5$ s), the independent motions of the walls and the diaphragm become apparent. Therefore, multiple dominant modes are present in the "semi-flexible" and "flexible" ranges, while a single dominant mode generally exists in the "rigid" and the "stiff" ranges. Similar consistent trends have also been observed for the symmetric and the stiffness-asymmetric systems. This observation has a practical implication, because the single-mode assumption may be appropriate in simplifying the seismic analysis of structures whose diaphragms are classified as "rigid" or "stiff".

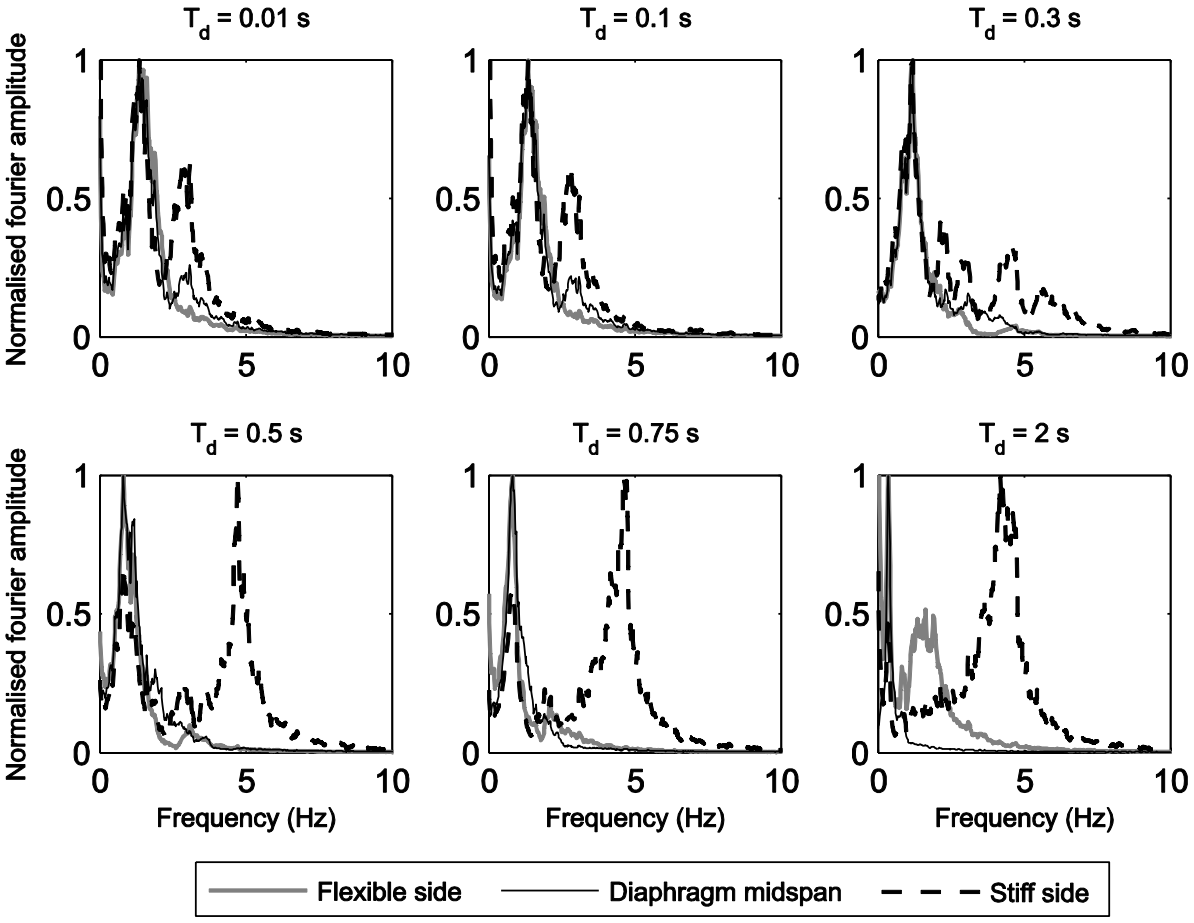

Figure 17. Normalised Fourier amplitudes of displacements for $T_y = 0.35$ s, $R_y = 2.5$ and $\varepsilon_{sx} = \varepsilon_{px} = 0.3$.

The transition from the "stiff" to the "semi-flexible" range (or transition from essentially a single-mode to a multi-mode response) may be considered to occur if the bending component of the diaphragm becomes relatively large in comparison to the other deformation components. One measure of this is the ratio $\lambda = \Delta_d/\Delta_w$. The values of λ calculated at the transition point using the mean peak displacements show asymptotic reductions with the increase in T_y, as shown in Figure 18 for all symmetric, stiffness- and

strength-asymmetric systems with $\rho_x/\rho_y = 1$. In addition, the range of calculated λ reduces with T_y, with $\lambda = 1/3$ providing a reasonable approximation to the median values for T_y of 0.35 and 0.6 s, which are in the velocity-sensitive range of the ground motion. For shorter period systems, this limit is a generally conservative measure of the transition point. Therefore, as an approximate (and conservative) measure, $\lambda = 1/3$ may be considered to signify the transition between the "stiff" to "semi-flexible" ranges of diaphragms.

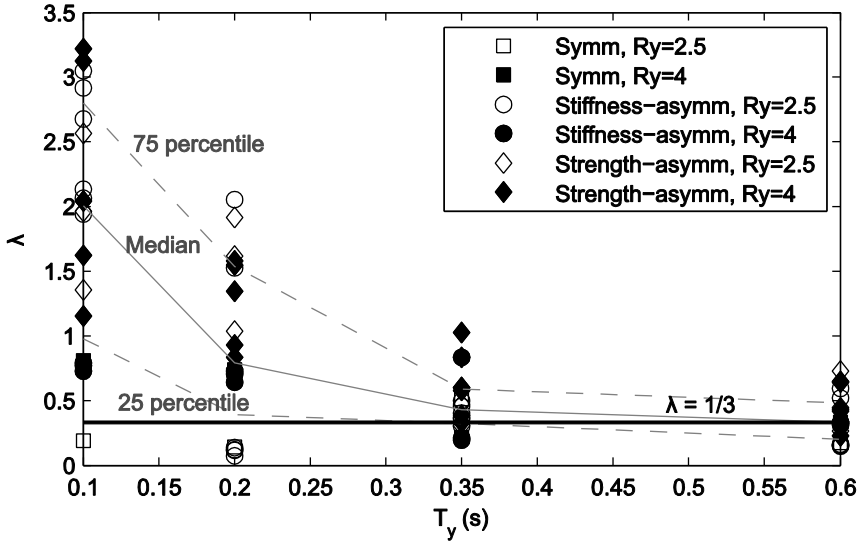

Figure 18. Variation of λ as a function of T_y, includes symmetric, stiffness- and strength-asymmetric configurations.

6. APPRAISAL OF SIMPLIFIED MODEL

The parametric analysis was conducted using idealised single-storey systems which did not fully capture the characteristics of actual URM buildings with flexible diaphragms (as discussed in Section 2). Hence, two case studies were conducted using more detailed numerical models to verify the applicability of the results obtained from the simplified models for URM buildings.

The two building models (Model A and Model B) were single-bay, two-storey URM constructions. The models were analysed using the equivalent frame analysis program TREMURI (Lagomarsino et al. 2013). The plan layouts of the models and their in-plane wall discretisations are shown in Figure 19. The direction of loading and the span direction of floor joists are also indicated. As summarised in Table 4, the buildings had different levels of stiffness and strength eccentricities. Model A had a small stiffness eccentricity of 0.07 and no significant strength eccentricity. Model B had stiffness and strength eccentricities of 0.32 and 0.08, respectively. The stiffness and strength of each in-plane loaded wall (Wall

1 and Wall 2) were calculated from a pushover analysis by idealising the pushover curve of each wall by an elastic-plastic simplification.

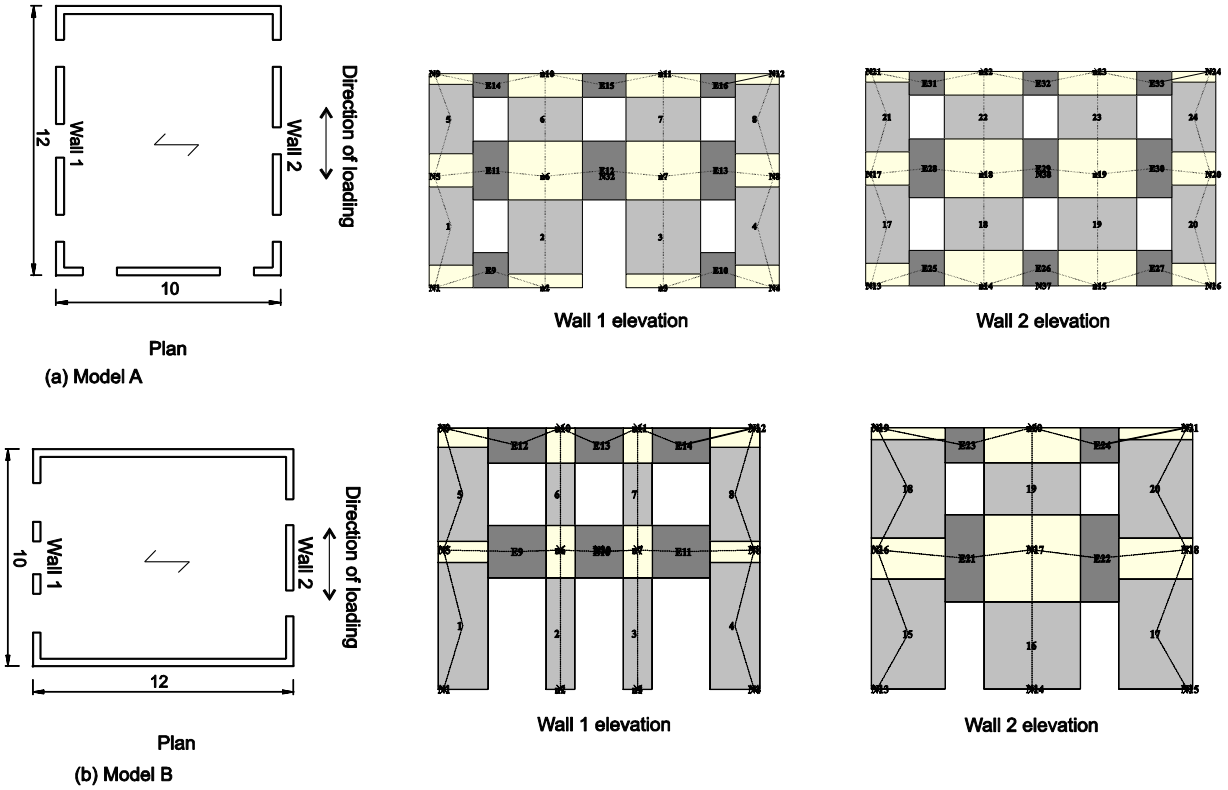

Figure 19. Building models analysed

Table 4. Parameters of case study building models

Parameter	Model A	Model B
T_y (s)	0.15	0.23
ε_{sx}	0.07	0.32
ε_{px}	0.0	0.08
ρ_x/ρ_y	0.74	1.27

The in-plane behaviours of the walls were modelled using the equivalent frame idealisation, in which the nonlinear behaviours of piers and spandrels are defined by the macroelement model of Penna et al. (2014). The macroelement model is able to capture the important response mechanisms of URM, including the coupled axial-rocking behaviour with limited compressive strength, and the cumulative shear damage resulting in strength and stiffness degradations. The stiffness contributions of the out-of-plane walls were considered to be small in comparison to those of in-plane direction, and were hence neglected. Four elastic membrane elements were used to represent a diaphragm with the stiffnesses

corresponding to the range of timber diaphragm constructions described in ASCE 41-13 (ASCE 2014). In addition, two relatively stiff diaphragms representing hypothetical retrofits were also analysed.

Nonlinear time-history analysis was conducted for each building, subjected to a suite of accelerograms scaled to match the design spectrum of AS 1170.4 (Standards Australia 2007) for Site Class C_e, with the period at the beginning of the constant velocity range T_C = 0.34 s. The ground motions were different to those used for the parametric study, and are listed in Appendix B. The records were scaled in magnitude until significant inelastic behaviours of both buildings were attained.

The analyses showed that inelastic damage was concentrated in the ground storey for both models. Figure 20 shows the mean peak interstorey drift ratios of the critical ground storey plotted against the average diaphragm period of the floor and the roof. Figure 20 shows that the response characteristics of both building models are consistent with the diaphragm classification developed using the simplified systems. Furthermore, the effects of diaphragm flexibility on the wall responses can be seen to depend on strength eccentricity. When the strength eccentricity is negligible, Model A indicates that the effects of diaphragm flexibility are similar for both flexible and stiff sides. When the strength eccentricity is present, however, results of Model B show that the diaphragm flexibility induces the response amplification of the flexible side and the rapid reduction of the stiff side. These observations are identical to the main characteristics of the responses of observed using simplified systems (Section 4).

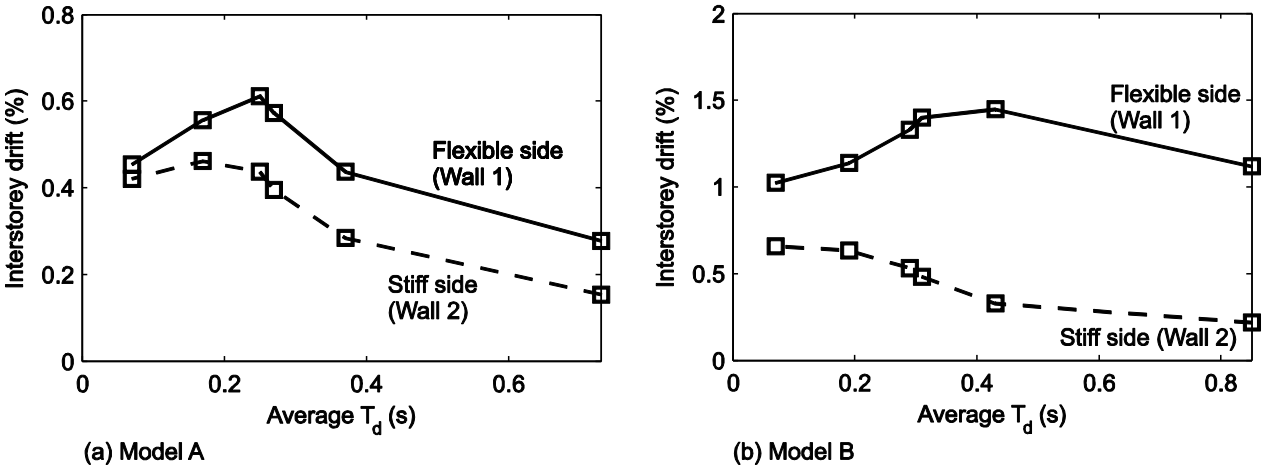

Figure 20. Mean peak interstorey drift ratios of flexible and stiff walls for (a) strength-symmetric Model A, (b) strength-asymmetric Model B

The applicability of the empirical expression developed using the simplified systems for URM buildings was also investigated. The maximum response amplification ratio of the flexible side (Eq. 1) was evaluated for Model B and compared against the numerical result. Using the values listed in Table 4, this ratio was evaluated to be 1.34. From Figure 20(b), the "exact" ratio (mean peak drift at T_d = 0.43 s

divided by the corresponding value at T_d = 0.09 s) is found to be 1.41, which is within 5% of the predicted value. This close correspondence suggests that the simplified system used in the parametric analysis was able to capture the main response characteristics of URM buildings with flexible diaphragms.

7. CONCLUSIONS

The effects of diaphragm flexibility on the seismic response of plan-asymmetric structures typical of URM buildings were investigated using simple inelastic models. A wide range of diaphragm stiffnesses were considered, ranging from practically rigid to almost completely flexible.

The analyses identified that the diaphragm flexibility can increase or reduce the displacement demands on the in-plane walls, depending on the level of diaphragm flexibility and the presence of stiffness and strength eccentricity. The reduction of the wall displacement is induced by the bending-dominant (vibrational) response of the diaphragm, and occurs when the diaphragms are relatively flexible for all systems considered in the study (symmetric, stiffness - and strength - asymmetric). The increased wall displacement predominantly occurs in plan-asymmetric systems, in particular those with strength eccentricity, when the diaphragm is relatively stiff. In these cases, the diaphragms tend to deform in a shear-dominant shape, and causes large displacement amplification of the flexible side of the structure.

In general, non-rigid diaphragms may be classified into four ranges, referred in this study as "rigid", "stiff", "semi-flexible", and "flexible", defined qualitatively on how incremental diaphragm flexibility affects the displacement demands of the in-plane walls. The “rigid” diaphragm range is characterised essentially by the rigid-body motions of the diaphragm, and hence incremental diaphragm flexibility has negligible effects on the wall responses. At the other end of the spectrum, in the “flexible” range, diaphragm flexibility also has little effects because the walls tend to behave as independent elements. The “stiff” range corresponds to the shear-dominant displacement shape of the diaphragm, which increases the displacements of the flexible side and reduces the stiff side, while the “semi-flexible” range corresponds to the bending-dominant diaphragm displacement, which causes the reductions of the displacements for both flexible and stiff walls. In particular, the transition from the "stiff" to the "semi-flexible" range has been identified to correspond with the transition from the essentially single-mode to the multi-mode behaviour. A measure of this transition point has been derived based on the displacement shape of the diaphragm.

Although simplified single-storey single-bay models were used in this study, general conclusions are expected to be applicable for multi-storey single-bay structures as the participations of higher modes

along the building height are typically negligible for low-rise URM structures. Further studies are however needed for buildings with additional internal walls, and for those with more complicated wall layouts.

ACKNOWLEDGEMENTS

The authors gratefully acknowledge the financial support provided by the Australian Research Council (ARC grant # DP120100848). The financial support provided by the Australian Postgraduate Award for the first author is also gratefully acknowledged. The financial support provided by Progetto ReLUIS 2015 – Linea Strutture in Muratura for the third author is also gratefully acknowledged.

REFERENCES

ASCE 41-13 (2014) "Seismic evaluation and retrofit of existing buildings", American Society of Civil Engineers, Reston, Virginia.

Brignola, A., Pampanin, S., and Podestà, S. (2012) "Experimental evaluation of in-plane stiffness of timber diaphragms", Earthquake Spectra 2012, 28(4), 1687-1709.

Carr, A. J. (2008) Ruaumoko user manual, University of Canterbury.

De-La-Colina, J. (1999) "In-plane floor flexibility effects on torsionally unbalanced systems", Earthquake Engineering and Structural Dynamics, 28(12), 1705-1715.

Fleischman, R. B. and Farrow, K. T. (2001) "Dynamic behavior of perimeter lateral-system structures with flexible diaphragms", Earthquake Engineering and Structural Dynamics, 30(5), 745-763.

Giongo, I., Dizhur, D., Tomasi, R., and Ingham, J. M. (2014) "Field testing of flexible timber diaphragms in an existing vintage URM building", Journal of Structural Engineering, 141, Special Issue: Field testing of Bridges and Buildings.

Jain, S. K. and Jennings, P. C. (1985) "Analytical models for low-rise buildings with flexible floor diaphragms", Earthquake Engineering and Structural Dynamics, 13 (2), 225-241.

Ju, S. H. and Lin, M. C. (1999) "Comparison of building analyses assuming rigid or flexible floors", Journal of Structural Engineering, 125 (1), 25-31.

Kim. S.-C. and White D. W. (2004) "Nonlinear analysis of a one-story low-rise masonry building with a flexible diaphragm subjected to seismic excitation", Engineering Structures, 26 (14), 2053-2067.

Lagomarsino, S., Penna, A., Galasco, A., and Cattari, S. (2013) "TREMURI program: An equivalent frame model for the nonlinear seismic analysis of masonry buildings", Engineering Structures, 56, 1787 – 1799.

Magenes, G. and Calvi, G. M. (1997) "In-plane seismic response of brick masonry walls", Earthquake Engineering and Structural Dynamics, 26 (11), 1091-1112.

Magenes, G., Penna, A., Rota, M., Galasco, A., and Senaldi, I. (2014) "Shaking table test of a full-scale stone masonry building with flexible diaphragms", International Journal of Architectural Heritage, 8(3), 349 – 375.

Moon, S.-K. and Lee, D.-G. (1994) "Effects of inplane floor slab flexibility on the seismic behavior of building structures", Engineering Structures, 16 (2), 129-144.

Pacific Earthquake Engineering Research Center (PEER). PEER NGA Database. http://peer.berkeley.edu/peer_ground_motion_database (accessed on 4 August 2014).

Penna, A. (2015). "Seismic assessment of existing and strengthened stone-masonry buildings: critical issues and possible strategies", Bulletin of Earthquake Engineering, 13 (4), 1051-1071.

Penna, A., Lagomarsino, S., and Galasco, A. (2014) "A nonlinear macroelement model for the seismic analysis of masonry buildings", Earthquake Engineering and Structural Dynamics, 43(2), 159 – 179.

Peruš, I. and Fajfar, P. (2005) "On the inelastic torsional response of single-storey structures under bi-axial excitation", Earthquake Engineering and Structural Dynamics, 34 (8), 931-941.

Priestley, M. J. N., Calvi, G. M. and Kowalsky, M. J. (2007) "Displacement-based seismic design of structures", IUSS press, Pavia, Italy.

Sadashiva, V. K., MacRae, G. A., Deam, B. L. and Spooner, M. S. (2012) "Quantifying the seismic response of structures with flexible diaphragms", Earthquake Engineering and Structural Dynamics, 41 (10), 1365-1389.

Saffarini, H.S. and Qudaimat, M. M. (1992) "In-plane floor deformations in RC structures", Journal of Structural Engineering, 118 (11), 3089-3102.

Senaldi, I., Magenes, G., Penna, A., and Galasco, A. (2014) "The effect of stiffened floor and roof diaphragms on the experimental seismic response of a full-scale unreinforced stone masonry buildings", Journal of Earthquake Engineering, 18(3), 407 – 443.

Standards Australia (2007). "Structural design actions Part 4: Earthquake actions in Australia, AS 1170.4", Standards Australia, Sydney.

Tena-Colunga, A. and Abrams, D. P. (1996) "Seismic behaviour of structures with flexible diaphragms", Journal of Structural Engineering, 122 (4), 439-445.

Tomaževic, M., Lutman, M., and Velechovsky, T. (1991) "The influence of rigidity of floor on the seismic behaviour of old stone-masonry buildings", European Earthquake Engineering, 3, 28 – 41.

Tomaževic, M., Lutman, M., and Velechovsky, T. (1993) "Aseismic strengthening of old stone-masonry buildings: is the replacement of wooden floors with R.C. slabs always necessary?", European Earthquake Engineering, 3, 28 – 41.

Whitney, R., and Agrawal, A. K. (2015) "Seismic performance of flexible timber diaphragms: Damping, force-displacement and natural period", Engineering Structures, 101, 583 – 590.

Wilson, A., Quenneville, P. and Ingham, J. (2013) "Natural period and seismic idealization of flexible timber diaphragms", Earthquake Spectra, 29 (3): 1003-1019.

Vintzileou, E., Mouzakis, C., Adami, C.-E., and Karapitta, L. (2015) "Seismic behaviour of three-leaf stone masonry buildings before and after interventions: Shaking table tests on a two-storey masonry model", Bulletin of Earthquake Engineering, 13(10), 3107 – 3133.

Appendix A – List of Main Symbols

Δ_d	Deformation of diaphragm relative to the average displacement of in-plane walls
Δ_w	Average displacement of in-plane walls
Δ_θ	Differential displacement of flexible and stiff sides caused by torsional rotation of diaphragm
Δ_s	Differential displacement of flexible and stiff sides caused by raking shear of diaphragm
ε_{sx}	Normalised stiffness eccentricity
ε_{px}	Normalised strength eccentricity
I_O	Mass moment of inertia of rigid diaphragm structure
K_y	Total stiffness in the direction of loading
λ	Ratio of Δ_d to Δ_w
m	Total mass
Ω_θ	Ratio of uncoupled torsional to lateral frequencies of rigid diaphragm system
R_y	Force reduction factor in the direction of loading
R_F	Ratio of strength in the orthogonal directions of the structure
ρ_y	Fraction of total mass attributed to each wall in the direction of loading
ρ_x	Fraction of total mass attributed to each wall in the direction orthogonal to loading
ρ_d	Fraction of total mass attributed to diaphragm
T_C	Period at the transition of acceleration- to velocity-sensitive ranges of the response spectrum
T_d	Fundamental period of diaphragm
T_y	Translational period of symmetric system under the rigid diaphragm configuration
$u_{1,max}$	Maximum value of peak displacement of the flexible side over all values of diaphragm stiffness

$u_{1,rig}$ Peak displacement of the flexible side for the rigid diaphragm configuration

u_{flex} Peak displacement of walls when diaphragm is completely flexible

u_{sdof} Peak displacement of individual walls

Appendix B – List of Accelerograms for Case Study

Table B.1. List of accelerograms used for case study

Event	Year	Station	M_w	Mechanism	Closest distance (km)	V_{s30} (m/sec)	Scale factor
Friuli	1976	Tolmezzo	6.5	Reverse	15.82	505.23	0.9492
Imperial Valley	1979	Compuertas	6.53	Strike slip	15.3	259.86	1.7846
Imperial Valley	1979	El Centro Array #12	6.53	Strike slip	17.94	196.88	1.9922
Irpinia	1980	Rionero In Vulture	6.2	Normal	22.69	574.88	2.412
Superstition Hills	1987	Brawley Airport	6.54	Strike slip	17.03	208.71	2.3956
Northridge	1994	Hollywood - Willoughby Ave	6.69	Reverse	23.07	347.7	1.4762
Northridge	1994	LA - 116th St School	6.69	Reverse	41.17	301	1.7326
Northridge	1994	LA - Baldwin Hills	6.69	Reverse	29.88	297.07	1.4162
Northridge	1994	Northridge - 17645 Saticoy St	6.69	Reverse	12.09	280.86	0.7668
Northridge	1994	Santa Susana Ground	6.69	Reverse	16.74	715.12	1.0751
Joshua Tree	1992	North Palm Springs Fire Sta #36	6.1	Strike slip	21.97	367.84	1.6272
Christchurch	2011	Canterbury Aero Club	6.2	Reverse Oblique	14.41	280.26	1.6631

CHAPTER 6

NONLINEAR STATIC PROCEDURES

Background

In this chapter, the applicability of three types of widely used nonlinear static (pushover) analysis methods are evaluated for unreinforced masonry buildings with flexible diaphragms. Three building models with different levels of stiffness eccentricity and pier failure mechanisms are used to investigate (1) the most suitable way in applying the various analysis methods, and (2) the method that yields the most accurate predictions, when compared to the "exact" nonlinear time-history analysis. The results of the study cast some doubts on the applicability of the Modal Pushover Analysis for unreinforced masonry buildings with flexible diaphragms. Practical recommendations are presented to identify when single-mode pushover analyses can be used with reasonable accuracy.

List of Manuscripts

Nakamura, Y., Derakhshan, H., Griffith, M. C., Magenes, G. and Sheikh, A. H. (2016) "Applicability of nonlinear static procedures for low-rise unreinforced masonry buildings with flexible diaphragms", submitted to Engineering Structures

Statement of Authorship

Title of Paper	Applicability of nonlinear static procedures for low-rise unreinforced masonry buildings with flexible diaphragms
Publication Status	☐ Published ☐ Accepted for Publication ☑ Submitted for Publication ☐ Unpublished and Unsubmitted work written in manuscript style
Publication Details	Nakamura, Y., Derakhshan, H., Griffith, M. C., Magenes, G. and Sheikh, A. H. (2016) "Applicability of nonlinear static procedures for low-rise unreinforced masonry buildings with flexible diaphragms", submitted to Engineering Structures

Principal Author

Name of Principal Author (Candidate)	Yasuto Nakamura
Contribution to the Paper	Prepared manuscript, developed analysis methodology, performed all analyses
Overall percentage (%)	85%
Certification:	This paper reports on original research I conducted during the period of my Higher Degree by Research candidature and is not subject to any obligations or contractual agreements with a third party that would constrain its inclusion in this thesis. I am the primary author of this paper.
Signature	Date 26/8/16

Co-Author Contributions

By signing the Statement of Authorship, each author certifies that:

i. the candidate's stated contribution to the publication is accurate (as detailed above);

ii. permission is granted for the candidate in include the publication in the thesis; and

iii. the sum of all co-author contributions is equal to 100% less the candidate's stated contribution.

Name of Co-Author	Hossein Derakhshan
Contribution to the Paper	Contributed to research and manuscript
Signature	Date 26 Aug 2016

Name of Co-Author	Michael C. Griffith
Contribution to the Paper	Supervised and contributed to research and manuscript
Signature	Date 30/08/2016

Name of Co-Author	Guido Magenes
Contribution to the Paper	Supervised and contributed to research and manuscript
Signature	Date 25/8/16

Name of Co-Author	Abdul H. Sheikh
Contribution to the Paper	Supervised and contributed to research and manuscript
Signature	Date 26/8/2016

Applicability of Nonlinear Static Procedures for Low-Rise Unreinforced Masonry Buildings with Flexible Diaphragms

ABSTRACT

The applicability of the N2 method, the modal pushover analysis (MPA) and an adaptive pushover analysis method are investigated for estimating the peak seismic responses of unreinforced masonry buildings with flexible diaphragms. The nonlinear static procedures are evaluated against the nonlinear time-history analyses of three low-rise building models with various levels of stiffness eccentricity, failure mechanisms of piers (rocking or shear), and a range of diaphragm stiffness representing timber floor and roof systems. The results indicate that the MPA is unsuitable for unreinforced masonry buildings with flexible diaphragms, if the building response is shear-dominated. The adaptive method provides the most accurate estimates when the diaphragms are relatively stiff. When the diaphragms are relatively flexible, none of the considered methods can provide accurate predictions of peak seismic demands. However, conservative results may be obtained using the N2 method, by taking the envelope of pushover analyses conducted using force distributions proportional to the uniform and linear displacement shapes along the height of the building. The present study also identifies the most suitable analysis parameters/methods in using various nonlinear static procedures, such as the location of the control node in the N2 method and the modal combination rules in the MPA, for unreinforced masonry buildings with flexible diaphragms.

keywords: pushover analysis, N2, MPA, adaptive, unreinforced masonry, flexible diaphragm

1. INTRODUCTION

An essential component of a performance-based seismic assessment is the computation of inelastic seismic response of a building subjected to a predetermined level of earthquake shaking. In computing the seismic response, it is well recognised that the linear elastic analysis used in traditional force-based assessment is inadequate in capturing the redistribution of internal forces, as well as the distribution of damage, after the onset of nonlinear behaviour (Magenes & Penna 2009). On the other hand, rigorous nonlinear time-history analysis (NTHA) of a multi degree of freedom (MDOF) model remains unfeasible for typical design/assessment tasks, due to the need to develop complex numerical models, the appropriate selection of a suite of ground motions and the large computational effort required.

To avoid these difficulties, nonlinear static procedures (NSPs) based on pushover analysis have been developed in the past decades, aimed at attaining a balance between the accuracy of analysis and the suitability for practical use.

The simplest form of NSPs considers the building to respond in an invariant displacement shape (or in a single mode) throughout the excitation. An example in this category is the N2 method (Fajfar & Gašperšič 1996; Fajfar 1999). By considering a single-mode response, the dynamic response of the MDOF structure can be reduced to that of an equivalent single degree of freedom (SDOF) system. This simpler equivalent SDOF is used to estimate the peak inelastic displacement (target displacement) at a selected location (control node) of the MDOF structure. The pushover analysis at that target displacement is considered to approximate the peak inelastic seismic response of the building.

A limitation of the single-mode pushover analysis method is that it cannot capture the responses of buildings containing multiple dominant modes. This limitation has led some researchers to propose multi-mode NSP, an example of which is the Modal Pushover Analysis (MPA) (Chopra & Goel 2002). In the MPA, the multi-mode effects are accounted for in an approximate manner by conducting separate pushover analyses for each significant elastic mode and the results of such "modal" pushover analyses are combined to obtain the total peak dynamic response. While the MPA considers the contribution of multiple modes, the elastic mode shapes are considered to remain unmodified throughout the excitation, even if an inelastic damage alters the dynamic property of the building.

The adaptive pushover methods were developed with the aim of capturing the changing characteristics of the structure as it enters the inelastic range. Various proposals have been made for modifying the pushover forces based on the instantaneous damage state of the structure (Aydinoğlu 2003; Antoniou & Pinho 2004a; Antoniou & Pinho 2004b; Kalkan & Kunnath 2006). An adaptive pushover procedure has also been developed for unreinforced masonry (URM) buildings (Galasco et al. 2006) with the primary aim of making the analysis independent of the location of the control node. In the procedure developed by Galasco et al. (2006), the pushover force distribution at the i^{th} step ($\mathbf{p}_i$) is constructed using the computed displacement shape of the previous analysis step ($\boldsymbol{\psi}_{i-1}$),

$$\mathbf{p}_i = \mathbf{m}\boldsymbol{\psi}_{i-1} \tag{1}$$

where $\mathbf{m}$ denotes the mass matrix of the building.

The initial application of the adaptive method found that constraints were needed on the force distribution, $\mathbf{p}_i$, in order to obtain realistic responses for buildings with flexible diaphragms (Galasco et al.

2006). While promising results are reported, this adaptive pushover procedure has not been investigated in the context of a NSP.

Even though the NSPs have become commonly used for the analysis of URM buildings in recent years, two broad issues require further studies for buildings with flexible diaphragms:

- The first issue is the uncertainties in the selection of analysis parameters when using the NSPs. These uncertainties include the suitable reference hysteresis behaviour assumed in calculating the target displacement, the suitable location of control node, the modal combination method used in MPA, and the procedure to convert the pushover curve to an equivalent SDOF system definition for the adaptive method, considering the continuously changing lateral force distribution pattern. Some of these uncertainties arise because the NSPs were originally developed for buildings with rigid diaphragms. For example, while the location of the control node can logically be placed at the centre of mass of roof for buildings if the diaphragms are rigid, the most suitable location is not immediately apparent when the diaphragms are flexible. Other issues concern the nonlinear static analysis of URM buildings more generally. For example, while the use of equivalent SDOF systems with idealised hysteresis models for estimating the target displacement have been studied for RC or steel frame buildings (Krawinkler & Seneviratna1998; Chopra et al. 2003) specific studies for URM buildings have been limited, with a notable exception (Graziotti et al. 2014). If a suitable idealised hysteresis rule can be identified, inelastic displacement ratios derived on the basis of extensive statistical studies for modern construction systems (Vidic et al. 1994; Ruiz-Garcia & Miranda 2003; Chopra & Chintanapakdee 2004) can be adopted also for URM buildings.

- The second issue requiring further studies is the identification of the applicable ranges of the NSPs. While intuition suggests that more advanced methods (e.g. MPA and the adaptive NSP) are able to provide better estimates of seismic responses than the single-mode N2 method for a wider range of diaphragm stiffness values, systematic evaluations have not been undertaken to verify the accuracies of various methods. Furthermore, no studies have been conducted to identify the factors affecting the accuracies of NSPs for URM buildings with flexible diaphragms.

The study reported herein aims to address these issues associated with the NSPs for URM buildings with flexible diaphragms. The applicability of the N2 method, the MPA and an adaptive NSP utilising the pushover algorithm of Galasco et al. (2006) are investigated for URM buildings with flexible diaphragms, using three building models with different levels of stiffness eccentricity and predominant failure

mechanisms (by rocking or shear). A wide range of diaphragm stiffnesses representative of timber floor systems are considered. The geometrical and engineering properties of these buildings and the earthquake loading scenarios are reported in Section 2. The most suitable analysis parameters for each NSP are identified in Section 3, by comparing the estimated control node displacements with the "exact" results obtained from the NTHA of the MDOF model. Finally, utilising the best analysis parameters for each NSP identified in Section 3, the relative accuracies of the NSPs are investigated in Section 4, followed by concluding remarks in Section 5.

2. DESCRIPTIONS OF BUILDINGS, NUMERICAL MODELS AND GROUND MOTIONS

2.1 Descriptions of Building Models

Three building models, broadly representative of low-rise isolated URM buildings commonly found in New Zealand and Australia (Russel 2010; Griffith et al. 2013) were analysed. The models differed in the number of storeys (2 or 3), number of bays (1 or 2), stiffness eccentricity and the predominant failure mechanisms. Table 1 summarises the key properties with Figure 1 showing the plan views of the buildings and the elevations of the in-plane loaded walls. The stiffness eccentricities were calculated for the first floor, considering the piers of the ground storey to be fixed at top and bottom (i.e. rigid spandrels). The densities of masonry and timber materials were 1800 kg/m^3 and 660 kg/m^3 respectively. Uniform floor live load of 4 kPa was assumed, with the seismic load factor of 0.3 in accordance with AS 1170.1 (Standards Australia 2002). The analyses were conducted under unidirectional loading, applied in the X directions of the models.

Table 1. Structural properties of the building models

Building	Number of storey	Number of bays	T_{rig}† (s)	Normalised stiffness eccentricity‡	Dominant failure mechanism¶
Model 1	2	1	0.231	0.36	Rocking
Model 2	2	1	0.151	0.1	Shear
Model 3	3	2	0.253	0.2	Shear

† fundamental period of the building with rigid diaphragms

‡ normalised eccentricity in the direction of excitation

¶ the shear failure was considered to be dominant if more than half the piers of the critical storey failed in shear

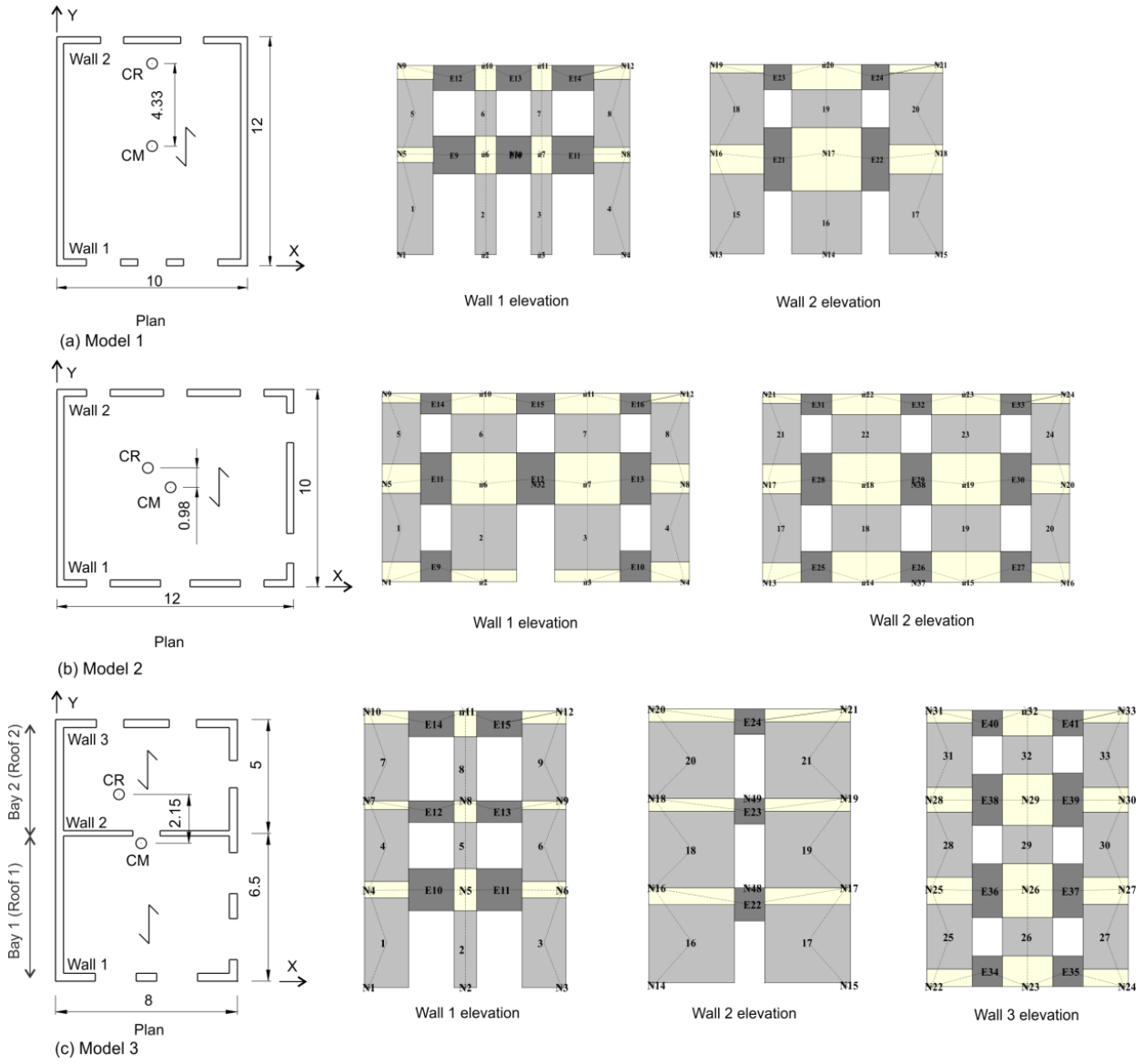

Figure 1. Plan and elevation views of the building models (dimensions in m)

The floor and roof diaphragms were representative of flexible (or non-rigid) timber systems with identical constructions at all floor levels. Six different configurations were considered for each model. They corresponded to single straight sheathing (D1), single diagonal sheathing (D2), double straight sheathing (D3), double layered panels (D4), and two additional levels representing hypothetical retrofits (D5 and D6). The reference diaphragm stiffness (G_d), expressed as the shear modulus multiplied by the equivalent diaphragm thickness are summarised in Table 2 based on the "expected" values given in ASCE 41-13 (ASCE 2014).

Table 2. Reference diaphragm stiffness values

Diaphragm	G_d (kN/m)	Description
D1	350	Single straight sheathing
D2	1400	Single diagonal sheathing, chorded
D3	2625	Double straight sheathing, chorded
D4	3150	Double layered panels, chorded
D5	7000	Hypothetical retrofit 1
D6	35000	Hypothetical retrofit 2

2.2 Numerical Modelling and Analysis

The TREMURI program (Lagomarsino et al. 2013) was used to model the buildings. The walls were modelled by the equivalent frame idealisation considering the in-plane wall actions. The inelastic responses of the piers and spandrels were represented by the macroelement formulation (Penna et al. 2014), which captures the rocking and shear behaviours separately (Figure 2). In the macroelement, the rocking response is modelled at the two ends by a set of compression-only springs with limited strengths. The P-Delta effect was considered to be negligible due to the small level of expected displacement in comparison to the width of piers, and hence, no strength degradation was considered for the rocking behaviour (Figure 2b). The shear behaviour is captured by the internal (middle) segment, and governed by a monotonically increasing damage parameter α, where $\alpha>1$ results in the strength degradation of the macroelement (Figure 2c). The material properties of masonry were obtained from an experimental study conducted by Knox (2012), using bricks obtained from damaged heritage buildings in the Christchurch earthquake with a weak mortar mix representative of older URM buildings (Table 3).

Each diaphragm was modelled using four elastic membrane elements, with translational degrees of freedom at the mid-span to capture its dynamic behaviour. The nodes belonging to the diaphragms and the walls were shared at wall corners and intersections. The shear stiffnesses of the membranes were set so that the diaphragm stiffnesses corresponded to the six configurations (Table 2), further modified to account for the stiffness contributions of the out-of-plane loaded walls using the procedure by Giongo et al. (2014). However, the dynamic behaviours of the out-of-plane responding walls were not explicitly modelled.

The nodal masses were assigned based on tributary areas considering the horizontal (inertial) loading. To obtain the nodal masses, the tributary masses were firstly computed separately for the diaphragm and wall nodes. Where the diaphragm and wall nodes coincide at wall corners and intersections, the computed wall and diaphragm nodal masses were then added. It is noted that assigning nodal masses in this manner is

appropriate for the dynamic analysis of low-rise buildings where the induced direction of the excitation is primarily horizontal. However, it does not give the correct internal force distributions under gravity loading. Hence, additional nodal forces (vertical loads and moments) were imposed on the structure to obtain correct gravity load distributions prior to carrying out the dynamic analyses.

The inherent (i.e. non-hysteretic) component of energy dissipation was modelled using the Rayleigh viscous damping model for the NTHA. TREMURI program uses Rayleigh damping proportional to the initial stiffness, and this approach is known to overestimate the inherent component of damping when the structure undergoes inelastic behaviour (Priestley & Grant 2005). The overestimation occurs because the Rayleigh viscous damping effectively increases with the elongation in the period of the structure. To address this issue, an approximate approach was used; specifically, a 5% initial damping ratio was assigned at (1) the lower frequency corresponding to the secant stiffness to collapse, identified as the point at which the base shear resistance reduced below 80% of peak value, and (2) higher frequency corresponding to the lowest elastic mode containing 90% mass participation. In calculating the lower frequency, an initial single-mode pushover analysis was carried out to identify the point of collapse. It is noted that a similar approach has been used by Mouyiannou et al. (2014) when carrying out NTHA in TREMURI.

Table 3. Masonry material properties used (calculated from Knox (2012))

Young's modulus	Shear modulus	Compressive strength	Cohesion	Friction coefficient
1385 MPa	740 MPa	5.74 MPa	0.101 MPa	0.152

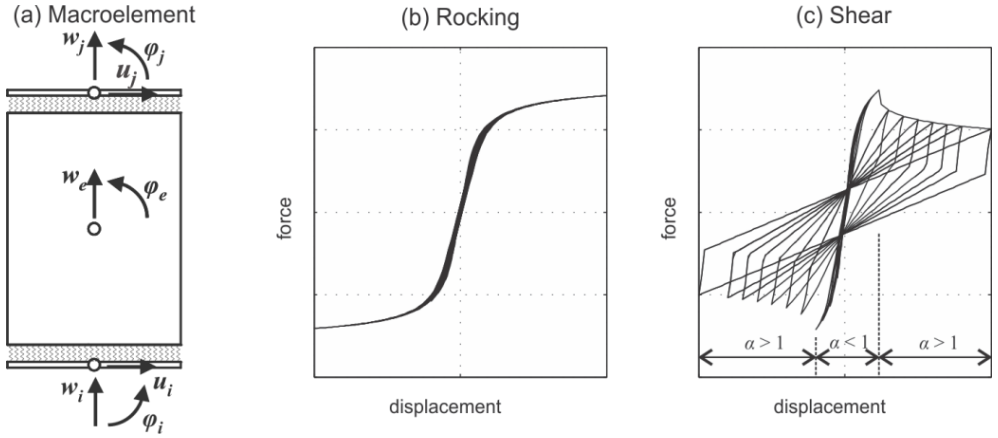

Figure 2. Macroelement model: (a) element kinematics, (b) rocking response and (c) shear response.

2.3 Ground Motions

Twelve natural accelerogams were selected from the database of Pacific Earthquake Engineering Research Centre (PEER 2015), and scaled to match the design spectrum of AS 1170.4 (Standards Australia 2007) for site class C_e (defined as shallow soil). In order to obtain records with magnitudes between 6 and 7 without excessive scaling, the peak ground acceleration (PGA) of the target spectrum was set to 0.26 g. The closest distance from the rupture plane ranges from 14 to 41 km. The records did not contain damaging near-field characteristics such as the forward directivity effect. A wide range of soil conditions were considered, as indicated by the average top 30 m shear velocity ($V_{s,30}$) ranging from 197 m/s to 715 m/s. Table 4 summarises the ground motion records used in the analysis. The mean 5% damped acceleration and displacement spectrum are shown in Figure 3. In addition to the PGA of 0.26 g, two additional intensity levels corresponding to the PGA of 0.13 g and 0.52 g were also considered in the analysis, in order to induce different levels of inelastic behaviours.

Table 4. List of ground motion records

Event	Station	Year	Magnitude	Component	R_{rup} (km)	$V_{s,30}$ (m/sec)
Friuli	Tolmezzo	1976	6.5	000	15.82	505.23
Imperial Valley	Compuertas	1979	6.53	015	15.3	259.86
Imperial Valley	El Centro Array #12	1979	6.53	140	17.94	196.88
Irpinia	Rionero In Vulture	1980	6.2	000	22.69	574.88
Superstition Hills	Brawley Airport	1987	6.54	225	17.03	208.71
Northridge	Hollywood - Willoughby Ave	1994	6.69	090	23.07	347.7
Northridge	LA - 116th St School	1994	6.69	090	41.17	301
Northridge	LA - Baldwin Hills	1994	6.69	090	29.88	297.07
Northridge	Northridge - 17645 Saticoy St	1994	6.69	090	12.09	280.86
Northridge	Santa Susana Ground	1994	6.69	000	16.74	715.12
Joshua Tree CA	North Palm Springs Fire Sta #36	1992	6.1	180	21.97	367.84
Christchurch	Canterbury Aero Club	2011	6.2	N40E	14.41	280.26

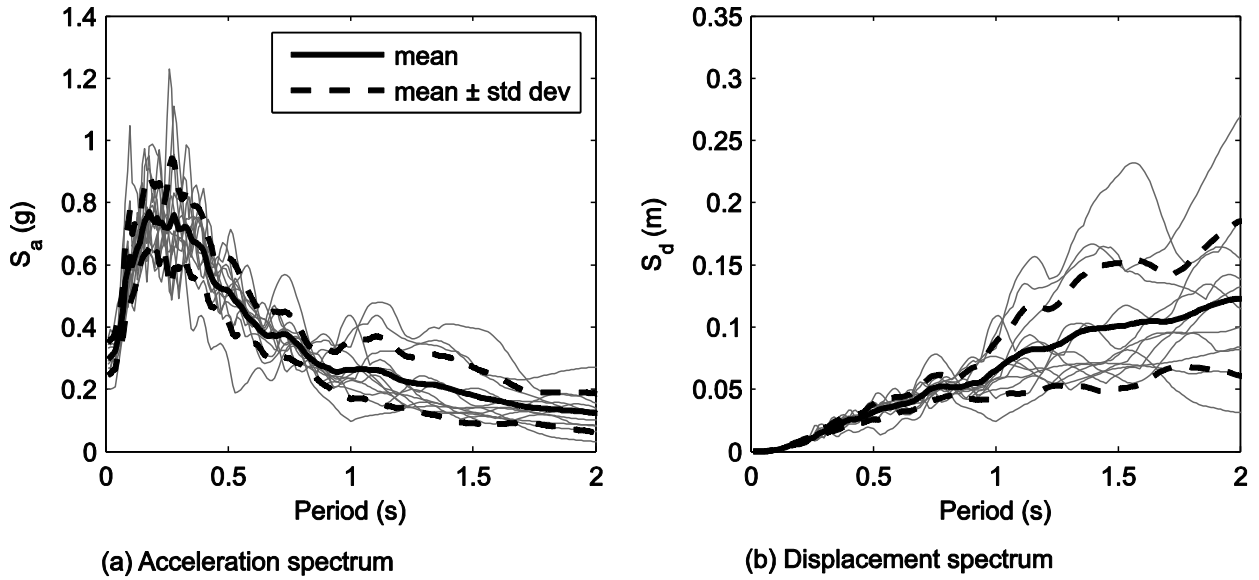

Figure 3. Mean spectra of ground motions with average PGA of 0.26 g

3. IDENTIFICATION OF SUITABLE ANALYSIS PARAMETERS

3.1 Parameters Investigated

As the existing NSPs have been developed for modern rigid diaphragm constructions, several uncertainties are associated with their application for URM buildings with flexible diaphragms. The analysis parameters investigated in the present study are summarised in Table 5, and are described in this section.

For the N2 method, the main uncertainties for the application of the method are (1) location of control node, and (2) the computation of target displacement using an equivalent SDOF system. In order to identify the most appropriate control node location, the accuracies of the target displacements computed at the control node placed at the roof levels of each in-plane loaded wall and the diaphragm mid-spans are investigated. In addition, four different hysteresis models are studied for calculating the target displacement using the NTHA of the equivalent SDOF systems. The hysteresis models correspond to elastic-plastic, thin Takeda, origin centered, and bilinear elastic rules (Figure 4).

It is noted that in practice, the computation of the target displacement needs to be carried out without conducting a NTHA of the equivalent SDOF system. In seismic codes and guidelines (CEN 2004; FEMA 2005; ASCE 2014), this is achieved by utilising empirical formulae that relates elastic spectral displacement to the inelastic spectral displacement. However, in order to eliminate statistical bias inherent

in the simplified spectrum-based approaches, the present study uses step-by-step NTHA of the equivalent SDOF system.

Several load patterns are also considered for the N2 method in the present study, namely (a) mass multiplied by "uniform" displacement shape (uniform pushover analysis), (b) mass multiplied by "linear" displacement shape along the height of the building (linear pushover analysis), which is similar to load patterns often specified in seismic codes, and (c) mass multiplied by displacement shape corresponding to that calculated using the response spectrum analysis with the square root of squares (SRSS) combination rule (SRSS pushover analysis).

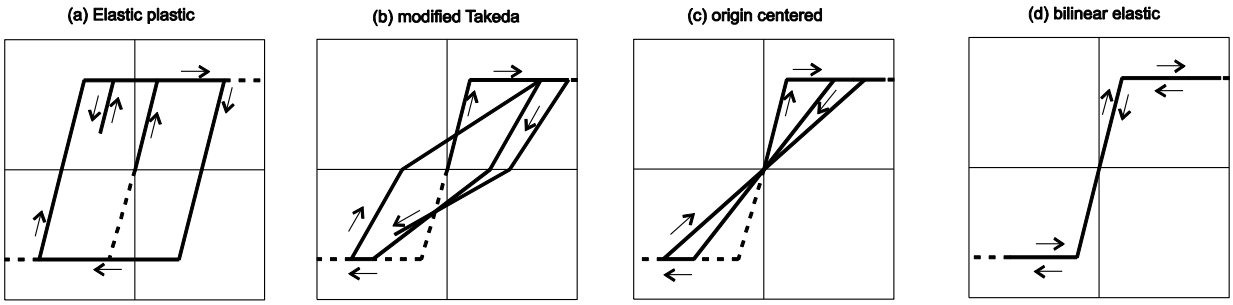

Figure 4. Hysteretic models investigated for the equivalent SDOF system

The analysis parameters investigated for the MPA are (1) location of control node, and (2) mode combination rules used for combining the "modal" pushover analysis results. The control node locations investigated are (a) location that displaces the most in the elastic range, and (b) location that displaces the most at the ultimate state of the structure. The considered combination rules consist of SRSS and the complete quadratic combination (CQC) rules. The calculation of the target displacement is conducted for each mode by the NTHA of the equivalent SDOF system, using the most suitable hysteresis model identified for the N2 method. In the present study, the number of modes considered encompassed more than 85% of mass participation.

The analysis parameter investigated for the adaptive NSP is the conversion of the pushover curve to the equivalent SDOF system, accounting for the continuously changing force distribution during the analysis. Three conversion methods are investigated[1]. The first approach (ADAP1) uses the current displacement shape of the structure to calculate the conversion parameters. The second method (ADAP2) is similar to the ADAP1, but uses the displacement shape back calculated from the pushover force profile of the current step. The difference between ADAP1 and ADAP2 is that the pushover force distribution ($\mathbf{p}_i$ in Eq.

[1] More detailed descriptions of the conversion methods are provided in Appendix B of this thesis.

1) is bounded in the present study in order to obtain realistic analysis results (Galasco et al. 2006), while the displacement response may lay outside the constraint distributions. The limiting force distributions correspond to the SRSS and uniform pushover analyses of the N2 method; the SRSS distribution may considered to be appropriate when the building is in the elastic range, while the uniform distribution represents the ultimate state of the building when a soft-storey occurs in the ground storey. The third approach (ADAP3) constructs the equivalent SDOF system based on conserving the work done on the MDOF structure by the pushover forces (Hernández-Montes et al. 2004). The target displacement is again obtained by the NTHA of the equivalent SDOF system, using the most suitable hysteresis model identified for the N2 method.

As the ADAP1 procedure uses the computed displacement shape, it is independent of the control node location. ADAP3 is also independent of the control node, as it does not require any displacement to be monitored during the pushover analysis. On the other hand, ADAP2 requires the control node in constructing the pushover curve, as the constraints imposed on the pushover force distribution lead to an inconsistency between the actual displacement shape and that used in the conversion. For ADAP2, the control node is placed at the mid-span degree of freedom of the most flexible roof for all building models.

Table 5. List of analysis parameters studied

Analysis Method	Investigated Parameters
N2 method	• Location of control node • Hysteresis model for the computation of target displacement using equivalent SDOF system • Lateral pushover force distribution
MPA	• Location of control node • Mode combination rule
Adaptive pushover method	• Conversion procedure from pushover curve to equivalent SDOF system

3.2 Results for N2 method

The suitability of using equivalent SDOF systems with idealised hysteresis rules for the calculation of target displacement is investigated first. Figure 5 shows the comparisons of the estimated target displacements against the peak displacements obtained from the NTHA of the MDOF model. The plots include all ground motions, building models, diaphragm stiffnesses, excitation intensities, and the assumed displacement shape, hence giving an overall idea of the relative accuracies of various hysteresis models. The presented results correspond to the analyses conducted using the mid-span of the most

flexible roof diaphragm as the control node. While not shown, qualitatively identical trends were also observed when the control node was placed at different locations of the building. The error of the target displacement estimations of the N2 method ($u_{c,N2}$) with respect to the NTHA results ($u_{c,NTHA}$) are quantified in Figure 5 using the root mean square of the displacement error normalised by the building height (h), as given by $\delta_{RMS} = \sqrt{\sum \left(\frac{u_{c,N2} - u_{c,NTHA}}{h}\right)^2}$.

The plots show that the two hysteresis models with limited to no hysteretic energy dissipation capacities (origin centered and bilinear elastic) give highly conservative estimates as the excitation intensity increases. The overestimations appear to increase exponentially, and significant errors can be expected as the inelastic behaviour increases. The elastic-plastic model, on the other hand, provides good predictions on average. However, the large variability about the equality line indicates the potential for significant errors (including underestimations) for individual ground motion. The most suitable hysteresis, that gives (on average) results closest to the NTHA analysis with the smallest variability, is the modified Takeda (thin) model. Indeed, the responses of URM walls generally show a combination of the rocking and shear failures, which are approximated most closely by the modified Takeda model.

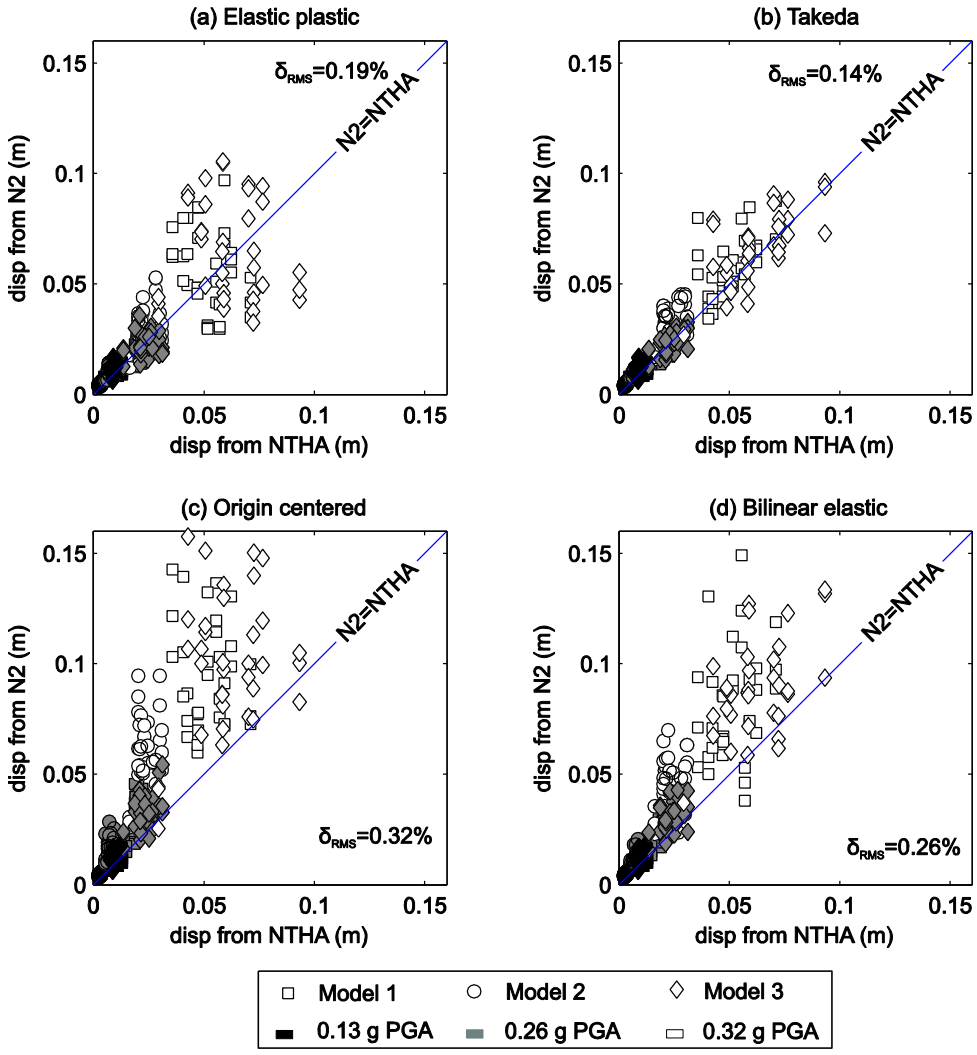

Figure 5. Comparisons of the target displacement estimates from the N2 method against NTHA with control node at the mid-span of the most flexible roof diaphragm, including all hysteresis models and pushover force distributions.

In assessing the suitability of the control node, it may be recognised that the location of the control node affects the pushover analysis insofar as determining how far the structure is to be pushed. Hence the most suitable control node location is where the estimated target displacement matches the NTHA results on average, with the smallest coefficient of variation (measure of scatter). The ratio (u_c^*) of the estimated target displacement to the NTHA displacement is used to evaluate the applicability of a control node,

$$u_c^* = \frac{u_{c,N2}}{u_{c,NTHA}} \tag{2}$$

Figure 6 and Figure 7 show the mean and coefficient of variation of the target displacement ratios against the average diaphragm period of the floors (T_d) for Model 2 and Model 3 respectively, subjected to the

largest ground motion intensity of 0.52 g. T_d is calculated from the stiffness and the tributary mass of the diaphragm. The control node location is varied between the top level of the in-plane loaded walls, and the mid-spans of the roof diaphragms. It is noted that in Model 3, the diaphragm between Wall 1 and Wall 2 (denoted as Roof 1 in Figure 1) is more flexible than the diaphragm between Wall 2 and Wall 3 (denoted as Roof 2 in Figure 1) due to the larger span length.

The mean ratios show that consistently good estimates are obtained when the control node is placed at the mid-span of the (most flexible) roof diaphragm. This is the only location where acceptable accuracy can be attained for all diaphragm stiffness levels, the assumed displacement shapes, and the building models (Model 1 showed similar trends to Model 2, and is not shown). Furthermore, the similar values of the coefficient of variation for the different control node locations indicate that there is no particular location that consistently gives the smallest coefficient of variation. The mid-span of the most flexible diaphragm (i.e. Roof 1 for Model 3) hence appears to be the most suitable location for the N2 method.

The estimation of the target displacement at the mid-span of the (most flexible) diaphragm is also reasonably consistent for different levels of inelastic behaviour. Figure 8 shows the mean target displacement ratios for the three models with the control node at the mid-span of the roof (Roof 1 for Model 3) for different levels of excitation. All building models remained practically elastic for the 0.13 g excitation, while significant inelastic responses were induced under the 0.52 g intensity. However, the mean target displacement ratios were relatively insensitive to the change in the response characteristics. The coefficient of variation of the predictions (Figure 9), however, generally increases with the excitation intensity.

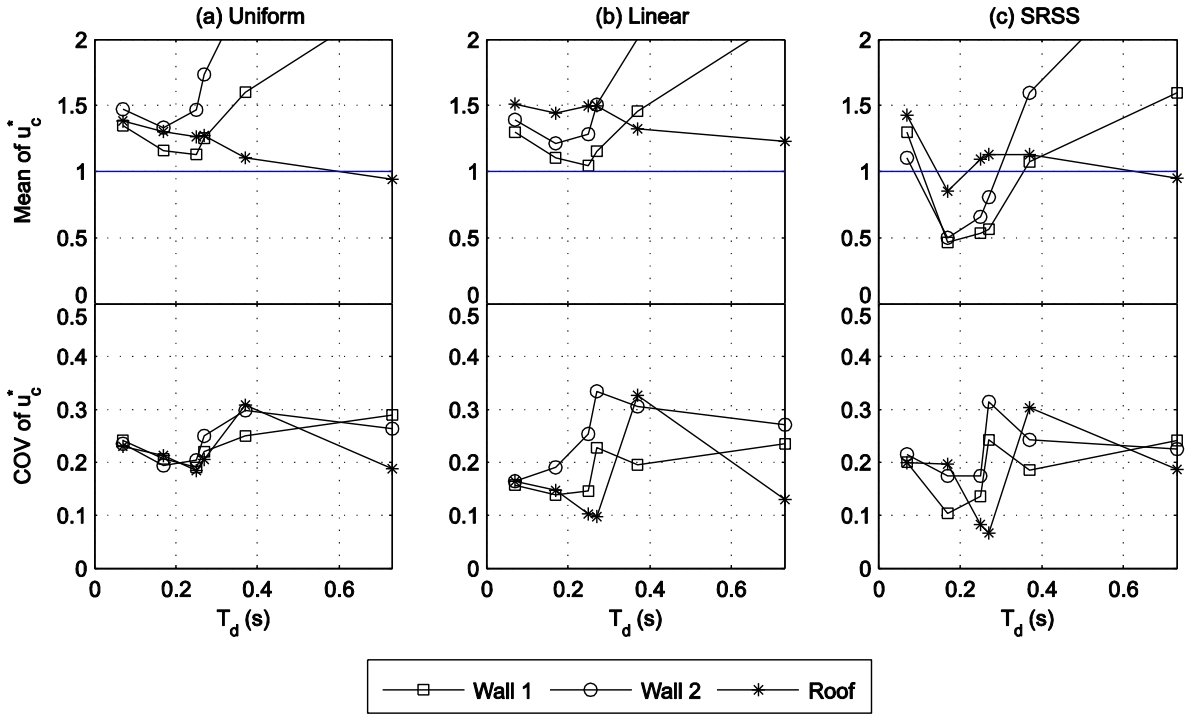

Figure 6. Mean and coefficient of variation of target displacement ratios for Model 2 under 0.52 g PGA, (a) uniform pushover force, (b) linear pushover force, and (c) SRSS pushover force.

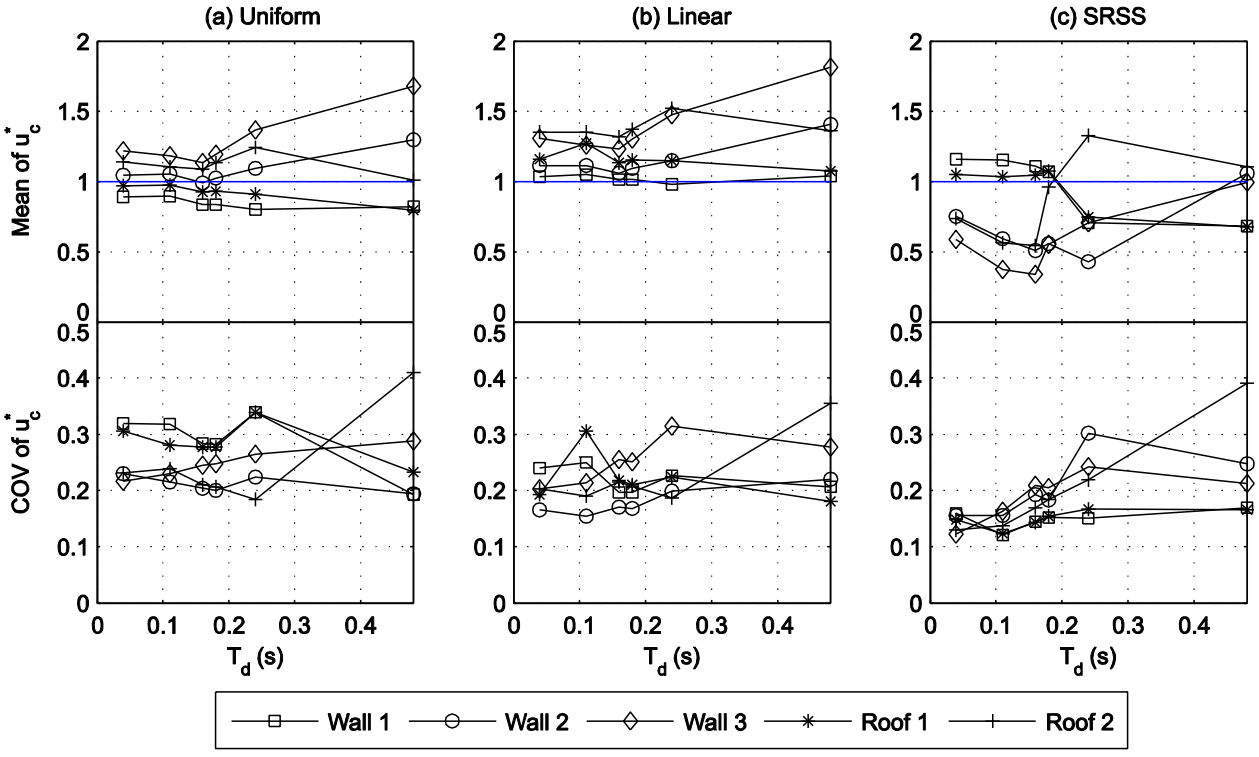

Figure 7. Mean and coefficient of variation of target displacement ratios for Model 3 under 0.52 g excitation, (a) uniform pushover force, (b) linear pushover force, and (c) SRSS pushover force.

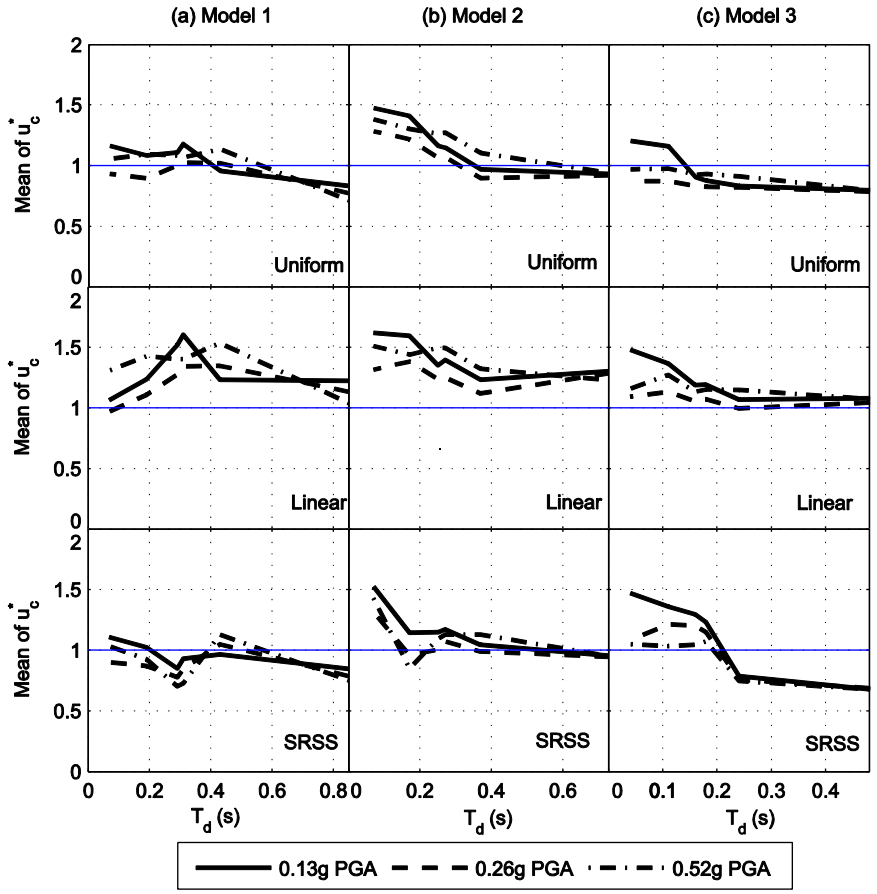

Figure 8. Sensitivity of the mean target displacement ratios to ground motion intensity.

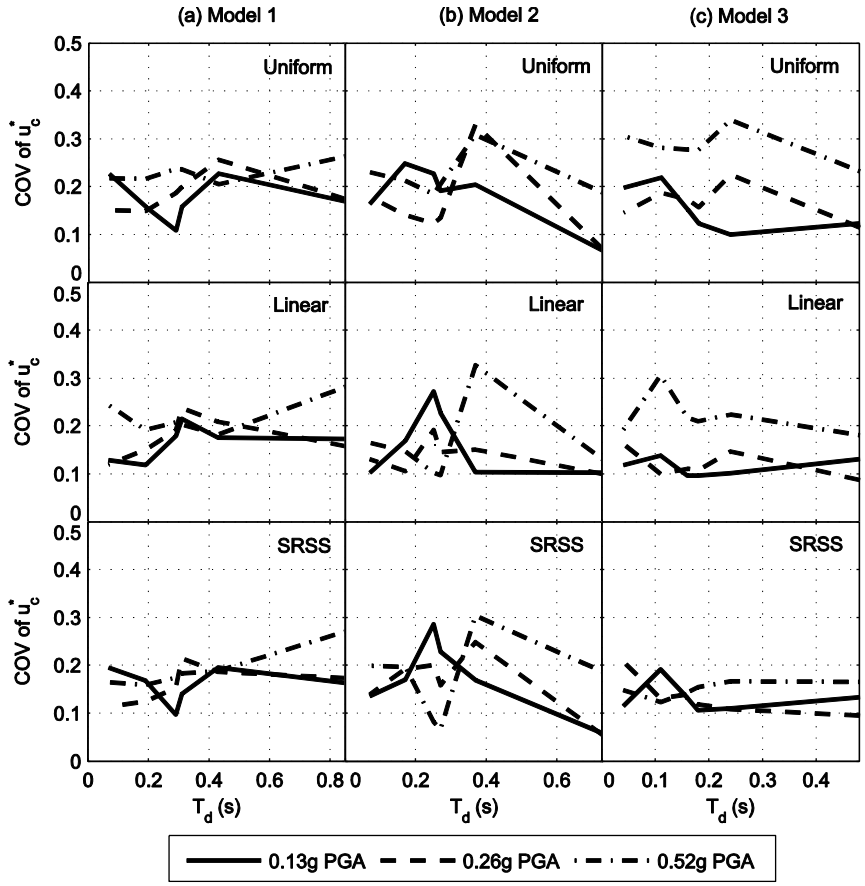

Figure 9. Sensitivity of the coefficient of variation of target displacement ratios to ground motion intensity.

3.3 Results for MPA

For the MPA, the most suitable location of control node, and the mode combination rules were investigated.

In Figure 10, the mean of the peak displacement ratios corresponding to various diaphragm stiffnesses are shown for the mid-spans of the (most flexible) roof for the three building models under the largest excitation of 0.52 g PGA, which induced significant inelastic behaviour. The displacement ratio is defined similarly to Eq. 2, with $u_{c,N2}$ replaced by the value computed from the MPA. The figure includes the control node locations that displace the most in the elastic range (case 1) and at the ultimate state (case 2), with either the SRSS or the CQC mode combination rules. In most cases, the results are not overly sensitive to the control node location, indicating that the location that displaces the most in the elastic range also generally undergoes the largest inelastic deformation. Where there are discrepancies, however, the more accurate results are obtained when the control node corresponds to the location that displaces the

most in the elastic range. This is attributed to the larger initial period of the equivalent SDOF system, which results in a larger target displacement.

The differences between the two combination rules are generally negligible, despite the fact that some modes were closely spaced due to the similar values of diaphragm stiffness at all floor levels. The CQC rule is nevertheless preferred in the present study as it gives more conservative predictions.

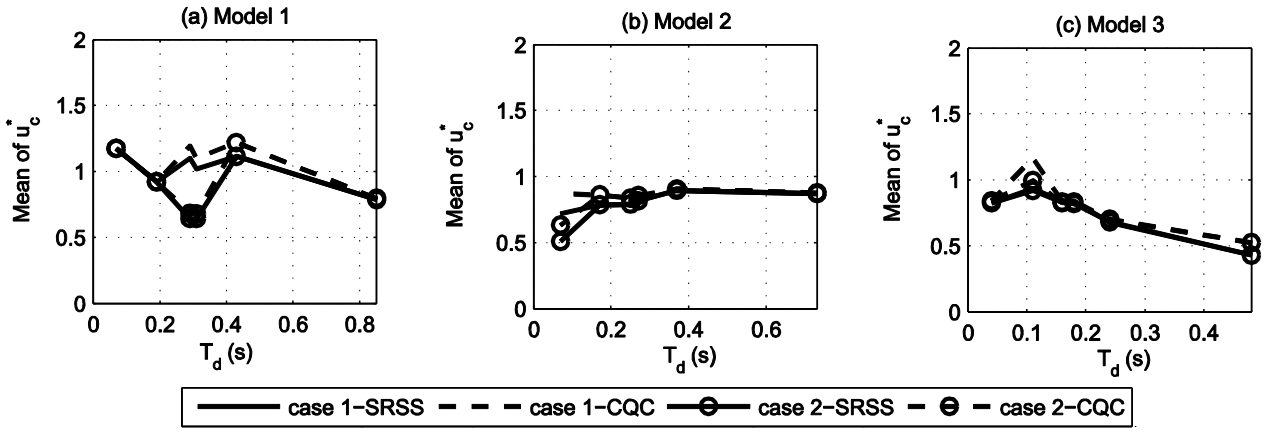

Figure 10. Comparisons of the mean displacement ratios at mid-spans of roof (roof 1 for Model 3), subject to 0.52 g PGA ground motion for the four different MPA cases.

3.4 Results for Adaptive Procedure

Three conversion procedures (ADAP1, ADAP2 and ADAP3, Section 3.1) are investigated for the adaptive NSP. The mean peak displacement ratios at the mid-spans of the roofs (Roof 1 for Model 3) are plotted against the diaphragm periods in Figure 11. The displacement ratio is calculated analogously to Eq. 2, using the computed value from the adaptive procedure in lieu of $u_{c,N2}$. The ADAP1 approach underestimates the peak displacements when the diaphragms become overly flexible. The underestimation occurs due to the disproportionate increase in the displacement of the diaphragm mass, which effectively reduces the mass of the equivalent SDOF system. The strength of the equivalent SDOF hence increases in comparison to its effective mass, which results in the reduced inelastic displacement for a given ground motion. In comparison, the ADAP2 and ADAP3 procedures provide more consistent results with the NTHA. In particular, ADAP3 generally gives more conservative results.

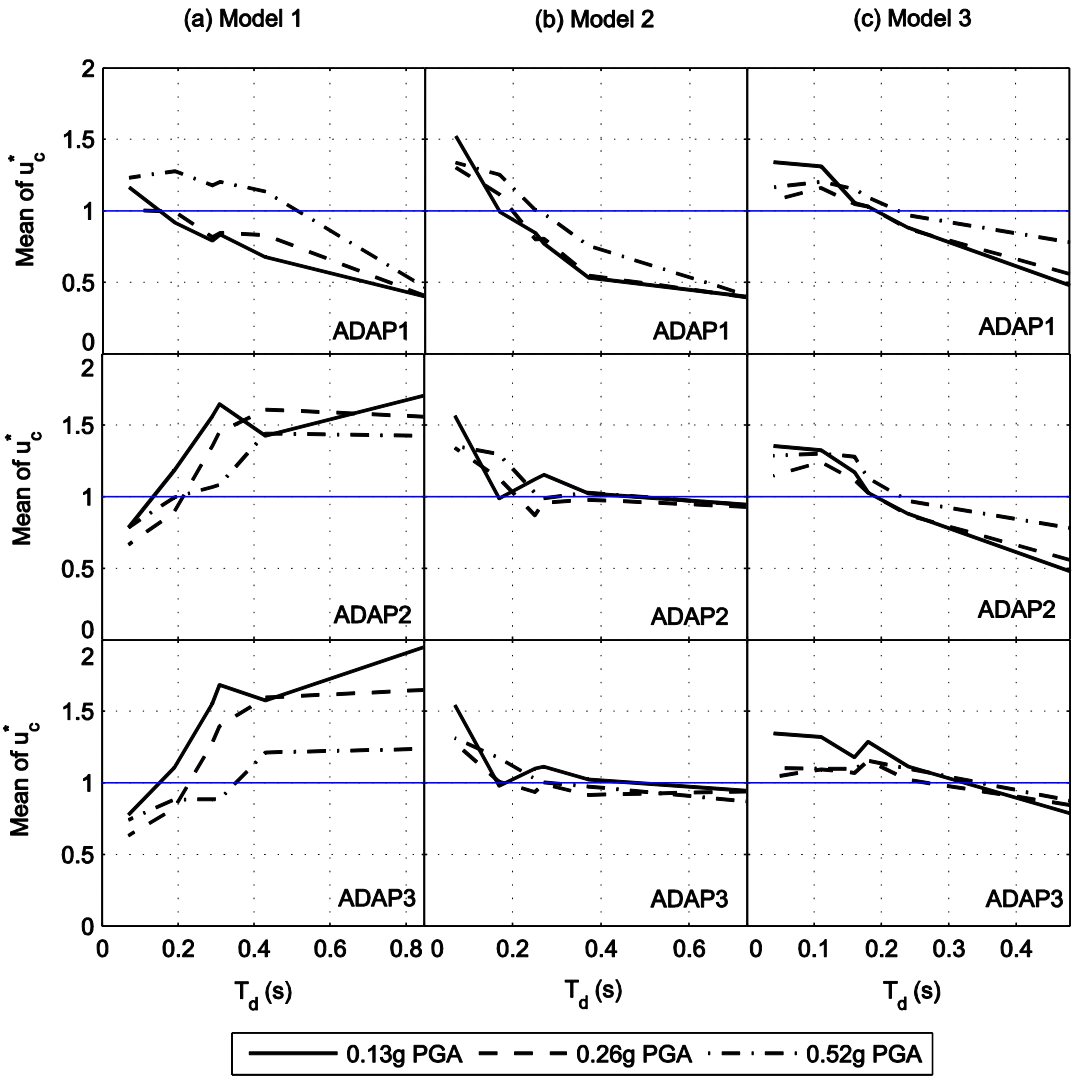

Figure 11. Comparisons of the mean displacement ratios at mid-spans of roof (Roof 1 for Model 3) for the three different conversion procedures for adaptive pushover analysis.

3.5 Summary

From the analyses conducted, following recommendations are given for the application of NSPs to URM buildings with flexible diaphragms. These recommendations will be adopted in studying the accuracies of various analysis methods in Section 4.

- For all methods: target displacement of the equivalent SDOF system to be obtained using modified Takeda or similar hysteresis.

- N2 method: control node to be located at the mid-span of the most flexible diaphragm at the roof level of the building.

- MPA method: (1) for each mode, control node to be placed at the location that displaces the most in the elastic range; (2) use CQC rule to combine the modal responses.

- Adaptive method: conversion to the equivalent SDOF system to be based on the equal work done on the MDOF structure by the pushover forces using the procedure of Hernández-Montes et al. (2006).

4. APPLICABILITY OF NONLINEAR STATIC PROCEDURES

4.1 N2 Method

The applicability of the N2 method is investigated by comparing the plan displacements at the roof level and interstorey drift ratios of in-plane loaded walls against the NTHA results. Three different pushover force distributions, uniform, linear and SRSS, are considered. The comparisons of the displacements at roof level are shown in Figure 12, while the interstorey drifts are shown in Figure 13, Figure 14 and Figure 15 for Models 1, 2 and 3 respectively, subjected to the largest 0.52g excitation.

The linear pushover analysis can be seen to give the most conservative roof displacement predictions for all building models. The estimated interstorey drifts are more uniform along the height than those obtained by the NTHA, leading to general overestimations of the upper-storey drifts for all diaphragm stiffnesses.

The uniform pushover analysis predicts more constant plan displacement shapes than the NTHA, and this leads to the underestimation of the flexible side and the overestimation of the stiff side when the stiffness eccentricity of the building is large (Models 1 and 3). For Model 2, when the stiffness eccentricity is small, the uniform pushover analysis over-predicts the responses of both in-plane loaded walls. The computed interstorey drift by the uniform pushover analysis is concentrated in the ground storey, which becomes most pronounced when shear damage is the dominant failure mechanism of the critical storey. The upper-storey drifts are typically underestimated by the uniform pushover analysis.

The SRSS force distribution generally gives better correlations with the NTHA for both the roof displacements and the interstorey drifts. However, large underestimations can occur (for example, Model 1 with D4 in Figure 13) when the diaphragms become flexible.

In general, regardless of the type of pushover force profile, the accuracy of the N2 method is mainly dependent on the level of diaphragm stiffness. Other factors, such as the level of stiffness eccentricity and

failure mechanism, appear to be of secondary importance in comparison. The exact NTHA results indicate that the interstorey drift demands reduce when the diaphragm flexibility is increased. The single-mode N2 method cannot capture this reduction associated with the multi-mode behaviour of the buildings, and their predictions increasingly overestimate those of the NTHA results. In addition, no single pushover force distribution is found to provide the most accurate predictions for all diaphragm stiffnesses. However, conservative displacement and interstorey drift estimates can be made if the envelope of the uniform and the linear pushover analysis results is considered.

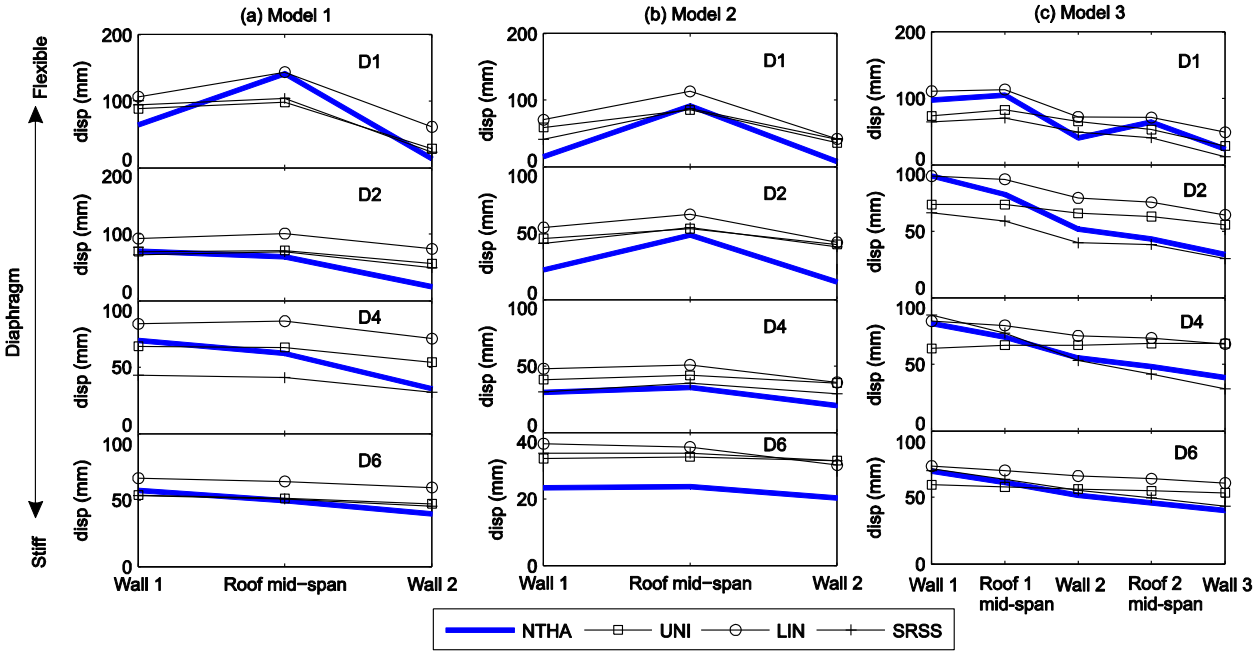

Figure 12. Comparisons of mean peak top displacements obtained from N2 method against the mean NTHA results, subjected to 0.52 g PGA (plan view).

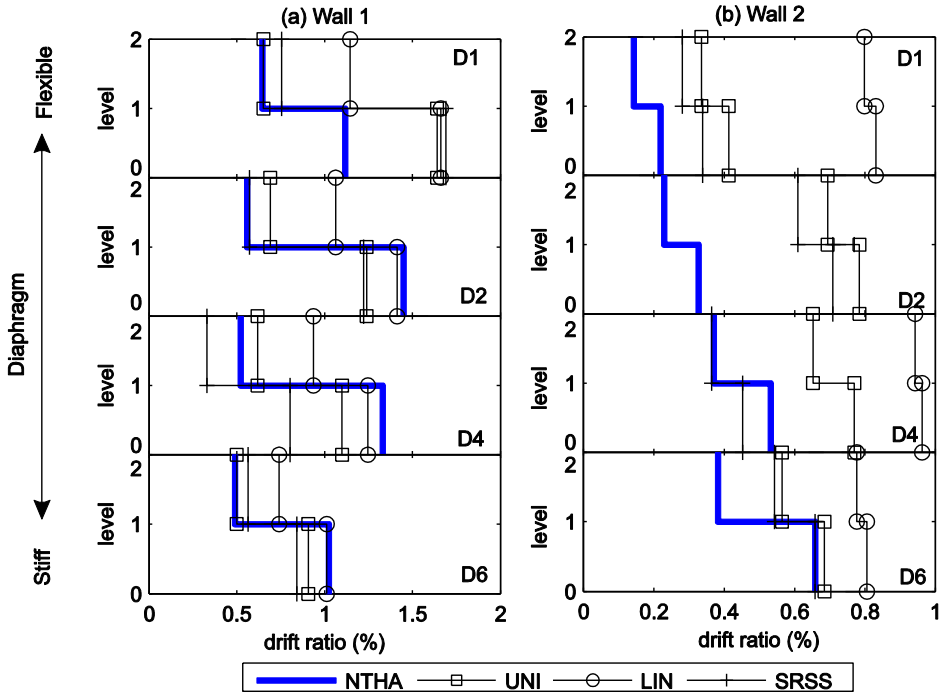

Figure 13. Comparisons of mean peak interstorey drifts from N2 method and NTHA for (a) flexible (wall 1) and (b) stiff (wall 2) in-plane walls of Model 1 subjected to 0.52 g PGA.

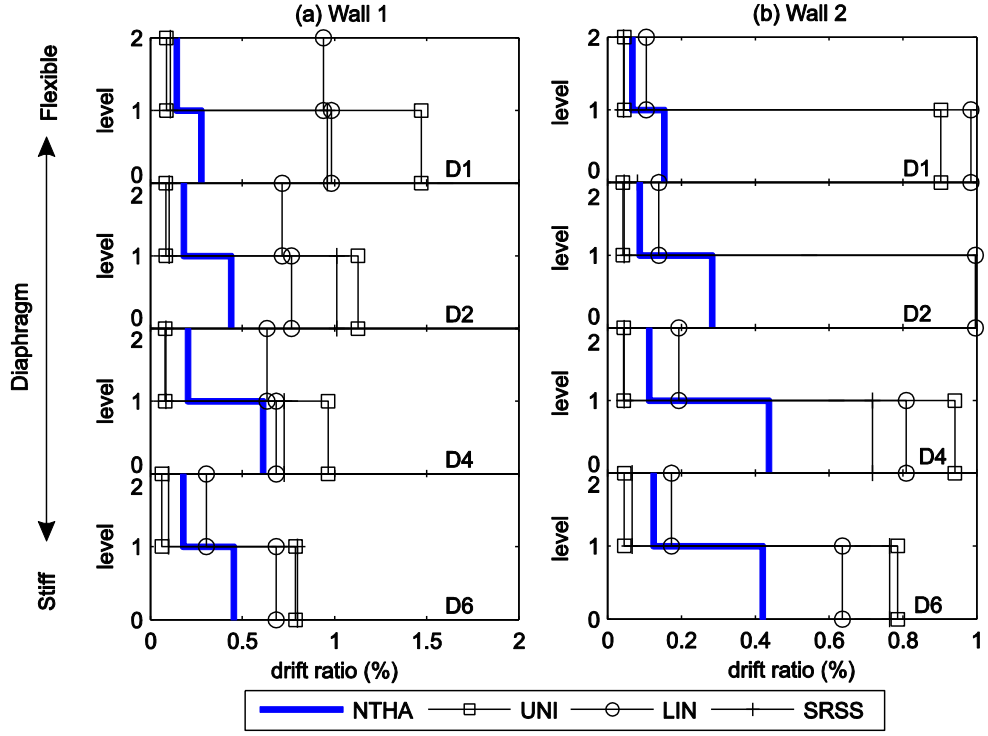

Figure 14. Comparisons of mean of peak interstorey drifts obtained from N2 method against mean NTHA (a) flexible (wall 1) and (b) stiff (wall 2) in-plane walls of Model 2 subjected to 0.52 g PGA.

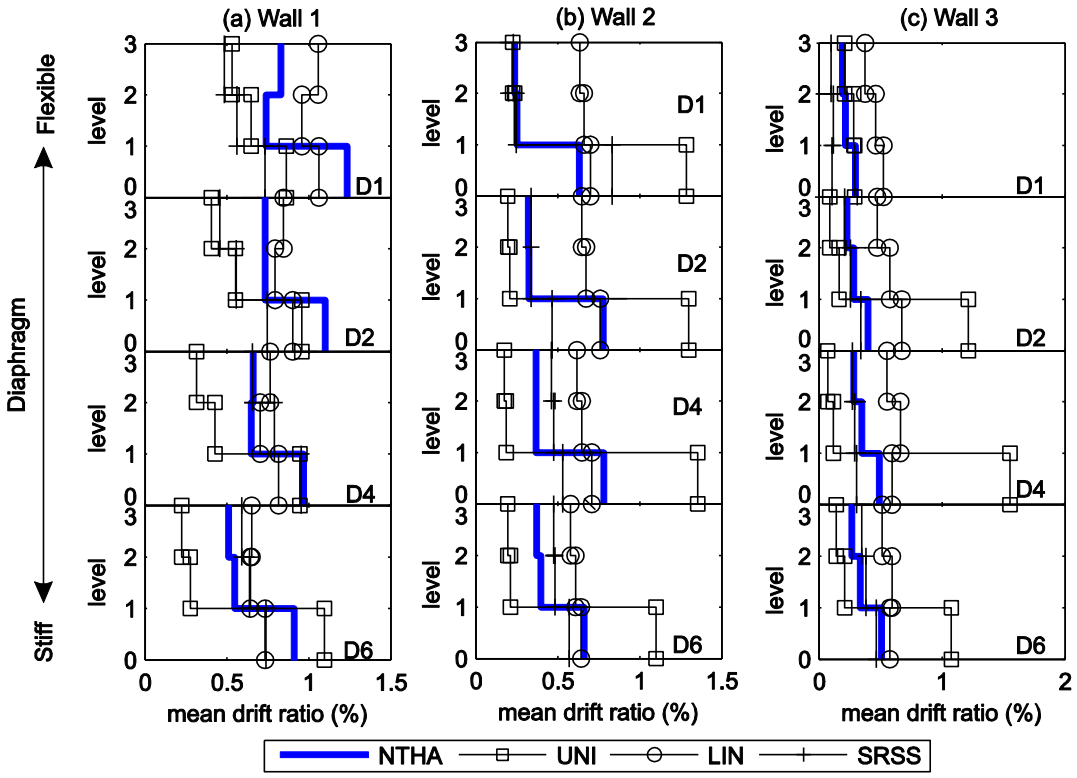

Figure 15. Comparisons of mean of peak interstorey drifts obtained from N2 method against mean NTHA for (a) flexible (wall 1) and (b) stiff (wall 2) in-plane walls of Model 3 subjected to 0.52 g PGA (elevation).

4.2 MPA

The plan displacement shapes computed from the MPA are compared against the NTHA in Figure 16 and Figure 17 subjected to the PGA of 0.13g and 0.52g respectively. When the building response is primarily elastic under the 0.13g excitation (Figure 16), the MPA provides accurate predictions of the NTHA results. This is expected because the MPA is identical to the RSA in the elastic range, and it appropriately accounts for the multi-mode behaviour through modal superposition. In contrast, the accuracy of the inelastic building response predictions under the 0.52g excitation (Figure 17) is dependent on the dominant failure mechanisms of the building models. For Model 1, in which the dominant failure mechanism is the rocking of piers, the MPA performs well. The accuracy in this case was comparable to the elastic response predictions. For Models 2 and 3 however, for which the piers failed mostly in shear, the MPA consistently underestimates the peak displacements.

The interstorey drifts for shear-dominated Models 2 and 3 also show large underestimations of the critical storey, as indicated in Figure 18 for Model 3 subjected to the 0.52g excitation. These underestimations are most pronounced when the diaphragms are relatively flexible and the multi-mode behaviour is prevalent.

The underestimations of the MPA are caused by the assumption of independent modal responses, and this is highlighted in the present study due to the definition of the macroelement used in the analysis. In the macroelement definition, the rocking behaviour is almost elastic (although nonlinear), while the shear behaviour is highly inelastic, defined by a monotonically increasing scalar parameter that accounts for the macroscopic representation of cumulative damage occurring at mortar joints. Such cumulative damage cannot be captured by assuming independent modal responses, and this leads to the underestimations of responses by the MPA when multiple modes contribute to building behaviour.

The assumption of the independent modal responses also creates a difficulty in identifying the damage level of the piers. This problem is illustrated in Figure 19, which shows the variations of axial and shear forces obtained during the modal pushover analyses, plotted against the strength interaction curves of the exterior pier of Model 2 located on the compression side. The plot also shows the combined results of the MPA and the peak values corresponding to the NTHA. The individual modal pushover analyses show that none of the analyses actually resulted in the failure of the pier. However, the combined result indicates that the pier would have failure in shear. Furthermore, the maximum compressive force on the pier remains in the range corresponding to the rocking failure for modes 2, 4 and 7, while for mode 6, the axial force enters into the range corresponding to shear failure. The combined shear force can also exceed the actual strength of the pier, which is a recognised limitation of the MPA (Goel and Chopra 2005). These issues attributed to the independent modal response assumption of the MPA make the accuracy of the method questionable when multiple dominant modes are present.

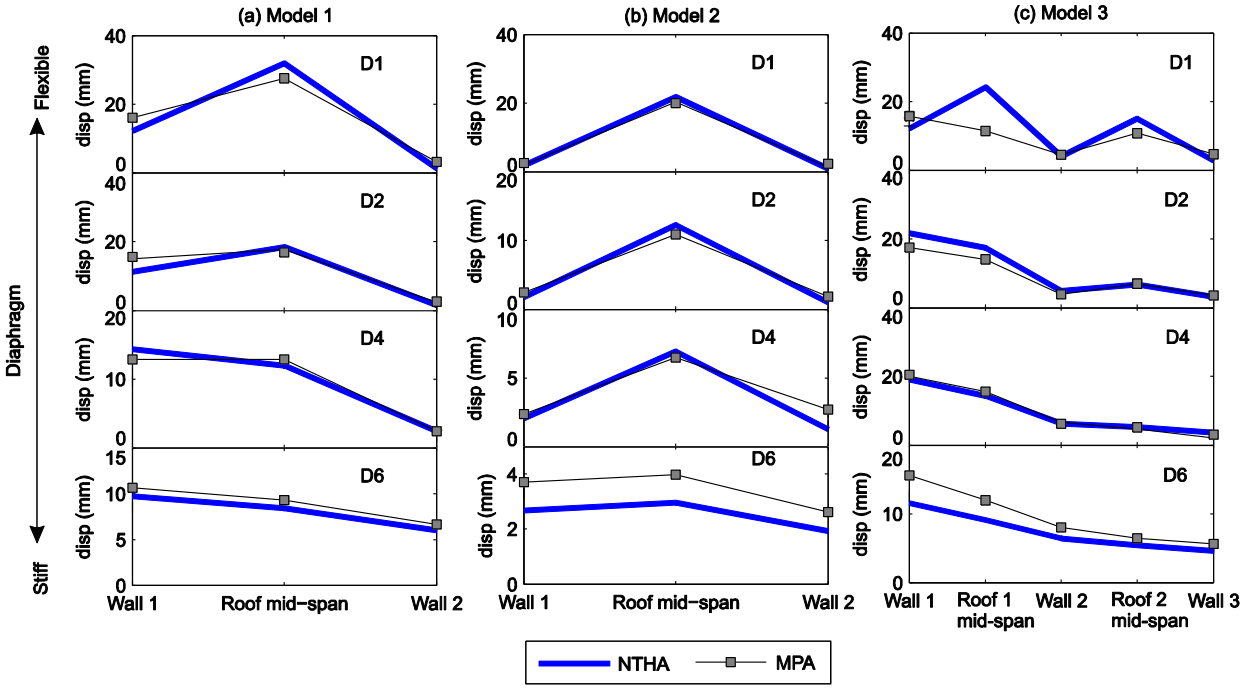

Figure 16. Comparisons of mean peak top displacements obtained from the MPA against the mean NTHA result, subjected to 0.18 g PGA (plan view).

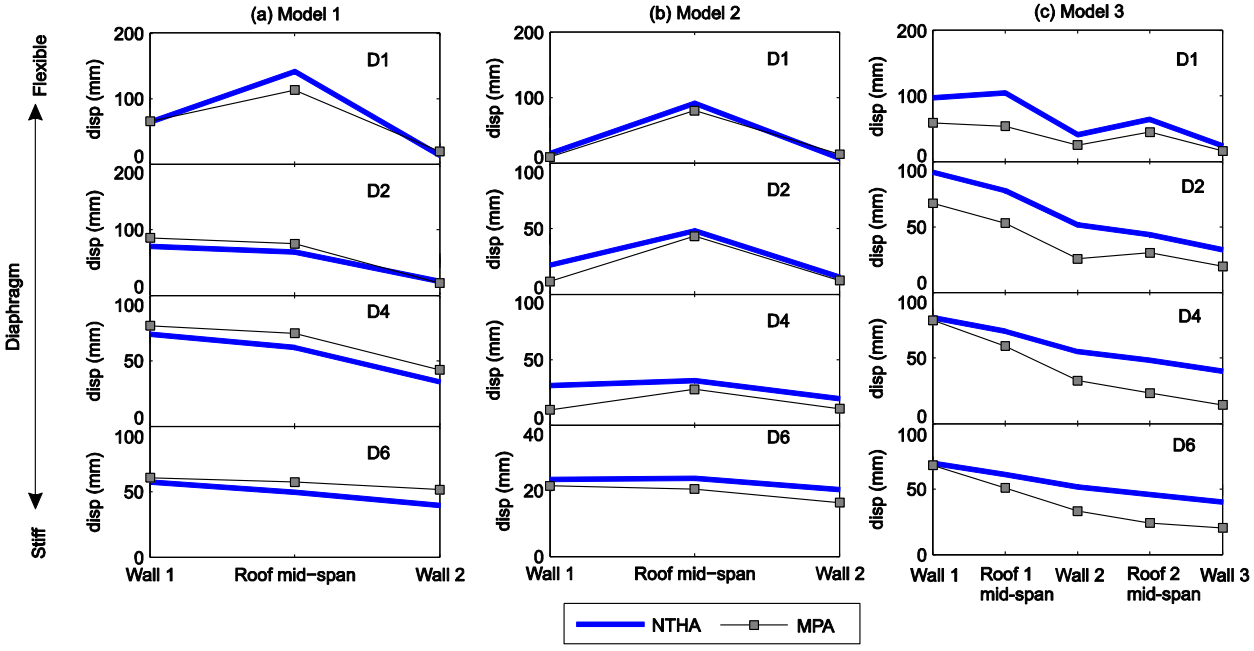

Figure 17. Comparisons of mean peak top displacements obtained from the MPA against the mean NTHA result, subjected to 0.52 g PGA (plan view).

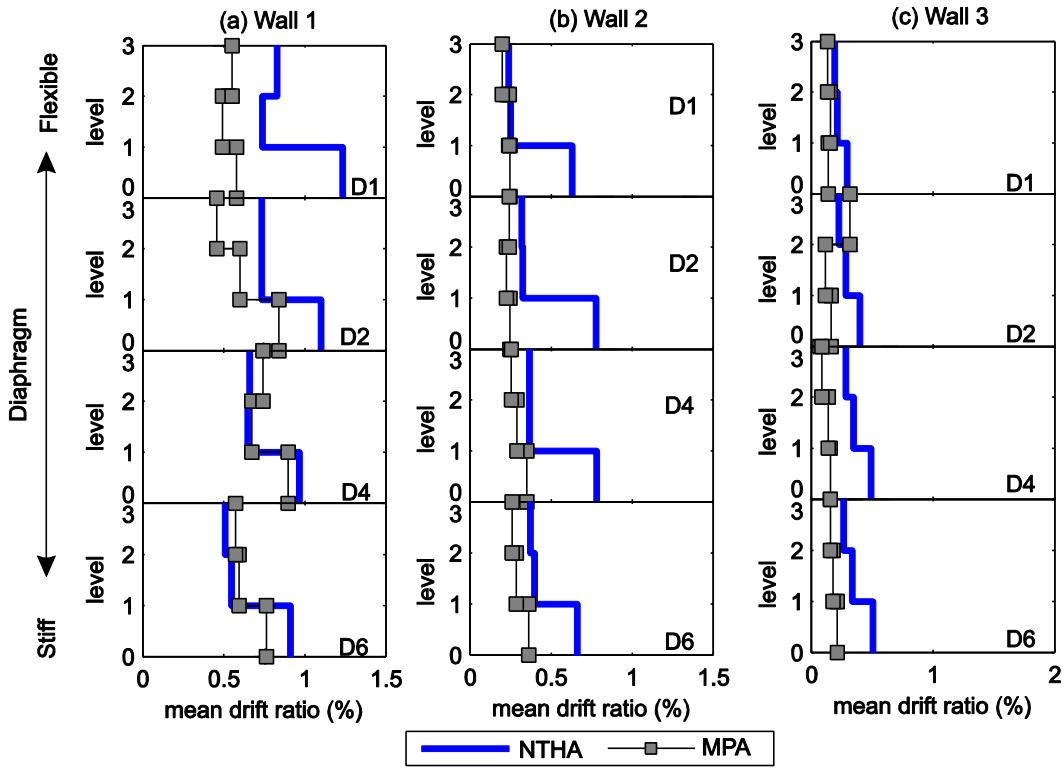

Figure 18. Comparisons of mean peak interstorey drifts obtained from the MPA against mean NTHA for the flexible (wall 1) in-plane walls subjected to 0.52 g PGA (elevation).

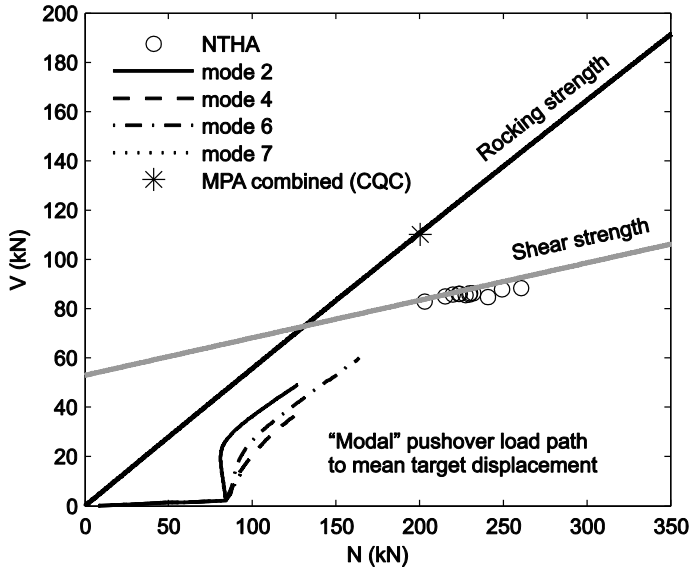

Figure 19. Axial - shear variations of "modal" pushover analysis in against the failure domain of the ground storey exterior pier of Model 2, corresponding to the 0.52 g PGA excitation.

4.3 Adaptive Pushover

The plan displacement shapes computed from the adaptive pushover analysis are compared against the NTHA in Figure 20 corresponding to the PGA of 0.52g. The interstorey drifts under the same excitation intensity are shown in Figure 21 for Model 3. In general, the adaptive pushover analysis captures the top displacements and interstorey drifts better than the N2 method or the MPA. However, the limitations similar to the N2 method can be observed; for all models, the reduced interstorey drifts associated with multi-mode behaviour is not accurately captured. This similarity with the N2 method occurs even though the pushover force distribution is continually modified during the analysis to account for the changing characteristics of the building behaviour, because the single-mode behaviour is essentially assumed at each analysis step.

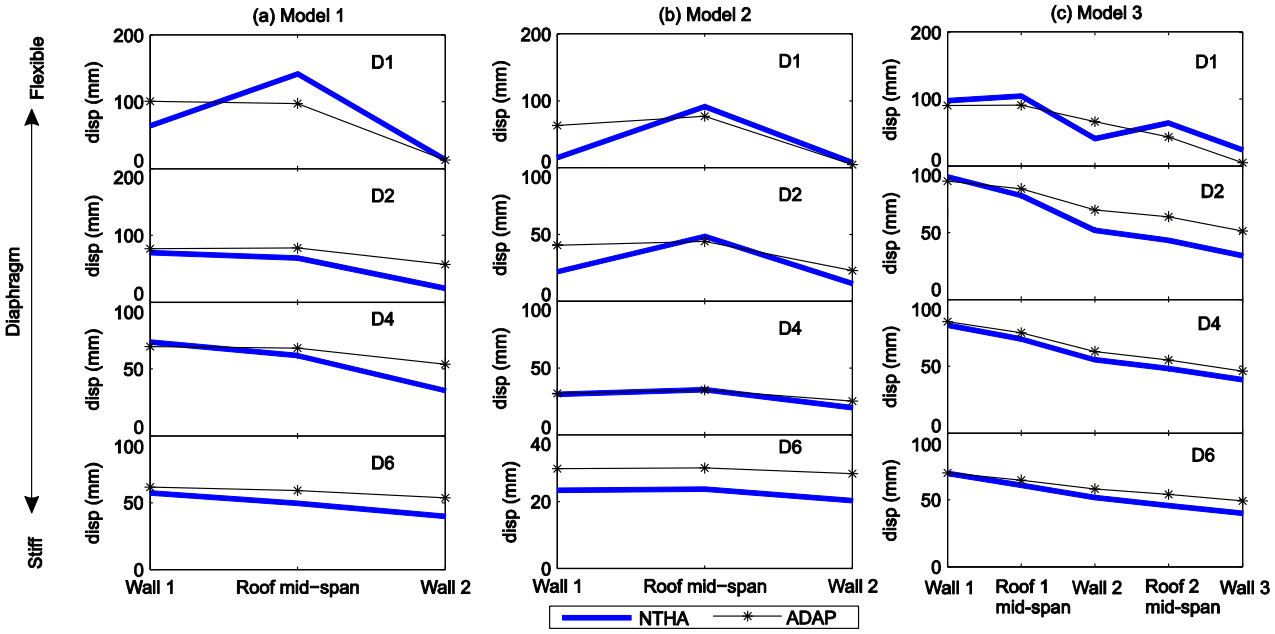

Figure 20. Comparisons of mean peak top displacements obtained from the adaptive pushover analysis against the mean NTHA result, subjected to 0.52 g PGA (plan view).

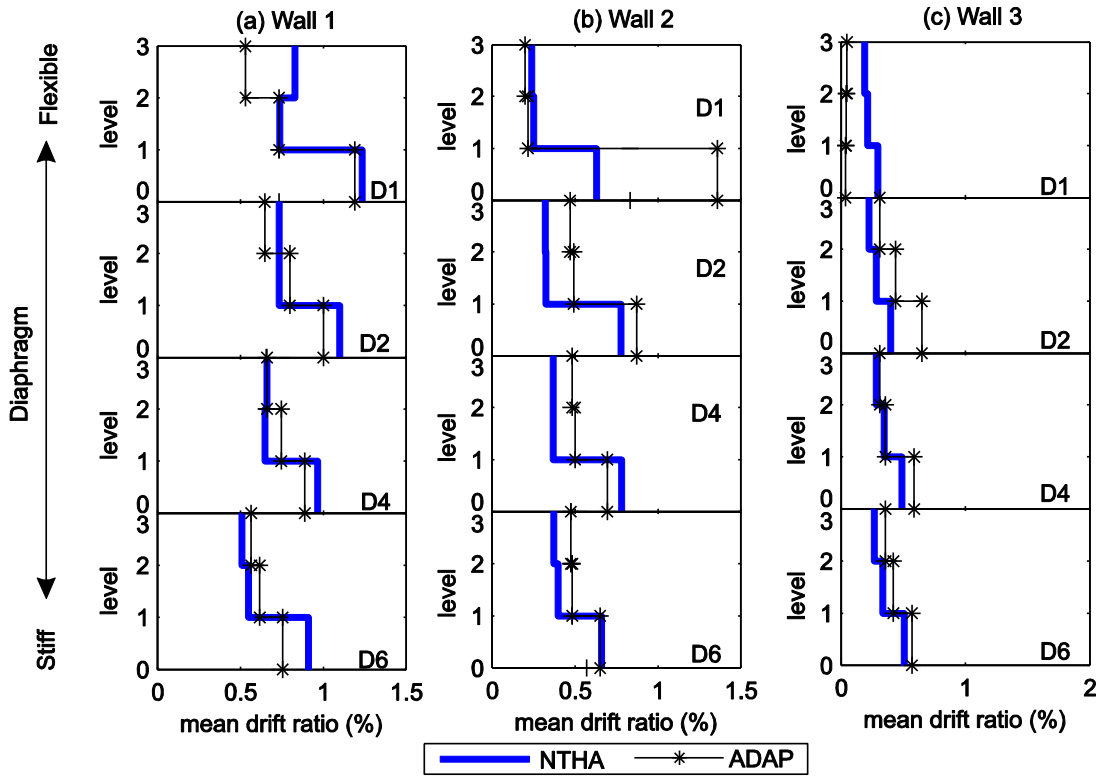

Figure 21. Comparisons of mean peak interstorey drifts obtained from the adaptive pushover analysis against mean NTHA for the in-plane walls of Model 3 subjected to 0.52 g PGA (elevation).

4.4 Diaphragm Deformation

The analyses indicate that the N2 method and the adaptive NSP typically underestimate the diaphragm deformation (Figure 12 and Figure 20), which is defined here as the mid-span displacement of the diaphragm relative to the average displacement of the supporting in-plane loaded walls.

In order to obtain more accurate estimates of the diaphragm deformation, a simple strategy is proposed based on the following assumptions: (1) the diaphragms remain elastic throughout the excitation, and (2) the in-plane loaded walls are sufficiently stiffer than the diaphragms so that they can be considered essentially rigid for the purpose of calculating diaphragm deformation. The first assumption is consistent with the numerical modelling used in the analyses. The second assumption may be considered reasonable when the diaphragm flexibility is relatively large. Using these assumptions, the peak diaphragm deformation can be approximated by the elastic spectral displacement value corresponding to the diaphragm period.

The accuracy of such simple spectrum approach is shown in Figure 22, where the ratios of the estimated peak diaphragm deformations from the response spectrum (S_d) to the exact value obtained from the

NTHA (Δ_d) are plotted against the NTHA results. The mean ratios show good agreement of the spectrum approach in predicting a wide range of diaphragm deformation values, with the average error approximately ranging between 70% to 150% of the NTHA. As expected, the standard deviations of the predictions (or the scatter of results) increase as the diaphragms become stiff because the assumption of rigid in-plane walls become inaccurate. It is noted that the proposed procedure has some similarities to the direct displacement-based design approach investigated by Whitney and Agrawal (2015).

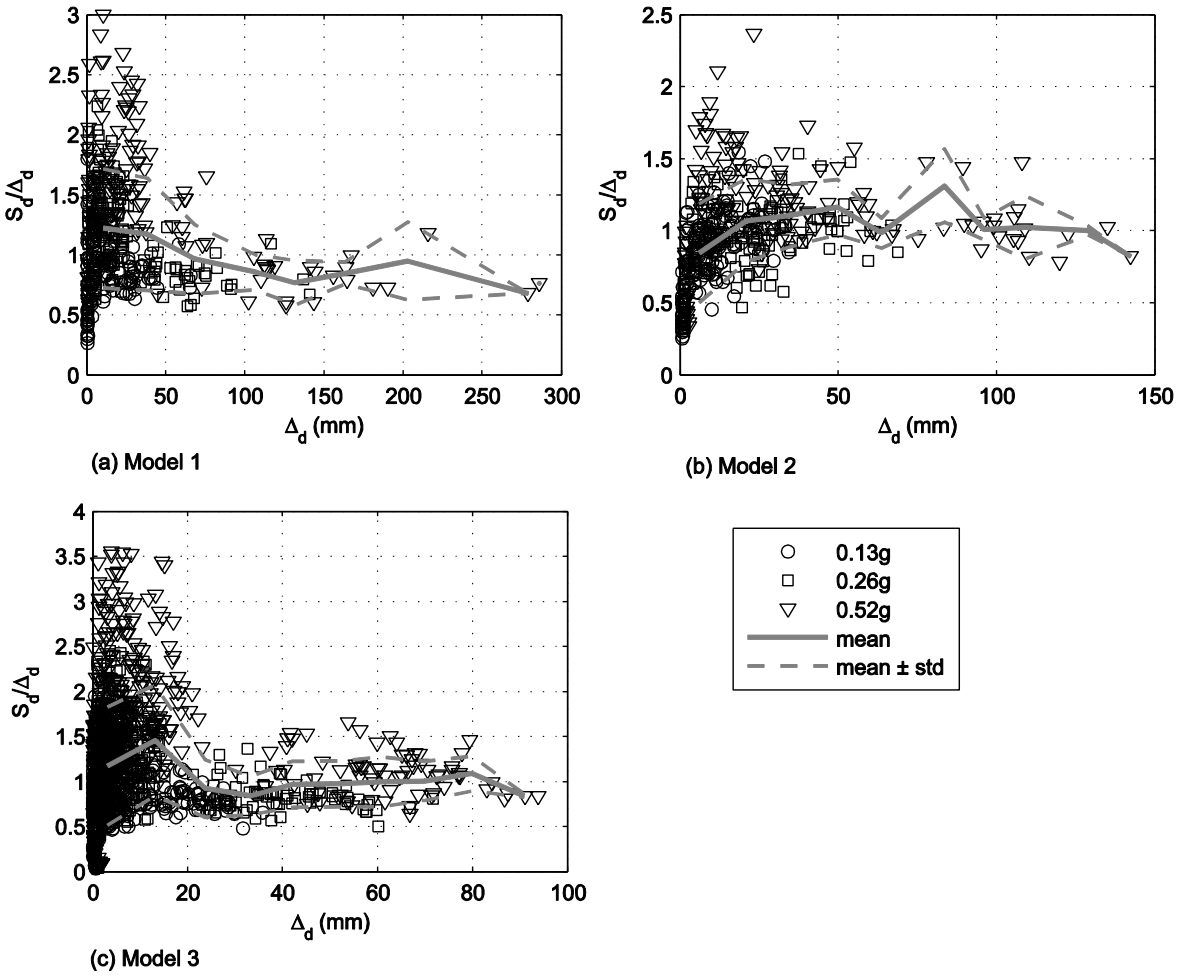

Figure 22. Peak ratios of spectral displacements to the diaphragm deformations calculated from NTHA

4.5 Discussions and Recommendations on the Use of Nonlinear Static Procedures

The analyses show that all considered pushover analysis methods have limited applicability. The accuracies of the methods are found to depend on two main factors, namely (1) the failure mechanism of the in-plane loaded walls, and (2) the level of diaphragm flexibility. While both factors affect the applicability of the investigated NSPs, the MPA is primarily dependent on the failure mechanism of the piers in the critical storey. In contrast, the applicability of the N2 methods and the adaptive procedures are

mainly dependent on the level of diaphragm flexibility. Based on these observations, recommendations are provided for the applicable ranges of various pushover analysis methods for URM buildings with flexible diaphragms.

The applicability of the MPA for URM buildings with flexible diaphragms in practice appears to be limited, due to the large underestimations of response estimates for buildings which undergo shear-dominant failures. Furthermore, it is difficult to identify the damage levels of walls when multiple modes are present in the building response. For these reasons, the use of the MPA is not recommended for URM buildings with flexible diaphragms.

For the N2 method and the adaptive NSP, the analyses become erroneous when the presence of multiple modes result in the reductions of the "exact" displacement (or interstorey drift) demands of the in-plane loaded walls. In a previous parametric study conducted using idealised single-storey systems, such multi-mode responses were identified to become significant when the ratio of the diaphragm deformation to the average wall displacement (Δ_w), $\lambda = \Delta_d/\Delta_w$, was approximately greater than 1/3. Hence a possible strategy for ensuring the accuracy of the N2 and the adaptive NSP is to firstly carry out the analyses and then to check that the maximum diaphragm deformation obtained at all floor levels satisfies the condition of $\lambda \leq 1/3$. The applicability of this strategy is illustrated in Figure 23, in which the ratios of the peak ground storey drifts obtained using the NSPs to the NTHA results ($\Delta^*_{w,1}$) are plotted against the maximum values of λ for each ground motion. It is noted that in calculating λ, the diaphragm deformations were obtained using the response spectrum approach (Section 4.4), while the average wall displacements were obtained from the NSPs. Figure 24 shows that $\lambda \leq 1/3$ appears to be a reasonable limit, if somewhat on the conservative side, to be placed on the results of the NSPs to ensure that the accuracy of the N2 and the adaptive NSP are at a comparable level to those of the rigid diaphragm configuration (i.e. when λ tends to zero). The plots also confirm that the adaptive NSP are generally more accurate than the N2 method when the $\lambda \leq 1/3$ condition is met.

Large errors can be associated with both the N2 method and the adaptive NSP when $\lambda > 1/3$. However, the analyses have shown that the N2 method can provide conservative results for all diaphragm stiffness values when the envelope of the uniform and linear pushover analyses is considered.

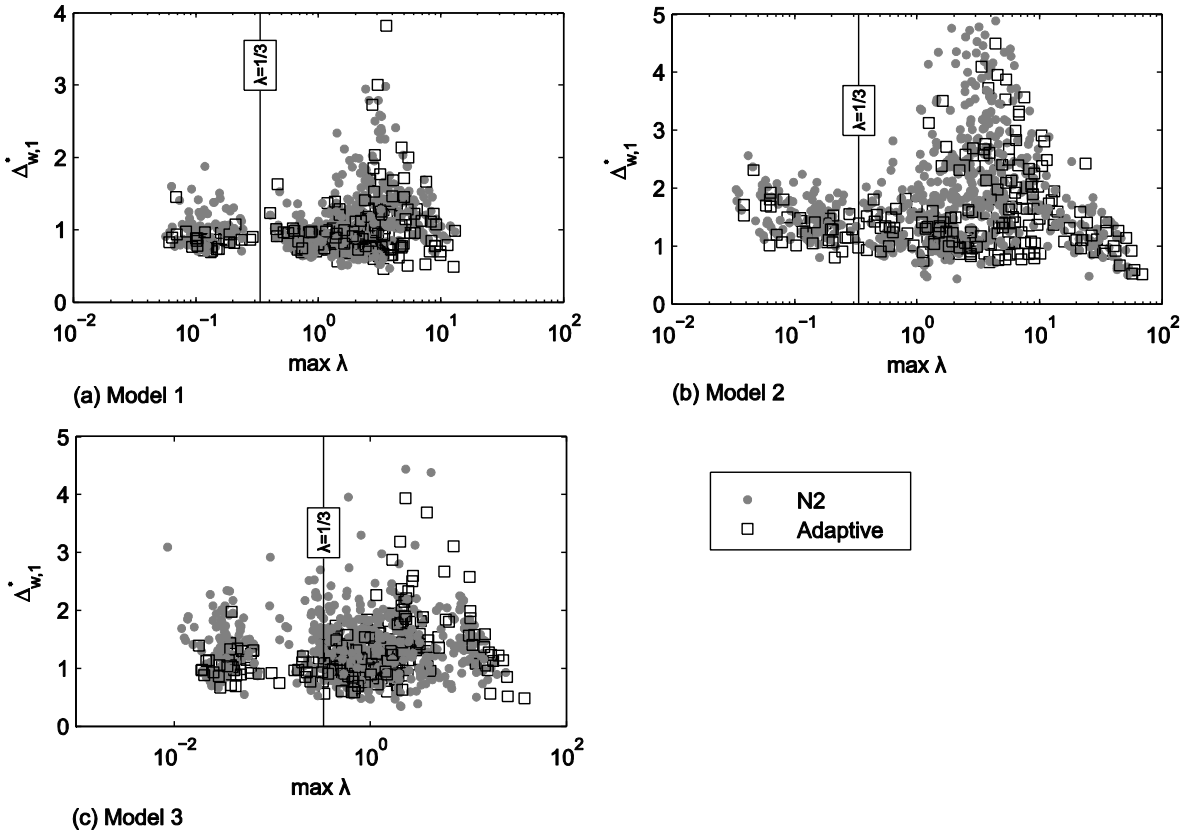

Figure 23. Ratios of ground storey drifts calculated by the N2 method and adaptive pushover analysis to the NTHA results, plotted against the maximum λ values. Data points include all pushover force distributions and ground motion excitation levels.

5. CONCLUSIONS

The applicability of the N2 method, MPA and the adaptive pushover method developed by Galasco et al. (2006) for estimating the peak seismic responses of URM buildings with flexible diaphragms were investigated, considering the NTHA of the MDOF models give the "exact" dynamic responses. Three building models with different levels of stiffness eccentricity, number of storeys, number of bays and the predominant failure mechanisms were considered.

The analyses indicated that the accuracy of the MPA was primarily dependent on the failure mechanism of the buildings, while those of the N2 and the adaptive method were influenced mainly by the level of diaphragm flexibility.

When the building response remained almost elastic, or when the piers predominantly responded in rocking, the MPA provided the most accurate predictions of the peak displacements and interstorey drifts. However, when the buildings experienced significant inelastic shear damage, the MPA consistently

underestimated the displacements and the critical interstorey drifts. The underestimations were attributed to the assumption of the independent "modal" responses in the MPA, which did not capture the cumulative nature of shear damage implemented in the numerical model. These results suggest that the MPA is not suitable for URM buildings with flexible diaphragms.

The adaptive method provided the most accurate predictions of the roof displacements and interstorey drifts ratios when the diaphragm was relatively stiff. The applicable range of the adaptive method can be given by $\lambda \leq 1/3$, where λ is the maximum ratio of the diaphragm deformation at a floor level to the average displacement of in-plane walls supporting the diaphragm at the same level. In calculating λ, the diaphragm deformation can be approximated using the displacement spectrum, and the wall displacements can be obtained from the pushover analysis.

When $\lambda > 1/3$, no investigated method could provide good predictions of the NTHA results. In this range of diaphragm flexibility, more advanced multi-mode adaptive pushover procedures may be needed, which require further studies. However, conservative results can be obtained by using the N2 method, by taking the envelope of the results obtained using the pushover force distributions corresponding to the uniform and linear displacement shapes.

Furthermore, the most consistent predictions of the target displacements are expected when analyses are carried out in the following manner:

- N2 method: control node to be located at the mid-span of the most flexible diaphragm at the roof level of the building.

- MPA method: (1) for each mode, control node to be placed at the location that displaces the most in the elastic range; (2) use CQC rule to combine the modal responses.

- Adaptive method: conversion to the equivalent SDOF system to be based on the equal work done on the MDOF structure by the pushover forces using the procedure of Hernández-Montes et al. (2006).

- The target displacement to be calculated using hysteresis models similar to thin Takeda model, or by spectrum-based approximate procedures developed using such models. Further studies are however recommended to identify/develop inelastic displacement ratio expressions appropriate for URM buildings.

ACKNOWLEDGEMENT

The authors gratefully acknowledge the financial support provided by the Australian Research Council (ARC grant # DP120100848). The financial support provided by the Australian Postgraduate Award for the first author is also gratefully acknowledged. The financial support provided by Progetto ReLUIS 2015 – Linea Strutture in Muratura for the third author is also gratefully acknowledged.

REFERENCES

Antoniou, S. and Pinho, R. (2004a) "Advantages and limitations of adaptive and non-adaptive force-based pushover procedures", Journal of Earthquake Engineering, 8(4), 497 – 522.

Antoniou, S. and Pinho, R. (2004b) "Development and verification of a displacement-based adaptive pushover procedure", Journal of Earthquake Engineering, 8(5), 643 – 661.

ASCE (2014) "Seismic evaluation and retrofit of existing buildings, ASCE/SEI 41-13", American Society of Civil Engineers, Reston, Virginia.

Aydinoğlu, M. N. (2003) "An incremental response spectrum analysis procedure based on inelastic spectral displacements for multi-mode seismic performance evaluation", Bulletin of Earthquake Engineering, 1, 3 – 36.

CEN (2004) "Eurocode 8: design of structures for earthquake resistance – part 1: general rules, seismic actions and rules for buildings", European Committee for Standardization, Brussels, Belgium.

Chopra, A. K. and Goel, R. K. (2002) "A modal pushover analysis procedure for estimating seismic demands for buildings", Earthquake Engineering and Structural Dynamics, 31, 561 – 582.

Chopra, A. K. and Chintanapakdee C. (2004) "Inelastic deformation ratios for design and evaluation of structures: Single-degree-of-freedom bilinear systems", Journal of Structural Engineering, 130(9), 1309 – 1319.

Chopra A. K., Goel, R. K. and Chintanapakdee C. (2003) "Statistics of single-degree-of-freedom estimate of displacement for pushover analysis of buildings", Journal of Structural Engineering, 129(4), 459 – 469.

Fajfar, P. and Gašperšič, P. (1996) "The N2 method for the seismic damage analysis of RC buildings", Earthquake Engineering and Structural Dynamics, 25, 31 – 46.

Fajfar, P. (1999) “Capacity spectrum method based on inelastic demand spectra”, Earthquake Engineering and Structural Dynamics, 28, 979 – 993.

FEMA (2005) “Improvement of nonlinear static seismic analysis procedures, FEMA 440”, Applied Technology Council, Washington.

Galasco, A., Lagomarsino, S. and Penna, A. (2006) “On the use of pushover analysis for existing masonry buildings”, Proceedings of 1st European Conference on Earthquake Engineering and Seismology, Geneva, Switzerland.

Giongo, I., Wilson, A, Dizhur, D. Y., Derakhshan, H., Tomasi, R., Griffith, M. C., Quenneville, P., and Ingham, J. M. (2014) “Detailed seismic assessment and improvement procedure for vintage flexible timber diaphragms”, Bulletin of the New Zealand Society for Earthquake Engineering, 47(2), 97 – 118.

Goel, R. K. and Chopra, A. K. (2005), “Extension of modal pushover analysis to compute member forces”, Earthquake Spectra, 21(1), 125 – 139.

Graziotti, F., Penna, A., Bossi, E., and Magenes, G. (2014) “Evaluation of displacement demand for unreinforced masonry buildings by equivalent SDOF systems”, Proceedings of the 9th International Conference on Structural Dynamcis, EURODYN 2014, Porto, Portugal.

Griffith, M. C., Moon, L., Ingham, J. M. and Derakhshan, H. (2013) “Implications of the Canterbury earthquake sequence for Adelaide, South Australia”, Proceedings of the 12th Canadian Masonry Symposium, Vancouver, British Columbia, June 2-5, 2013.

Hernández-Montes, E., Kwon, O.-S., and Aschheim, M. A. (2004) “An energy-based formulation for first- and multiple-mode nonlinear static (pushover) analyses”, Journal of Earthquake Engineering, 8(1), 69 – 88.

Kalkan, E. and Kunnath, S. K. (2006) “Adaptive modal combination procedure for nonlinear static analysis of building structures”, Journal of Structural Engineering, 132(11), 1721 – 1731.

Knox, C. L. (2012) “Assessment of perforated unreinforced masonry walls responding in-plane”, PhD thesis, Department of Civil and Environmental Engineering, University of Auckland.

Krawinkler, H. and Seneviratna G. D. P. K. (1998) “Pros and cons of pushover analysis of seismic performance evaluation”, Engineering Structures, 20(4-6), 452 – 464.

Lagomarsino, S., Penna, A., Galasco, A. and Cattari, S. (2013) “TREMURI program: an equivalent frame model for the nonlinear seismic analysis of masonry buildings”, Engineering Structures, 56, 1787 – 1799.

Magenes, G. and Penna, A. (2009) “Existing masonry buildings: General code issues and methods of analysis and assessment”, Proceedings of Eurocode 8 Perspectives from the Italian Standpoint Workshop, Naples, Italy.

Mouyiannou, A., Rota, M., Penna, A. and Magenes, G. (2014) "Identification of suitable limit states from nonlinear dynamic analyses of masonry structures", Journal of Earthquake Engineering, 18(2), 231 - 263.

Pacific Earthquake Engineering Center (PEER). PEER NGA-West database. Accessed on 5th of January, 2015.

Penna, A., Lagomarsino, S. and Galasco, A. (2014) “A nonlinear macroement model for the seismic analysis of masonry buildings”, Earthquake Engineering and Structural Dynamics, 43(2), 159 – 179.

Priestley, M. J. N. and Grant, D. N. (2005) "Viscous damping in seismic design and analysis", Journal of Earthquake Engineering, 9(S2), 229 - 255.

Ruiz-García, J. and Miranda, E. (2003) “Inelastic displacement ratios for evaluation of existing structures”, Earthquake Engineering and Structural Dynamics, 32, 1237 – 1258.

Russel, A. (2010) “Characterisation and seismic assessment of unreinforced masonry buildings”, PhD thesis, Department of Civil and Environmental Engineering, University of Auckland.

Standards Australia (2002) “AS/NZS 1170.1-2002: Structural design actions – Permanent, imposed and other actions”, Standards Australia, Sydney.

Standards Australia (2007) “AS 1170.4-2007: Earthquake actions in Australia”, Standards Australia, Sydney.

Vidic, T., Fajfar, P. and Fischinger, M. (1994) “Consistent inelastic design spectra: strength and displacement”, Earthquake Engineering and Structural Dynamics, 23, 507 – 521.

Whitney, R. and Agrawal, A. K. (2015) “Seismic performance of flexible timber diaphragms: Damping, force-displacement and natural period”, Engineering Structures, 101, 583 – 590.

CHAPTER 7

CONCLUSIONS AND RECOMMENDATIONS

1. CONCLUSIONS

The research presented in this thesis focused on enhancing the understanding of the global seismic behaviour of URM buildings, and contributing towards the improved seismic analysis methods when the floor and roof diaphragms are flexible. The specific objectives of this research were: (1) development of a comprehensive understanding of the seismic behaviour of URM buildings with flexible diaphragms; (2) investigation of accuracies of existing analysis methods; and (3) contributing towards the improvement of analysis methods for URM buildings with flexible diaphragms. The main conclusions of the present research are summarised in the following for each objective.

1.1 Seismic Behaviour of URM Buildings with Flexible Diaphragms

Diaphragm flexibility has significant influences on the global responses of buildings, and on the seismic demands imposed on the lateral load resisting walls. Modal analysis has shown that for symmetric buildings, two important modes are typically present. The deformations of the diaphragms are typically concentrated in the lower mode, while the responses of the in-plane loaded walls are contained in the higher mode. In the elastic range, the increased diaphragm flexibility generally leads to the reduced peak base shear force because of the independent responses of the masses attributed to the diaphragms and in-plane loaded walls.

In the inelastic range, the diaphragm flexibility can induce two different effects, depending on the level of diaphragm stiffness and the plan-asymmetry, especially the strength eccentricity, of the building. When a strength eccentricity is present, large amplification of the displacement demand of the flexible side can occur. However, for all building configurations, large diaphragm flexibility was observed to lead to the reduced in-plane wall demands, in a manner similar to the elastic system.

In general, non-rigid diaphragms can be categorised into four ranges – “rigid”, “stiff”, “semi-flexible”, and “flexible” – based on how incremental diaphragm flexibility affects the peak displacement demands of the in-plane loaded walls. The “rigid” diaphragm range is characterised essentially by the rigid-body motion of the diaphragm, and incremental diaphragm flexibility has little effects on the wall responses. In

the “stiff” diaphragm range, incremental diaphragm flexibility causes the amplification of the displacement of the flexible side, and reduction of the displacement of the stiff side. In the “semi-rigid” range, incremental diaphragm flexibility reduces the peak demand on the flexible side of the building, and the “flexible” range corresponds to the almost independent responses of the diaphragm and the walls.

The maximum displacement amplification of the flexible side occurs at the transition from the “stiff” to the “semi-flexible” diaphragm ranges. An empirical expression of the maximum amplification has been derived as a function of strength eccentricity. This transition point also approximately corresponds to the transition from an essentially single-mode to the multi-mode dominant behaviour of the building. A simple measure of the diaphragm stiffness corresponding to this transition point has been derived as $\lambda = \Delta_d/\Delta_w = 1/3$, where Δ_d is the peak deformation of the diaphragm mid-span relative to the supporting walls, and Δ_w is the average displacement of the supporting walls.

1.2 Accuracy of Existing Seismic Analysis Methods

Both linear and nonlinear static analysis methods were investigated. Existing linear analysis methods are based on a simplifying assumption of the dynamic interaction occurring between the flexible diaphragms and the in-plane loaded walls, and the accuracies of the methods depend on the level of diaphragm flexibility. The analysis procedure contained in ASCE 41-13 (ASCE 2014) is reasonably accurate when the diaphragms are stiff. However, its accuracy reduces as the diaphragm flexibility increases. On the other hand, the method by Knox (2012) is more accurate when the diaphragms are relatively flexible, but its accuracy reduces as the diaphragms become stiff.

The applicability of the investigated nonlinear static methods, namely the N2 method (Fajfar and Gašperšič 1996), the MPA (Chopra and Goel 2002) and an adaptive pushover analysis by Galasco et al. (2006), also depend on the level of diaphragm flexibility. However, for the MPA, the accuracy of the method also depends significantly on the dominant failure mechanism of the piers (rocking or shear). Because of the dependence on the failure mechanism, as well as the difficulties in identifying the damage level of piers and spandrels, the MPA is not recommended as a suitable method in estimating the peak seismic response of URM buildings with flexible diaphragms.

The most accurate predictions of the nonlinear responses are expected when the adaptive pushover method is used. However, it is also recommended that the use of the single-mode adaptive method to be limited to the case when the maximum value of $\lambda = \Delta_d/\Delta_w$ for all diaphragms in a building is less than or equal to 1/3. In calculating λ, the diaphragm deformation can be obtained from the elastic spectral displacement corresponding to the diaphragm period. Consistently conservative predictions can also be

obtained for all levels of diaphragm stiffness using the N2 method, by taking the envelope of the analyses conducted using pushover forces proportional to the uniform and linear displacement shapes along the height of the structure.

1.3 Improvement of Seismic Analysis Methods

Using the two important modes identified from the modal analysis, an improved linear analysis procedure has been proposed. The proposed method directly accounts for the dynamic interaction between the flexible diaphragms and in-plane loaded walls. A set of analysis charts has been developed for the design spectrum of NZS 1170.5 (New Zealand Standard 2004) to facilitate the simplified code-based application of the method. Similar charts can readily be developed for other code-specified spectra.

The most suitable manner for the application of the existing nonlinear static procedures for URM buildings with flexible diaphragms has also been identified. Most accurate predictions of the target displacements are expected when analyses are carried out in the following manner:

- N2 method: control node to be located at the mid-span of the most flexible diaphragm at the roof level of the building.

- MPA: (1) for each mode, control node to be placed at the location that displaces the most in the elastic range, and (2) use CQC method to combine the modal responses.

- Adaptive method: conversion of the pushover curve to the equivalent SDOF system to be based on the equal work done on the MDOF structure by the pushover forces, using the procedure of Hernández-Montes et al. (2006).

- The target displacement to be calculated using equivalent SDOF system with hysteresis models similar to thin Takeda model, or by spectrum-based approximate expressions developed using such hysteresis models.

2. RECOMMENDATIONS

The outcomes of the present research lead to several areas of future research into the improvement of seismic analysis methods for URM buildings with flexible diaphragms.

Firstly, there is a need for an improved numerical model capable of accurately capturing the three-dimensional behaviour of URM buildings with flexible diaphragms. Such a numerical model should

include all the salient characteristics of URM buildings with flexible diaphragms; namely the orthotropic nature of timber diaphragms, the limited (or poor) connections between diaphragms and the masonry walls, and the dynamic behaviour of the out-of-plane responding walls.

At present, the linear static method remains popular in practice. Therefore, further investigations in improving the accuracy of the linear static method appears to be appropriate. The procedure developed in this study can be extended to incorporate the redistribution of the internal forces as part of the linear static analysis method, in order to better capture the likely distribution of damage.

The results of the present research suggest that improving the nonlinear static analysis method for URM buildings with flexible diaphragms requires the consideration of both the changing nature of structural response into the inelastic range and the multi-mode behaviour arising from diaphragm flexibility. Hence, it is suggested that further studies to be undertaken to develop a multi-mode adaptive pushover method for URM buildings with flexible diaphragms. It would be particularly valuable to have such method coded in widely available analysis software, such as TREMURI.

Finally, while the present research has indicated the suitability of using equivalent SDOF systems with modified Takeda (or similar) hysteresis model to estimate the target displacement in a manner similar to modern construction systems, further systematic statistical evaluations are recommended. The question of whether the equivalent nonlinear SDOF system (as used in this research) or the equivalent linear system with increased viscous damping is more appropriate for URM buildings, should also be addressed.

REFERENCES

ASCE (2014) "Seismic evaluation and retrofit of existing buildings, ASCE/SEI 41-13", American Society of Civil Engineers, Reston, Virginia.

Chopra, A. K. and Goel, R. K. (2002) "A modal pushover analysis procedure for estimating seismic demands for buildings", Earthquake Engineering and Structural Dynamics, 31, 561 – 582.

Fajfar, P. and Gašperšič, P. (1996) "The N2 method for the seismic damage analysis of RC buildings", Earthquake Engineering and Structural Dynamics, 25, 31 – 46.

Galasco, A., Lagomarsino, S. and Penna, A. (2006) "On the use of pushover analysis for existing masonry buildings", Proceedings of 1st European Conference on Earthquake Engineering and Seismology, Geneva, Switzerland.

Hernández-Montes, E., Kwon, O.-S., and Aschheim, M. A. (2004) “An energy-based formulation for first- and multiple-mode nonlinear static (pushover) analyses”, Journal of Earthquake Engineering, 8(1), 69 – 88.

Knox, C. (2012) "Assessment of perforated unreinforced masonry walls responding in-plane", PhD thesis, Department of Civil and Environmental Engineering, University of Auckland.

New Zealand Standard (2004) “Structural design actions Part 5: Earthquake actions - New Zealand”, NZS 1170.5:2004. Standards New Zealand, Wellington, New Zealand.

APPENDIX A

EXAMPLE TREMURI INPUT FILE

A1. INTRODUCTION

In Chapters 4 to 6, the equivalent frame analyses were carried out using TREMURI software. This appendix presents an example TREMURI input file, incorporating four membrane elements to model a flexible diaphragm as described in Chapter 4.

A2. EXAMPLE TREMURI INPUT FILE

```
Tremuri 1 7 1
/Settings
Default
Best 1
/walls
1 0.175 0.175 0.0
2 0.175 11.825 0.0
3 0.175 0.175 90°
4 9.825 0.175 90°
5 0.175 6 0.0
6 5 0.175 90°
/Material_properties
! masonry
1 1385000000 740000000 18 5740000 130000 130000 1 1 1 0.111 2.5 0.3
! steel
2 200000000000 83333333333 7810 350000000
! rigid (massless)
3 200000000000 83333333333 0.0
/nodes_2d
2 1  3.63 0.0 N
3 1  6.03 0.0 N
6 1  3.63 4.0 R 18 0.29 0.45 0.45 0.7 0.8
7 1  6.03 4.0 R 18 0.29 0.45 0.45 0.7 0.8
10 1 3.63 7.5 R 18 0.23 0.45 0.45 0.0 1.0
11 1 6.03 7.5 R 18 0.23 0.45 0.45 0.0 1.0
20 2 4.825 7.5 R 18 0.23 1.5 1.5 0.0 1
/nodes_3d
```

1 2 1 3 0.0 N N
4 2 1 4 0.0 N N
5 2 1 3 4.0 R 18 0.29 0.175 1.38 0.253 0.353 N
8 2 1 4 4.0 R 18 0.29 1.38 0.175 0.253 0.353 N
9 2 1 3 7.5 R 18 0.23 0.175 1.38 0.0 0.553 N
12 2 1 4 7.5 R 18 0.23 1.38 0.175 0.0 0.553 N
13 2 2 3 0.0 N N
14 2 2 6 0.0 N N
15 2 2 4 0.0 N N
16 2 2 3 4.0 R 18 0.29 0.175 2.125 0.336 0.836 N
17 2 2 6 4.0 R 18 0.29 1.5 1.5 1.0 1.5 N
18 2 2 4 4.0 R 18 0.29 2.125 0.175 0.336 0.836 N
19 2 2 3 7.5 R 18 0.23 0.175 2.125 0.0 0.336 N
21 2 2 4 7.5 R 18 0.23 2.125 0.175 0.0 0.336 N
22 2 2 6 9.1 N N
23 2 4 5 0.0 N N
24 2 4 5 4.0 N N
25 2 4 5 7.5 N N
26 2 3 5 0.0 N N
27 2 3 5 4.0 N N
28 2 3 5 7.5 N N
29 2 1 6 0.0 N N
30 2 1 6 4.0 N N
31 2 1 6 9.1 N N
32 2 5 6 0.0 N N
33 2 5 6 4.0 N N
34 2 5 6 9.1 N N
/macroelements
1 1 1 5 0.6 1.824 1.55 3.647 0.35 1 0
2 1 2 6 3.625 1.6 0.9 3.2 0.35 1 0
3 1 3 7 6.025 1.6 0.9 3.2 0.35 1 0
4 1 4 8 9.05 1.824 1.55 3.647 0.35 1 0
5 1 5 9 0.6 5.6 1.55 2.695 0.23 1 0
6 1 6 10 3.625 5.6 0.9 1.8 0.23 1 0
7 1 7 11 6.025 5.6 0.9 1.8 0.23 1 0
8 1 8 12 9.05 5.6 1.55 2.695 0.23 1 0
9 1 5 6 2.275 3.95 1.5 1.8 0.29 1 1
10 1 6 7 4.825 3.95 1.5 1.5 0.29 1 1
11 1 7 8 7.375 3.95 1.5 1.8 0.29 1 1
12 1 9 10 2.275 7 1 1.8 0.23 1 1
13 1 10 11 4.825 7 1 1.5 0.23 1 1
14 1 11 12 7.375 7 1 1.8 0.23 1 1
15 2 13 16 0.975 1.582 2.3 3.164 0.35 1 0

16 2 14 17 4.825 1.25 3 2.5 0.35 1 0
17 2 15 18 8.675 1.582 2.3 3.164 0.35 1 0
18 2 16 19 0.975 5.75 2.3 2.828 0.23 1 0
19 2 17 20 4.825 5.75 3 1.5 0.23 1 0
20 2 18 21 8.675 5.75 2.3 2.828 0.23 1 0
21 2 16 17 2.725 3.75 2.5 1.2 0.29 1 1
22 2 17 18 6.925 3.75 2.5 1.2 0.29 1 1
23 2 19 20 2.725 7 1.0 1.2 0.23 1 1
24 2 20 21 6.925 7 1.0 1.2 0.23 1 1
25 4 23 24 5.825 2.0 12.0 4.0 0.35 1 0
26 4 24 25 5.825 5.75 12.0 3.5 0.23 1 0
27 3 26 27 5.825 2.0 12.0 4.0 0.35 1 0
28 3 27 28 5.825 5.75 12.0 3.5 0.23 1 0
/Beam_elastic
! rigid arms for walls 3 and 4
100 3 5 27 3 10 5 0 0
101 3 27 16 3 10 5 0 0
102 3 9 28 3 10 5 0 0
103 3 28 19 3 10 5 0 0
104 4 8 24 3 10 5 0 0
105 4 24 18 3 10 5 0 0
106 4 12 25 3 10 5 0 0
107 4 25 21 3 10 5 0 0
! diaphragm dummy elements
200 5 26 27 3 10E-6 10E-14 0 0
201 5 27 28 3 10E-6 10E-14 0 0
202 5 32 33 3 10 10E-14 0 0
203 5 33 34 3 10 10E-14 0 0
204 5 23 24 3 10E-6 10E-14 0 0
205 5 24 25 3 10E-6 10E-14 0 0
206 6 29 30 3 10 10E-14 0 0
207 6 30 31 3 10 10E-14 0 0
208 6 32 33 3 10 10E-14 0 0
209 6 33 34 3 10 10E-14 0 0
210 6 14 17 3 10E-6 10E-14 0 0
211 6 17 22 3 10 10E-14 0 0
/floors
1 5 30 33 27 0.02 10000000000 10000000000 0.0 70928850 0.0
2 30 8 24 33 0.02 10000000000 10000000000 0.0 70928850 0.0
3 33 24 18 17 0.02 10000000000 10000000000 0.0 70928850 0.0
4 27 33 17 16 0.02 10000000000 10000000000 0.0 70928850 0.0
5 9 31 34 28 0.02 10000000000 10000000000 0.0 70276400 0.0
6 31 12 25 34 0.02 10000000000 10000000000 0.0 70276400 0.0

7 34 25 21 22 0.02 10000000000 10000000000 0.0 70276400 0.0
8 28 34 22 19 0.02 10000000000 10000000000 0.0 70276400 0.0
/mass
1 5250.42 -0.206893449 -1.018186825 -0.973517639
2 1034.208 0 0 -0.912
3 1034.208 0 0 -0.912
4 5250.42 -0.206893449 -1.018186825 -0.973517639
5 10583.62601 -0.463926744 -0.958250652 0.340962603
6 0 0 0 0
7 0 0 0 0
8 10583.62601 0.463926744 -0.958250652 0.340962603
9 5102.401055 -0.655352238 -0.796748283 0.54276848
10 0 0 0 0
11 0 0 0 0
12 5102.401055 0.655352238 -0.796748283 0.54276848
13 5788.2825 -0.388763231 0.923574216 -0.923527986
14 2989.98 0 0 -0.791
15 5788.2825 0.388763231 0.923574216 -0.923527986
16 12555.16781 -0.675334829 0.807776262 0.373655201
17 10738.34867 0 0 0.393490825
18 12555.16781 0.675334829 0.807776262 0.373655201
19 5465.085755 -0.769591378 0.743872917 0.509248939
20 0 0 0 0
21 5465.085755 0.769591378 0.743872917 0.509248939
22 5881.987416 0 0.337037945 0.999176568
23 7339.5 0 0 -1
24 13923.82527 0.204850463 0 0.261911795
25 5581.368336 0.294235108 0 0.661609433
26 7339.5 0 0 -1
27 13923.82527 -0.204850463 0 0.261911795
28 5581.368336 -0.294235108 0 0.661609433
29 0 0 0 0
30 8425.17767 0 -0.40868073 0.241406143
31 7225.417416 0 -0.2743721 1.217548066
32 0 0 0 0
33 4727.245795 0 0 0
34 2721.747579 0 0 0
/Restraints
1 v v v v v
2 v v v
3 v v v
4 v v v v v
13 v v v v v

14 v v v v v
15 v v v v v
23 v v v v v
26 v v v v v
29 v v v v v
32 v v v v v
! diaphragm restraint
30 0 0 0 0 v
31 0 0 0 0 v
22 0 0 0 0 v
/cf 10 0.0001 1500
5 0 0 -48624 0 40422
6 0 -44033 643
7 0 -44033 -394
8 0 0 -48624 0 -40422
9 0 0 -38421 -19448 21295
10 0 -28754 151
11 0 -28754 41
12 0 0 -38421 -19448 -21295
16 0 0 -70278 0 82430
17 0 0 -106270 0 0
18 0 0 -70278 0 -82430
19 0 0 -43508 19448 36688
20 0 -53488 0
21 0 0 -43508 19448 -36688
24 0 0 -256807 0 0
25 0 0 -111988 0 0
27 0 0 -256807 0 0
28 0 0 -111988 0 0
33 0 0 -46374 0 0
/po 500 0.0001 300 34 ux 0.25 0.25 0
5 454.37 0 0.0 0.0 0.0 0.0
6 1.3866 0.0 0.0
7 1.3866 0.0 0.0
8 454.37 0 0.0 0.0 0.0 0.0
9 1278 0 0.0 0.0 0.0 0.0
10 3.4616 0.0 0.0
11 3.4616 0.0 0.0
12 1278 0 0.0 0.0 0.0 0.0
16 1390.7 0 0.0 0.0 0.0 0.0
17 1193.6 0 0.0 0.0 0.0 0.0
18 1390.7 0 0.0 0.0 0.0 0.0
19 1721.3 0 0.0 0.0 0.0 0.0

20 8.3823 0.0 0.0
21 1721.3 0 0.0 0.0 0.0 0.0
22 1846.1 0 0.0 0.0 0.0 0.0
24 7969 0 0.0 0.0 0.0 0.0
25 4936.4 0 0.0 0.0 0.0 0.0
27 7969 0 0.0 0.0 0.0 0.0
28 4936.4 0 0.0 0.0 0.0 0.0
30 360.39 0 0.0 0.0 0.0 0.0
31 1804.1 0 0.0 0.0 0.0 0.0
33 2660 0 0.0 0.0 0.0 0.0
34 2370.3 0 0.0 0.0 0.0 0.0

APPENDIX B

CONVERSION METHODS OF ADAPTIVE PUSHOVER CURVES

B1. INTRODUCTION

The three conversion methods ADAP1, ADAP2 and ADAP3 introduced in Chapter 6 are described in more detail in this Appendix.

B2. DESCRIPTIONS OF METHODS

As described in Chapter 2, for single-mode nonlinear static procedure, the properties of the equivalent SDOF system (equivalent mass and force-displacement relationship) can be derived from the pushover curve by the following conversions

Equivalent mass:

$$m^* = \boldsymbol{\phi}^{\mathrm{T}}\boldsymbol{m}\boldsymbol{\iota} \tag{B.1}$$

Equivalent displacement:

$$d^* = \frac{u_r}{\Gamma} \tag{B.2}$$

Equivalent normalised force:

$$f^* = \frac{V_b}{\Gamma m^*} \tag{B.3}$$

The equation of motion of the equivalent SDOF system (equivalent to Eq. 12 of Chapter 2, but presented in a slightly modified form by dividing both sides of the equation by m^*):

$$\ddot{d}^* + f^* = -\ddot{u}_g \tag{B.4}$$

where $\boldsymbol{m}$ is the mass matrix, $\boldsymbol{\phi}$ is the assumed displacement shape, $\boldsymbol{\iota}$ is the kinetic transmission vector of ground motion, u_r is the displacement of the control node, V_b is the base shear and $\Gamma = \boldsymbol{\phi}^{\mathrm{T}}\boldsymbol{m}\boldsymbol{\iota}/\boldsymbol{\phi}^{\mathrm{T}}\boldsymbol{m}\boldsymbol{\phi}$.

When an adaptive pushover analysis is performed, the assumed displacement shape varies from one pushover analysis step to the next; in the adaptive pushover algorithm investigated in Chapter 6, $\boldsymbol{\phi}$ at a given pushover analysis step is equal to the displacement shape analysed in the previous step. In addition, the investigated adaptive pushover algorithm also limits the pushover force distributions (obtained by mass multiplied by the displacement shape) to be between the uniform and SRSS force patterns.

ADAP1 directly adopts the expressions Eq. B.1 to Eq. B.3 to calculate the properties of the equivalent SDOF system. The displacement vector $\boldsymbol{\phi}_i$ at the ith step is used to calculate the values m_i^*, d_i^* and Γ_i.

ADAP2 also uses expressions Eq. B.1 to Eq. B.3 directly at each step. However, the vector $\boldsymbol{\phi}_i$ used in the conversion is not the assumed displacement shape, but the value back calculated from the pushover force pattern. As the force pattern is bounded, the vector $\boldsymbol{\phi}_i$ used in the conversion may not be proportional to the assumed displacement shape.

ADAP3 is based on the equivalence of the work done by the pushover forces and the energy absorbed by a SDOF system. This approach is conceptually similar to the energy-based conversion proposed by Hernández-Montes et al. (2004). The incremental work done by the pushover forces is firstly calculated as

$$\Delta W_i = \boldsymbol{p}_i(\boldsymbol{u}_i - \boldsymbol{u}_{i-1}) \tag{B.5}$$

where $\boldsymbol{p}_i$ and $\boldsymbol{u}_i$ are the pushover force and the calculated displacements respectively, at the ith analysis step.

The incremental displacement satisfying energy equivalence is obtained by equating the work done by the base shear,

$$\Delta D_i = \frac{\Delta W_i}{V_{b,i}} \tag{B.6}$$

The base shear can be expressed in a manner similar to the standard modal expression, using the displacement shape $\boldsymbol{\phi}_i$ at the ith step,

$$V_{b,i} = \omega_i^2 \Gamma_i m_i^* D_i \tag{B.7}$$

where D_i is the summation of displacements calculated in Eq B.6 up to the ith step, and ω_i may be interpreted as a linearised frequency corresponding to the secant stiffness from the origin to the ith analysis step on the pushover curve.

Rearranging Eq. B.7,

$$\omega_i^2 D_i = \frac{V_{b,i}}{\Gamma_i m_i^*} \tag{B.8}$$

Comparing Eq. B.8 to the standard equation of motion of SDOF system (e.g. Chopra 2007) shows that the displacement of the equivalent SDOF system is

$$d_i^* = D_i \tag{B.9}$$

and the restoring force of the equivalent SDOF system is

$$f_i^* = \frac{V_{b,i}}{\Gamma_i m_i^*} \tag{B.10}$$

The ADAP3 approach uses Eq. B9 and Eq. B.10 at each point on the pushover curve to obtain the equivalent SDOF system definition.

REFERENCES

Chopra, A. K. (2007) "Dynamics of structures – theory and applications to earthquake engineering", 3rd Edition. Pearson Prentice Hall, New Jersey.

Hernández-Montes, E., Kwon, O.-S., and Aschheim, M. A. (2004) "An energy-based formulation for first- and multiple-mode nonlinear static (pushover) analyses", Journal of Earthquake Engineering, 8(1), 69 – 88.

APPENDIX C

ACCURACY OF SINGLE-MODE PUSHOVER ANALYSIS METHOD

Background

This Appendix contains the paper titled "Estimating the accuracy of single-mode pushover analysis method" presented at the 10th Pacific Conference on Earthquake Engineering. The paper investigates a technique for estimating the magnitude of error involved when using the single-mode pushover analysis for URM buildings with flexible diaphragms.

This Appendix presents additional material related to Chapter 6.

ABSTRACT

Nonlinear static analyses of unreinforced masonry buildings are typically carried out assuming a single-mode response of the structure. While this assumption is appropriate when the floor and the roof diaphragms are rigid in their own planes, many existing unreinforced masonry buildings have flexible timber diaphragms, for which the applicability of a single-mode pushover analysis becomes questionable.

This paper explores whether the accuracy of a single-mode pushover analysis can be estimated from the results of the pushover analysis itself. From the theoretical consideration, a key parameter that reflects the validity of the single-mode pushover analysis is shown to be the sensitivity of the analysis to the control node location, and a measure of the control node sensitivity is proposed. Preliminary parametric studies conducted on idealised single-storey systems and a two-storey building show that the proposed measure can provide an indicative error of the single-mode pushover analysis.

1. INTRODUCTION

Nonlinear static (pushover) methods have become widely used for the seismic demand estimation of buildings, with various forms of the method specified in Eurocode 8 (CEN 2004), ATC-40 (ATC 1996) and ASCE 41-13 (ASCE 2014). In association with the advances in the development of efficient numerical tools, the use of pushover analysis has also become common for the evaluation of unreinforced masonry (URM) buildings (Magenes and Penna 2009).

The pushover methods currently used for masonry buildings almost exclusively correspond to the single-degree-of-freedom (SDOF) representation of the structure, in which the pushover analysis is carried out using invariant lateral forces. Typically, the lateral forces are assumed to be proportional to mass (uniform displacement shape) or to mass multiplied by a linear (inverted triangular) shape along the height of the building. The former approximates the soft-storey behaviour, while the latter is more appropriate when the inelastic deformations are distributed throughout the building or when the walls behave as weakly coupled cantilevers. Such single-mode pushover (SPO) analysis is known to be an acceptable approximation for low-rise regular buildings with rigid diaphragms. However, existing URM buildings often have flexible timber floor and roof diaphragms, and several studies have questioned the indiscriminate use of the SPO analysis when the diaphragms are flexible (Costley and Abrams 1995; Mendes and Lourenço 2009). Although refined pushover methods, for example a multi-mode procedure (Chopra and Goel 2002), can be extended to buildings with flexible diaphragms, it is important to be able to estimate when a SPO analysis can be applied with sufficiently accurate results. This is particularly so

for URM buildings, of which the majority may be considered to be simple structures, for which correspondingly simple analysis procedures are preferred in practice.

In this paper, the theoretical background of the SPO analysis is firstly summarised, showing that a reliable SPO analysis should be independent of the control node location. The differences in the predicted responses obtained using different control nodes are considered to reflect the inaccuracy of the SPO analysis, and a measure of the control node sensitivity is proposed. Parametric analyses on idealised single-storey systems and a two-storey building suggest that the proposed measure can provide an indicative error of the SPO analysis.

2. THEORETICAL BACKGROUND

The theoretical basis of the SPO analysis relies on the assumption of an invariant deflected shape $\boldsymbol{\phi}$ of the structure throughout the excitation (Fajfar and Gašperšič 1996; Krawinkler and Seneviratna 1997), which is used to reduce the multi degree of freedom (MDOF) structure to an equivalent SDOF system.

Consider the nonlinear MDOF equation of motion,

$$\boldsymbol{m}\ddot{\boldsymbol{u}} + \boldsymbol{c}\dot{\boldsymbol{u}} + \boldsymbol{f_s}(\boldsymbol{u}, \dot{\boldsymbol{u}}) = -\boldsymbol{m\iota}\ddot{u}_g(t) \tag{1}$$

where $\boldsymbol{m}$ and $\boldsymbol{c}$ are the mass and the damping matrices respectively, $\boldsymbol{u}$ is the relative displacement vector, $\boldsymbol{f_s}$ is the vector of nonlinear resisting forces, $\boldsymbol{\iota}$ is the influence vector of the ground motion and $\ddot{u}_g$ is the ground acceleration. Introducing the assumption of the invariant displacement profile,

$$\boldsymbol{u} = \boldsymbol{\phi} q(t) \tag{2}$$

Substituting Eq. 2 into Eq. 1, pre-multiplying by $\boldsymbol{\phi}^{\mathrm{T}}$ and simplifying the equation in a manner analogous to the standard modal decomposition (Chopra 2007) gives the equation of motion of the equivalent SDOF system,

$$\ddot{D} + 2\xi\omega\dot{D} + \frac{F_s\left(D, \dot{D}\right)}{L} = -\ddot{u}_g(t) \tag{3}$$

where $F_s = \boldsymbol{\phi}^{\mathrm{T}}\boldsymbol{f_s}$, $L = \boldsymbol{\phi}^{\mathrm{T}}\boldsymbol{m\iota}$, $D = \frac{q}{\Gamma}$, and $\Gamma = \frac{\boldsymbol{\phi}^{\mathrm{T}}\boldsymbol{m\iota}}{\boldsymbol{\phi}^{\mathrm{T}}\boldsymbol{m\phi}}$. The damping term is expressed by the initial frequency ω and the damping ratio ξ corresponding to the assumed displacement shape, defined so that $\frac{\boldsymbol{\phi}^{\mathrm{T}}\boldsymbol{c\phi}}{\boldsymbol{\phi}^{\mathrm{T}}\boldsymbol{m\phi}} = 2\xi\omega$.

The SPO analysis approximates the force-displacement relationship of the equivalent SDOF system (F_s/L-D) by the base shear – control node displacement (V_b-u_k) relationship (pushover curve) of a static pushover analysis of the structure subjected to incremental lateral forces proportional to $\boldsymbol{m\phi}$ (Fajfar and Gašperšič 1996). It should be noted that the pushover curve is not a unique property of the structure as it depends on the choice of $\boldsymbol{\phi}$ and the location of the control node. The conversion between the pushover curve and F_s/L-D (capacity curve) of the equivalent SDOF system is given by

$$D = \frac{u_k}{\Gamma \phi_k} \tag{4}$$

$$\frac{F_s}{L} = \frac{V_b}{\Gamma L} \tag{5}$$

In the N2 method, the displacement profile is normalised to the control node location, i.e. ϕ_k=1.

The capacity curve is typically simplified by a bilinear idealisation to enable the solution of Eq. 3. Eq. 3 can be solved rigorously by the nonlinear time history analysis (NTHA) of the equivalent SDOF system. Alternatively, the peak value of D may be obtained using approximate techniques such as the equivalent linearisation (Capacity Spectrum Method), the use of the modification factors on the elastic displacement (Displacement Coefficient Method) or the use of the inelastic spectrum (N2 method). Once the peak value of D is obtained, Eq. 4 can be inverted to obtain the peak displacement estimate of the control node. The results of the pushover analysis at the peak control node displacement gives the approximate peak seismic demands (e.g. displacements, inter-storey drifts, member chord rotations) of the structure.

3. MEASURE OF CONTROL NODE SENSITIVITY

A pushover analysis satisfying Eq. 2 is independent of the control node location. This can be seen by considering analyses with the same assumed displacement shape, but using two different control nodes j and k. The only difference between the two analyses is the displacement definition of the equivalent SDOF systems, D_j and D_k, as given by Eq. 4. If Eq. 2 is re-written as

$$\frac{u_j}{u_k} = \frac{\phi_j}{\phi_k} \tag{6}$$

and substituted into D_j,

$$D_j = \frac{u_j}{\Gamma \phi_j} = \frac{u_k}{\Gamma \phi_j}\frac{\phi_j}{\phi_k} = D_k = D \tag{7}$$

The two equivalent SDOF systems are hence identical to each other, and the same peak displacement will be obtained when Eq. 3 is solved. Similar consideration shows that the structural responses (e.g. displacement, inter-storey drifts) are also identical when $\boldsymbol{\phi}$ reflects the exact displacement shape.

However, the SPO analysis is generally *not* independent of the control node because (1) a building entering in the nonlinear response regime continuously changes its displacement shape, and (2) the multi-mode behaviour becomes prominent as the diaphragm flexibility increases, neither of which can be captured by a single invariant displaced shape. If a control node k is used in the SPO analysis, the degree to which the predicted responses depend on the choice of the control node may be expressed in the form of error as (referred to as control node sensitivity, CS)

$$CS = \left| \frac{r_k}{r_j} - 1 \right|, \qquad j \neq k \tag{8}$$

where r_k is a response of interest from the pushover analysis using the reference control node k, and r_j is the corresponding result using some other control node $j \neq k$. The value of CS varies depending on the response parameter used (e.g. displacements, inter-storey drifts, chord rotations), the selected control node locations, and for the different locations/members of the structure. If several control nodes are used for the additional analyses (i.e. for node *j* in Eq. 8), the maximum value of CS can be used as the control node sensitivity.

An invariant displacement shape could approximate the nonlinear displacements if the structure is appropriately designed, for instance by distributing the seismic demand uniformly throughout the structure, so that the likely displacement shape of the structure is known. However, in most cases of existing structures, the distribution of the nonlinear deformation demand cannot be identified a priori, and the assumption of a fixed displacement shape is generally incorrect. This problem has led in the past to the proposal of adaptive pushover methods (Galasco et al. 2006) where the evolving nature of the displacement shape is accounted for in the pushover procedure. Nevertheless, for a SPO analysis to give correct results, Eq. 2 must be valid, so that the pushover analysis will give consistent results irrespective of the choice of the control node. Hence it may be supposed that a correlation exists between the control node sensitivity and the accuracy of the SPO analysis and Eq. 8 to provide an indicative measure of the accuracy of the non-adaptive, fixed shape SPO analysis. This premise is investigated in the following section.

4. NUMERICAL ANALYSIS

4.1 Idealised Single-storey System

A parametric analysis was conducted using idealised single-bay single-storey systems with one-way stiffness and strength eccentricities (Fig. 1(a), 1(b)). Simple single-storey systems representing the most basic response characteristics of buildings with flexible diaphragms were used in order to eliminate the uncertainties associated with the height-wise distribution of the pushover forces and to enable the rigorous solution of the equation of motion of the equivalent SDOF system. Therefore the inaccuracy of the SPO analysis resulting from the diaphragm flexibility can be isolated. The parameters of the model are defined by (1) plan dimensions L_x and L_y, (2) total mass, (3) period of the rigid diaphragm system T_y, (4) ratio of the uncoupled torsional to translational frequencies of the rigid diaphragm condition Ω_θ, (5) stiffness eccentricity ε_{sx}, (6) strength eccentricity ε_{px}, (7) force reduction factor under the rigid diaphragm condition in the direction of excitation R_y, (8) ratio of strengths in the orthogonal direction to the direction of excitation R_F, (9) fraction of masses attributed to the walls (ρ_{w1}, ρ_{w2} etc.) and the diaphragm ρ_d, and (10) fundamental period of the diaphragm as a shear beam T_d. The systems used in this study had the following constant properties; L_x=12 m, L_y=18 m, total mass of 25 tons, T_y = 0.35 s, Ω_θ = 1, R_F = 1, ρ_{w1}=ρ_{w2}=ρ_{w3}=ρ_{w4} = 0.225, ρ_d=0.1 and the constant modal damping ratio of 5%. The inelastic behaviour of the spring was represented by a Takeda model. The wall masses were lumped at the locations of wall springs, while the diaphragm mass was distributed across the diaphragm elements. The diaphragms were modelled by elastic membrane elements, with each line of nodes constrained to move together in each orthogonal direction, so that the diaphragm deformation was governed by its shear modulus calculated from T_d. The stiffness eccentricity ε_{sx} amounted to 0.3L_x. The strength parameters were varied as shown in Table 1 to create systems with two levels of yielding (R_y=2.5 or 4), that had either a symmetric distribution of wall strength (ε_{px}=0), or the strength eccentricity equal to the stiffness eccentricity ($\varepsilon_{px} = \varepsilon_{sx}$). The diaphragm period was varied between 0.01 s and 2 s.

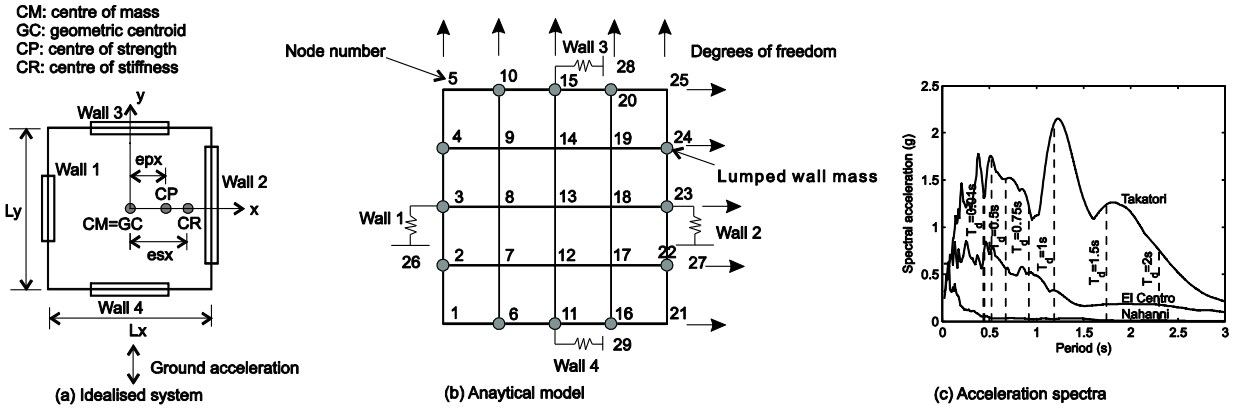

Figure 1. Idealised model and ground motions used in the analysis.

Table 1. Models used in the analysis

Model	R_y	ε_{px}
M1	2.5	0.0
M2	2.5	0.3
M3	4	0.0
M4	4	0.3

Three unscaled ground motions of different frequency content and intensities were used in the analysis. The ground motions were (1) El Centro earthquake recorded on 19th May 1940, (2) Nahanni earthquake recorded on 23th of December 1985, and (3) Kobe earthquake recorded at Takatori station on 16th January 1995. Figure 1(c) shows the 5% damped elastic spectra of the records together with the fundamental periods of the considered systems.

The NTHA of the system was considered to provide the "exact" peak displacements, $\boldsymbol{u}_{THA}$. As the variation of pushover forces along the height of the building was irrelevant for the single-storey model, the SPO analysis was conducted using pushover forces proportional to the distribution of mass in the direction of loading. The response of the equivalent SDOF system was calculated rigorously by solving the nonlinear equation of motion (Eq. 3) using the bilinearised F_S/L-D relationship, and the peak displacement of the equivalent SDOF system was converted back to the control node displacement by inverting Eq. 4. The pushover analysis at that control node displacement gave the estimated peak displacements, $\boldsymbol{u}_{SPO}$.

The accuracy of the SPO analysis was measured by the peak displacement error (PDE)

$$PDE = \frac{u_{SPO}}{u_{THA}} - 1 \tag{9}$$

which were evaluated for the displacements at wall 1, wall 2 and the diaphragm mid-span.

The control node sensitivity (CS) defined in Eq. 8 were calculated from the displacements obtained by the SPO analysis with the reference control node at the diaphragm mid-span, and the additional analyses using control nodes on wall 1 and wall 2. The maximum values of CS were then recorded for wall 1, wall 2 and the diaphragm mid-span. Note that the CS values are calculated solely from pushover analysis, while the PDE expresses the accuracy of SPO with respect to NTHA.

Figure 2 shows the typical displacement predictions of SPO analysis when the control node is varied between wall 1, wall 2 and the diaphragm mid-span (shown for model M3 subjected to the El Centro record). The predictions clearly show the increased sensitivity to the control node location as the diaphragm flexibility increases.

Figure 3 shows the values of CS and the corresponding PDE. Also indicated on the plots are the equality relationship between the absolute value of the PDE and the CS. A good correlation between the PDE and the CS can be observed for the El Centro record, with the CS providing an indicative upper-bound error of the SPO analysis. This indicates that the exact responses tend to lie within the range of responses predicted by the SPO analyses using different control nodes, as confirmed in Figure 2. For the Nahanni and the Takatori records, the correlation is not as clear as for the El Centro record. Large overestimations can be observed for both records when CS is in the range of 0.3 to 0.6, which imply that the SPO analysis tends to be conservative, regardless of the location of the control node. In fact, a SPO analysis is likely to overestimate the actual responses when the diaphragm becomes flexible because the analysis assumes the majority of the seismic mass (the value depends on the assumed displacement shape) to participate in a single mode, while the actual response is governed by a multi-mode behaviour in which some out-of-phase cancelling of responses would occur. The underestimation errors of the SPO analysis, however, are consistently bound by the CS for all records.

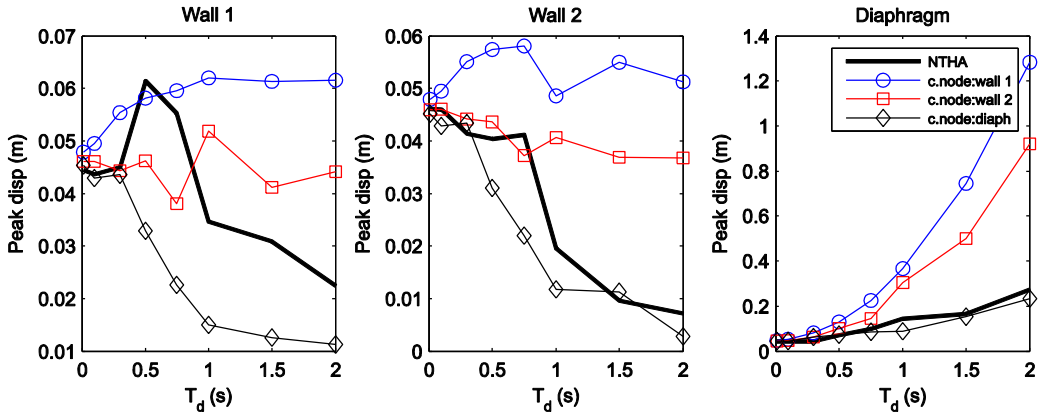

Figure 2. Peak displacement predictions by SPO analysis using different control nodes for M3 subjected to El Centro accelerogram.

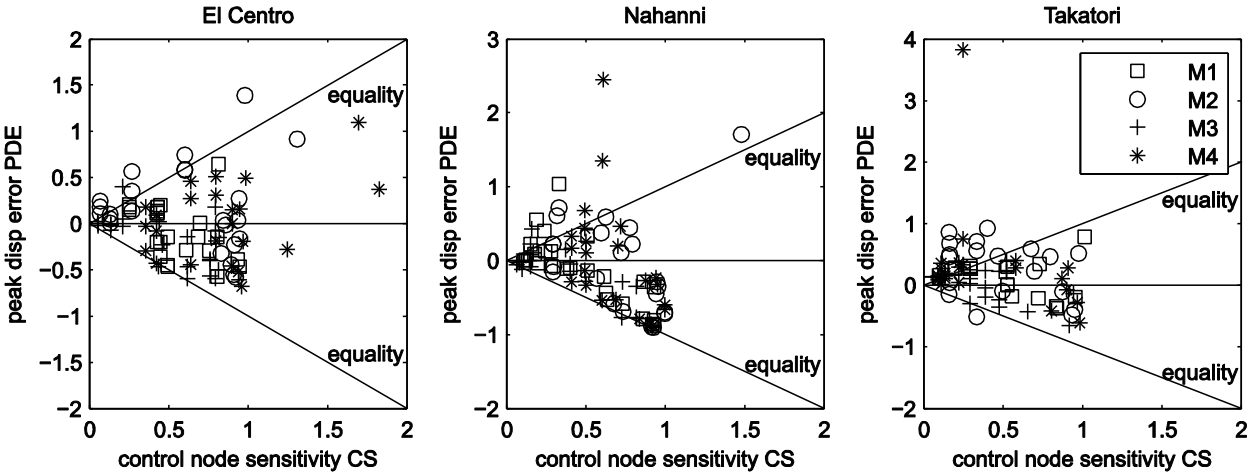

Figure 3. Correlation between peak displacement error and the control node sensitivity.

4.2 Two-storey Stone Masonry Building

The use of the control node sensitivity in gauging the accuracy of the SPO analysis is further investigated using a full-scale stone masonry building with strengthened timber floor and roof, which was tested under shake-table excitations at EUCENTRE (Magenes et al. 2014). The building was subjected to the 1979 Montenegro earthquake measured at the Ulcinj-Hotel Albatros station, scaling the peak acceleration from 0.06 g to 1.16 g. The building was modelled using TREMURI (Lagomarsino et al. 2013) with each wall represented by the equivalent frame idealisation of their in-plane behaviour. The out-of-plane wall behaviour was not explicitly modelled. The deformable lengths of the equivalent frames (i.e. piers and spandrels) were modelled using the macroelement formulation (Penna et al. 2014), which accounts for the axial-rocking interaction and shear-softening behaviours of URM. Each diaphragm was approximately represented by four elastic membrane finite elements to capture its vibrational behaviour (Figure 4), with the floor mass distributed to the perimeter walls and the diaphragm centre nodes based on simple tributary area consideration under lateral (inertial) loading. Additional static forces were applied on the walls to ensure the correct gravity stresses. This modelling approach was validated against the test data, with an acceptable accuracy (Fig. 5).

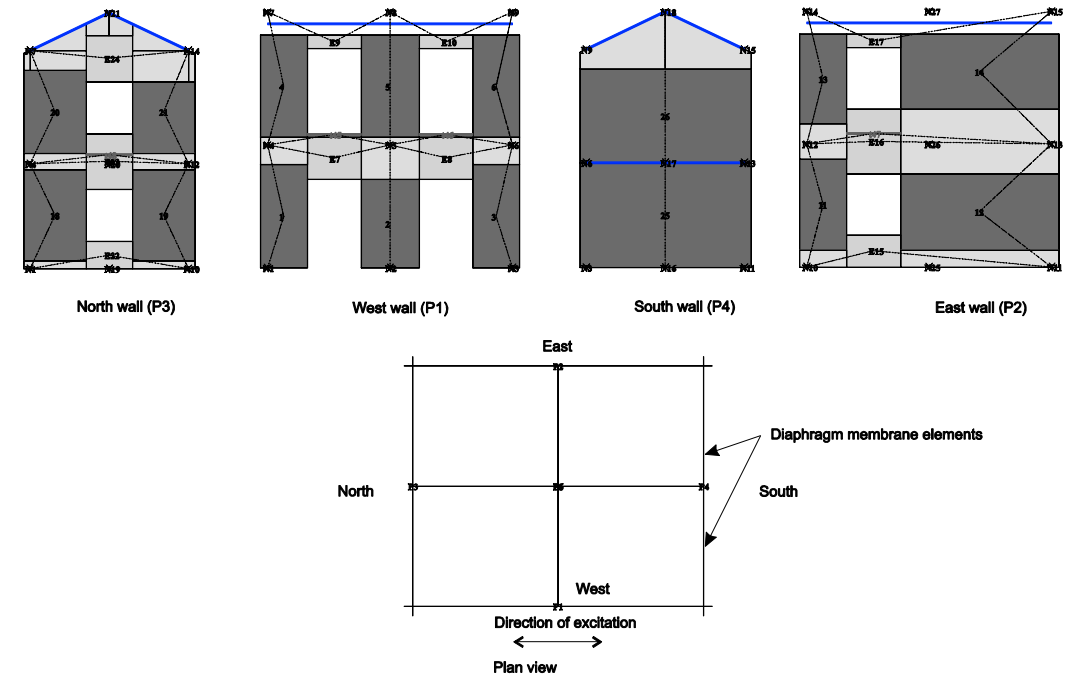

Figure 4. TREMURI model of tested building.

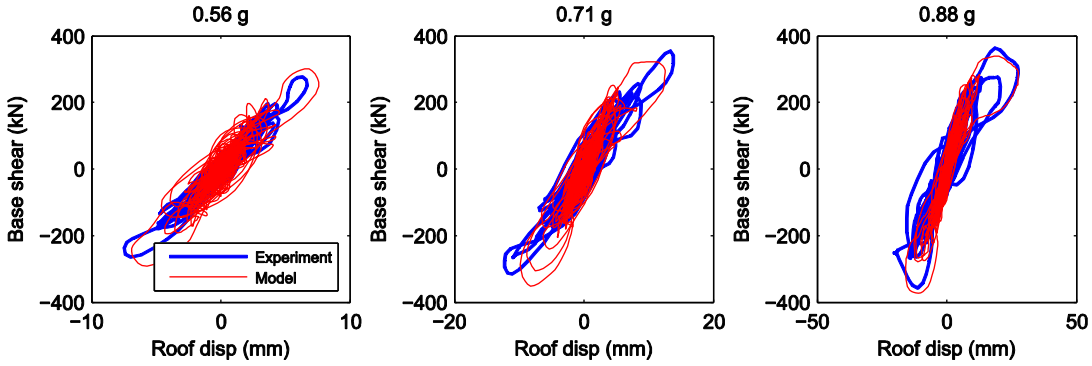

Figure 5. Comparison of numerical model against test data for 0.56 g to 0.88 g (penultimate) excitation levels.

Using the validated model, the diaphragm stiffness was reduced to 1.0, 0.75, 0.5 and 0.25 times the as-built configuration in order to simulate diaphragms of increasingly flexible constructions. The NTHA was conducted for each diaphragm configuration subjected to the 0.71 g and 0.88 g excitations. These analyses were considered to give the "exact" responses of the buildings for the purpose of assessing errors in the SPO analysis.

The SPO analyses were conducted using pushover forces proportional to mass and mass multiplied by a linear profile along the height of the structure. These two profiles are often considered to envelope the actual inelastic response (Galasco et al. 2006). Instead of rigorously solving the equation of motion of the equivalent SDOF system, the target displacement was estimated by the formulation of the N2 method

(Vidic et al. 1994; Fajfar 1999). The CS for the displacements and the inter-storey drifts at each level of the west wall, east wall, and the diaphragm mid-spans were calculated using the roof mid-span as the reference control node, with the additional analyses conducted using the control nodes at the roof levels of the two longitudinal walls.

Figure 6 shows the PDE and the peak inter-storey drift errors (IDE), which is defined analogously to Eq. 9 using inter-storey drifts, against the corresponding CS for the uniform and the linear displacement profiles. For the uniform displacement shape, the CS correlates well with both the PDE and the IDE. As observed for the idealised single-storey system, the CS can be seen to approximate the indicative upper-bound error of the analysis. For the linear displacement shape, the poor correlation is attributed to the actual response of the upper-storey west wall and the diaphragm not being bound by the SPO analyses with different control nodes (Fig. 7). However, for both assumed displacement shapes, the underestimation is again well bound by the CS and the SPO analysis generally tends to overestimate the "exact" NTHA responses.

An interest observation can be made regarding Figure 7, by noting that the three different predictions correspond to the same pushover analysis. The differences between them arise from the different levels of inelastic deformation depending on the control node location. Hence they indicate the progression of the nonlinear displacement under the pushover analysis conducted assuming a linear displacement shape. It can be seen that the analysis initially indicate larger upper storey deformation (for control node on east wall), but with an increased loading, the damage becomes concentrated at the ground storey (slight unloading takes place for the west wall). Hence even when the linear displacement is assumed, the pushover analysis ultimately indicates the concentration of inelastic damage at the ground storey, which is more consistent with the NTHA results, for which a uniform displacement shape may be considered more appropriate.

It may be noted that the SPO analysis does not converge to the exact response as the CS becomes small. Even for the uniform displacement shape, the PDE and the IDE of approximately 20% to 50% can be observed when the CS becomes negligible. This error is attributed to the inaccuracies inherent in the bilinear idealisation of the pushover curve and the empirical formulation used to estimate the peak displacement.

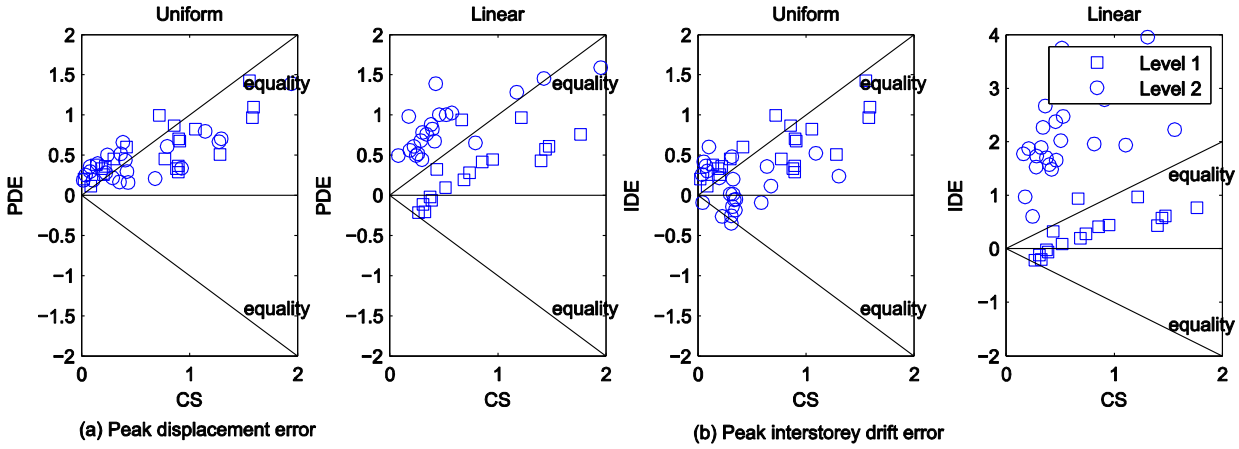

Figure 6. Correlation between control node sensitivity and peak displacement and interstorey drift errors.

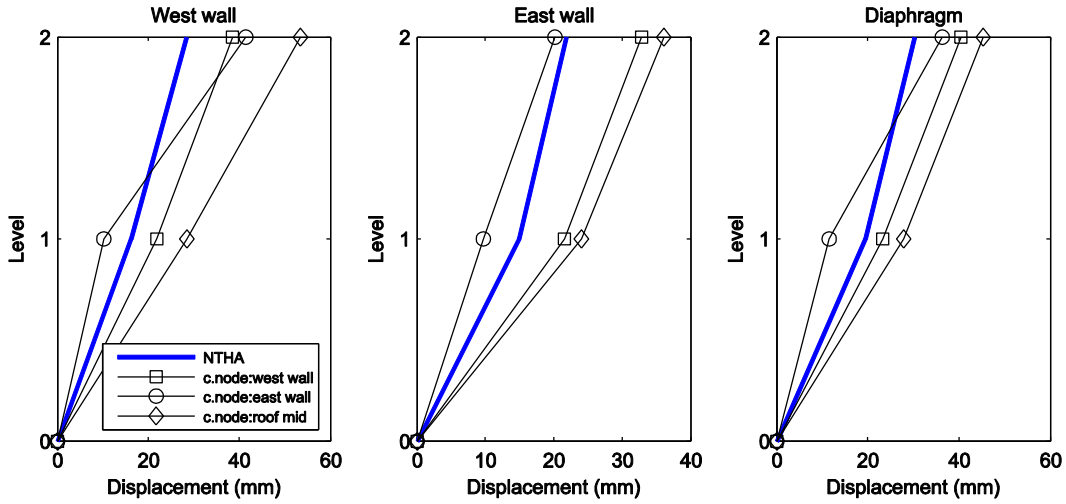

Figure 7. Comparison of NTHA of building model with diaphragm stiffness 0.5 times the as-built condition subjected to the 0.85 g excitation, with pushover analyses using linear displacement shape. The upper-storey displacements of the NTHA fall outside the predictions of the SPO analyses using different control nodes.

5. CONCLUSIONS

a measure for estimating the accuracy of a single-mode pushover analysis was investigated based on the sensitivity of the pushover analysis predictions to the variations in the control node location. From the limited number of analyses carried out, the proposed measure of the control node sensitivity was generally found to correlate with the accuracy of the SPO analysis. Provided that the displacement shape assumed in the pushover analysis was appropriate (i.e. consistent with the dominating failure mechanism) and several different control nodes are used, for example at the flexible and stiff walls and the roof mid-span, the SPO analysis tended to envelope the exact responses. In such cases, the proposed measure provided the upper-bound errors of the SPO analysis. Even when the SPO analyses did not envelope the

exact response, they generally provided conservative estimates of the responses. Notably, the underestimation error was consistently bound by the proposed measure. Therefore, limiting the control node sensitivity to an acceptable value could be one of the requirements needed to avoid unsafe use of the SPO analysis for URM buildings with flexible diaphragms.

REFERENCES

ASCE (2014) "Seismic evaluation and retrofit of existing buildings ASCE/SEI 41-13", American Society of Civil Engineers, Reston, Virginia.

ATC (1996) "ATC-40: Seismic evaluation and retrofit of concrete buildings, volume 1", Applied Technology Council, Redwood City, California.

CEN (2004) "EC8-1 – Eurocode 8: design of structures for earthquake resistance – part 1: general rules, seismic actions and rules for buildings. EN1998-1:2004", CEN, Brussels.

Chopra, A. K. and Goel, R. K. (2002) "A modal pushover analysis procedure for estimating seismic demands for buildings", Earthquake Engineering and Structural Dynamics, 31, 561 – 582.

Chopra, A. K. (2007) "Dynamics of structures - theory and applications to earthquake engineering, third edition", Pearson Prentice Hall, Upper Saddle River, New Jersey.

Costley, A. C. and Abrams, D. P. (1995) "Dynamic response of unreinforced masonry buildings with flexible diaphragms, SRS No. 695", University of Illinois at Urbana-Champaign, Illinois.

Fajfar, P. and Gašperšič, P. (1996) "The N2 method for the seismic damage analysis of RC buildings", Earthquake Engineering and Structural Dynamics, 24, 31 – 46.

Fajfar, P. (1999) "Capacity spectrum method based on inelastic demand spectra", Earthquake Engineering and Structural Dynamics, 28, 979 – 993.

Galasco, A., Lagomarsino, S. and Penna, A. (2006) "On the use of pushover analysis for existing masonry buildings", Proc. of 1st European Conference on Earthquake Engineering and Seismology, Geneva, 3-8 September.

Krawinkler, H. and Seneviratna, G. D. P. K. (1997) "Pros and cons of a pushover analysis of seismic performance evaluation", Engineering Structures, 20(4-6), 452 – 464.

Lagomarsino, S., Penna, A., Galasco, A. and Cattari, S. (2013) "TREMURI program: an equivalent frame model for the nonlinear seismic analysis of masonry buildings", Engineering Structures, 56, 1787 – 1799.

Magenes, G. and Penna, A. (2009) "Existing masonry buildings: general code issues and methods of analysis and assessment", Proc. of Eurocode 8 perspectives from the Italian Standpoint Workshop, Napoli, Italy.

Magenes, G., Penna, A., Senaldi, I., Rota, M. and Galasco, A. (2014) "Shaking table test of a strengthened full-scale stone masonry building with flexible diaphragms", International Journal of Architectural Heritage: Conservation, Analysis, and Restoration, 8(3), 349 – 375.

Mendes, N. and Lourenço, PB. (2009) "Seismic assessment of “Gaioleiro” buildings in Lisbon, Portugal", Journal of Earthquake Engineering, 14(1), 80 – 101.

Penna, A., Lagomarsino, S. and Galasco, A. (2014) "A nonlinear macroelement model for the seismic analysis of masonry buildings", Earthquake Engineering and Structural Dynamics, 43(2). 159 – 179.

Vidic, T., Fajfar, P. and Fischinger, M. (1996) "Consistent inelastic design spectra: strength and displacement", Earthquake Engineering and Structural Dynamics, 23, 507 – 521.